



HAL
open science

The origins of biomolecular asymmetry : study of extraterrestrial matter by two-dimensional gas chromatography

Raphaël Pepino

► **To cite this version:**

Raphaël Pepino. The origins of biomolecular asymmetry : study of extraterrestrial matter by two-dimensional gas chromatography. Analytical chemistry. Université Côte d'Azur, 2022. English. NNT : 2022COAZ4036 . tel-03827079

HAL Id: tel-03827079

<https://theses.hal.science/tel-03827079v1>

Submitted on 24 Oct 2022

HAL is a multi-disciplinary open access archive for the deposit and dissemination of scientific research documents, whether they are published or not. The documents may come from teaching and research institutions in France or abroad, or from public or private research centers.

L'archive ouverte pluridisciplinaire **HAL**, est destinée au dépôt et à la diffusion de documents scientifiques de niveau recherche, publiés ou non, émanant des établissements d'enseignement et de recherche français ou étrangers, des laboratoires publics ou privés.



$$\rho \left(\frac{\partial v}{\partial t} + v \cdot \nabla v \right) = -\nabla p + \nabla \cdot T + f$$

$$e^{i\pi} + 1 = 0$$

THÈSE DE DOCTORAT

Les origines de l'asymétrie biomoléculaire

Étude de la matière extraterrestre par chromatographie
bidimensionnelle en phase gazeuse

Raphaël PEPINO

Institut de Chimie de Nice (ICN)

Présentée en vue de l'obtention
du grade de docteur en chimie
de l'Université Côte d'Azur

Dirigée par : Dr. Cornelia Meinert

Soutenue le : 13 juillet 2022

Devant le jury, composé de :

Caroline West, Professeure, Université
d'Orléans, Rapportrice & Présidente du Jury
Arnaud Buch, Professeur, Université Paris-
Saclay, Rapporteur
Pauline Poinot, Maîtresse de conférences,
HDR, Université de Poitiers, Examinatrice
Thomas Michel, Maître de conférences,
HDR, Université Côte d'Azur, Examineur



European
Research
Council





UNIVERSITÉ
CÔTE D'AZUR



ICN Institut de
Chimie de Nice



European
Research
Council

Université Côte d'Azur

École Doctorale de Sciences Fondamentales et Appliquées (EDSFA)

Institut de Chimie de Nice (ICN)

THÈSE DE DOCTORAT

Présentée en vue de l'obtention du grade de docteur en chimie de l'Université Côte d'Azur par

Raphaël PEPINO

THE ORIGINS OF BIOMOLECULAR ASYMMETRY

Study of extraterrestrial matter by two-dimensional gas chromatography

Dirigée par Dr. Cornelia Meinert

Soutenue le 13 juillet 2022

Devant le jury composé de :

RAPPORTEURS

Caroline West, Professeure, Université d'Orléans, Présidente du Jury

Arnaud Buch, Professeur, Université Paris-Saclay

EXAMINATEURS

Pauline Poinot, Maîtresse de conférences, HDR, Université de Poitiers

Thomas Michel, Maître de conférences, HDR, Université Côte d'Azur

LES ORIGINES DE L'ASYMETRIE BIOMOLECULAIRE

Etude de la matière extraterrestre par chromatographie bidimensionnelle en phase gazeuse

Résumé : La définition de la "vie" n'a pas encore fait l'objet d'un consensus scientifique, mais elle peut être comprise comme des organismes ayant un cycle de vie construit sur des cellules pouvant subir diverses réactions chimiques (métabolisme). Ces organismes sont maintenus dans un état d'homéostasie mais peuvent croître par division cellulaire, se reproduire, évoluer et s'adapter à leur environnement. Malgré son abondance actuelle sur Terre, il faut garder à l'esprit que la vie est apparue à un moment donné, s'est répandue et a donné lieu à une diversité et une complexité considérable. Au niveau moléculaire, la vie est apparue sur Terre grâce à des blocs de construction chimiques clés capables de polymériser et/ou de s'auto-assembler, générant des macromolécules telles que l'ADN, l'ARN et les protéines. Ces structures ont la caractéristique unique et cruciale d'être constituées de monomères chiraux, dont un seul énantiomère a été sélectionné pour construire la vie. Cette prédominance d'un énantiomère sur l'autre est commune à tous les organismes et est appelée *homochiralité*. Abiotiquement, cette particularité est difficile à décrire car elle implique la sélection d'un énantiomère par rapport à son image miroir, ce qui n'est généralement pas le cas sans support biologique : des proportions racémiques sont censées être obtenues dans ces conditions. Cet événement de rupture de symétrie, ou la création d'un excès énantiomérique suivi de son amplification est toujours une question en suspens mais est d'une importance fondamentale pour tenter d'expliquer l'apparition de la vie. Parmi les hypothèses existantes présentées ici, un scénario plausible pourrait être l'interaction entre la lumière polarisée circulairement (CPL) et la matière organique, induisant des excès énantiomériques. En effet, une photolyse et/ou une photosynthèse énantiosélective utilisant cette lumière chirale pourrait s'être produite sur des particules de poussière dans le milieu interstellaire (ISM), et des composés enrichis en énantiomères pourraient avoir été incorporés dans des météorites et des astéroïdes qui ont ensuiteensemencé la Terre primitive. Par conséquent, l'étude des matériaux extraterrestres tels que les météorites, les astéroïdes et les comètes devient essentielle pour obtenir des indices sur l'origine de la vie. La littérature soutient l'existence d'une source extraterrestre de composés enrichis en énantiomères, tels que les acides aminés L et les sucres D, ainsi que la détection de CPL dans l'ISM. Les moyens d'étudier ces excès sont discutés en combinant un outil analytique puissant tel que la chromatographie en phase gazeuse multidimensionnelle intégrale couplée à un spectromètre de masse à temps de vol (GC×GC-TOFMS) pour analyser des mélanges complexes, et des procédures de dérivation appropriées pour améliorer la volatilité, la détection et l'énantioséparation de biomolécules chirales. La dérivation des acides aminés a été

largement étudiée tandis que la dérivation des sucres est plus délicate en raison de leur cyclisation, et doit être adaptée à l'objectif de l'analyse. Pour étudier simultanément les acides aminés et les sucres dans des échantillons extraterrestres ou analogues, une méthodologie pour l'échantillonnage, l'extraction, la purification et le fractionnement de ces échantillons a été développée en utilisant la chromatographie par échange d'ions. Les applications de cette méthodologie, ou de certaines de ses parties, sur des échantillons issus de la synthèse d'acides aminés à partir d'hexaméthylènetétramine et de la synthèse de sucres à partir de formaldéhyde dans des conditions simulant les processus d'altération du corps parent des météorites sont mises en évidence.

Mots-clés : Chiralité, origine de la vie, GC×GC, dérivation, acides aminés, sucres.

THE ORIGINS OF BIOMOLECULAR ASYMMETRY

Study of extraterrestrial matter by two-dimensional gas chromatography

Abstract: The definition of “life” has not yet reached scientific consensus, but it can be understood as organisms with a life cycle built on cells that can undergo various chemical reactions of metabolism. These organisms are maintained in a state of homeostasis but can grow by cell division, reproduce, evolve, and adapt to their environment. Despite its current abundance on Earth, it must be kept in mind that life appeared at some point, spread and resulted in considerable diversity and complexity. At the molecular level, life emerged on Earth through key chemical building blocks capable of polymerizing and/or self-assembling, generating macromolecules such as DNA, RNA and proteins. These structures have the unique and crucial feature of being made of chiral monomers, and only one enantiomer has been selected to build life. This predominance of an enantiomer over the other is common to all organisms and called *homochirality*. Abiotically, this particularity is difficult to describe because it implies the selection of one enantiomer over its mirror image that is not generally the case without a biological support: racemic proportions are supposed to be obtained under these conditions. This symmetry breaking event, or the creation of an enantiomeric excess followed by its amplification, is still an ongoing question but is of fundamental importance for the appearance of life. Among the existing hypotheses presented herein, a plausible scenario could be the interaction between circularly polarized light (CPL) with organic matter inducing enantiomeric excesses. Indeed, enantioselective photolysis and/or photosynthesis using chiral light could have occurred on dust particles in the interstellar medium (ISM) and enantiomerically enriched compounds could have been incorporated in meteorites and asteroids that later seeded the early Earth.

Therefore, the study of extraterrestrial materials such as meteorites, asteroids and comets become essential to obtain clues about the origin of life. The literature supports the existence of an extraterrestrial source of enantio-enriched building blocks, such as L-amino acids and D-sugars, along with the detection of CPL in the ISM. The means to investigate these excesses are discussed by combining a powerful analytical tool such as comprehensive multidimensional gas chromatography coupled to a time-of-flight mass spectrometer (GC×GC-TOFMS) to analyze complex mixtures and suitable derivatization procedures to improve volatility, detection and enantioseparation of chiral biomolecules. Amino acid derivatization has been studied extensively, whereas sugar derivatization is more challenging due to their cyclization behavior and must be adapted to the purpose of the analysis. To simultaneously investigate amino acids and sugars in extraterrestrial or analogous samples, a methodology for sampling, extraction, purification, and fractionation of these samples has been developed using ion exchange chromatography. Applications of this methodology, or parts of it, on samples such as the synthesis of amino acids starting from hexamethylenetetramine and the synthesis of sugars starting from formaldehyde under conditions simulating meteorite parent body alteration processes are highlighted.

Keywords: Chirality, origin-of-life, GC×GC, derivatization, amino acids, sugars.

REMERCIEMENTS

Je tiens en premier lieu à remercier Pr. Caroline West ainsi que Pr. Arnaud Buch d'avoir accepté d'évaluer mes travaux de thèse en tant que rapporteurs, ainsi que Dr. Pauline Poinot et Dr. Thomas Michel d'en être les examinateurs. Vos expertises en chimie analytique ainsi qu'en extraction d'échantillons sont très appréciées, je vous adresse mes plus sincères remerciements.

Je tiens en second lieu à remercier celle sans qui ces travaux n'auraient pas été possibles, ma directrice de thèse, Dr. Cornelia Meinert. Sa bienveillance, sa gaieté, ses connaissances, ses compétences, son professionnalisme et son dévouement à la recherche ont su rendre ces années très enrichissantes d'un point de vue personnel et professionnel. Je ne saurais comment exprimer ma gratitude pour ces années d'apprentissage !

Je tiens à remercier Vassilissa Vinogradoff et Adeline Garcia pour nos différentes collaborations au cours de ces années et l'approvisionnement en échantillons toujours très complexes. Ce fut un plaisir d'échanger avec vous.

Je remercie également les membres de l'équipe, Jana, Vanessa, Guillaume et Adrien qui ont contribué à ces travaux, aux bons moments et aux coups durs qui se résolvaient la plupart du temps avec de bons W. ou KB. J'ai une pensée pour les stagiaires qui ont pu rejoindre l'équipe au cours de ces années, Nina et Valentin. Je vous souhaite à tous une très bonne continuation.

Je souhaiterais remercier tous les collègues et amis de l'institut que j'ai eu la chance de connaître au cours de ces années. Je pense à Jean-Jacques, Emilie, Bénédicte, Kim, Valentin, Camille, Adèle, Manon, Maïlys, Clément, Maria, Maxence, Jody, Matej, Cédric, Emilie, Corentin, Aurélien, Simon, Ben, Lorenzo, Kévin ... et bien sûr tous ceux que j'ai oublié de citer. Que de souvenirs avec chacun d'entre vous.

J'adresse mes plus pogneux remerciements à la F.F.P. pour toutes ces réflexions qui ont animé ces années mouvementées. Ses membres fondateurs, Adrien, Président d'honneur émérite, Guigui, Trésorier stratège, et Steve, Responsable communication intercontinentale, ont su rendre ces expériences de pensée formatrices sur le plan personnel, intellectuel, et même parfois financier. J'ai également une pensée pour Sarah, intrépide membre active de cette institution. J'espère avoir été digne de ma fonction de Président désigné pour ces quelques années. Puisse la Kambing ne pas m'en tenir rigueur.

J'aimerais remercier ceux avec qui j'ai pu partager des moments privilégiés, philosophiques, intemporels, insensés ... Je pense à Kim, Séb, Clément, Camille, Damien, Chalette, Val, et les pogneurs bien sûr.

Je remercie les membres de Deltaplus, Matthieu, Sévan et Vincent. Le Bretal a vu le jour au moment opportun et a rythmé ces dernières années. Le Pil rythmera probablement les suivantes !

Je remercie mes amis qui me supportent depuis notre plus tendre enfance et qui continuent à le faire aujourd'hui. P.L., Romain, Vincent, Nico, Joris et Pierre, vous êtes de ceux qui ne désespèrent pas face à un castis, ça n'a pas de prix. Je remercie également Anastasia, Alexia et Erika pour leur implication dans cette communauté. J'ai une pensée particulière pour P.L. et Anastasia dont le soutien depuis toutes ces années et particulièrement ces derniers mois redonne toujours le sourire, un grand merci !

Ces remerciements ne pourraient pas s'achever sans exprimer ma sincère gratitude à ma famille. Je remercie mes parents d'avoir toujours été aussi affectueux et investis depuis toutes ces années, votre soutien compte énormément ! Je remercie mes frères Guillaume et Florent qui ont toujours été là pour moi, et aussi pour occuper les samedis et le confinement, vous êtes géniaux ! Je remercie également mes belles-sœurs Aurélie et Noémie pour leur gentillesse et mes nièces, Elise et Julia, toujours pleines d'énergie. Je n'oublie évidemment pas Toto, Ema, Léo, Aldo et Françoise. On partage des choses extraordinaires depuis toutes ces années, je vous en remercie.

Enfin, mes derniers remerciements s'adressent à toi, Maëva. Tu es quelqu'un d'extraordinaire et pleine d'énergie, je te remercie pour ton soutien, ta patience, ta présence, ton rire contagieux. Nos routes se sont croisées au beau milieu d'un chemin semé d'embûches, mais d'autres horizons plus radieux arrivent, j'en suis persuadé.

TABLE OF CONTENTS

TABLE OF CONTENTS	XIII
LIST OF ABBREVIATIONS	XVII
LIST OF FIGURES	XIX
LIST OF TABLES	XXI
PREFACE	1
CHAPTER I – ORIGINS OF LIFE AND HOMOCHIRALITY	5
1.1 INTRODUCTION & OBJECTIVES	7
1.2 DETERMINATE SYMMETRY BREAKING MECHANISMS & AMPLIFICATION PROCESSES	9
1.2.1 Parity violation in the weak force	10
1.2.2 Circularly polarized light	11
1.2.3 Viedma ripening	13
1.2.4 Catalysis-based amplification	14
1.2.5 Other asymmetric amplification models	15
1.2.6 Conclusion	16
1.3 BIOSIGNATURES IN INTERSTELLAR ICE ANALOGS	16
1.3.1 Interstellar medium & grain model	16
1.3.2 Interstellar ice analogs	18
1.4 BIOSIGNATURES IN EXTRATERRESTRIAL MATTER	21
1.4.1 Meteorites	21
1.4.2 Comets	25
1.4.3 Asteroids	26
1.4.4 Conclusion	28
1.5 EXTRATERRESTRIAL SYNTHESIS OF BIOSIGNATURES	28
1.5.1 Amino acids	28
1.5.2 Sugars	29
1.5.3 Hexamethylenetetramine relevant biosignature	30
1.5.4 Conclusion	32
1.6 CONCLUSION	32
CHAPTER II - CHIRAL RESOLUTION AND ANALYSIS OF BIOSIGNATURES	33
2.1 COMPREHENSIVE TWO-DIMENSIONAL GAS CHROMATOGRAPHY (GC×GC)	35
2.1.1 General principle of operation	35
2.1.2 Modulators	36
2.1.2.1 Principle of operation	36
2.1.2.2 Technologic evolutions	37
2.1.2.3 Detectability	39
2.1.2.4 Time-of-flight mass spectrometry	39
2.1.3 Stationary phases	41
2.1.3.1 Cyclodextrins	41
2.1.3.1.1 General structure	41
2.1.3.1.2 Chiral recognition principle	42
2.1.3.1.3 Lipodex E	43
2.1.3.1.4 CP-Chirasil-Dex CB	43
2.1.3.2 New stationary phases for multidimensional gas chromatography	44
2.1.4 Derivatization in gas chromatography	44
2.2 TARGET COMPOUNDS CONSIDERATIONS	45

2.2.1	Carbohydrates	45
2.2.1.1	<i>Classifications</i>	45
2.2.1.1.1	Degree of polymerization & functions	45
2.2.1.1.2	Carbon number, stereochemistry & predominant forms	46
2.2.1.2	<i>Carbohydrate derivatization strategies</i>	49
2.2.1.2.1	Reduction	49
2.2.1.2.2	Oximation	50
2.2.1.2.3	Aldonitrile acetate	50
2.2.1.2.4	N,O-Bis(trimethylsilyl)trifluoroacetamide	51
2.2.1.2.5	Methylboronic acid/trifluoroacetic anhydride	52
2.2.1.2.6	(S)-2-Butanol/trifluoroacetic anhydride	53
2.2.2	Amino acids	53
2.2.2.1	<i>Classification</i>	53
2.2.2.2	<i>Amino acid derivatization strategies</i>	54
2.2.2.2.1	N,N-dimethylformamide/dimethylacetal	55
2.2.2.2.2	N-(tert-butyltrimethylsilyl)-N-methyltrifluoroacetamide (MTBSTFA) & N,O-bis(trimethylsilyl)trifluoroacetamide (BSTFA)	55
2.2.2.2.3	Ethylchloroformate/heptafluorobutanol	56
2.2.2.2.4	Methanol/trifluoroacetic anhydride	57
2.3	ION EXCHANGE CHROMATOGRAPHY	59
2.3.1	Resin properties	59
2.3.2	Relative selectivity of counter-ions	60
2.3.3	Separation mechanisms	60
2.3.4	Principle of ion exchange chromatography	61
2.3.5	Resin conditioning	62
2.4	EXTRACTION OF EXTRATERRESTRIAL ORGANIC MATTER	63
2.4.1	Solvent extraction of soluble organic compounds	63
2.4.2	Hydrolysis of meteoritic amino acids	66
2.5	CONCLUSION	66
CHAPTER III – TOWARD THE DEVELOPMENT OF A COMPLETE ANALYTICAL PROCEDURE TO INVESTIGATE EXTRATERRESTRIAL AND LABORATORY-PRODUCED EXTRATERRESTRIAL SAMPLES		69
3.1	GENERAL APPROACH	71
3.2	DERIVATIZATION & GC×GC ANALYSIS	72
3.2.1	MeOH/TFAA derivatization of amino acids	72
3.2.1.1	<i>Materials and methods</i>	72
3.2.1.1.1	Reagents	72
3.2.1.1.2	Derivatization	73
3.2.1.1.3	GC×GC-TOFMS	73
3.2.1.2	<i>Identification of amino acids</i>	74
3.2.1.2.1	Mass spectrum & fragmentations	74
3.2.1.3	<i>Overall resolution & enantioseparation</i>	76
3.2.1.4	<i>Repeatability</i>	79
3.2.1.5	<i>Linearity</i>	79
3.2.1.6	<i>Limit of detection</i>	81
3.2.1.7	<i>Enantiomeric excess conservation</i>	85
3.2.1.8	<i>Stability</i>	87
3.2.1.9	<i>Conclusion</i>	88
3.2.2	MBA/TFAA derivatization of sugars & sugar related compounds	88

3.2.2.1	<i>Materials and methods</i>	88
3.2.2.1.1	Reagents	88
3.2.2.1.2	Derivatization	89
3.2.2.1.3	GC×GC-TOFMS	89
3.2.2.2	<i>Identification of sugars and sugar related compounds</i>	89
3.2.2.2.1	Sugars	90
3.2.2.2.2	Sugar alcohols	92
3.2.2.3	<i>Overall resolution and enantioseparation</i>	93
3.2.2.4	<i>Conclusion</i>	93
3.3	PURIFICATION & FRACTIONATION	94
3.3.1	Materials & methods	94
3.3.1.1	<i>Materials & Reagents</i>	94
3.3.1.2	<i>Column preparation & conditioning</i>	95
3.3.1.3	<i>Sample purification and fractionation</i>	97
3.3.2	Amino acid recoveries	98
3.3.3	Early developments	101
3.3.3.1	<i>Recoveries of alanine and ribose</i>	101
3.3.3.2	<i>Drying impact</i>	102
3.3.4	Conclusion	103
3.4	SAMPLING & EXTRACTION	103
3.4.1	Materials & methods	103
3.4.2	Degradation of amino acids during hydrolysis	104
3.4.2.1	<i>Procedure</i>	104
3.4.2.2	<i>Results & discussion</i>	104
3.4.3	Degradation of amino acids in the presence of sugars	105
3.4.3.1	<i>Procedure</i>	105
3.4.4	Conclusion	106
3.5	CONCLUSION	106
CHAPTER IV	– APPLICATIONS OF THE OPTIMIZED METHOD TO COMPLEX SAMPLES	107
4.1	AMINO ACID SYNTHESIS STARTING FROM HEXAMETHYLENTETRAMINE	109
4.1.1	Materials and methods	109
4.1.2	Amino acids content	110
4.1.3	Other detected amino acids	112
4.1.4	Conclusion	113
4.2	MINERAL-CATALYZED FORMOSE REACTION UNDER HYDROTHERMAL CONDITIONS	114
4.2.1	Materials and methods	114
4.2.2	Derivatization approach	115
4.2.3	Evolution of sugars content	119
4.2.4	Evolution of sugar alcohols content	122
4.2.5	Enantiomeric excesses investigation	124
4.2.6	Conclusion	124
	CONCLUSION & PERSPECTIVES	127
	REFERENCES	133
	SUPPLEMENTARY MATERIALS	155

LIST OF ABBREVIATIONS

DNA	Deoxyribonucleic acid
RNA	Ribonucleic acid
PAH	Polycyclic aromatic hydrocarbon
PVED	Parity violation energy difference
CPL	Circularly polarized light
IR	Infrared
UV	Ultraviolet
ee	Enantiomeric excess
PECD	Photoelectron circular dichroism spectroscopy
CC	Carbonaceous chondrite
ppb	Parts per billions
AA	Amino acid
ISM	Interstellar medium
HMT	Hexamethylenetetramine
HMT*	2-Hydroxymethyltetritol
GC	Gas chromatography
GC×GC	Comprehensive two-dimensional gas chromatography
GC³	Three-dimensional gas chromatography
LC	Liquid chromatography
HPLC	High-performance liquid chromatography
MS	Mass spectrometry
TOFMS	Time-of-flight mass spectrometry
Quad	Quadrupole
CD	Cyclodextrin
ANA	Aldonitrile acetate
MBA	Methylboronic acid
BSTFA	<i>N,O</i> -bis(trimethylsilyl)trifluoroacetamide
TFAA	Trifluoroacetic anhydride
TFA	Trifluoroacetyl
(S)-2-BuOH	(<i>S</i>)-2-Butanol
OPA/NAC	<i>ortho</i> -phthalaldehyde/ <i>N</i> -acetylcysteine
ECHFBE	<i>N(O,S)</i> -ethoxycarbonyl heptafluorobutyl ester
DMF/DMA	<i>N,N</i> -dimethylformamide/dimethylacetal
Lipodex E	Octakis-(3- <i>O</i> -butyryl-2,6-Di- <i>O</i> -pentyl)- γ -cyclodextrin stationary phase
CP-Chirasil Dex CB	Heptakis-(2,3,6-tri- <i>O</i> -methyl)- β -cyclodextrine stationary phase
DB-WAX	Polyethylene glycol stationary phase

MTBSTFA	<i>N</i> -methyl- <i>N</i> -(<i>tert</i> -butyldimethylsilyl)-trifluoroacetamide
TMS	Trimethylsilyl
MeOH	Methanol
AcOCl	Acetyl chloride
IPA	Isopropanol
DCM	Dichloromethane
PTFE	Polytetrafluoroethylene
<i>m/z</i>	Mass/charge ratio
LOD	Limit of detection
MDL	Method detection limit
IDL	Instrument detection limit
P_M	Modulation period
NIST	National institute of standards and technology
EI	Electron ionization
ATP	Adenosine triphosphate
ROSINA	Rosetta orbiter spectrometer for ion and neutral analysis
IOM	Insoluble organic matter
NEO	Near-Earth object
<i>m</i>-ECD	Micro-electron capture detector
TCD	Thermal conductivity detector
FID	Flame ionization detector
RS	Relative selectivity
IEC	Ion exchange chromatography
CH	Carbohydrate
S	Sugar
BV	Bed volume
AccQ-Tag	6-Aminoquinolyl- <i>N</i> -hydroxysuccinimidyl carbamate
TIC	Total-ion current

LIST OF FIGURES

Figure 1. Structure of the deoxyribonucleic acid.	7
Figure 2. Genetic material built from chiral molecules.	8
Figure 3. Schematic representation of the construction of circularly polarized light.	11
Figure 4. Induced ees as a function of circularly polarized light orientation and wavelength.	12
Figure 5. Model of interstellar ice chemistry (grain model).	17
Figure 6. Sublimation chamber used for interstellar ice analogs studies.	18
Figure 7. Strecker synthesis of an α -amino acid from an aldehyde and Michael addition of ammonia to acrylonitrile leading to a β -amino acid under abiotic conditions.	29
Figure 8. Formose reaction chemical network.	30
Figure 9. Synthesis of hexamethylene tetranime (HMT) from formaldehyde and ammonia reagents.	31
Figure 10. Plausible chemical pathway leading to HMT under abiotic conditions using methanol, ammonia and UV-light.	31
Figure 11. Schematic of two-dimensional gas chromatography (GC \times GC).	36
Figure 12. Schematic of the modulation process.	36
Figure 13. Chemical structure of cyclodextrins.	41
Figure 14. Example of sugar acid, sugar alcohol, sugar aldehyde and sugar ketose for a three-carbon monosaccharide.	46
Figure 15. Classification of aldoses (monosaccharides) according to their carbon number.	47
Figure 16. Classification of ketoses (monosaccharides) according to their carbon number.	47
Figure 17. Intramolecular cyclization of ribose into anomers in solution.	48
Figure 18. Illustration of molecular duplication and loss of chiral information during the reduction of some D-aldopentoses.	49
Figure 19. Oximation derivatization starting from ribose.	50
Figure 20. Aldonitrile acetate derivatization starting from glyceraldehyde.	51
Figure 21. N,O-Bis(trimethylsilyl)trifluoroacetamide derivatization on ribose.	51
Figure 22. Methylboronic acid/trifluoroacetic anhydride derivatization on C ₃ , C ₅ and C ₆ monosaccharides.	52
Figure 23. (S)-2-butanol/trifluoroacetic anhydride derivatization on ribose.	53
Figure 24. N,N-dimethylformamide/dimethylacetal derivatization (DMF/DMA) of amino acids.	55
Figure 25. N-(tert-butyltrimethylsilyl)-N-methyltrifluoroacetamide (MTBSTFA) derivatization of amino acids.	56
Figure 26. Ethylchloroformate/heptafluorobutanol derivatization (ECHFBF) of amino acids.	56
Figure 27. Two-dimensional chromatogram of ECHFBF derivatized amino acids and analyzed on Chirasil-Val coupled to DB-WAX columns.	57
Figure 28. Methanol/trifluoroacetic anhydride derivatization (MeOH/TFAA) of amino acids.	58
Figure 29. Structure and properties of a cation exchange resin.	59
Figure 30. Principle of cation exchange chromatography for the separation of carbohydrates and amino acids.	62
Figure 31. General scheme of sampling, extraction, fractionation and purification, derivatization and analysis of a meteorite sample.	71
Figure 32. Mass spectrum & fragmentation of alanine as N-trifluoroacetyl methyl ester derivative.	75
Figure 33. Two-dimensional chromatogram of MeOH/TFAA derivatized amino acids analyzed on a Lipodex E coupled to a DB-WAX column.	77
Figure 34. Two-dimensional chromatogram of MeOH/TFAA derivatized amino acids analyzed on a CP-Chirasil-Dex CB coupled to a DB-WAX column.	77
Figure 35. Calibration curve for D-Alanine and L-Alanine using ECHFBF derivatization.	84
Figure 36. Evolution of ee over four concentrations of five 5% L-doped amino acids.	86
Figure 37. Two-dimensional chromatogram of MBA/TFAA derivatized sugars analyzed on a CP-Chirasil-Dex CB coupled to a DB-WAX column.	94

Figure 38. Schematic of glass tubes containing IEC resin and Teflon frits.	97
Figure 39. Recoveries of amino acids after ion exchange chromatography and MeOH/TFAA derivatized.	99
Figure 40. Two-dimensional chromatograms of Iva retention time area highlighting derivatization reagents background noise induced by IEC.	100
Figure 41. Schematic of the HMT sample processing.	110
Figure 42. Proposed pathway for the formation of amino acids from the decomposition of HMT followed by the formose reaction in the presence of ammonia.	113
Figure 43. Two-dimensional chromatogram of MBA/TFAA derivatized FGO2 sample analyzed on CP-Chirasil-Dex CB coupled to DB-WAX columns.	117
Figure 44. Two-dimensional chromatogram of (S)-BuOH/TFAA derivatized FGO2 sample analyzed on CP-Chirasil-Dex CB coupled to DB-WAX columns.	117
Figure 45. Two-dimensional chromatograms of FGO2, FG2 α , FGO7 and FG7 α .	118
Figure 46. Evolution of sugar content using calcium hydroxide and olivine as catalysts for the formose reaction on days 2, 7 and 45.	121
Figure 47. Evolution of sugar alcohols and dihydroxyacetone content using calcium hydroxide and olivine as catalysts for the formose reaction on days 2, 7, and 45.	123
Figure 48. D-Enantiomeric excess in calcium hydroxide and olivine catalyzed formose reaction on day 2.	125
Figure S 1. Alanine residual plot calculated from the calibration curve.	162

LIST OF TABLES

Table 1. Components of the interstellar medium.	17
Table 2. Average petrological characteristics of carbonaceous chondrites.	22
Table 3. Amino acid amounts in Murchison and their calculation in mol/L for our analyses.	24
Table 4. Example of amounts of sugars and sugar-related compounds in Murchison and their calculation for our analyses.	25
Table 5. Evolution of early thermal and valve modulators used in GC×GC.	38
Table 6. Acquisition rate of GC×GC compatible detectors.	40
Table 7. Physical and chemical properties of native cyclodextrins.	42
Table 8. Anomer ratios for a series of aldoses in aqueous solution.	48
Table 9. 20 to 22 proteinogenic amino acids including the 9 essential amino acids.	54
Table 10. Relative counter ion selectivity for AG 50W-X8 resin.	60
Table 11. List of mechanisms involved in ion exchange chromatography.	61
Table 12. Extraction methods of various targeted compounds in meteoritic samples.	64
Table 13. Characterization of N-trifluoroacetyl methyl ester amino acid derivatives by mass spectra, retention time and method detection limit.	78
Table 14. Repeatability tests on 9 samples analyzed once for each amino acid at 5×10^{-5} M.	79
Table 15. Regression data of the MeOH/TFAA calibration curve.	80
Table 16. Relative standard deviation of 8 samples analyzed once using 5×10^{-8} M of each amino acid.	82
Table 17. Investigation of alanine contamination using 2 mL of dried reagent, hydrolyzed with H ₂ O/AcOCl and derivatized as ECHFBE derivatives.	83
Table 18. Alanine contamination in three different grades of TFAA.	85
Table 19. Recovery tests after 7 days using 5×10^{-5} M for each amino acid.	87
Table 20. Characterization of MBA/TFAA sugar derivatives by mass spectra and retention time.	91
Table 21. Comparison of 5% ee, doped amino acids at 10^{-5} M with and without ion exchange chromatography.	100
Table 22. Recovery of DL-alanine and DL-ribose by ion exchange chromatography for 3 and 4 bed volumes and with 1 M NH ₄ OH.	101
Table 23. Recoveries of DL-alanine and DL-ribose using ion exchange chromatography for 4 BV and using 2 M NH ₄ OH.	102
Table 24. Ribose recovery depending on the drying procedure before derivatization.	102
Table 25. Amino acids recoveries after water extraction.	104
Table 26. Recoveries of Ala and Iva after mortar-doped serpentine, water hydrolysis and IEC.	105
Table 27. Comparison of the amino acid content reported in the original study and in the present work.	111
Table 28. Comparison of the amino acids content between the work of V.Vinogradoff et al. and the presented study.	112
Table 29. Overview of samples studied in this work.	115
Table 30. Qualitative analysis of some relevant formose reaction products using BSTFA derivatization.	118
Table S 1. Mass spectrum & fragmentation patterns of N-trifluoroacetyl amino acid methyl ester derivatives.	157
Table S 2. Mass spectrum of MBA/TFAA derivatized sugars and sugar related compounds.	163
Table S 3. Regression data of the MBA/TFAA calibration curve, used for days 2 and 7.	167
Table S 4. Regression data of the MBA/TFAA calibration curve, used for day 45.	168

PREFACE

Countless scientific and philosophical questions about the origins of life remain unanswered and may never find a meaningful explanation. Yet, a question as simple as “what is life?” remains itself an open debate¹. It can, however, be understood as organisms having a life cycle built on cells that can undergo various chemical reactions of metabolism. These organisms are maintained in a state of homeostasis but can grow by cell division, reproduce, evolve, and adapt to their environment. Since ancient times, scientists have believed that life arose spontaneously under favorable conditions from non-living matter, through what is called spontaneous generation. According to this theory, worms, maggots, and insects for example, could arise from organic matter (heterogenesis) from dead flesh or from inorganic matter (abiogenesis) such as dust particles.

Since Miller-Urey’s 1952 experiment, which simulated early Earth conditions using simple molecules such as methane, ammonia, dihydrogen, water, and electrical sparks that synthesized amino acids abiotically, a door was left-open to the likelihood of life’s building blocks to *randomly* appear on Earth in a mixture of primitive gases. The experiment prompted serious criticism of the conditions necessary for such reactions to occur. Temperature, pH, concentrations, dihydrogen content and a reducing atmosphere were all pointed out. Nevertheless, it paved the way for further investigations, as this *primordial soup* concept has since been widely explored. Hydrothermal vents, using volcanic hotspots as energetic source were later proposed as potential location for the origin of life due to their high methane, ammonia, and mineral composition. Wet-dry cycles constitute a later study, suggesting that biosignatures, like amino acids polymerize into oligo and polypeptides *via* alternating cycles of wet nighttime cooling and hot daytime drying cycles near lakes. In addition, meteorite studies have highlighted the possibility of an extraterrestrial seeding process of early Earth with various prebiotic molecules, raising many questions about the role of asteroids, comets and the interstellar medium in the synthesis and delivery of these compounds.

Ultimately, tracing the origins of life involves a multidisciplinary investigation at the interface between chemistry, biology, physics, astrophysics, and geology. In this context, particular emphasis is placed on meteorites and extraterrestrial samples, as well as on the means to extract and analyze them.

CHAPTER I

Origins of life and homochirality

1.1 INTRODUCTION & OBJECTIVES

Living organisms are assembled using specific chemical building blocks, leading to complex structures and self-assembly at the molecular level. Compounds such as lipids, carbohydrates (sugars), nucleobases, phosphates and amino acids are essential for the proper functioning of organisms. The combination of some of these molecules covalently and/or supramolecularly bond together can give rise to structures essential to life, such as DNA (**Figure 1**), which encodes the genetic information through chains of nucleotides, or proteins, assuring many roles, including enzyme catalysis.

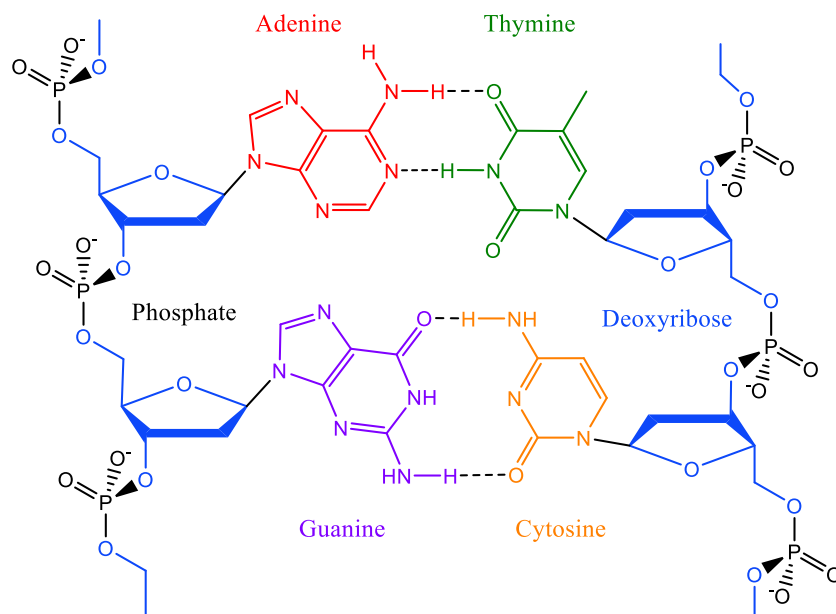


Figure 1. Structure of the deoxyribonucleic acid. In blue, the D-2-deoxyribose is highlighted and in black, the phosphate. Both constitute the skeleton of the DNA. In color, the nucleobases are highlighted and establish H-bonds between the pairs.

Interestingly, it was discovered that the monomers involved in DNA and proteins have a specific configuration, as shown in **Figure 2**. These monomers are chiral and therefore cannot be superimposed on their mirror image. This chiral property is conferred by asymmetric carbons that are linked to four different atoms or groups and lead to an *R* or *S* configuration. As molecules can contain several asymmetric carbons, enantiomers are defined as compounds having all of them of opposite configuration while the others are called diastereomers. In the case of amino acids and sugars, enantiomers are defined as D or L after the historical definition of optically active (+)-glyceraldehyde as D-glyceraldehyde. Thus, DNA is built from D-sugars (along with phosphates and nucleobases), while proteins use exclusively L-amino acids. On a larger scale, atypical structures of DNA and proteins are evidenced as a double helix and an α -

helix or β -sheet respectively. These examples show that the genetic material of life depends on enantiomers, which is in some ways difficult to understand given that abiotic chemical reactions tend to produce compounds in racemic proportions.

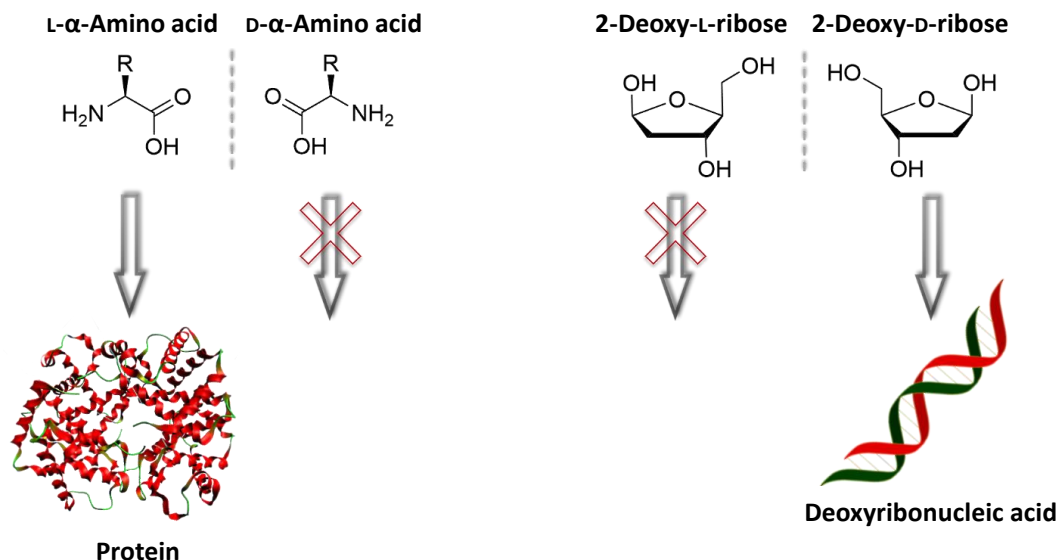


Figure 2. Genetic material built from chiral molecules.

Intuitively, a D or L predominance in biomolecules makes sense, as it allows for better recognition and replication in enzymatic reactions. Interestingly, a complete opposition – i.e., a "mirror world" using D-amino acids and L-sugars – should yield identically efficient life². Indeed, DNA, for example, would have the same double helix structure, but with L-nucleotides instead of D-nucleotides, which would give an opposite direction to the helix. It should also be noted that although life is primarily built on one specific configuration – D-sugars and L-amino acids – the other enantiomer exists in living organisms³⁻⁵. Furthermore, to obtain such polymers, it is questionable whether homochiral prebiotic building blocks are exclusively required. Theoretical calculations have shown that homochirality and polymers should go hand in hand, and that polymerization kinetics are altered by cross-inhibition of enantiomers⁶. Nevertheless, having an excess of one enantiomer should only enhance this selectivity-based process.

Many questions then arise from this asymmetry present in all living organisms – also called biological *homochirality*. Several major questions stand out: how and where the building blocks of life were formed as well as how and where the enantiomeric selection could have been occurred and amplified to lead to present homochiral life. Obviously, no scientific consensus has been reached on these two subjects, but several hypotheses have been developed and opened the way to promising leads.

Since temperatures were high during the Earth's formation, it is unlikely that hydrocarbon chains were preserved under these harsh conditions. A plausible hypothesis remains that is that extraterrestrial carbonaceous materials fed the Earth after it cooled. Indeed, more than 160 molecular species^{7,8} including carboxylic acids, alcohols, aldehydes, amines, ethers, hydrocarbons and polycyclic aromatic hydrocarbons (PAHs) have been found in the gas or solid phase – at various frequencies – in star-forming regions reinforcing an extraterrestrial carbon source. Thus, meteorites are of great interest because many biosignatures such as amino acids and sugar derivatives have been revealed after their analysis. Assuming such extraterrestrial delivery, the chemical reactions producing these biosignatures must be compatible with interstellar conditions and subsequent survival under early Earth' geochemical conditions. This severely restricts the pathways for obtaining amino acids and sugars, which are generally explained by a Strecker reaction for amino acids and a formose reaction for sugars.

With respect to homochirality, it is not clear whether it has a deterministic or probabilistic origin. This problem is usually approached as a two-step process: the first part consists of symmetry breaking associated with the creation of small enantiomeric excesses, and the second part consists of the propagation of these small *ees* through amplification processes. Since small enantiomeric excesses have been found in meteorites, it is likely that the symmetry breaking event occurred in space under interstellar conditions. These excesses may have subsequently seeded and spread on Earth.

Objectives

The questions on the original source of biosignatures and the origin of homochirality are addressed in the first chapter of this manuscript. As any *ee* found in extraterrestrial material and brought to the early Earth is of special interest to potentially answer the question on the origin of life, the analytical techniques useful to analyze them are detailed in the second chapter. The main objective of this thesis concerns the development of an analytical method to extract, purify, fractionate, derivatize and analyze an extraterrestrial sample and is outlined in the third chapter. Finally, the application of the developed methodologies on relevant extraterrestrial samples are reported in the fourth chapter.

1.2 DETERMINATE SYMMETRY BREAKING MECHANISMS & AMPLIFICATION PROCESSES

Apart from the necessity that life chose one molecular handedness of each of its fundamental chiral building blocks because of its efficiency in developing more complex structures during evolution, abiotic theories explaining initial symmetry breaking event can be grouped into random and determinate

mechanisms. Random mechanisms are the result of spontaneous symmetry breaking by crystallization, asymmetric adsorption onto minerals, and/or polymerization with minerals⁹. Several determined chiral influences have been proposed over time, but only two hypotheses are the most popular and detailed here: parity violation in the weak force and circularly polarized light¹⁰. The third true chiral influence (*true chirality* has been defined as parity-odd and time-even by L.D. Barron¹¹) concerns static magnetic fields collinear with unpolarized light¹². Other hypotheses have been proposed but are not considered because they are not truly chiral.

1.2.1 Parity violation in the weak force

The four fundamental interactions – gravitational, electromagnetic, strong nuclear and weak nuclear – were *assumed* to possess parity properties. However, the weak nuclear force was shown to violate parity in 1957 by Wu *et al.*¹³ using ⁶⁰Co. A cooled and magnetically aligned unstable isotope of Co (⁶⁰Co) was used, as it decays to ⁶⁰Ni by β -decay. An electron, an antineutrino and gamma rays are emitted during this decay. Since electromagnetic waves are known to respect the conservation of parity, the rate of emission of gamma rays was compared to the rate of emission of electrons in two distinct directions at low temperature. It was then shown that the electrons were emitted in a privileged direction – opposite to the gamma rays and the nuclear spin vector – thus violating parity.

The chemical implications of this parity violation concern two types of weak interactions: the charged current interaction and the weak neutral current¹⁴. The first is responsible for the emission of left-handed beta electrons during beta decay and radiolyses the enantiomers at different rates *via* electromagnetic interactions. The second is responsible for the energy differences between the enantiomers (PVED) due to the different interactions between the nuclei and the electrons. The range of this interaction is shorter and like that of the electromagnetic interaction. Theoretical calculations of the difference in parity violation energy (PVED) between the D and L amino acid enantiomers suggest that the L form would be slightly predominant over the D form due to its lower intrinsic energy. The order of magnitude of this energy difference has been estimated^{15,16} to be $10^{-14} - 10^{-13}$ J/mol but cannot be verified experimentally given the extremely small value of the expected difference. Another general skepticism is that the surprisingly found energetic advantage of the *biologically just fitting*, namely the L-amino acid enantiomer depended on the exact conformation of the compound, which is rather variable in its structure in vacuo, solid state, or dissolved (in water) state¹⁷. Moreover, PVED would be insufficient to lead to an amplification in the autocatalytic Soai reaction despite its efficiency in amplifying very small *ees*¹⁸. Also,

other theoretical calculations tend to say that beta radiolysis creates a larger chiral perturbation than weak neutral currents, up to six orders of magnitude¹⁹.

1.2.2 Circularly polarized light

Circularly polarized light (CPL) shown in **Figure 3** is a true chiral entity¹¹ capable of interacting differentially with chiral material through photochemical reactions and revealing the optical activity of an enantiomer. Three different mechanisms of photochemistry triggered by CPL have been reported so far. *Asymmetric photolysis* corresponding to the selective decomposition of one enantiomer over the other, *asymmetric photosynthesis* corresponding to the selective synthesis of one enantiomer and *photoisomerization* concerning the selective rearrangement of one enantiomer into the other²⁰. Thus, the interaction of CPL with chiral molecules can lead to the creation of enantiomeric excesses.

Supernovae were first considered as a potential source of extraterrestrial CPL because of the synchrotron radiation they emit, which could lead to the creation of enantiomeric excesses. However, CPL has not been detected in neutron star regions and this hypothesis has been ruled out²¹. On the other hand, infrared (IR)-CPL has been revealed in several star-forming regions such as the Orion nebulae OMC-1²² and BN/KL²³ with polarization rates up to 17% and in NGC6334-V²⁴ with polarization rates up to 22%. The evidence of these large-scale CPL regions reinforces the potential role of CPL in triggering *ees* in extraterrestrial material. Circularly polarized light could be the result of Mie scattering of linearly polarized light due to non-spherical dust grains aligned in a magnetic field^{25,26} or other processes of multiple scattering, dichroism, or twisted magnetic field lines^{27,28}. Calculations have confirmed that such IR-CPL intensities could also extend into the UV range and that absorption by interstellar dust prevents its direct detection²².

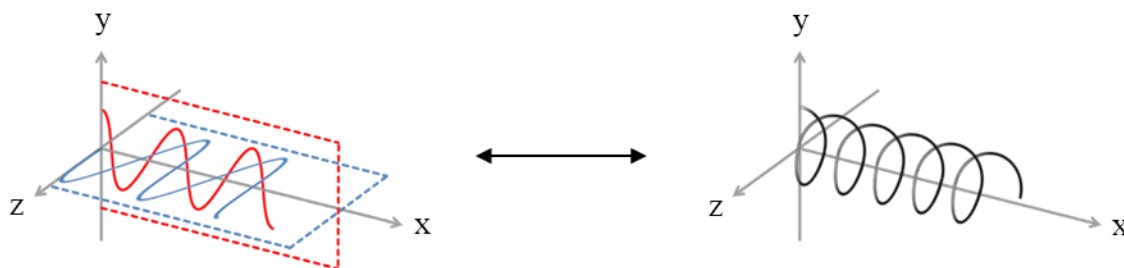


Figure 3. Schematic representation of the construction of circularly polarized light. Vertically and horizontally polarized waves are combined with a $\lambda/4$ wavelength shift and lead to CPL which has a helical path.

Because circularly polarized light is a true chiral entity that can be circularly polarized to the left (*l*-CPL) or right (*r*-CPL), circular dichroism ($\Delta\epsilon$) measurements can be performed on enantiopure compounds. Circular dichroism reports the difference in the molar extinction coefficient of an enantiopure compound between the two CPL helices at a given wavelength. In other words, it represents the difference in absorption of an enantiomer between *l*-CPL and *r*-CPL. Often, the anisotropy factor g – defined as $\Delta\epsilon/\epsilon$ (**Equation 1**) – which better describes the kinetics using the rate constants k_D and k_L for D and L enantiomers, and the photoreactions involved using the molar absorption coefficients ϵ_D and ϵ_L for D and L enantiomers, respectively, is used to predict any net effect of the CPL in asymmetric photoreactions (**Figure 4**). In addition, the induced *ee* can be related to the anisotropy factor to predict its maximum value^{29,30}. In **Equation 2**, the *ee* also depends on the extent of photolysis ξ . Ultimately, the chiral photoinduced formation of a specific enantiomer and the extent of *ee* depend on the wavelength and helicity of the CPL.

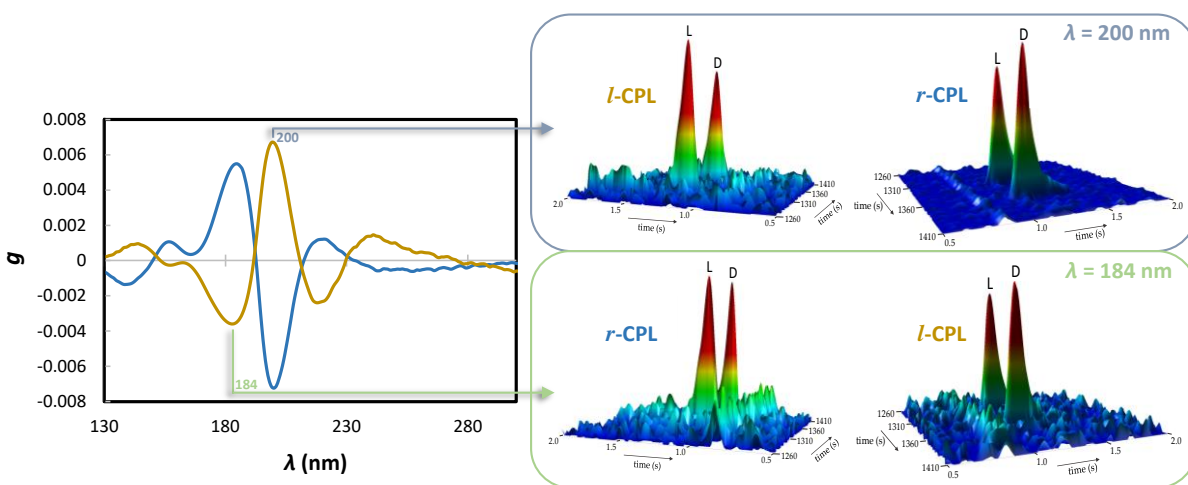


Figure 4. Induced *ees* as a function of circularly polarized light orientation and wavelength. (Left) Anisotropy spectrum of D-alanine (gold) and L-alanine (blue) in the solid state. (Right) Enantioselective GCxGC analysis of initially racemic alanine irradiated with the *l*-CPL anisotropic maximum ($\lambda=200$ nm, top) and the *r*-CPL anisotropic maximum ($\lambda=184$ nm, bottom).

$$g = \frac{\Delta\epsilon}{\epsilon} = 2 \times \frac{\epsilon_{l\text{-CPL}} - \epsilon_{r\text{-CPL}}}{\epsilon_{l\text{-CPL}} + \epsilon_{r\text{-CPL}}} = 2 \times \frac{\epsilon_D - \epsilon_L}{\epsilon_D + \epsilon_L} = 2 \times \frac{k_D - k_L}{k_D + k_L} \quad \text{Equation 1}$$

$$ee \geq \left(1 - \left(1 - \xi\right)^{\frac{g}{2}}\right) \times 100 \quad \text{Equation 2}$$

The first experiments using CPL were performed by Kuhn & Braun³¹ in the liquid phase using a racemic mixture of ethyl α -bromopropanoic ester which paved the way for enantioselective photolysis experiments of racemic amino acids decades later³². The reported *ees* for leucine in liquid solution (212.8 nm) were -2.5% and 1.98% using *l*-CPL and *r*-CPL, respectively. The first enantioselective laboratory syntheses using CPL were performed in 1971 by H. Kagan *et al.*³³ using helicenes. The optical rotations reported in these experiments were approximately $[\alpha]_D = -21 \pm 1^\circ$ using *r*-CPL and $[\alpha]_D = 21 \pm 1^\circ$ using *l*-CPL. Since then, CD and anisotropy studies of relevant biosignatures such as amino acids^{34,35} and sugars^{36,37} have been performed under various conditions, followed by corresponding asymmetric photolysis experiments. In the solid phase, racemic films of leucine exhibited an *ee* of 2.6% with *r*-CPL and -0.88% with *l*-CPL at 182 nm³⁸. After being studied in the liquid and solid phase^{29,39}, amino acids were recently studied in the gas phase to circumvent intermolecular and solvent interactions⁴⁰ by synchrotron radiation circular dichroism⁴¹ and photoelectron circular dichroism spectroscopy (PECD). PECD experiments on alanine at the astrochemically relevant Lyman- α line (10.2 eV \approx 121 nm) revealed an *ee* of about 4% in the photoproducts⁴². It should be noted that the magnitude of *ees* induced by CPLs is comparable to, but generally lower than the ones found in meteorites⁴³, supporting the UV-CPL hypothesis. Thus, given the observable and reproducible laboratory results on *ee* induction, CPL appears to be a promising candidate in terms of the initial symmetry-breaking event in the biomolecules of life.

Nevertheless, chance and determined mechanisms alone are insufficient to explain biological homochirality given the low *ees* obtained, which are of the order of a few percent only. An amplification mechanism to increase this imbalance is therefore mandatory. Several amplification models have been proposed that may be responsible for this phenomenon. *Chemical* models use chemical transformations such as catalysis-based amplification to preferentially synthesize an enantiomer⁴⁴, while *physical* models exploit physicochemical properties such as solubility, crystallization rates, or physical behavior of phases to enantioenrich a phase^{44,45}.

1.2.3 Viedma ripening

Spontaneous deracemization of enantiomers has been used as a separation technique, but only a few compounds, about 15%⁴⁶, show this predisposition. This is because conglomerate crystallization and solution racemization must occur at the same time under given conditions. Originally discovered by the crystallization of sodium chlorate NaClO₃⁴⁷, it has since given way to other techniques. During the Viedma ripening process, the solution must be saturated, stirred and may be racemic. Under these conditions, re-nucleation cannot take place, only growth dynamics and dissolution are affected. The use of glass beads

to shake the flask is interesting because it leads to many smaller crystals with higher solubility and thus to a slight supersaturation of the compound in solution. To compensate for this effect, the accretion rate on the existing NaClO₃ crystals is increased. The important characteristic of NaClO₃ is its achiral nature in solution which gives it the ability to accrete indifferently on D or L crystals. It rather depends on the size of the existing crystal according to the Ostwald maturation process⁴⁸, where large crystals are favored. Thus, if a chiral crystal predominates randomly, this will eventually lead to the growth of this enantiomeric solid and the creation of an *ee*. Since this is an unnatural equilibrium change, this attrition-promoted deracemization of conglomerates has been termed Viedma ripening, in reference to the Ostwald ripening cited above. In addition to NaClO₃, a biologically relevant amino acid derivative was reported⁴⁹, providing the first confirmation of the feasibility of this process. This enantioenrichment was also performed on the proteinogenic amino acid aspartic by C. Viedma *et al.*⁴⁶ as it is the only one of the 20 proteinogenic amino acids capable of crystallizing as homochiral D and L crystals^{45,46}.

1.2.4 Catalysis-based amplification

Catalytic amplification mechanisms rely on far-from-equilibrium conditions consistent with prebiotic conditions and were introduced by F.C. Frank⁵⁰ using model equations. Several hypotheses have been described over time, such as the *asymmetric autocatalytic reaction*, the *reaction with asymmetric self-amplification*, the *asymmetric catalytic reaction with a "hyperpositive" nonlinear effect*, and the *asymmetric catalytic reaction without nonlinear effects*, and have been reviewed by K. P. Bryliakov⁵¹. The genesis of these mechanisms lies in a slight enantiomeric imbalance due to random fluctuations or a deterministic symmetry-breaking event described previously. This imbalance can lead to an amplification because one enantiomer catalyzes its own formation or is potentially able to inhibit the synthesis of the other enantiomer.

The first and most famous experiment highlighting an *asymmetric autocatalytic reaction* scenario was reported by K. Soai *et al.*^{52,53} using alkylzincs. The so-called "Soai reaction" is very sensitive to very small enantiomeric imbalances. In their follow-up work⁵², the *ee* reported after several autocatalytic runs showed a huge increase from 2 to 5% *ee* to 90% using a pyrimidine-like molecule containing a secondary alcohol.

Other catalysis-based amplifications cited take advantage of a chiral catalyst leading to the achiral oxidized form of the initial product and only one of the two enantiomers^{54,55}, a chiral auxiliary whose *ee* (\approx 5%) leads to a higher product *ee* (\approx 50%)⁵⁶, and a catalyst that allows for a racemoselective, reversible catalytic

reaction combined with precipitation-induced chiral amplification⁵⁷. Using the latter, S. Miyagawa *et al.*⁵⁸ recently showed that spontaneous absolute asymmetric Strecker synthesis could be achieved in a prebiotic environment as enantioenriched chiral amino acid intermediates were obtained from achiral conditions. More importantly, R. Breslow *et al.*⁵⁹ showed a synergistic process between L-amino acids and D-sugars in a formose reaction, consistent with the current trend of life's homochirality. Finally, the RNA synthesis of Powner/Sutherland⁶⁰ combined with the work of Hein *et al.*⁶¹ offers an enantioselective prebiotic synthesis of activated RNA nucleotide monomers from glyceraldehyde. Therefore, catalysis-based mechanisms are promising candidates as *ee* amplification processes.

1.2.5 Other asymmetric amplification models

Various other models have been proposed, and can be classified as chemical, physical, or even a combination of both. The *eutectic* model or the *eve crystal* are physical models, the former being based on the differences in amino acid solubility between homochiral and heterochiral crystals⁶². Heterochiral crystals are less soluble and give one enantiomer the opportunity to predominate in solution. At the eutectic point, the *ee* of the aqueous solution is generally high, 46% for valine and 99% for serine⁶³. However, chiral amplification is impossible for all amino acids because some of them form conglomerates such as threonine and arginine. Other research has also demonstrated the role of small molecules in modifying the composition of *ee* eutectic *via* cocrystallization⁶⁴. Using oxalic acid in water, the *ee* of threonine at the eutectic point was found to be 50% (instead of 0%) while using fumaric acid in water, the *ee* increased from 47% to 99% for valine⁶⁵. The latter uses similar conditions to Viedma ripening but also includes the control of the temperature. As the solution is cooled, only one nucleus can be generated due to the low nucleation kinetics. Further nucleation will be favored because the first homochiral crystal is mechanically disintegrated into smaller crystals⁶⁶.

In terms of chemical amplification, we can mention incomplete reaction and polymerization. The former is based on kinetic differences between enantiomers during a stereoselective reaction leading to *ees* if the reaction is not complete. Tyrosine methyl ester was enriched in the L-enantiomer from 27.4% to 30.8% *via* its thermal dimerization after 40% completion⁶⁷. Polymerization of leucine at approximately 50% completion led to increased *ee* values in the final product⁶⁸. Starting with a 27% L-*ee* solution, poly-leucine was found to have an L-*ee* of 39.5% and left the remaining monomers enriched in D. The combination of the two has been treated extensively by M. Klussman *et al.*⁶⁴ and Hein *et al.*⁶¹ using physical enrichment of the enantiomers through catalytic amplification followed by selective crystallization.

1.2.6 Conclusion

In summary, among all deterministic symmetry breaking processes, CPL is a plausible candidate able to induce *ees* in many chiral biomolecules, hence initiated further studies of the interstellar medium and related chemical reactivities. On the other hand, the amplification mechanisms are various and different in nature. Only catalysis-based mechanisms create *ees* permanently, while alternative mechanisms concentrate and separate enantiomers. The amplification process will not be developed further in this manuscript; however, it could have occurred either on Earth under primitive Earth conditions or in space under interstellar conditions.

1.3 BIOSIGNATURES IN INTERSTELLAR ICE ANALOGS

As the possible scenario of seeding the Earth with interstellar matter is addressed in this thesis, the composition and chemical reactivity in interstellar environments as well as means of replicating these chemistries in the laboratory are briefly considered in the following.

1.3.1 Interstellar medium & grain model

The interstellar medium (ISM) is defined as the matter and radiation occurring between the stars in a galaxy and can itself be divided into several components according to temperature, density, and state of matter. These components are briefly detailed in **Table 1** and show a great diversity of physicochemical conditions in different regions. These huge differences are thought to arise from energy injection by supernovas *via* shock wave compressions and radiative processes resulting from turbulent behavior of the ISM^{69,70}. The major components of the ISM are H₂ gas (75%) and He (24%)²⁸ but account for only a few percent of the Galactic mass. The remaining percentage is attributed to silicates and carbon-based particles forming dust suitable for gas accretion and chemical reactions. Among the carbon-containing species, CO is the most abundant with a H₂/CO ratio of about 10⁴ while the abundance of other compounds varies with the ISM region⁷¹.

Given the numerous complex compounds that can be found in the ISM, laboratory simulations attempt to partially reproduce the composition, temperature, pressure, and/or radiation to gain access to primitive extraterrestrial-like samples. A model of interstellar dust grains (**Figure 5**) has been developed and aims to reproduce the surface chemistry of such extraterrestrial samples. Dust grains only represent about 1% of the total ISM mass but are fundamental as third bodies to host chemical reactions⁷². A five-step interaction mechanism has also been proposed to calculate the formation of simple molecules⁷³. The

products of these experiments are referred to as interstellar ice analogs and will be detailed in the next section.

Table 1. Components of the interstellar medium. From P. Ehrenfreund et al.⁷⁰ and adapted from D.H. Wooden et al.⁷¹

ISM component	Designation	Temperature (K)	Density [cm ⁻³]	Hydrogen state
Hot ionized medium	Coronal gas	10 ⁶	0.003	H ⁺
Warm ionized medium	Diffuse ionized gas H II	10 ⁴	>10	H ⁺
Warm neutral medium	Intercloud H I	10 ⁴	0.1	H ⁰
Atomic cold neutral medium	Diffuse clouds	100	10-100	H ⁰ + H ₂
Molecular cold neutral medium	Dark, molecular, and dense clouds	<50	10 ³ -10 ⁵	H ₂
Molecular hot cores	Protostellar cores	100-300	>10 ⁶	H ₂

Many processes such as UV radiation⁷⁴ (desorption and/or destruction of small molecules), cosmic rays⁷⁵ (creation of secondary electrons capable of triggering chemical reactions), low-energy protons⁷⁶ (formation of new radicals and molecular compounds) can be involved in ice chemistry. Finally, these dust particles may undergo heating as they move between regions of the ISM such as hot cores, increasing their temperature from 10 K to about 200 K. This heating effect has been shown to be essential for heavy radicals to be mobilized and participate in the formation of complex organic molecules^{75,77}.

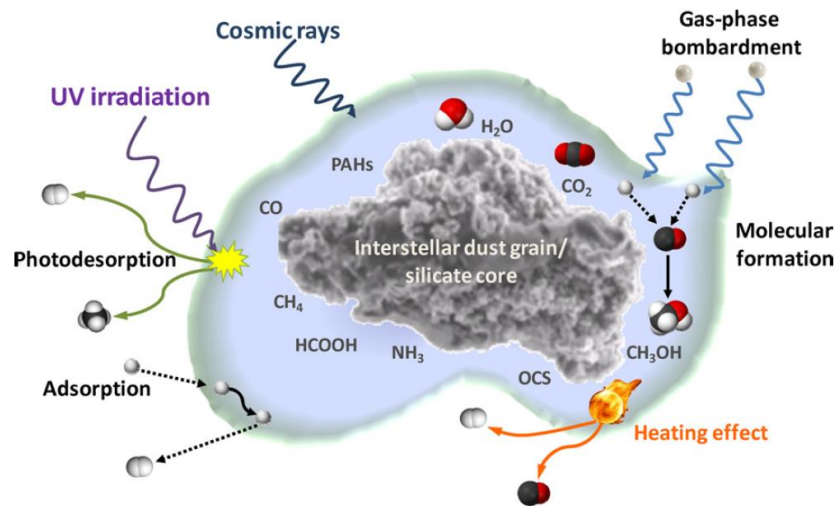


Figure 5. Model of interstellar ice chemistry (grain model). From C. Meinert et al.²⁸

1.3.2 Interstellar ice analogs

Depending on their composition, which is mainly H₂O, CH₃OH, CO, CO₂, CH₄, NH₃, H₂CO and HCOOH^{78,79}, they can be classified into polar ice^{80,81} having high H₂O content with low amounts of CH₃OH, CH₄, and NH₃, as well as apolar ice⁸² with high CO, CO₂, N₂, and O₂ content. In addition, the influence of water ice morphology is still an issue, as water can be amorphous or crystalline depending on the exact temperature conditions⁸³. Below 150 K, water ice resulting from the direct condensation of steam is amorphous and two categories are distinguished. Below 10 K, amorphous water is dense, while above 10 K, it is lighter and more common. Naturally, this is also a major concern for extraterrestrial samples, as they may have undergone aqueous alteration over time.

Figure 6 shows a typical experimental setup for experiments to simulate the complex chemistry of interstellar ice. Vacuum pumps and a cryostat ensure that interstellar conditions (≈ 10 K and $\approx 10^{-8}$ Torr) are reproduced while gaseous compounds condense on a window for subsequent irradiation with an energy source to trigger chemical reactions. An IR source and detector can be used to monitor the *in situ* evolution of the ice composition.

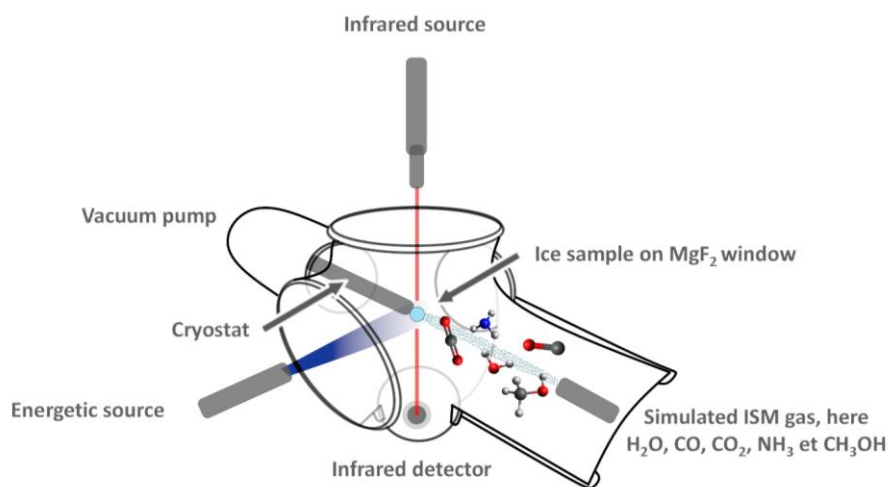


Figure 6. Sublimation chamber used for interstellar ice analogs studies.

Amino acid syntheses *via* this type of set-up were performed by Bernstein *et al.*⁸⁴ and led to the detection of glycine, alanine and serine using H₂O, CH₃OH, NH₃ and HCN under UV light on a nickel substrate. Contaminations were ruled out by ¹³C labeling and racemic proportions were obtained for alanine and serine. Another implication of these results is the non-required liquid conditions on the parent bodies.

Indeed, molecular clouds could thus be the seat of amino acid syntheses *via* photochemical reactions. Besides, Muñoz Caro *et al.*⁸⁵ identified 16 amino acids using H₂O, CH₃OH, NH₃, CO and CO₂ under UV light on an aluminum substrate. Of these amino acids, 6 were found to be proteinogenic and some of them have been reported in previous analyses of meteorites. In addition, diamine compounds were found in these simulated interstellar ices and the authors suggested that they might also be present in meteorites. Another striking finding was the high proportion of hexamethylenetetramine, which could be a source of prebiotic compounds, as discussed in **1.5 Extraterrestrial synthesis of biosignatures**. In these experiments, enantioselective analysis was generally performed to justify the non-contamination of the samples because no *ees* were expected. However, Bernstein *et al.*⁸⁴ anticipated at the time the use of UV-CPL in these samples as a potential means to induce *ees*. Years later, initial investigations into the possibility of creating enantiomeric excesses using UV-CPL illuminating a simple gas mixture of H₂O, CH₃OH, and NH₃ under interstellar conditions showed that L-*ees* of up to 1.34% ± 0.40% can be obtained⁸⁶. The authors related the results to previous work on the Murchison meteorite⁸⁷ where alanine was found in 1.2% excess making this scenario plausible. However, the difficulty of explaining the huge *ee* values of isovaline, up to 18.5%⁸⁸, with the use of UV-CPL alone was pointed out. Speculations on the nature of the amplification mechanism, *via* aqueous alteration, has also been made⁸⁹.

Phosphine, PH₃, is another abiotically relevant molecule because it has been detected in the circumstellar envelope of a carbon star⁹⁰. It is also thought that it may find an origin on interstellar grains using atomic phosphorus and hydrogen, in a water-like scenario with atomic oxygen and hydrogen. Phosphorus, especially in its oxidized form of phosphate, plays a crucial role in biology. However, its origin on the early Earth is unlikely due to the limited solubility of inorganic phosphorus under early Earth conditions. Thus, alternative extraterrestrial pathways have been proposed as a source of this element with different degrees of oxidation. From phosphine, carbon dioxide, and water under ionizing interstellar conditions, A.M. Turner *et al.*⁹¹ successfully synthesized phosphorus oxoacids such as phosphinic acid H₃PO₂ P(I), phosphonic acid H₃PO₃ P(III), phosphoric acid H₃PO₄ P(V), and pyrophosphoric acid H₄P₂O₇ P(V). Radical recombination and/or the insertion of electronically excited atomic oxygen obtained by the decomposition of water from carbon dioxide are reported as initiating processes that could have increased the complexity of the phosphinic acid H₃PO₂ formed first. The authors also addressed that the absence of triphosphoric acid H₅P₃O₁₀ would be an indicator that the increasing complexity ends with H₄P₂O₇ in the molecular clouds. Triphosphoric acid is considered very important because it is a precursor of the phosphorus backbone of adenosine triphosphate (ATP), providing energy to living cells. Furthermore, the presence of phosphoric acid and its eventual delivery to Earth would support the

findings reported by I. Nam *et al.*⁹² on sugar phosphates and ribonucleosides. Although thermodynamically and kinetically unfavored in bulk solution, phosphorylation was found to be more efficient using microdroplets and yielded over 6% D-ribose-1-phosphate. It also revealed the presence of uridine, leading the authors to consider microdroplets as a favorable environment for prebiotic ribonucleoside synthesis. Using phosphine, methane and water, Turner *et al.*⁹³ detected alkylphosphonic acids such as methylphosphonic acid [CH₃P(O)(OH)₂], ethylphosphonic acid and propylphosphonic acid. This validates the detection of alkylphosphonic acids in the Murchison meteorite⁹⁴ and could be the primitive source of bioavailable phosphorus for early organisms.

As previously described, ribose and 2-deoxyribose are fundamental constituents of RNA and DNA as well as other sugars for various nucleic acids. Using H₂O, CH₃OH, and NH₃ subjected to UV light under interstellar conditions, Meinert *et al.*⁹⁵ identified a variety of sugar alcohols (arabitol, xylitol, threitol), sugar acids (ribonic acid, arabinoic acid, xylonic acid), and sugars including arabinose, lyxose, xylose and ribose. Ribose has been later detected for the first time in the Murchison meteorite⁹⁶. As the authors point out, such a diversity of compounds can only be achieved by a formose-type reaction detailed in **1.5 Extraterrestrial synthesis of biosignatures**. The particularity lies in a non-required divalent catalyst such as calcium, lead or titanium ions⁹⁷ for this reaction to occur but a photochemical-driven mechanism.

Nucleobases are essential constituents of DNA and were synthesized abiotically by Y. Oba *et al.*⁹⁸ using H₂O, CO, NH₃, and CH₃OH under UV light and thermal processes. Specifically, pyrimidine (cytosine, uracil and thymine) and purine (adenine, xanthine and hypoxanthine) nucleobases were detected. Although previous studies exist on their synthesis under abiotic conditions using formamide⁹⁹ or urea¹⁰⁰, these compounds and the conditions under which the nucleobases were obtained are less relevant to astrophysical conditions. The reported amounts were found to correlate well with the Murchison meteorite because a factor of 100 was observed between amino acids and nucleobases.

Ultimately, these simulated interstellar ice samples highlight possible formation pathways of relevant organic molecules including chiral biomolecules in extraterrestrial samples. However, such interstellar ice analogs *only* focus on specific conditions of temperature, pressure, and composition. Minerals, which are known to play a catalytic role and are suspected of triggering *ees* in amino acids, have so far been excluded from these studies. Analyses of real samples such as meteorites, asteroids, and comets provide a more difficult but more accurate picture of the compounds likely to be delivered to Earth and should be correlated with these experiments. Thus, the composition of extraterrestrial materials will be highlighted in the following section.

1.4 BIOSIGNATURES IN EXTRATERRESTRIAL MATTER

1.4.1 Meteorites

Meteorites are solid fragments of extraterrestrial matter such as comets and asteroids that have survived the entry into a planet's atmosphere. During the atmospheric entry phase, these objects are called meteors because friction, pressure and chemical reactions increase their temperature until a fireball, commonly called a shooting star, is observed. They can be considered either as *falls* if they can be linked to an actual observation of a fall, or as *finds* if they cannot. In terms of classification, they are divided into 3 categories: *chondrites* (undifferentiated meteorites), *achondrites* (differentiated meteorites) or *primitive achondrites*. Chondrites come from bodies that have preserved the original matter of the solar system and contain chondrules (spheres of 1 to 2 mm) while achondrites are igneous rocks from differentiated parent bodies (asteroids, planets), which means that they were huge enough to melt and organize themselves in several layers. Primitive achondrites possess partial characteristics of both categories: an achondritic texture (without chondrules) and a primitive chemical signature of their original chondritic parent body. Among chondrites, three major classes are distinguished: carbonaceous (C), ordinary (O) and enstatite (E). Each class can be divided into groups and further subdivided into subgroups.

The nomenclature of carbonaceous chondrites such as CI, CM, CR, CV, CO, CH, CB, CK are related to the type of specimen¹⁰¹. For example, CM stands for Carbonaceous Mighei-like meteorite. Parameters such as average chondrule diameter, matrix/chondrule ratios, metal abundance, mineral content, and composition of each group are briefly reviewed in **Table 2**. Carbonaceous chondrites can contain up to 5% carbon in the form of organic matter, carbonates, and other materials such as graphite, diamond, and silicon carbide¹⁰². Of the organic matter, about 25% are free and available, i.e. soluble compounds that are easily extracted with solvents (SOM), while the remaining 75% are bound, complex, insoluble compounds such as polyaromatic hydrocarbons¹⁰² (IOM). Carbonaceous chondrites represent only a small fraction, about 4%, of meteorite falls and finds^{28,103,104} but are not representative of their true proportion because they undergo rapid weathering. Another classification parameter is the aqueous and thermal alteration of the parent body that impacts the mineralogy and texture of the chondrite. This alteration is classified on a scale of 1 to 6, 1 representing the most aqueous alteration and 6 the least.

Table 2. Average petrological characteristics of carbonaceous chondrites. From and inspired by M.K. Weisberg et al.¹⁰¹

	CI	CM	CO	CV	CK	CR	CH	CB
Chondrule (%)	<< 1	20*	48	45	45	50 – 60	70	20 – 40
Matrix (%)	> 99	70*	34	40	40	30 – 50	5	<< 1
CAI-AOA (%)	<< 1	5	13	10	10	0.5	0.1	<< 1
Metal (%)	0	0.1	1 – 5	0 – 5	0 – 5	5 – 8	20	60 – 80
Diameter (mm)	NA	0.3	0.15	1.0	1.0	0.7	0.02	0.2 – 1

*Highly variable values. Percentages are expressed as volume fractions. CAI – Calcium – aluminium-rich in inclusion. AOA – Amoeboid olivine aggregate.

Particular emphasis has been put on the analysis of carbonaceous chondrites (CC) because of their high and diverse composition of organic compounds. Among these CC meteorites, the Murchison meteorite is emblematic because 96 amino acids¹⁰⁵, derivatives of C₃ to C₆ sugars¹⁰⁶, *N*-heterocycles, hydroxy acids, aldehydes, ketones, aliphatic and aromatic hydrocarbons¹⁰⁷ have been detected. A very exciting discovery concerning these molecules are the reported *ees*: up to 18% for L-amino acids and up to 82% for D-sugar derivatives. As previously mentioned, this L *ee* corresponds to isovaline which is a particular amino acid in the analysis of extraterrestrial samples. Indeed, as it is a non-biological amino acid, contaminations can be discarded, and it has the advantage of being less prone to racemization¹⁰⁸. It is therefore often targeted for the research of *ees*. Interestingly, the sign of these *ees* curiously tends to be the same as found in all present-day life forms. Other major biological building blocks, such as ribose, were also detected, but it is not yet known whether sugar molecules including ribose possess an *ee*¹⁰⁹. Given these results, it is likely that these key chiral building blocks of life may have had an extraterrestrial origin. However, the analysis of meteorites is still a challenge in terms of terrestrial contaminations. For this reason, *in situ* measurements on asteroids or comets have been attempted to overcome this problem of biological contamination and will be discussed in the following sections.

Since one of the goals of the present work is to develop an analytical method to quantify amino acids and sugars and their possible *ee* in meteoritic samples, it is necessary to ensure that these biosignatures can be quantified as a function of the chosen sample mass. Thus, it is necessary to estimate how much can be expected in a sample like the Murchison meteorite. Murchison has been well studied since its fall and data on the amounts of amino acids and sugars are available as ppb values. The objective is to obtain an order of magnitude of the amino acid concentration to adapt and optimize the analytical procedure accordingly. Considering the analysis of a sample of 1 g of Murchison, the expected concentration in a final volume – before gas chromatographic analysis – of 50 μ L can be expressed as follows in **Equation 3**.

$$[AA]_s = \frac{m_{AA}}{M_{AA} \times V_F} = \frac{m_S \times Q_{AA} \times 10^{-9}}{M_{AA} \times V_F} = \frac{1 \times Q_{AA} \times 10^{-9}}{M_{AA} \times 50 \times 10^{-6}} \quad \text{Equation 3}$$

$[AA]_s$ is the concentration of the amino acid in the sample (mol/L)

m_{AA} is the mass of the amino acid in the sample (g)

M_{AA} is the molar mass of the amino acid (g/mol)

V_F is the final volume before injection in which the AA is solubilized (L)

m_S is the mass of the sample (g)

Q_{AA} is the concentration of the amino acid in the sample, in ppb (ng/g)

As can be seen in **Table 3**, the order of magnitude of amino acid concentration is in the 10^{-5} – 10^{-4} M range for 1 g of a Murchison sample. If only 0.1 g of Murchison sample would be available, the amino acids are expected to be present in a concentration range of 10^{-6} – 10^{-5} M. The amino acids presented here were selected from the data of T. Koga & H. Naraoka¹¹⁰. It is also interesting to note that the hydrolysis step, according to this data set, releases a significant proportion of oligomerized amino acids that would not otherwise be quantified. Thus, it appears as a basic and necessary step in the analytical method. Similarly, the expected amounts for sugars and sugar-related compounds in Murchison were calculated and are reported in **Table 4**. Compared to amino acids, the amounts are approximately 10 times lower within the range of 10^{-5} – 10^{-6} M per 1 g of Murchison material. Some exceptions are low molecular weight compounds such as ethylene glycol, glycerol, and glyceric acid. As an overall trend, the abundances decrease with the number of sugar carbon. Other interesting compounds such as deoxy sugar acids including 2-deoxypentonic acid and 3-deoxyhexonic acid as well as dicarboxylic acids have also been reported¹¹¹.

Both values for amino acids and sugars are essential for developing and selecting adequate analytical methods as they directly define the limits of detection and quantification. However, these limits must be as low as possible in order to successfully differentiate the compounds from the matrix noise involved in such a complex sample.

Table 3. Amino acid amounts in Murchison (in ppb) and their calculation in mol/L for our analyses. Data taken from T. Koga & H. Naraoka¹¹⁰. Amino acids were derivatized as N-trifluoroacetyl O-methyl esters and analyzed by GC-MS equipped with a Chirasil-L-Val column. Standard deviations are not reported in this table for clarity but are available in T. Koga & H. Naraoka¹¹⁰.

Amino acid	H ₂ O (ppb)	H ₂ O + HCl (ppb)	M (g/mol)	H ₂ O (M)	H ₂ O + HCl (M)
Glycine	1373	3566	75.1	3.7 x 10 ⁻⁴	9.5 x 10 ⁻⁴
D-Alanine	318	570	89.1	7.1 x 10 ⁻⁵	1.3 x 10 ⁻⁴
L-Alanine	398	1130	89.1	8.9 x 10 ⁻⁵	2.5 x 10 ⁻⁴
Sarcosine	201	298	89.1	4.5 x 10 ⁻⁵	6.7 x 10 ⁻⁵
D-Serine	267	394	105.1	5.1 x 10 ⁻⁵	7.5 x 10 ⁻⁵
L-Serine	318	1261	105.1	6.1 x 10 ⁻⁵	2.4 x 10 ⁻⁴
β-Alanine	1064	1721	89.1	2.4 x 10 ⁻⁴	3.9 x 10 ⁻⁴
2-Aib	863	1015	103.1	1.7 x 10 ⁻⁴	2.0 x 10 ⁻⁴
D-2-Aba	532	873	103.1	1.0 x 10 ⁻⁴	1.7 x 10 ⁻⁴
L-2-Aba	541	944	103.1	1.0 x 10 ⁻⁴	1.8 x 10 ⁻⁴
D-Aspartic acid	108	301	133.1	1.6 x 10 ⁻⁵	4.5 x 10 ⁻⁵
L-Aspartic acid	267	1048	133.1	4.0 x 10 ⁻⁵	1.6 x 10 ⁻⁴
D-Threonine	tr.	tr.	119.1	-	-
L-Threonine	173	691	119.1	2.9 x 10 ⁻⁵	1.2 x 10 ⁻⁴
D-3-Aba	147	200	103.1	2.9 x 10 ⁻⁵	3.9 x 10 ⁻⁵
L-3-Aba	146	193	103.1	2.8 x 10 ⁻⁵	3.7 x 10 ⁻⁵
D-3-Aib	150	235	103.1	2.9 x 10 ⁻⁵	4.6 x 10 ⁻⁵
L-3-Aib	131	204	103.1	2.5 x 10 ⁻⁵	4.0 x 10 ⁻⁵
4-Aba	1244	1882	103.1	2.4 x 10 ⁻⁴	3.7 x 10 ⁻⁴
D-Valine	58	87	117.2	9.9 x 10 ⁻⁶	1.5 x 10 ⁻⁵
L-Valine	129	548	117.2	2.2 x 10 ⁻⁵	9.4 x 10 ⁻⁵
D-Norvaline	75	129	117.2	1.3 x 10 ⁻⁵	2.2 x 10 ⁻⁵
L-Norvaline	67	119	117.2	1.1 x 10 ⁻⁵	2.0 x 10 ⁻⁵
DL-Isovaline	1418	1668	117.2	2.4 x 10 ⁻⁴	2.8 x 10 ⁻⁴
D-Glutamic acid	172	314	147.1	2.3 x 10 ⁻⁵	4.3 x 10 ⁻⁵
L-Glutamic acid	426	1214	147.1	5.8 x 10 ⁻⁵	1.7 x 10 ⁻⁴
D-Leucine	17	80	131.2	2.6 x 10 ⁻⁶	1.2 x 10 ⁻⁵
L-Leucine	170	1058	131.2	2.6 x 10 ⁻⁵	1.6 x 10 ⁻⁴
D-Isoleucine	101	273	131.2	1.5 x 10 ⁻⁵	4.2 x 10 ⁻⁵
L-Isoleucine	251	947	131.2	3.8 x 10 ⁻⁵	1.4 x 10 ⁻⁴

Table 4. Example of amounts of sugars and sugar-related compounds in Murchison (in pmol/g or ppb) and their calculation for our analyses. Data taken from Y. Furukawa et al.¹¹² and G. Cooper et al.¹¹³

	Compounds	pmol/g or ppb	M (g/mol)	Content (M)
Sugar alcohols	Ethylene glycol	320000	62.07	6.4×10^{-3}
	Glycerol	160000	92.09	3.2×10^{-3}
	Erythritol	14*	122.12	2.8×10^{-7}
	DL-Threitol	14*	122.12	2.8×10^{-7}
	Adonitol	0	152.15	0
	DL-Arabinitol	0	152.15	0
	Xylitol	0	152.15	0
Sugar acids	Glyceric acid	80000	106.08	1.6×10^{-3}
	Threonic acid	4000	136.1	8.0×10^{-5}
	Erythronic acid	4000	136.1	8.0×10^{-5}
	Ribonic acid	589	166.13	1.2×10^{-5}
	Arabinonic acid	963	166.13	1.9×10^{-5}
	Gluconic acid	273	196.16	5.5×10^{-6}
	Mannonic acid	743	196.16	1.5×10^{-5}
Sugars	Ribose	25	150.13	3.3×10^{-6}
	Arabinose	120	150.13	1.6×10^{-5}
	Xylose	180	150.13	2.4×10^{-5}
	Lyxose	6.7	150.13	8.9×10^{-7}

*Values reported for another meteorite, ALH 85013, which is lower than the quantities in Murchison. Maximum values are 26 pmol/g for erythritol & 32 pmol/g for threitol. pmol/g values were converted to ppb using molar mass and a 1000 factor for further calculation.

1.4.2 Comets

First described as "dirty snowballs" by Whipple in 1950¹¹⁴, comets are composed of a mixture of ices and dust originally formed outside the solar system. They are considered to be remnants from the time of solar system formation¹¹⁵. Several parts of a comet can be distinguished: the *nucleus*, which is a small solid part composed of rock, dust, and ices of H₂O, CO, CO₂, CH₃OH, and H₂CO¹¹⁶, the *coma*, which is a visible atmosphere of ice and dust¹¹⁷ due to the outgassing process of the nucleus when it is heated, and the *tail(s)*, which are the result of the pressure of the solar wind and the Sun's radiation on the coma. Two distinct tails are usually observed: a gas tail formed by ions following the (magnetic) streamline of the solar wind and a dust tail, often curved and left behind.

Comets are generally more primitive than asteroids and meteorites because the still-frozen ice shows less weathering and thermal processing¹¹⁸. Comets have a high orbital eccentricity and can therefore be studied near the Earth rather than in the outer solar system which would prevent their close-up investigation¹¹⁸. The Rosetta mission, for example, was designed to analyze the surface of comet

67P/Churyumov-Gerasimenko. Its *Philae* lander was supposed to reach the site of *Agilkia* but ended up at its final site of *Abydos* due to several bounces on the cometary surface¹¹⁹ despite a sophisticated damping device to mitigate these bounces, an active descent system that was supposed to provide gaseous thrust as well as anchor harpoons to hold the lander to the surface. Unfortunately, the former did not activate while the latter did not deploy. As a result, the lander was left in an unfavorable position and orientation for the sampling and drilling device that was supposed to collect and deliver cometary surface material to the COSAC and Ptolemy analyzers. Nevertheless, the COSAC instrument operated several times in sniffing mode¹²⁰, where the mass spectrometer analyzed compounds that passively entered the instrument without the aid of the sample-and-drill device. These analyses led to comparison studies with the National institute of standards and technology (NIST) database to find the best fit for all peaks. In the end, 16 species were putatively identified¹²⁰, several of which, such as aldehydes, ketones, amines, and hydrogen cyanide, are thought to be molecules essential for abiotic amino acid synthesis.

Fortunately, the Rosetta orbiter spectrometer for ion and neutral analysis (ROSINA) on board the Rosetta parent probe revealed the presence of the simplest amino acid, glycine¹²¹, between 15 and 30 km from the core center. Two other nitrogen-bearing compounds, methylamine and ethylamine, were detected synchronously. K. Altwegg *et al.*¹²¹ pointed out that glycine is the only amino acid that could form without liquid water, which would explain its only detection in the comet's coma. Given its low sublimation temperature, about 150 °C¹²², they speculated that glycine is released from dust grain mantles that heat up in the coma. For comparison, alanine has a sublimation temperature in the same range, around 200 °C¹²², but was not detected. Its absence was therefore attributed to the unlikely aqueous alteration of comets.

Another interesting finding is the presence of phosphorus, which is present in multiple forms in living organisms, one of which is the DNA shown in **Figure 1**. However, its origin is unknown because only the exact mass of the ionized phosphorus has been found. The parent molecules could be PO¹²³, PN¹²⁴, CP¹²⁵ or HCP¹²⁶ because they have already been detected in the ISM. The presence of elemental phosphorus was suspected in the comet Halley dust signature¹²⁷ but the lack of sufficient mass resolution prevented any differentiation with other ions such as CH₂OH⁺ with a $m/z = 31$.

1.4.3 Asteroids

Links between meteorites and asteroids were first established with the low albedo asteroid Bamberga¹²⁸ which was found to be similar to carbonaceous chondrites. It is now estimated that these carbonaceous

C-type asteroids represent about 70% of all known asteroids¹²⁹. The presence of organic and other compounds is typically studied in the visible and near-infrared at wavelengths between 0.5 and 4 μm , as $\text{Fe}^{2+} - \text{Fe}^{3+}$ charge transfer absorption occurs at 0.7 μm , anhydrous silicates at 1 μm , water in hydrated minerals at 3 μm , and organic compounds between 3.3 and 3.6 μm , which is characteristic of the CH and NH chemical groups¹²⁹. D.P. Cruikshank *et al.*¹³⁰ in 1987 first reported the putative presence of C-H bonds in the asteroid Elektra at 3.4 μm , and in 2010 H. Campins *et al.*¹³¹ and S.A. Rivkin *et al.*¹³² suggested the presence of aliphatic CH_2 and CH_3 groups on the asteroid Themis at 3.3 μm and 3.4 μm . Unambiguous detection of organics using ground-based observations is tricky and this was also the case for the dwarf planet Ceres. The Dawn probe targeted Ceres from orbit in 2015 and confirmed the detection of aliphatic organic compounds. Given the depth of the observed 3.4 μm band, the abundance of insoluble organic matter (IOM) relative to carbonaceous chondrites has also been discussed^{133,134}.

In situ analyses are useful but also limited because many compromises must be made when designing a spacecraft. Thus, sample return missions are desirable because the best analytical tools available on Earth can be applied for these samples. Apart from the Apollo mission and the Stardust mission, which aimed to collect material from the lunar soil and comet dust particles, respectively, Hayabusa was the first sample return mission targeting an asteroid. Approximately 1 mg of asteroid Itokawa was successfully returned to Earth in 2010, but no amino acids were unambiguously identified¹³⁵. Glycine, alanine, 2-aminoisobutyric acid, and isovaline could not be proven to be indigenous because procedural blanks showed similar values of glycine and alanine while 2-aminoisobutyric acid and isovaline were only detected in one of the analyzed fragments. Missions such as Hayabusa2 or Osiris-REX are current examples of successful recovery of extraterrestrial material from carbonaceous near-Earth objects (NEOs). Hayabusa2 successfully sampled and returned 5.4 g of material to Earth from the asteroid Ryugu in December 2020. Preliminary results published by T. Yada *et al.*¹³⁶ using spectroscopy and microscopy showed the presence of hydroxyls at 2.72 μm , the presence of organics or carbonates at 3.4 μm , and the presence of a nitrogen-rich phase at 3.1 μm . In 2022, E.T. Parker *et al.*¹³⁷ identified non-proteinogenic amino acids such as β -alanine and β -aminoisobutyric acid for the first time using liquid chromatography with fluorescence detection and time-of-flight spectrometry in Hayabusa samples. On the other hand, Osiris-REX successfully sampled at least 60 g of the asteroid Bennu in October 2020 and is expected to land on Earth in September 2023.

Unfortunately, the masses collected by these sample return missions are small compared to the masses available from meteorites on Earth. Access to these valuable samples is therefore very limited.

1.4.4 Conclusion

Among extraterrestrial samples, meteorites are the most readily available but present a risk of terrestrial contamination. *In situ* analysis overcomes this difficulty but requires compromises in terms of analytical performance. Sample return missions are currently the best solution because they combine low risks of sample contamination and the use of high-performance analytical tools. Several biosignatures have been detected in these extraterrestrial samples and the following section aims at presenting the chemical reactions that could be responsible for their synthesis, especially for amino acids and sugars.

1.5 EXTRATERRESTRIAL SYNTHESIS OF BIOSIGNATURES

1.5.1 Amino acids

The pathway of amino acid synthesis in parent bodies has still not been resolved despite extensive studies of meteorites. The diversity of aldehydes and ketones found in these samples could have led to amino acids *via* a Strecker-type reaction involving ammonia and hydrogen cyanide, followed by hydrolysis *via* aqueous alteration on the parent body. This scenario is supported by the presence of α -hydroxy carboxylic and α -hydroxy dicarboxylic acids¹³⁸. According to this hypothesis, α -methylated amino acids such as isovaline and 2-aminoisobutyric acid, abundant in meteorites, could also be formed. Other pathways such as reductive amination of α -keto acids¹³⁹, carboxylation of amines using CO₂ and proton irradiation¹⁴⁰, and mineral-catalyzed reactions from H₂, CO, and NH₃¹⁴¹ have also been suggested. Nevertheless, a Strecker-type reaction cannot account for the generation of β -, γ -, and δ -amino acids thus questioning this scenario as plausible.

The synthesis of β -amino acids *via* a Michael addition to α,β -unsaturated nitriles coupled with reduction hydrolysis was considered¹⁰⁷. Michael addition, discovered in the late 19th century and shown in **Figure 7**, was adapted to the synthesis of β -alanine¹⁴² and was considered as a prebiotic way to obtain β -amino acids. Finally, γ - and δ -amino acids could be the result of the decarboxylation of α -amino-dicarboxylic acids¹⁴³ or the hydrolysis of lactams¹⁴⁴, an unlikely scenario given the unestablished source of the latter. In addition, aqueous alteration of cyanide-based polymers by hydrolysis has also been proposed¹⁴⁵, as well as radical mechanisms involving nitriles as precursors and gas-phase ion-molecule mechanisms¹⁴⁶. Nevertheless, Strecker's synthesis, discovered in 1850¹⁴⁷ and describing a route to obtain amino acids from an aldehyde (or ketone), ammonium chloride, and potassium cyanide, remains a good candidate for amino acid synthesis. The Strecker synthesis, shown in **Figure 7**, can be performed using ammonia and hydrogen cyanide. This synthesis is a 2-step reaction where the aldehyde reacts with ammonia *via* a

condensation reaction to lead to an α -aminonitrile that is then hydrolyzed to form an amino acid. The use of a primary or secondary amine instead of ammonia leads to *N*-substituted amino acids. In addition, racemic mixtures are obtained using this Strecker synthesis. Asymmetric synthesis and asymmetric catalysis were mentioned previously in **1.2.4 Catalysis-based amplification**. The former requires asymmetric amino reagents while the latter requires a chiral catalyst.

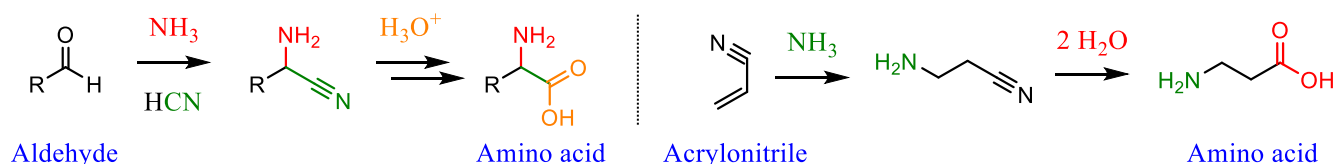


Figure 7. Strecker synthesis of an α -amino acid from an aldehyde (left) and Michael addition of ammonia to acrylonitrile leading to a β -amino acid (right) under abiotic conditions.

1.5.2 Sugars

The pathways for the synthesis of sugars under abiotic conditions have still not been solved, but several leads are being considered. The most famous is the Butlerov reaction¹⁴⁸, also known as the formose reaction. Discovered in 1861, the formose reaction describes a pathway for obtaining a plethora of long-chain sugars and sugar-related compounds from formaldehyde, as shown in **Figure 8**. The successive combination of isomerization and/or aldol reactions from formaldehyde leads to the complexification of the starting material to aldoses and ketoses. Basic conditions and a divalent metal such as calcium to coordinate the sugar oxygen atoms¹⁴⁹ were initially used as catalysts. The role of minerals has also been studied, and about half¹⁵⁰ of 34 tested minerals have been found to catalyze the formose reaction.

In addition, hydrothermal vent-like conditions using CaCO₃¹⁵¹ or interstellar-like¹⁵² conditions have been studied for the formation of various sugar compounds. A major concern is the availability of formaldehyde in interstellar ices or on the early Earth, as it is easily hydrated or can undergo a Cannizzaro reaction leading to formic acid and methanol. In addition, the sugars synthesized by the formose reaction are known to have a short lifetime¹⁵³ (ribose half-life is 73 min at pH 7.0 and 100 °C and 44 years at pH 7.0 and 0 °C), which compromises the mentioned conditions. In the case of hydrothermal vents, Omran¹⁵¹ proposed silica-CaCO₃ chemical gardens that could potentially allow for the accumulation (in addition to catalysis) of free sugars as the precipitate membranes formed are kept in disequilibrium from the outside.

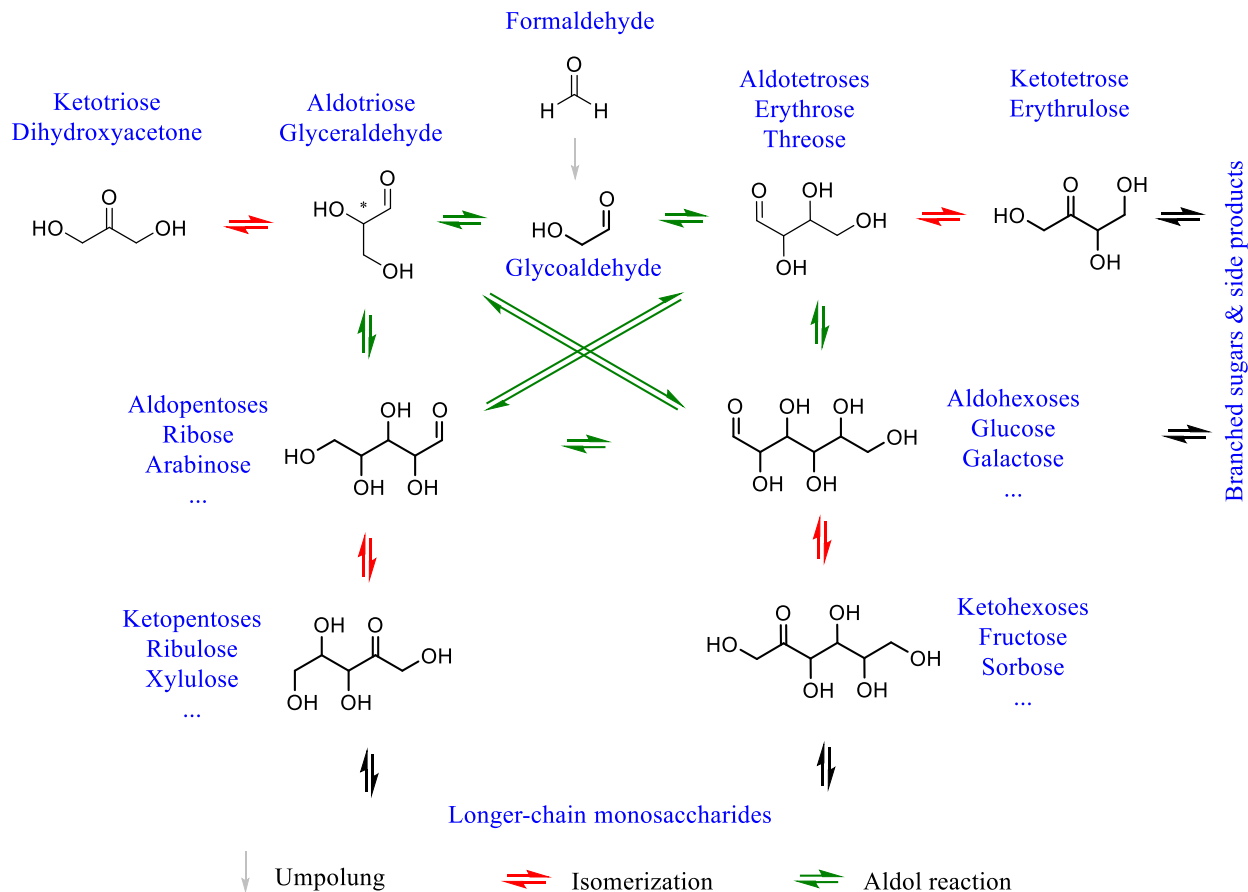


Figure 8. Formose reaction chemical network. Inspired by M. Haas et al.¹⁵⁴

1.5.3 Hexamethylenetetramine relevant biosignature

Hexamethylenetetramine (HMT) is a heterocyclic organic compound containing 4 nitrogen atoms linked to 6 methylene groups, as shown in **Figure 9**. It is symmetrical and has a cage-like molecular structure. HMT is usually obtained using formaldehyde and ammonia in liquid or vapor state by a condensation reaction. The search for pathways to form prebiotic molecules under abiotic conditions is still ongoing, but HMT is considered a key molecule to solve this problem because its acid hydrolysis can lead to several amino acids¹⁵⁵. Indeed, laboratory-synthesized interstellar ice analogs can contain significant amounts of HMT and HMT derivatives, especially when methanol is used in the initial reagent mixture¹⁵⁶. Furthermore, methanol abundances in the ISM support this scenario where these molecules are likely to be incorporated into interstellar ices and lead to abiotic chemistries on the surface of grains^{157,158}. The formose reaction and the inclusion of ammonia in the formose reaction are generally discussed to justify the role of HMT as a source of formaldehyde and ammonia¹⁵⁹ and as a feedstock for Maillard-type

reactions. It cannot be reduced to these reactions alone as it is probably a complex network of chemical reactions¹⁵⁹.

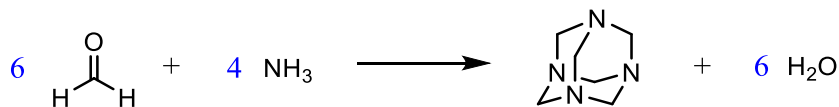


Figure 9. Synthesis of hexamethylenetetramine (HMT) from formaldehyde and ammonia reagents.

Despite its importance, HMT was only recently detected in meteorites¹⁵⁸ where derivatives such as methyl-HMT, amino-HMT, hydroxyl-HMT, hydroxymethyl-HMT, methoxy-HMT or monohydroxymethyl-HMT reinforced the indigenous origin of HMT. Unfortunately, spectroscopic techniques such as rotational spectroscopy or infrared spectroscopy do not allow direct detection of HMT in extraterrestrial environments. The first technique cannot be used due to the symmetric nature of HMT which does not give the molecule a permanent dipole moment¹⁵⁸. The second involves difficulties in reliably confirming an absorption band of HMT because deep C-H, C-N and N-H bands are found in interstellar ices¹⁵⁸. Its detection in meteorites has long been unsuccessful because standard protocols use water or acid hydrolysis at 100 °C for 24 hours that can degrade HMT^{156,160}. Mild temperature, suitable solvent conditions and desalting followed by HPLC (High-performance liquid chromatography) analysis have been used to successfully detect HMT. Formation pathways were proposed (**Figure 10**) from formaldehyde or methanol after irreversible irradiation and ammonia, leading to 1,3,5-triazinane as an intermediate and followed by the addition of formaldehyde on each nitrogen.

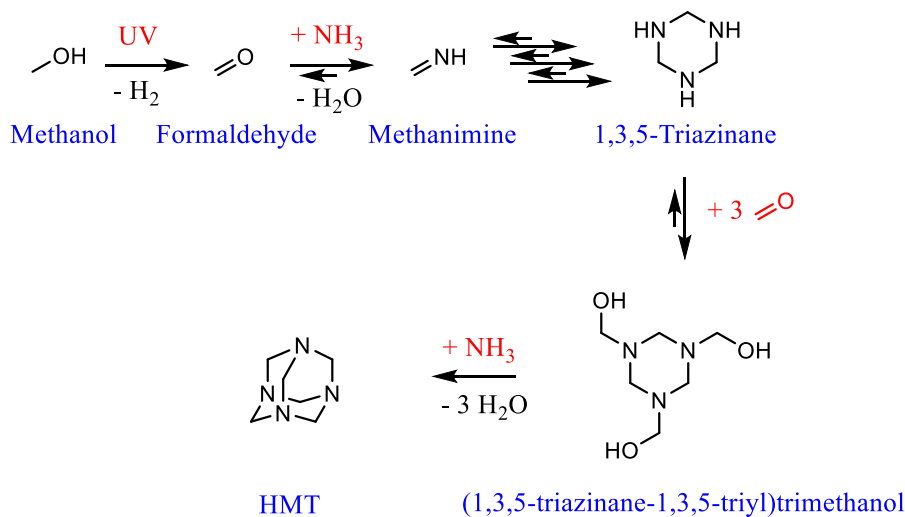


Figure 10. Plausible chemical pathway leading to HMT under abiotic conditions using methanol, ammonia and UV-light. Inspired by M. Caro et al.¹⁶¹ and M.P. Bernstein et al.¹⁶².

1.5.4 Conclusion

The conditions under which biosignatures are synthesized under interstellar conditions are still debated and not fully elucidated. Amino acids could be the result of multiple reactions such as Strecker synthesis and Michael addition, while sugars could probably originate from the formose reaction but suffer from rapid degradation. Other biosignatures such as HMT are another leads as intermediates to amino acids and a storage of formaldehyde for the formose reaction.

1.6 CONCLUSION

Numerous biosignatures have been found in extraterrestrial samples with *ees* of the same sign as found in living organisms. On the other hand, simulated cometary ice samples using CPL showed the presence of chiral biomolecules with small *ees*, that depend on the wavelength and helicity of the chiral photons used. Since the mechanisms and processes responsible for the synthesis of biosignatures and creation of extraterrestrial *ees* are not fully understood, additional analyses are required for understanding the origin of biomolecular homochirality. The following chapter aims to describe the materials and techniques that can be used to study such extraterrestrial *ees*.

CHAPTER II

Chiral resolution and analysis of biosignatures

2.1 COMPREHENSIVE TWO-DIMENSIONAL GAS CHROMATOGRAPHY (GC×GC)

Comprehensive two-dimensional gas chromatography is an advanced technology that evolved from conventional gas chromatography, which has been a common technique for analyzing volatile compounds for decades. The lack of full peak resolution in rather complex environmental samples has driven the evolution of gas chromatography through the use of *heart-cut* techniques that allow another separative run of an unresolved portion of the sample on a different column¹⁶³. At this point, the idea of performing complete heart-cut analyses emerged, but the main concern was to preserve separation on each individual column¹⁶⁴. The splitting devices used at that time have undergone many improvements and have been called modulators since 1991¹⁶⁵.

2.1.1 General principle of operation

A few microliters of liquid sample are introduced into the injector, which is maintained at high temperature, allowing the sample to change from liquid to gaseous state. The first oven is maintained at a temperature at least 20 °C below the boiling point of the sample solvent – to condense and concentrate the analytes at the beginning of the first column. A preferably inert carrier gas passes the two columns during the analysis and allows the migration of the analytes *via* their partition between the mobile phase (gas) and the stationary phase (column). This migration is assisted by the temperature, the oven being progressively heated to release the less volatile compounds. Compared to conventional GC, GC×GC can exhibit two different heated elements: the modulator and the second oven. Both allow for the successful transfer of effluents, minimizing peak broadening, and optimize the separation on the second dimension. The modulator traps the analytes between the columns and releases them periodically to preserve the separation in each dimension. The set of columns should preferably be chosen to be orthogonal, i.e. that the separation mechanism for each stationary phase is distinct to maximize peak capacity¹⁶⁶. The length of the 2nd column, which is approximately 1.5 m, is much shorter than the 1st column which is typically 25 m, and hence, is commonly compared to as very fast GC analysis¹⁶⁷. It should be noted that the addition of a second column does not change the total analysis time. The analytes are detected and quantified by a detector with a high acquisition frequency of at least 50 to 100 Hz, because of the resulting narrow peak widths of the secondary column. The typical width of these peaks is 100 to 200 ms, which corresponds to 10 to 5 Hz. Since about 10 data points are needed to reliably define each Gaussian peak, the acquisition rates of the detectors must be at least as high as those mentioned above. A simplified GC×GC scheme is shown in **Figure 11**.

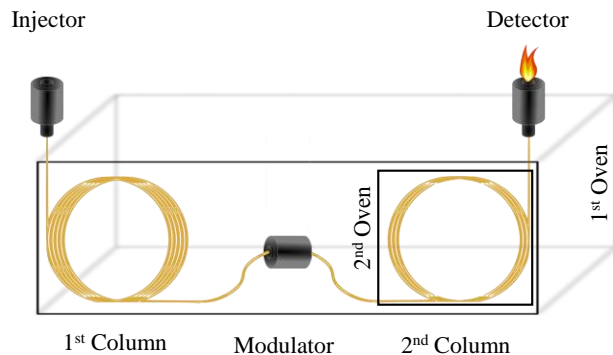


Figure 11. Schematic of two-dimensional gas chromatography (GCxGC).

2.1.2 Modulators

2.1.2.1 Principle of operation

The main roles of the modulator are to ensure a periodic re-injection of all the effluent from the first column into the second column as well as a conservation of the separation on each column, allowing a complete analysis defined by Giddings¹⁶⁸ in 1984. These criteria can be met through a multi-step modulator operating process. It collects, concentrates, focuses and re-injects effluents into the second column as shown in **Figure 12**.

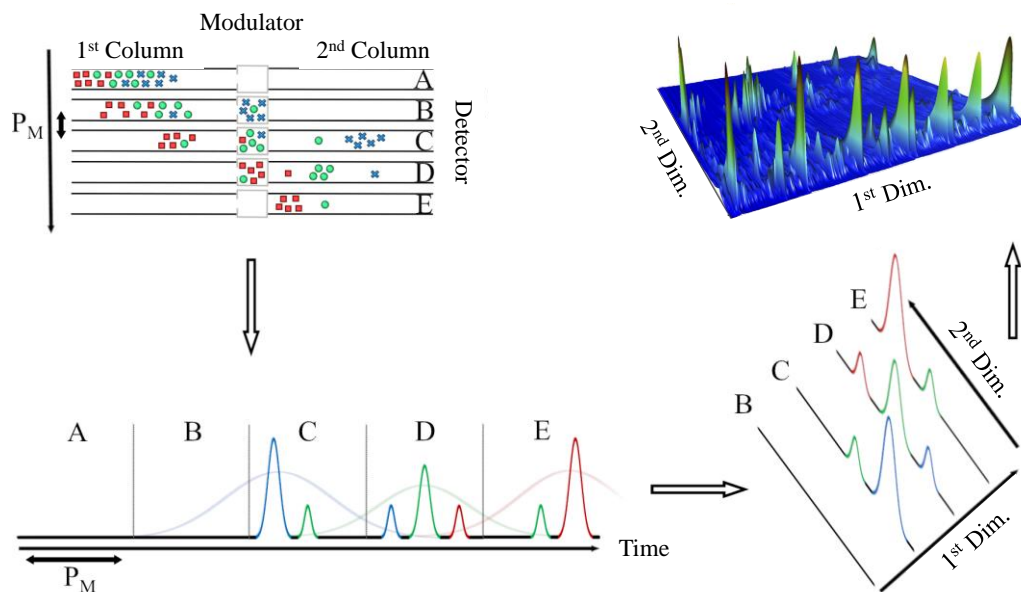


Figure 12. Schematic of the modulation process. (Top left) Successive steps from A to E showing the periodic trapping and release of the modulator between the two columns. (Bottom left) Response of the detector as a function of time. Shaded lines represent the detector response if no second column and no modulator were installed. (Bottom right) Schematic software reconstruction of the chromatogram as a stack of slices. (Top right) Three-dimensional view of the two-dimensional chromatogram.

As a result, conventional GC peaks, typically 10-30 seconds wide on the first dimension, are sliced multiple times and arrive as 200 ms peaks after the second dimension at the detector. The time between each re-injection (pulse) is called the modulation period (P_M) and corresponds to the elution time on the second dimension, which is typically between 2 and 6 seconds depending on the compound and secondary column interactions.

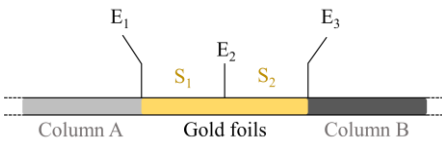
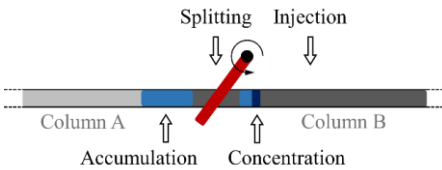
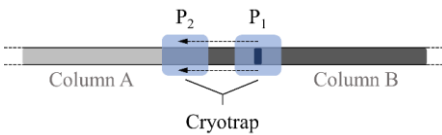
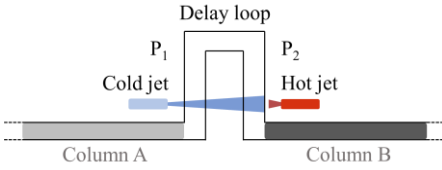
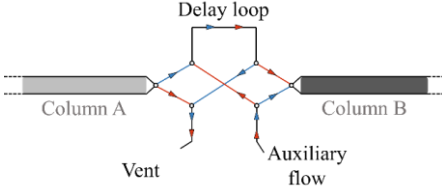
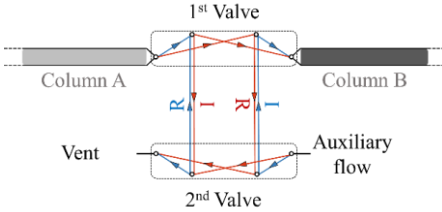
2.1.2.2 Technologic evolutions

Table 5 is intended to provide an overview of the operating principle and historical background of some well-known modulators. Two main categories stand out: thermal modulators and valve modulators. Thermal modulators, based on thermal desorption, were the first modulators ever made but are nowadays mostly cryogenic due to their major performance¹⁶⁹. The use of hot and cold jets with liquid nitrogen is in vogue because the low temperature cooling using liquid nitrogen with a boiling point of -196 °C is very efficient.

Valve modulators are based on pneumatic devices to cleverly reroute the effluent between columns. However, they can suffer from peak disruption because a high flow rate from the secondary column is required. Rapid re-injection of analytes is of great importance as it minimizes peak broadening, maximizes detectability, and increases maximum peak capacity. Currently, none of them stand out as they each have their advantages and disadvantages¹⁶⁹ regarding robustness, reproducibility, universality, narrow injection pulse, fast modulation period, duty cycle, quality, and cost. The main disadvantages of thermal modulators are (i) an observed analyte breakthrough, i.e. analytes are not fully trapped by the modulator and pass into the second column during the P_M and (ii) incomplete desorption, i.e. analytes are not fully released or not released quickly enough during the heating step at the end of P_M ¹⁶⁹. The main drawbacks of valve modulators are the high flow rates required in the second dimension and low duty cycles, resulting in limited applicability and loss of detectability thresholds^{169,170}.

The development of new thermal modulators may concern the use of cryogen-free modulators as this has a financial and logistical impact. In this regard, ceramic cooling blocks coupled with cooling fans have been designed¹⁷¹ as well as the Peltier modulator¹⁷² and have shown similar performance results compared to a commercially available N₂ modulator. Moreover, there are commercially available consumable-free modulators, such as the ZX2 from Zoex. The development of new valve modulators may involve the use of thermally robust¹⁷³ and chemically inert materials, reduction of the 2nd column flow rate¹⁷⁴ to be compatible with the MS and avoid disturbing the flow rate as well as higher duty cycles¹⁶⁹.

Table 5. Evolution of early thermal and valve modulators used in GC×GC.

Modulator	Principle	Remarks
<p>Thermal desorption modulator¹⁶⁵</p> 	<p>Modulator using conductive gold foil between the columns. The periodic application of an electric current between electrodes E₁ and E₂, then E₂ and E₃ alternately, allows the successive release/ desorption of the analytes trapped in sections S₁ and S₂ thanks to an increase in temperature.</p>	<ul style="list-style-type: none"> * 1st integral 2D GC * Slow injection * Overlapping of Analytes
<p>Rotating thermal modulator^{175,176}</p> 	<p>Modulator using a high temperature rotator with a periodic motion. The 4 key steps are accumulation, splitting, focusing and acceleration of the analytes for injection. The retention of the accumulation and focusing steps is achieved by the thick stationary phase of the second column.</p>	<ul style="list-style-type: none"> * 1st commercial modulator * Difficult alignment of column & rotator * High temperature * Thermal expansion
<p>Longitudinally modulated cryogenic modulator¹⁷⁷</p> 	<p>The modulator uses a cryogenic fluid to trap the analytes. It is designed to periodically switch from the P₁ position, where it traps the analytes, to the P₂ position, where it releases them <i>via</i> the high temperature of the oven.</p>	<ul style="list-style-type: none"> * 1st cryogenic modulator * Maintenance of mechanical parts
<p>Cryogenic jet modulator¹⁷⁸</p> 	<p>Modulator using a cryogenic jet and a hot jet. The analytes are trapped in the delay loop using the cold jet on both columns at P₁ and released using the hot jet at P₂.</p>	<ul style="list-style-type: none"> * High reproducibility * No peak broadening
<p>Differential flow modulator¹⁷⁹</p> 	<p>Modulator using a 6-port solenoid valve. The connections are switched periodically to accumulate (blue) and then inject the collected analytes from the delay loop into column B (red).</p>	<ul style="list-style-type: none"> * Injection band similar to cryogenic jet * Robust * Limited temperature (solenoid valve) * 80% Transfer
<p>Wang differential flow¹⁸⁰</p> 	<p>Modulator using two 4-port solenoid valves. Connections are switched periodically to accumulate (R, red only) and inject (I, blue only) simultaneously into each phase.</p>	<ul style="list-style-type: none"> * Injection band similar to cryogenic jet * Robust * High temperature * 100% Transfer

2.1.2.3 Detectability

The combination of peak compression, mass conservation, and inter-column focusing results in narrow, sharp peaks with 10- to 70-fold higher signal intensities compared to conventional GC¹⁸¹. However, the evaluation of better detectability needs to be correlated with the noise levels. Indeed, the noise level is proportional to the square root of the acquisition rate of the detector. High values of acquisition rate, around 100 Hz, are necessary for GC×GC to reliably define narrow peaks and thus reduce the effective detectability gain. According to Lee *et al.*¹⁶⁶, this effective value – corrected enhancement – for isolated peaks is typically 4 to 5. Nevertheless, the detectability improvement is particularly valuable for the study of trace analytes¹⁸². Emphasis should therefore be placed on the development of modulators and column configurations to reduce the peak width on secondary columns. As demonstrated by Lee *et al.*¹⁶⁶, there is a decreasing exponential function bounding the peak amplitude enhancement i.e., the ratio of secondary column peak amplitude over the first column peak amplitude, to the secondary column peak width. As the authors argued, a considerable increase in amplitude could be achieved if the width of the secondary peaks were about 100 ms or even 200 ms which is currently the case in most applications. Detectability is also influenced by the acquisition speed of the detector¹⁸³, which will be briefly discussed below.

2.1.2.4 Time-of-flight mass spectrometry

As previously mentioned, high acquisition speed detectors are mandatory in GC×GC to ensure the acquisition of well-defined Gaussian peaks. Common detectors meeting this criterion are the micro-electron capture detector (m-ECD), thermal conductivity detector (TCD), flame ionization detector (FID), and mass spectrometry (MS) with respective acquisition rates detailed in **Table 6**. R.C. Blase *et al.*¹⁸³ studied the effect of the acquisition rate at 10 Hz and 200 Hz using GC×GC-FID and found an increase in peak area by a factor of 20, an increase in peak height by a factor of 8, and a decrease in peak width by a factor of 5. Although it is possible to use detectors with low acquisition rates, analysts may risk missing or overlooking analytes with narrow band widths. It also implies overall poor GC×GC performances. Thus, high acquisition rates are generally preferred at the expense of a larger volume of data files. The advantage of m-ECD, despite its low acquisition rate, is its extreme selectivity towards halogenated compounds and thus its improved detectability which may justify its use depending on the application. TCD and FID are also excellent and easy-to-use candidates with high acquisition rates, however, they suffer from their versatility because no distinction between compounds can be made besides the retention time.

Table 6. Acquisition rate of GC×GC compatible detectors.

	ECD	TCD	FID	MS
Acquisition rate (Hz)	≤ 50	≤ 300	≤ 500	Quad: ≤ 50* & TOF: 100-500

*In selected ion mode (SIM) which restrains spectral data acquisition. Full spectrum acquisition is in the 10 Hz range.

Finally, mass spectrometry is often the best compromise because it benefits from both, speed of acquisition and analysis of spectral data. Since a mass spectrometer consists of several components such as an ion source, a mass analyzer and a detector, a distinction is made between quadrupole (Quad) and time-of-flight (TOF) mass analyzers. Their difference in acquisition rate is due to their operating process: a Quad is a scanning mass analyzer using rods to create electric fields allowing trajectory control of ions of a given m/z ratio, whereas a TOF is a non-scanning mass analyzer using electric fields to accelerate all ions with the same kinetic energy and separate them according to their time of flight needed to reach the detector¹⁸⁴. The main advantage of a TOF over a Quad is the ability to acquire a full range of mass spectra without compromising speed and sensitivity. However, the sensitivity of the Quad can be increased by using the selected ion monitoring (SIM) mode for better quantitative analysis.

After elution from the secondary column, analytes are most often bombarded in the ion source of a mass selective detector with a 70 eV electron beam to ionize the molecules and further leads to their fragmentation as they exhibit high excess energies. Electron ionization (EI) is the most common ionization technique used in GC because it provides a high degree of fragmentation and detailed mass spectra. It is referred to as hard ionization mode as opposed to soft ionization. Once the ions are created, they are pushed into the mass analyzer with the help of a repeller and accelerated by an electric field. All ions have the same kinetic energy and will be sorted by their time of flight over a given path length, as their velocity depends on their mass through their m/z ratio¹⁸⁵. The resolution can be improved and the kinetic energy of ions of the same m/z corrected by using a reflectron at the end of the flight path that increases the total distance¹⁸⁶. After traveling through the field-free drift region, the ions are detected either using a microchannel plate detector, electron multiplier, Faraday cup, or channel photomultiplier¹⁸⁵ that also amplify the signal which is then recorded using a time-to-digital converter (TCD) or analog-to-digital converter (ADC).

The resulting mass spectrum of each analyte is characteristic and often called a fingerprint. Fragmentation patterns provide structural information about the molecule, as functional groups tend to show the same dissociation behavior after ionization. Other more specific rearrangements also occur and are related to the structure of the molecule.

2.1.3 Stationary phases

The heart of each gas chromatographic separation is the column and its respective stationary phase used to resolve a multitude of analytes in a mixture. A gas chromatographic column should therefore always be chosen very carefully and adapted to the given application. In the following, I will highlight the most prominent chiral columns used for the enantioseparation of chiral amino acids and sugar compounds.

2.1.3.1 Cyclodextrins

2.1.3.1.1 General structure

Cyclodextrins (CDs) are cyclic oligosaccharides that possess a conical structure allowing non-covalent host-guest inclusion in its cavity. CDs are constructed from D-glucopyranose units in chair conformation and obtained by treatment of starch with amylase enzymes called cyclodextrinases¹⁸⁷. The hydrolysis of starch by amylases is not very specific and ends up forming a mixture of α -, β -, γ -, δ -cyclodextrins as well as CDs containing up to 13 glucose units through α -1,4 linkages¹⁸⁸. From these mixtures, α -, β -, γ -, δ -cyclodextrins were successfully isolated by selective precipitation using organic compounds. Smaller CDs, containing less than 6 glucose units, however, are not encountered because steric hindrance would stretch the glucose units. Examples of native and modified cyclodextrins are shown in **Figure 13**.

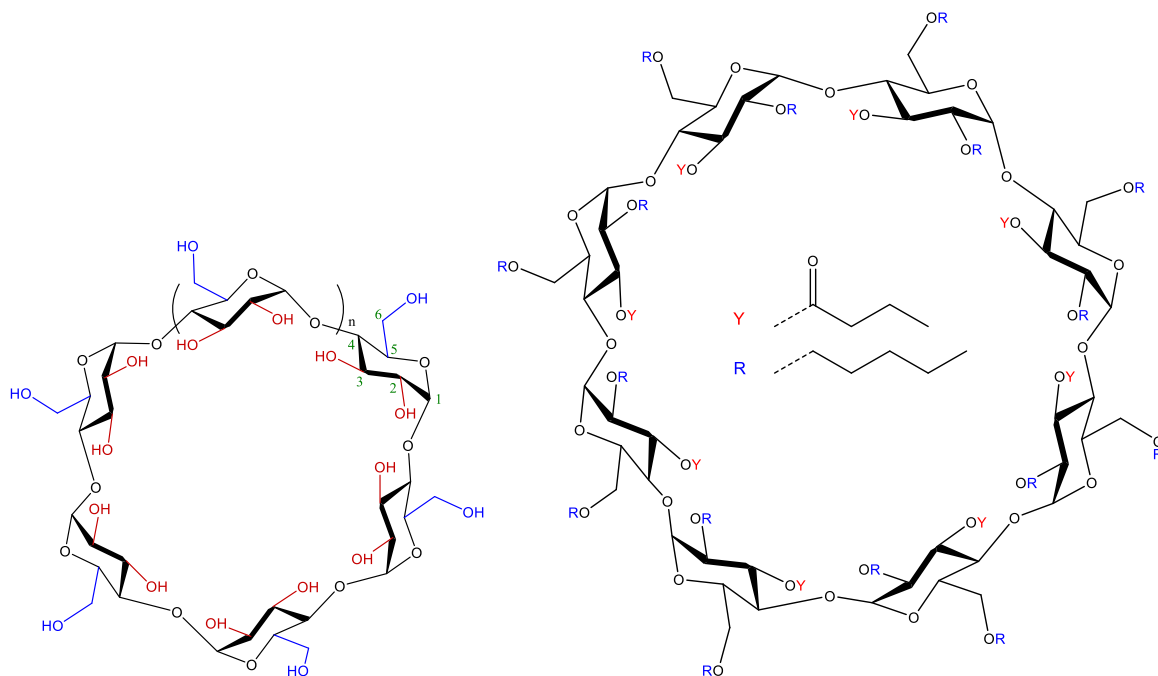


Figure 13. Chemical structure of cyclodextrins. (Left) Chemical structure of native α ($n=6$) cyclodextrins composed of D-glucopyranose units in chair conformation. The primary alcohols, in blue, represent the narrowest tapered ends while the secondary alcohols, in red, represent the widest tapered end. (Right) Chemical structure of octakis-(3-O-butyl-2,6-Di-O-pentyl)- γ -cyclodextrin.

Because CDs are represented as shallow cones, it is interesting to highlight their dual hydrophilic-hydrophobic nature. The inner part of the cavity is represented as a surface (as a plane for each glucose unit) containing protons, H3 and H5, and solitary pairs of glycosidic oxygens conferring a hydrophobic behavior to the cavity¹⁸⁹. On the other hand, the tapered ends have hydroxyl groups exhibiting hydrophilic behavior. Thus, CDs are described as "all-purpose molecular containers for organic, inorganic, organometallic, and metal organic compounds that may be neutral, cationic, anionic or even radical"¹⁹⁰. Some physicochemical parameters of different cyclodextrins are detailed in **Table 7**.

Table 7. Physical and chemical properties of native cyclodextrins. Derived and inspired by Dai et al.¹⁹¹.

Properties	α -CD	β -CD	γ -CD
Number of glucose units	6 (n=1)	7 (n=2)	8 (n=3)
Formula (anhydrous)	C ₃₆ H ₆₀ O ₃₀	C ₄₂ H ₇₀ O ₃₅	C ₄₈ H ₈₀ O ₄₀
Molecular weight	972.85	1134.99	1297.12
Approximate cavity volume (nm ³)	1.74	2.62	4.27
Cavity external diameter (nm)	0.49	0.62	0.79
α_D (deg.)	+150.5	+162.0	+177.4
pKa (25 °C)	12.33	12.20	12.08
Solubility (g/100 mL water, 25 °C)	14.5	1.85	23.2

2.1.3.1.2 Chiral recognition principle

Cyclodextrins are inherently chiral; they can form diastereomeric complexes with chiral guests. When this complex shows a higher stability for one enantiomer of the guest molecule, enantioselective recognition can be considered to occur. The difference in stability between the complex formed with one enantiomer compared to the other will define the efficiency of this chiral discrimination process.

The driving forces involved in cavity inclusion complexation of compounds are mainly van der Waals forces (Keesom, Debye and London) and hydrophobic interactions. To a lesser extent, hydrogen bonding and steric hindrance can impact the complexation behavior. The shape selectivity properties of CDs are suitable for all types of isomer separation, including enantiomers, which differ only in their stereochemistry. Indeed, although the size of the cavities allows for the inclusion of e.g., single (α) or multiple substituted phenyl rings (β and γ), it is the hydroxyl group at the edge of CDs that allow chiral recognition with the asymmetric center of the analyte. These properties have led to the development of modified CDs to control solubility, hydrophobicity, cavity outer diameter, and chiral recognition for example. Thousands of these derivatives currently exist with various ring sizes and chemical functionalizations¹⁹².

Modifications of CDs occur only at the hydroxyl groups which are nucleophilic, and these compete for electrophilic attack. Selective modification is therefore difficult but possible because these hydroxyl groups are not equivalent. The hydroxyls in position 2 are acidic, the hydroxyls in position 3 are sterically hindered, and the hydroxyls in position 6 are basic, which gives them increased nucleophilic behavior¹⁹¹. Depending on the reactivity of the reagent, a single derivatization of the hydroxyl group in position 6 can be achieved. For example, a monosubstitution¹⁹³ using *p*-toluenesulfonyl chloride, a disubstitution¹⁹⁴ using arenedisulfonyl chloride and a persubstitution¹⁹⁵ have been reported.

Two stationary phases are described in more detail in the next sections as they were used for the amino acid and sugar analysis studies. Many CDs can be used for *ee* analysis but it should be noted that the separation strongly depends on the derivatization used, which will be further discussed in **2.1.4**

Derivatization in gas chromatography.

2.1.3.1.3 Lipodex E

Commercialized as Lipodex E, octakis-(3-*O*-butyryl-2,6-Di-*O*-pentyl)- γ -cyclodextrin is a fully substituted γ -cyclodextrin (**Figure 13**). The prefix octakis, *oktáki*s in ancient Greek means *eight times*, which means that all glucose units of the γ -cyclodextrin are substituted with 3-*O*-butyryl-2,6-di-*O*-pentyl. The Lipodex E stationary phase was first introduced by König *et al.*¹⁹⁶ in 1989 as a highly versatile cyclodextrin derivative for the separation of proteinogenic and nonproteinogenic amino acids, α - and β -hydroxy acids, polyhydroxy compounds, alcohols, ketones, lactones, cyclopropane derivatives, cyclic acetals, amines and alkyl halides. Native γ -cyclodextrin was successively treated with 1-bromopentane under basic conditions (NaOH) followed by butyric anhydride under basic conditions (triethylamine) and 4-dimethylaminopyridine as nucleophilic catalyst. The hydroxyl groups at position 2 and 6 are converted to ethers in the first step by an S_N2 reaction while steric hindrance at position 3 prevents the substitution from occurring. In the second step, the hydroxyl at position 3 is acylated and gives an ester due to the nucleophilic attack of the hydroxyl on the anhydride. The ethers in position 2 and 6 do not react with the anhydride because they are less nucleophilic and because no inorganic catalyst is used.

2.1.3.1.4 CP-Chirasil-Dex CB

Commercialized as CP-Chirasil-Dex CB, heptakis-(2,3,6-tri-*O*-methyl)- β -cyclodextrin is a fully methyl substituted β -cyclodextrin containing seven glucose units bound to a polysiloxane backbone. In the search of best enantiomeric separation of volatile organics for *in situ* analysis, C. Freissinet *et al.*¹⁹⁷ showed that this stationary phase is the most suitable compared to ChiralDEX β -PM which is the same as CP-Chirasil-

Dex CB but is not bound to a polysiloxane backbone as well as CP-Chirasil L-Val which is typically used for amino acid analysis. Indeed, among the 14 chiral compounds investigated of four different chemical families, 11, 7 and 3 of them showed an enantiomeric separation on CP-Chirasil-Dex CB, Chiraldex β -PM and CP-Chirasil L-Val, respectively. This stationary phase has already been employed for meteorite analyses of amino acids, hydroxy acids, amines¹⁹⁸ and sugars¹¹³.

2.1.3.2 *New stationary phases for multidimensional gas chromatography*

Ionic liquids have attracted a lot of interest due to their dual nature (polar and ionic), allowing optimized orthogonality between the stationary phases. Stationary phases based on ionic liquids may therefore find increased use as secondary columns in comprehensive two-dimensional gas chromatography to improve the general resolution and peak capacity of complex mixtures. They have better selectivity and thermal stability than conventional phases¹⁹⁹. The first use of these ionic liquids in multidimensional gas chromatography was performed by G. R. Lambertus *et al.*²⁰⁰ and many others have been designed since for targeted analytes²⁰¹. Another important feature is the water and oxygen stability at high temperatures, allowing water to be used as an injection solvent and getting rid of tedious pretreatments. Ionic liquids were even used to perform a GC³ (three-dimensional GC)²⁰² analysis where the column configuration was: 20 m apolar \times 4 m ionic liquid \times 1 m polar. As the authors pointed out, it is still difficult to exploit the third retention space because the two columns used are polar and the sample lacks *polarity diversity*.

2.1.4 Derivatization in gas chromatography

The derivatization process is a chemical modification of target compounds to obtain better properties for their analysis. The main purpose of this modification is to improve their volatility for GC analysis. However, this is not the only purpose and/or consequence of this procedure²⁰³, which are listed below. **Volatility** is improved by lowering the boiling point through the addition of functional groups that decrease the overall polarity of the target molecule. Indeed, polar groups such as -OH, -NH, or -SH can establish strong H-bond interactions and must be converted to -OR, -NR, or -SR groups which also protects the stationary phase. **Stability** is improved by inhibiting intra and intermolecular reactions that may occur during heating in the injector and oven during gas chromatographic analysis. **Detectability** is improved by amplifying the intensity response through a better conversion of the compounds and/or the use of a specific detector. **Chromatographic behavior** is improved as compounds with modified functional groups interact differently with the stationary phase, resulting in different retention times and separations/enantioseparations. **Other improved benefits** include minimized interferences with the

matrix (robustness), separation of analytes from the matrix and shorter retention times. As previously stated, derivatization reagents must be reactive electrophiles to remove hydrogens held by alcohols, carboxylic acids, or amines, as these functional groups are nucleophilic and often encountered. For convenience, the reagents must be stable, affordable, and available.

Enantioselective separation of chiral analytes can theoretically be achieved by two different routes. The first uses achiral reagents and a chiral stationary phase, while the second uses chiral agents and an achiral stationary phase to separate diastereomers. The latter requires several conditions to be used with confidence in terms of small *ee* determination: enantiomeric purity of the reagent, non-racemization of the reagent and reactants, equal reaction rates between the reagent and the two enantiomers, and equal detector response of the diastereomers^{204,205}. Therefore, the use of achiral reagents in combination with a chiral stationary phase is often considered to be the better approach for efficient enantioseparation and precise *ee* determination, even though it may still suffer from racemization of the analytes during the derivatization reaction. Depending on the target molecules and derivatization method, however, racemization can be less critical as racemization of α -amino acids for example has been reported to be less than 0.1% (*ee* = 0.2%) from an enantiopure solution²⁰⁵ using ethanol/trifluoroacetic anhydride derivatization. Racemization is derivatization-dependent and can therefore be more critical. Regarding sugars, the situation is slightly different because many epimerization reactions can be involved, including racemization. Cooper *et al.*¹¹³ reported that there was no racemization but only oxidation of sugar molecules to sugar acids, with unchanged *ee* in the derivatization products using an alkyl/trifluoroacetic anhydride derivatization.

Finally, it is possible to combine a chiral reagent with a chiral stationary phase to improve chromatographic separation. Theoretically, the concerns regarding *ee* should remain the same, but depending on the derivative, chiral or achiral columns may be more appropriate.

2.2 TARGET COMPOUNDS CONSIDERATIONS

2.2.1 Carbohydrates

2.2.1.1 Classifications

2.2.1.1.1 Degree of polymerization & functions

Carbohydrates (CHs) were originally chemically defined as compounds of formula $C_m(H_2O)_n$ (*m* is generally equal to *n*) but are now considered as carbohydrates when $m, n > 2$ and inherit an "ose" suffix. Compounds

such as acetic acid, formaldehyde or glycolaldehyde meet these requirements but are excluded. The first way to classify carbohydrates is to distinguish them according to their degree of polymerization, ranging from 1 to about a million for amylopectins²¹¹. Three main categories are used: sugars (mono- and disaccharides), oligosaccharides and polysaccharides²¹². Monosaccharides are the fundamental monomers and the smallest unit used to construct di-, oligo-, and polysaccharides. A monosaccharide unit is polyhydroxylated (alcohol functions) and may be called an aldose (aldehyde) or ketose (ketone) depending on the chemical function of the carbonyl²¹³. Sugar acids and sugar alcohols also exist and contain a carboxylic acid and an alcohol terminal group, respectively, as shown in **Figure 14**. The bonding between monomers is called a glycosidic bond and involves the hemiacetal group of one monosaccharide and the hydroxyl group of another.

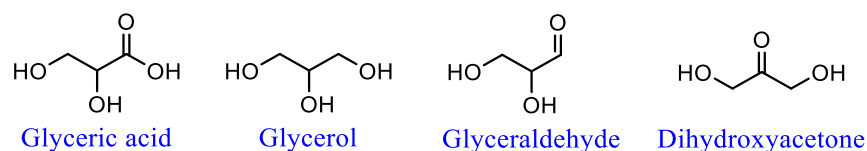


Figure 14. Example of sugar acid, sugar alcohol, sugar aldehyde and sugar ketose for a three-carbon monosaccharide.

2.2.1.1.2 Carbon number, stereochemistry & predominant forms

The number of carbon atoms used to build monosaccharides is another classification parameter. Monosaccharides range from three carbons (triose) to nine carbons (nonose), as shown in **Figure 15** and **Figure 16**. In terms of stereochemistry, they can be found in their D or L form depending on the configuration of the penultimate stereogenic carbon. Other configurations of stereogenic carbons have led to compounds with new names.

Furthermore, the appearance of a new stereogenic carbon due to an intramolecular nucleophilic attack between an alcohol group and the terminal carbonyl function is specific to carbohydrates. This carbon is called an anomeric carbon which is a special case of an epimeric hemiacetal carbon. The open-chain form of monosaccharides therefore leads to cyclic carbohydrates such as furanoses – 5-carbon ring – and pyranoses – 6-carbon ring. There is an equilibrium between these forms, which depends on temperature, concentration and solvent²¹⁴. The cyclic forms, **Table 8**, are extremely predominant over the straight chain form in water and the pyranose form is in the majority over the furanose form²¹⁵.

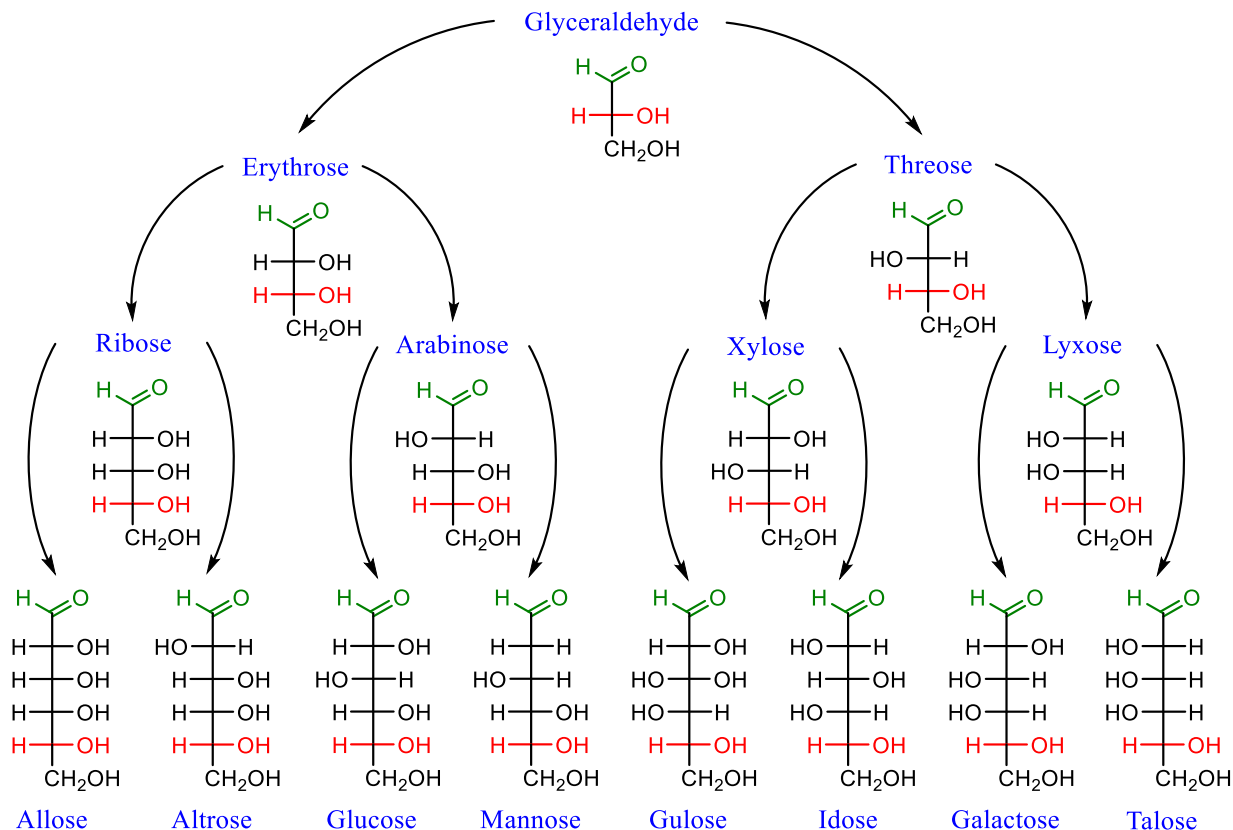


Figure 15. Classification of aldoses (monosaccharides) according to their carbon number. In green is highlighted the aldehyde function and in red the enantiomeric configuration for which the *D* is obtained. From top to bottom, each line represents the addition of one carbon from triose (aldotriose) to hexose (aldohexose).

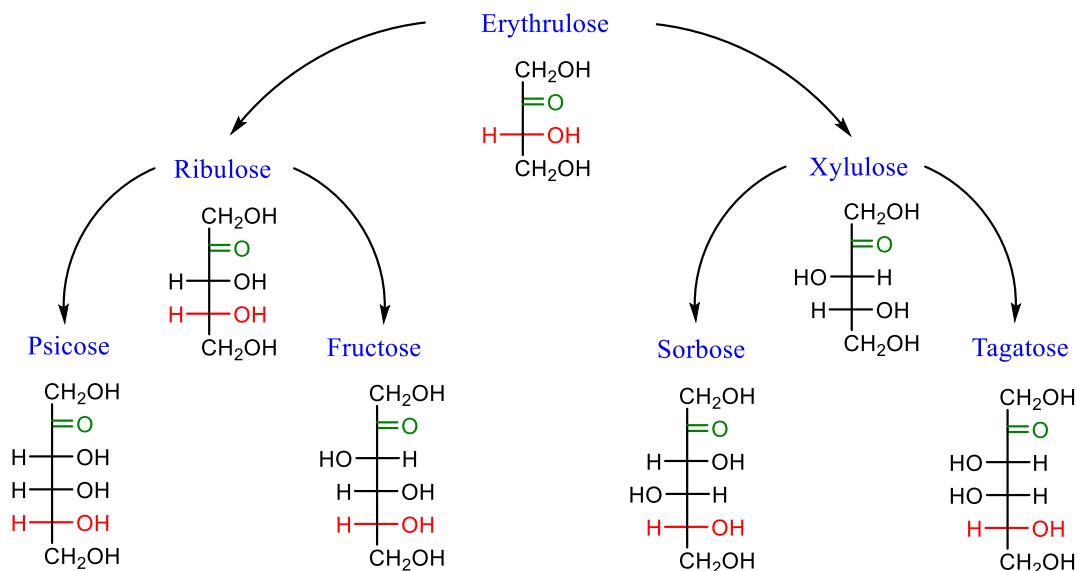


Figure 16. Classification of ketoses (monosaccharides) according to their carbon number. In green is highlighted the ketone function and in red the enantiomeric configuration for which the *D* is obtained. From top to bottom, each line represents the addition of one carbon from tetrose (ketotetrose) to hexose (ketoheptose).

Table 8. Anomer ratios for a series of aldoses in aqueous solution. Taken from²¹⁵

Monosaccharide	α -p	β -p	Total p	α -f	β -f	Total f
D-Ribose	20	56	76	6	18	24
D-Arabinose	63	34	97			3
D-Allose	18	70	88	5	7	12
D-Altrose	27	40	67	20	13	33
D-Glucose	36	64	100			< 1
D-Mannose	67	33	100			< 1
D-Galactose	27	73	100			< 1

p: pyranose form, f: furanose form

As the nucleophilic attack can take place equally on both sides of the carbonyl, two possible anomers can be formed. The pair of anomers is designated as the α -anomer with the alcohol group pointing down and the β -anomer with the alcohol group pointing upwards at the anomeric carbon C-1 in the Haworth projections. Consequently, a total of 5 different stereoisomers of one single sugar enantiomer can be found in equilibrium due to intramolecular cyclization at the anomeric carbon and the competition of forming 5- and 6-carbon membered rings (**Figure 17**). This means that up to 10 forms (5 D and 5 L) can be encountered for each carbohydrate.

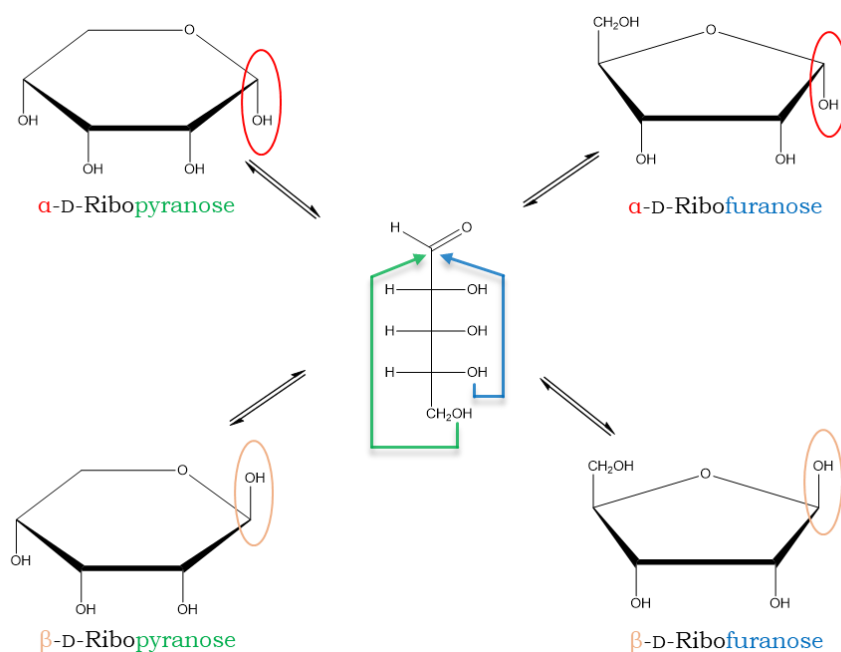


Figure 17. Intramolecular cyclization of ribose into anomers in solution.

2.2.1.2 Carbohydrate derivatization strategies

Several disadvantages of the equilibrium mixtures of the straight and cyclic forms of monosaccharides on the enantioselective analysis can be pointed out. The first disadvantage is the decrease in intensity associated with the numerous existing forms. Considering the aldoses in **Table 8**, 2 to 5 forms in total are present for one sugar enantiomer. However, the derivatization procedure may have an impact on the equilibrium composition of these forms. The second disadvantage is the high number of chromatographic peaks that can lead to difficulties in resolving such a complex mixture as well as achieving sufficient enantioseparation, even when using a powerful separation technique like GC×GC. Several specific derivatization approaches have been developed to overcome these limitations, but each has its strengths and weaknesses. Below, different approaches are presented, and the strengths and weaknesses are discussed in order to carefully choose one of them for our applications.

2.2.1.2.1 Reduction

The most intuitive solution would be to reduce the number of forms by preventing cyclization from occurring²¹⁶. This means inhibiting the reactivity of the carbonyl to constrain the carbohydrate to its linear form. Reduction can successfully fulfill this role but has strong drawbacks in terms of stereochemistry.

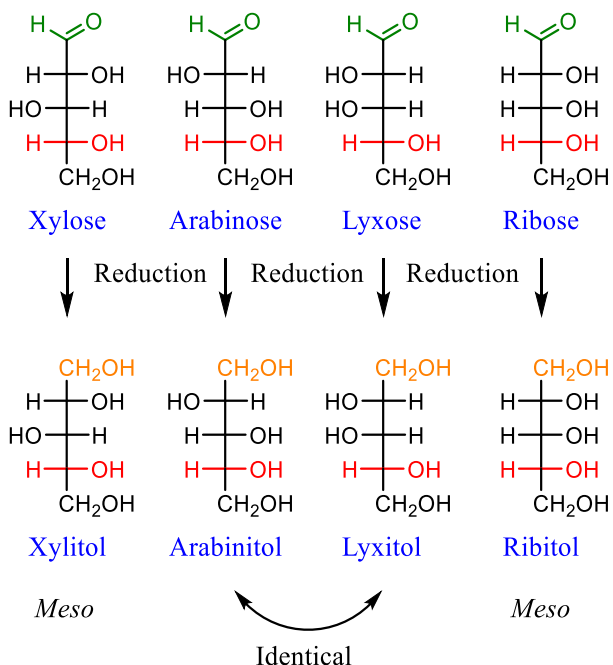


Figure 18. Illustration of molecular duplication (left and right) and loss of chiral information (middle) during the reduction of some D-aldopentoses.

It either leads to the loss of chiral information through the formation of a *meso* compound, or to the fact that the same sugar alcohol gives indistinguishable precursors, as shown in **Figure 18**. This phenomenon appears for some C₄, C₅ and C₆ sugars as pointed out by Cooper *et al.*²¹⁷. In the search for *ee* in extraterrestrial samples, this method cannot be employed despite its cyclization-preventing feature.

2.2.1.2.2 Oximation

Carbohydrate oximes, **Figure 19**, can be formed by a condensation reaction between hydroxylamine and an aldehyde or ketone of a carbohydrate. In this case, the chiral information is not lost, and the number of stereoisomers for one enantiomer is reduced to 2 instead of 5 because the C=N bond involves an *E/Z* configuration. Subsequent derivatization of the remaining hydroxyl groups to trimethylsilyl²¹⁸ (TMS) ethers or trifluoroacetyl²¹⁹ (TFA) esters can be performed. The method is suitable for C₃ to C₇ sugars and disaccharides²¹⁹. Despite the reported good resolution of C₃ and C₄ sugars²²⁰, both *E* and *Z* compounds are not always resolved²¹⁹.

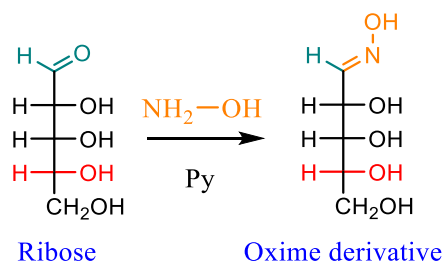


Figure 19. Oximation derivatization starting from ribose.

2.2.1.2.3 Aldonitrile acetate

Introduced by Guerrant & Moss²²¹, monosaccharides are constrained in their straight form because the nitrile function prevents any cyclization reaction. As with oximes, the first step involves the transformation of the carbonyl of the monosaccharide using hydroxylamine. Moreover, during this step, the presence of methanol and pyridine increases the basicity and thus the nucleophilic behavior of the hydroxylamine. The heating during the first step allows the formation of the nitrile function by the elimination of a molecule of water. The addition of acetic anhydride in the second step converts the hydroxyl groups to esters.

These reactions are part of the Wohl²²² degradation that converts a C₆ to a C₅ monosaccharide that uses a final additional step involving sodium methoxide as a strong base to convert the esters to alcohols *via* a saponification reaction and the nitrile to aldehyde *via* reductive hydrolysis. The conditions for the steps shown are similar to those used in the first step of the Wohl degradation.

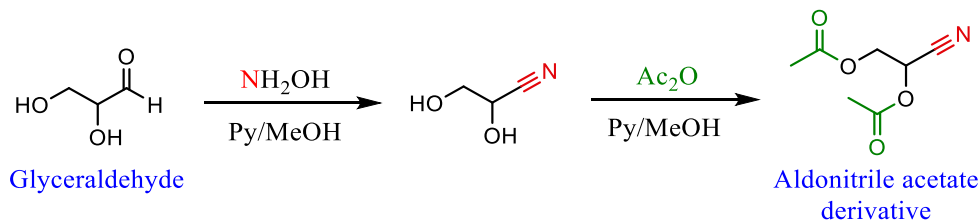


Figure 20. Aldonitrile acetate derivatization starting from glyceraldehyde.

The main advantages of this derivatization, **Figure 20**, concern the detection and enantioseparation of glyceraldehyde with good reproducibility. However, the C₄, C₅, and C₆ sugars suffer from a lack of enantioseparation²²³, which is a significant drawback for the evaluation of potential *ee* values in extraterrestrial samples.

2.2.1.2.4 *N,O*-Bis(trimethylsilyl)trifluoroacetamide

As with amino acids, which will be discussed later, *N,O*-bis(trimethylsilyl)trifluoroacetamide derivatization (BSTFA), **Figure 21**, leads to tris(trimethylsilyl) derivatives by substituting the labile hydrogens of the hydroxyl and carboxyl groups of sugars. In contrast, MTBSTFA, which leads to *tert*-butyldimethylsilyl derivatives, should be avoided because steric hindrance does not allow for the detection of sugars²²⁴. Indeed, silylation is a bimolecular nucleophilic substitution (S_N2). Aldoses, ketoses, sugar alcohols, and sugar acids can be identified and resolved using CP-Chirasil-Dex CB coupled to DB-Wax columns (GC×GC)⁹⁵. In addition, the cyclic forms pyranose and furanose can be distinguished based on their mass spectra. Thus, this is a very versatile and convenient derivatization method. However, no enantioseparation was reported using a chiral stationary phase like CP-Chirasil-Dex CB⁹⁵. This major drawback therefore makes this method unsuitable for *ee* analysis and will not be considered.

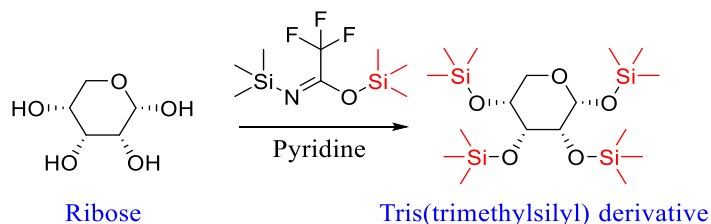


Figure 21. *N,O*-Bis(trimethylsilyl)trifluoroacetamide derivatization on ribose.

2.2.1.2.5 Methylboronic acid/trifluoroacetic anhydride

Monosaccharides are constrained to a cyclic form *via* a condensation reaction involving vicinal or isolated diols and methylboronic acid (MBA) to form a methylboronic ester. Originally designed for C₅ and C₆ sugars, the unique feature of this derivatization is the need for several alcohols to be close enough to link them by removing labile hydrogens with MBA. However, as shown in **Figure 22**, when the monosaccharide – here glucose – has an odd number of alcohols or if they are too far apart to be derivatized, a second derivatization step is necessary. Silylation using *N,O*-bis(trimethylsilyl)trifluoroacetamide (BSTFA) is a typical route, as outlined by Von Donger *et al.*²²⁵. Acylation²²⁶, using trifluoroacetic anhydride would be an alternative.

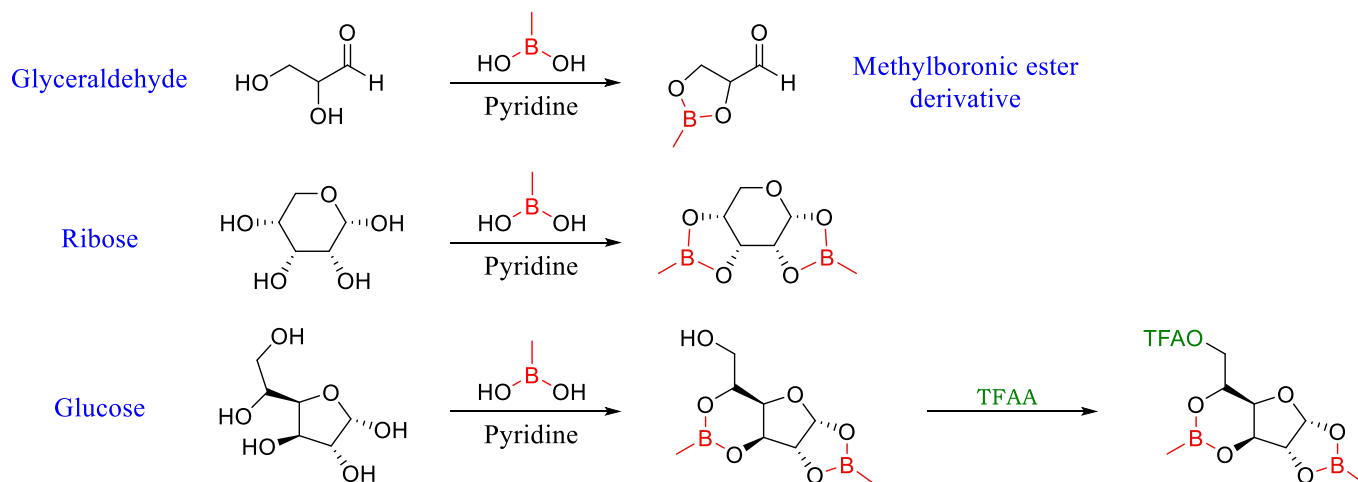


Figure 22. Methylboronic acid/trifluoroacetic anhydride derivatization on C₃, C₅ and C₆ monosaccharides.

Rings with five and six atoms are favored and called dioxaborolanes and dioxaborinanes respectively. In the case of ribose, the only form found is that shown in **Figure 22**: a boronic ester cannot be formed between C1 (acetal) and C4 because the ring formed would be too constrained. Moreover, this addition could only occur between C2 and C3, leaving the hydroxyl groups of C1 and C4 free for a second derivatization step, but this compound was not observed. Using MBA only, arabinose, fucose, xylose, ribose and rhamnose were detected, whereas lyxose, fructose, galactose, mannose and glucose detection required a second derivatization step using BSTFA or acetic anhydride.

The use of TFAA to derivatize the remaining free hydroxyl groups significantly reduces the intensity of the C₃ and C₅ derivatized sugars with MBA alone. A significant advantage of the MBA/TFAA derivatization method is the formation of only one compound per enantiomer leading to less cluttered chromatograms which is especially important for trace analysis. Single carbon addition for two alcohols is also timely for

of carbons, the side chain group, and especially according to the location of the functional groups. The location of the amine can be either in α , β , γ , or δ to the carboxylic acid. Hundreds²²⁷ of amino acids have been discovered in nature, but life is built on 20 of them that are all α and L-configured except glycine being the only achiral amino acid. These are called proteinogenic because of their incorporation into proteins during RNA translation. Selenocysteine and pyrrolysine²²⁸ are considered the 21st and 22nd proteinogenic amino acids because they have been reported to be incorporated into the proteins of some organisms. Of these proteinogenic amino acids, **Table 9**, only nine are considered essential because they cannot be synthesized by the human body. All other necessary amino acids can be synthesized from the nine essential amino acids.

Table 9. 20 to 22 (in yellow) proteinogenic amino acids including the 9 essential amino acids (in grey).

Alanine	Arginine	Asparagine	Aspartic Acid	Cysteine	Glutamic Acid
Glutamine	Glycine	Histidine	Isoleucine	Leucine	Lysine
Methionine	Phenylalanine	Proline	Serine	Threonine	Tryptophan
	Tyrosine	Valine	Selenocysteine	Pyrrolysine	

2.2.2.2 Amino acid derivatization strategies

Unlike carbohydrates, amino acids do not suffer from the reduction in intensity of multiple stereoisomers. However, the diversity of existing amino acids poses many challenges with respect to their separation and detection. Intensity, separation, and enantioseparation are essential to reliably calculate enantiomeric excesses in extraterrestrial samples. Since these compounds are not volatile – the melting point of glycine is about 230 °C – a derivatization step is necessary. In this regard, numerous attempts to develop an exceptional method have led to a wide variety of available techniques. Common derivatization procedures for meteorite analyses were reviewed by Simkus *et al.*²²⁹, highlighting 11 general amino acid derivatization routes. Of these, trifluoroacetic anhydride/alkyl (TFAA/alkyl) derivatization for GC and phthalaldehyde/NAC (OPA/NAC) derivatization for LC appear to be widely used to study amino acids from various meteorites. Volatility, intensity, enantioseparation, and versatility of all amino acids are still key factors in determining whether a derivatization is suitable for the analysis of a meteorite sample. The TFAA/alkyl functionalization meets some of these requirements. In particular, the high response of isovaline which is of great importance in finding clues to the origin of homochirality¹⁰⁸ in comparison to other methods is advantageous. Here, several amino acid derivatizations will be discussed.

2.2.2.2.1 *N,N*-dimethylformamide/dimethylacetal

Among amino acid derivatization reactions, *N,N*-dimethylformamide dimethylacetal (DMF/DMA), **Figure 24**, appears to be a rapid and simple route to successfully convert and detect most amino acids. Using this one-step method, 19 out of 20 proteinogenic amino acids were identified and 10 were enantioseparated on a CP-Chirasil-Dex CB (heptakis-(2,3,6-tri-*O*-methyl)- β -cyclodextrin)²³⁰ column. However, it should be noted that for 6 out of 10 amino acids, the enantioresolution is less than 1. This method is considered an excellent candidate for *in situ* analyses in diverse space missions because it meets many requirements. It can be easily automated having a short reaction time of 3 minutes at 140 °C. Moreover, it produces relatively low weight compounds that require only limited *m/z* ranges for adequate detection which is beneficial for space missions and their restricted instrumental and analytical performances. Among these 10 enantioseparated amino acids, only asparagine, aspartic acid, proline and serine showed partial racemization while tyrosine showed complete racemization. Compromises had to be made to optimize yield and avoid as much as possible racemization that occurs at high temperature, as well as by-products. This method is therefore not the best compromise for amino acid *ee* analysis of meteoritic samples.

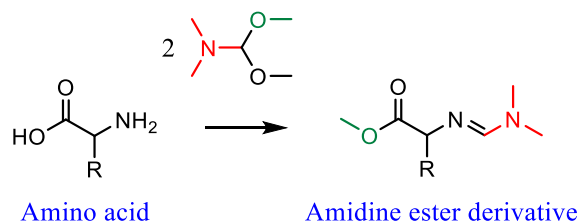


Figure 24. *N,N*-dimethylformamide/dimethylacetal derivatization (DMF/DMA) of amino acids.

2.2.2.2.2 *N*-(*tert*-butyldimethylsilyl)-*N*-methyltrifluoroacetamide (MTBSTFA) & *N,O*-bis(trimethylsilyl)trifluoroacetamide (BSTFA)

BSTFA leading to trimethylsilyl derivatives and MTBSTFA leading to *tert*-butyldimethylsilyl derivatives, **Figure 25**, are very versatile chemical reagents, allowing the simultaneous and rapid derivatization of amino and carboxylic groups. The one-step MTBSTFA reaction achieves yields in the range of 90-100%²³¹ and does not require separation of the derivatives prior to GC analysis, as is the case for other silylated derivatives. Silylation reactions involve the nucleophilic attack of the targeted heteroatoms of the analyte and thus require a good leaving group such as trifluoroacetamide to avoid a back reaction after derivatization²³¹. Depending on the molecule, not all labile hydrogens can be substituted due to steric hindrance²³². Silylation reagents are also less prone to hydrolysis, making them more suitable for *in situ* analysis.

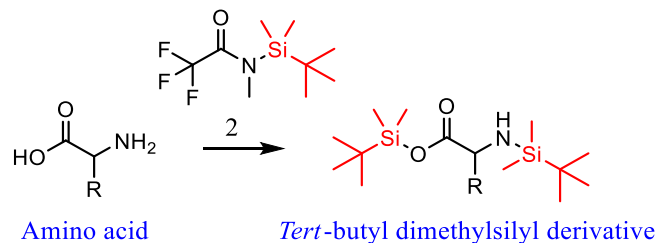


Figure 25. *N*-(tert-butyl dimethylsilyl)-*N*-methyltrifluoroacetamide (MTBSTFA) derivatization of amino acids.

2.2.2.2.3 Ethylchloroformate/heptafluorobutanol

The successive reaction of ethyl chloroformate and heptafluorobutanol on amino acids as a one-pot mixture leads to the formation of *N*(*O,S*)-ethoxycarbonylheptafluorobutylester derivatives. A by-product can be obtained after decarboxylation between the two reactions, **Figure 26**. This side-product corresponds to the compound that would have been obtained using ethanol instead of heptafluorobutanol. Overall good separation and enantioseparation²³³, **Figure 27**, are obtained with detection limits generally between 10^{-6} and 10^{-7} M, but several orders of magnitude higher for isovaline, sarcosine, and 2-aminoisobutyric acid. Nevertheless, the *ees* found in the Murchison meteorite using this method are reliable since the *ee_L* of alanine is 3.51 ± 0.74 and 4.61 ± 0.83 for isovaline using three standard deviations. As isovaline is of great interest in understanding the origin of chiral biases in meteoritic samples (**1.4.1 Meteorites**), this method was not considered in my studies.

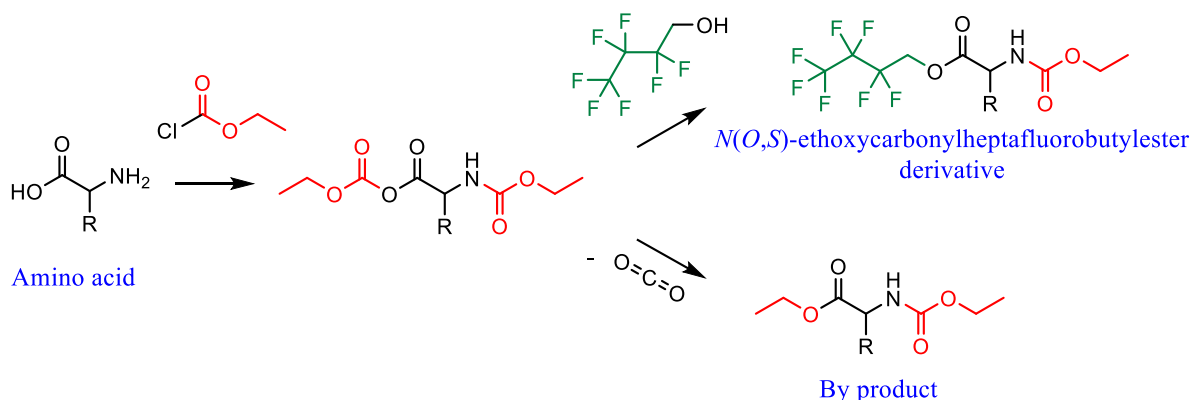


Figure 26. Ethylchloroformate/heptafluorobutanol derivatization (ECHFBE) of amino acids.

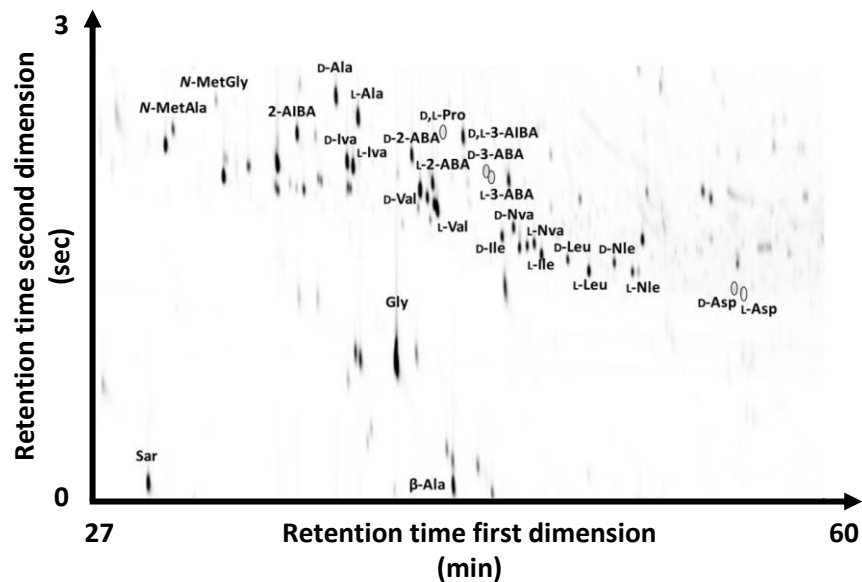


Figure 27. Two-dimensional chromatogram of ECHFBE derivatized amino acids and analyzed on Chirasil-Val coupled to DB-WAX columns²³³.

2.2.2.2.4 Methanol/trifluoroacetic anhydride

Methanol/trifluoroacetic anhydride derivatization (MeOH/TFAA), **Figure 28**, was described in the mid-20th century by Weygand & Röpsch²³⁴. Repeatability problems were then reported due to the volatility of the synthesized derivatives. Numerous attempts to overcome a possible loss of products have led authors to adapt or redesign the methodology, the conditions or even the derivatization itself.

This two-step derivatization involves successive heating steps and drying that are considered critical compared to other methods such as BuOH/TFAA or IPA/TFAA^{235,236}. With respect to methodology, the drying steps have been reported to be performed using either a rotary evaporator, P₂O₅/NaOH under vacuum²³⁷ or a nitrogen stream²³⁸. Studies using nitrogen stream have shown that a 10% loss can be induced on *N*-TFA methyl ester derivatives at room temperature. Equally 10% loss occurred at 100 °C when *N*-TFA *n*-butyl esters were dried under a nitrogen stream²³⁸. Using a rotary evaporator, up to 36% of alanine are lost²³⁹. Recently, careful drying using a nitrogen stream followed by drying at room temperature has been reported²⁴⁰. Complete drying was not performed to avoid evaporation of the amino acid derivatives. Instead, a relatively large amount of solvent was added for later analysis. It is likely that this quenches the TFAA-initiated reaction without losing the derivatized compounds.

Different conditions exist for each reaction in this two-step derivatization. Originally, HCl gas was used to perform the first acid-catalyzed esterification step by bubbling it into the chosen alcohol. Despite its easy

removal under a nitrogen stream, HCl paved the way for another practical alternative using acetyl chloride and an alcohol to produce dry HCl *in situ*. It is interesting to note that although the alcohol/acetyl chloride ratio might have an optimal value for isopropanol²⁴¹, various values for this esterification step depending on the alcohol are reported. As methanol is less sterically hindered than isopropanol, it might therefore be less sensitive to the importance of this ratio. Currently, a methanol/acetyl chloride ratio of 4:1 (v:v) is commonly used²⁴². Along with this ratio, the reaction time and temperature of isopropanol have been studied and are critical for the amino acid tryptophan, and slightly for valine²⁴¹. Indeed, care must be taken to ensure a good conversion without degradation due to overheating. To perform the second step, TFAA is rarely used as a pure reagent. Dichloromethane is the historical polar solvent for this reaction and is still widely used. However, nonpolar solvents such as hexane have also been used²⁴⁰ or polar solvents such as trifluoroacetic acid²⁴³.

The derivatization procedure has also been modified to avoid problems during isotopic measurements of amino acids. A 1:2:5 (v:v:v) acetic anhydride/triethylamine/acetone mixture replaced the 4:1 (v:v) DCM/TFAA mixture to remove fluorine from the derivatives²⁴⁴ because fluorine could be a toxic catalyst for the oxidation reactor. Among the modified procedures, the use of an insoluble sulfonated polystyrene resin in the hydrogen form as an acid catalyst²⁴⁵ for the first step is noteworthy. This type of resin is now a common means of purifying extraterrestrial amino acids from impurities *via* ion exchange chromatography. At low and neutral pH, the amino acids bind to the resin due to their positive charge. It is interesting to keep in mind that during the purification process, resin breakthrough in the amino acid fraction could result in loss of compounds. Indeed, using a TFAA/solvent reaction, the amino acids could still be bound to the resin and not be derivatized due to the low pH. To overcome this problem, it should either be established that no resin breakthrough occurs or the derivatization should be adapted to be performed in alkaline medium, using for example a methyl trifluoroacetate/trimethylamine mixture²⁴⁵.

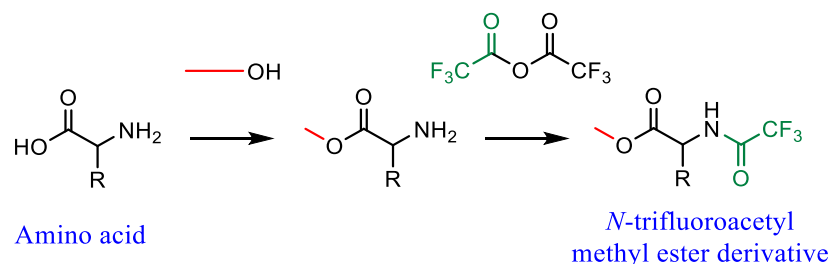


Figure 28. Methanol/trifluoroacetic anhydride derivatization (MeOH/TFAA) of amino acids.

Fox *et al.*²⁴² showed that using this derivatization, isovaline is baseline resolved on a Lipodex E column along with nearly 40 non-proteinogenic amino acid enantiomers being resolved. Unfortunately, no information on the detection limit of isovaline has been reported in this study. Thus, given the potential applicability for meteorite analyses, this method was selected for further study using non-proteinogenic and proteinogenic amino acids.

2.3 ION EXCHANGE CHROMATOGRAPHY

Prior to the derivatization step, meteoritic samples are usually purified using ion exchange chromatography (IEC) to remove salts and metal cations but can also be used to fractionate samples in two or several distinct fractions containing selected classes of compounds. It is also an additional filtering step to remove meteorites' solid particles.

2.3.1 Resin properties

The resin used throughout my studies was a sulfonated poly(styrene-*co*-divinylbenzene) copolymer obtained by post-sulfonation. The divinylbenzene leads to cross-linking and a three-dimensional network. The pore size of the beads depends directly on the cross-linking rate of the resin. Low cross-linking values, as shown in **Figure 29**, are associated with open and permeable structures with respect to high molecular weight compounds. They are also less resistant in terms of swelling and shrinkage, and less efficient/selective in separating compounds.

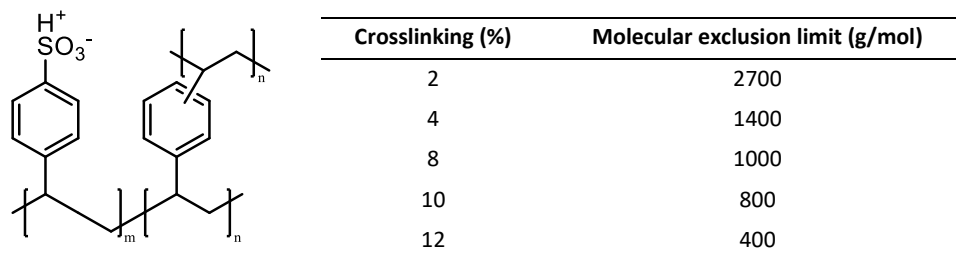


Figure 29. Structure and properties of a cation exchange resin. (Left) Sulfonated poly(styrene-*co*-divinylbenzene) copolymer used as ion exchange resin in the H⁺ form. (Right) Approximate equivalence between cross-linking values and molecular weight exclusion limit.

Particle sizes are often specified in mesh and are specifically chosen for the application. Large particles (20 – 50 and 50 – 100 mesh / 850 – 300 and 300 – 150 μm) are used primarily for large preparative applications and batch operations. Medium-sized particles (100 – 200 mesh / 150 – 75 μm) are used

primarily in column chromatography for analytical and laboratory scale preparative applications. Smaller particles (200 – 400 mesh / 75 – 38 μm) are used for high resolution analytical separations²⁰⁶.

2.3.2 Relative selectivity of counter-ions

Depending on the counterion used, the ion exchange properties can vary. Conversion from one form to another is possible by saturating the resin beads with the chosen counterion. A low selectivity is usually chosen in order to easily exchange the sample ions when they are introduced. The H^+ form can be easily obtained using concentrated HCl and is quite versatile given the relative selectivity available in **Table 10**. The higher the relative selectivity (RS), the stronger the binding between the resin and the counterion. The RS gap is a performance indicator of how well the sample ions will bind. It also defines the ease of transition from one form to another.

Table 10. Relative counter ion selectivity for AG 50W-X8 resin. From the instruction manual²⁰⁶.

Li^+	H^+	Na^+	NH_4^+	Mg^{2+}	Fe^{2+}	Zn^{2+}	Cu^{2+}	Cu^+
0.85	1	1.5	1.95	2.5	2.55	2.7	2.9	5.3

2.3.3 Separation mechanisms

Several separation mechanisms can occur when using an ion exchange resin and are presented in **Table 11**. Resins can be used either as an HPLC stationary phase or as a preparative step for subsequent analysis²⁰⁷.

In the context of extraterrestrial samples, its main function is to remove salts and metal ions from the amino acid fraction²⁰⁹. It can be performed before²¹⁰ or after the derivatization step. However, it may pose some risks when performed after derivatization (GC) because the target molecules are volatile and must be concentrated after ion exchange chromatography. Desalting is an important step to remove contaminants that could potentially interfere with subsequent derivatization. In addition, it has also been used to fractionate compounds according to their chemical functions. Thus, in our case it is a convenient way to obtain multiple fractions: one fraction containing sugar molecules and another fraction containing amino acids from a single sample¹⁴⁴. In this case, only a few mechanisms are prevalent and useful. Ion exchange is the main mechanism to retain only amino acids. Ion-moderated partitioning can be mentioned to some extent because some metals must be removed from the sample. Similarly, interactions with sulfonate groups and the matrix necessarily occur with amino acids and sugars. Finally, the flow rate of the column has a significant impact on the separation and must be tailored to the

application. For example, an elution rate of 5 – 10 cm/min is recommended for trace ion removal²⁰⁶. Since ion exchange chromatography is used here as a separation step rather than a fine separation tool, such an elution rate seems appropriate for the sample requirements.

Table 11. List of mechanisms involved in ion exchange chromatography. Inspired by Huber et al.²⁰⁸ and Huck et al.²⁰⁷

Mechanism	Description
Ion exchange	The cationic compounds compete on the copolymer surface through the sulfonate active site. There is a relative selectivity for each counterion with respect to the H ⁺ counterion.
Ion exclusion	The anionic compounds are repelled from the negatively charged matrix. It is directly related to the degree of dissociation of the ionic species. This mechanism loses its intensity with increasing molecular weight.
Size exclusion	The compounds are physically separated according to their size. This exclusion depends on the degree of cross-linking. The percentage of cross-linking influences the pore size of the resin beads.
Ion moderated partition chromatography	Metal cations can be attached to the sulfonate group and create a coordination complex with other compounds. Chelates are formed by pyranose rings and metal cations, for example.
Interaction with sulfonate groups	Compounds are adsorbed onto the sulfonate groups through hydrogen bonding and dipole-dipole forces or are separated by differences in water polarity induced by the sulfonate group. The intraparticle water is more polar than the mobile phase water.
Interaction with matrix	Reverse phase partitioning can occur due to the apolar resin backbone and the polar mobile phase. This mechanism becomes more dominant when surfactant analytes are used.

2.3.4 Principle of ion exchange chromatography

Upon sample addition (**Figure 30**), positively charged species compete with H⁺ ions at the sulfonate binding sites. As shown by the relative selectivity of counter ions in **Table 10**, cations generally have a greater affinity for the sulfonate binding site than H⁺ ions and are therefore exchanged and retained on the polymer resin beads. The use of water as the first elution solvent allows neutral and negatively charged species to elute directly, without being retained. Carbohydrates have pK_A values around 10-12 and are therefore neutral. Then, selective elution of amino acids can be achieved using appropriate pH and ionic strength. The use of ammonium hydroxide NH₄OH as a second elution solvent outperforms the R-NH₃⁺ amino acids due to its *high* NH₄⁺ concentration despite their similar affinity. It should also be noted that the introduction of ammonium hydroxide raises the pH above the pK_A of the ammonium ion with $pK_{A_A} \approx 9 - 10$, $pK_{A_C} \approx 2 - 2.5$ being the pK_A of the ammonium and carboxylate ions, respectively.

Indeed, at 2 M NH₄OH, $pH = 7 + \frac{1}{2} pK_A + \frac{1}{2} \log C = 7 + \frac{9.2}{2} + \frac{\log 2}{2} = 11.8$ for a weak base.

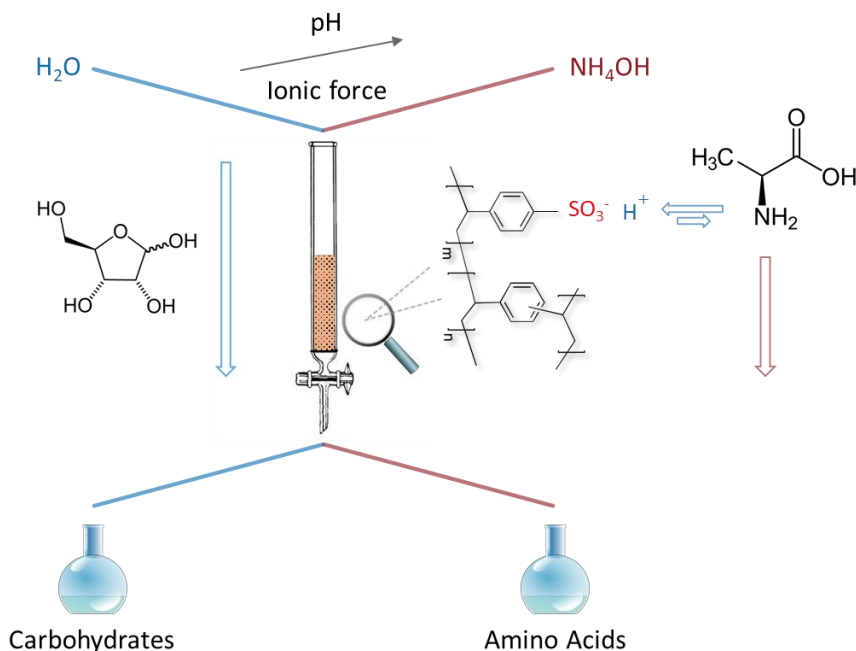


Figure 30. Principle of cation exchange chromatography for the separation of carbohydrates and amino acids.

This calculation provides an order of magnitude because the equation is for a dilute solution, between 10^{-6} M and 1 M. At this elevated pH, the ammonia group in the amino acids becomes mostly neutral when released from the exchange resin. This is unfortunately not often – if ever – stated in the literature. Once eluted, the amino acid fractions need to be concentrated using e. g. a rotary evaporator as several bed volumes are required to achieve their complete elution. Derivatization is usually performed after this “fractionation/purification” step. However, one has to keep in mind the basicity of the amino acid fraction which can have an impact on the efficiency of the derivatization reaction.

2.3.5 Resin conditioning

The ion exchange resin can potentially be a source of contamination and should therefore be cleaned before use. Equilibration is typically performed using 3-bed buffer volumes²⁰⁶. However, a successive elution of water-basic solution-water-acid solution-water to condition the resin can also be considered. The basic solution is used to remove the H^+ ions already present and elute any contaminants bound to the resin. The acidic solution is used to regenerate the resin with H^+ ions. Water is used to gently raise or lower the pH of the solution in which the resin is located, and to equilibrate the resin before use. This is because pH shocks can lead to cracks in the resin beads, resulting in less efficient and/or less reliable

separation. In addition, cracks can form due to the resin dry out during elution. Care must be taken to ensure that there is always sufficient solvent above the resin bed level.

2.4 EXTRACTION OF EXTRATERRESTRIAL ORGANIC MATTER

2.4.1 Solvent extraction of soluble organic compounds

Extraction is often the second step in the analysis of soluble organic matter of meteoritic samples and should not be neglected because subsequent sample handling and analyses depend on its success. The recovery rate after one extraction step is generally estimated to be about 80% for rock and soil samples²⁴⁶ but must be adapted in the case of extraterrestrial samples. As Rodier *et al.*²⁴⁶ pointed out, time, temperature, and solvent must be optimized to ensure maximum recoveries without experiencing compound degradation or side reactions between the target compounds or with the matrix. Compromises must be made regarding the solvent selected because its polarity must match the targeted compounds: the broader the class of compounds studied, the less efficient the extraction step. **Table 12** aims to summarize the different conditions employed to extract and study organic compounds in meteorites. Note that the targeted compounds are highlighted for better extraction context.

As can be seen in the table below, past experiments favored the use of apolar solvents while water is currently often chosen due to its polarity and ability to solubilize amino acids and sugars. It is also used for less polar compounds such as aliphatic amines, carboxylic acids and hydroxy acids. Slightly concentrated HCl can be used as a support to facilitate the release of organic compounds from the meteorite matrix. However, depending on the conditions used, deleterious reactions may occur. Target compounds can be altered by the Maillard reaction²⁴⁷, Strecker degradation as well as by dimerization, oxidation, and oximation⁴³.

Interestingly, in the context of Mars soil analyses, A. Buch *et al.*²⁴⁸, demonstrated that isopropanol could be an alternative to water and achieved recoveries of 80% for alanine and glycine, and 25% for serine. The carboxylic acids also studied, showed recoveries ranging from 5% to 80%, making this solvent more versatile in terms of extraction than ethyl acetate, acetonitrile, dichloromethane, and ethanol. With these solvents, the recoveries of these amino acids are generally close to zero. Thus, a more extensive study using a 1:1 (v:v) water and isopropanol mixture to optimize the extraction of amino and carboxylic acids was performed, and showed a wider extraction range²⁴⁹.

Table 12. Extraction methods of various targeted compounds in meteoritic samples.

Sample	Mass (mg)	Solvent	T (°C)	Time (h)	Targeted compounds	Reference
11	< 1400	Dichloromethane 2 mL	100	24	Aldehydes Ketones	Aponte ²⁵⁰ 2019
10-15	< 350	H ₂ O 1 mL	100	24	Monocarboxylic acids	Aponte ²⁵¹ 2019
1	100	H ₂ O / mL	100	20	Amino- & hydroxy-acids Amines & carboxylic acids	Pizzarello ²⁵² 2018
5	400-1100	HCl 1 mL (0.1 M) H ₂ O 1 mL	100	24	Amines Amino acids	Aponte ²⁵³ 2016
1	900	0.5 M HCl 1 mL	100	24	Aliphatic amines	Aponte ²⁵⁴ 2014
2	2000	1N NaOH 10 mL	RT	2.5	Monocarboxylic acids	Aponte ²⁵⁵ 2014
1	10	H ₂ O 2 mL Dichloromethane/methanol	100	24	Aliphatic compounds	Pizzarello ²⁵⁶ 2013
8	50-250	H ₂ O / mL	100	24	Amino acids, hydroxyacids, polyols, amines, monocarboxylic acids	Pizzarello ²⁵⁷ 2012
1-2	3994	H ₂ O 2 mL Dichloromethane/methanol 2 mL	100	24	Amino acids, ammonia, amines	Pizzarello ²⁵⁸ 2011
3	1000, 485, 165	H ₂ O 1 – 4 mL	100	20	Hydroxy acids	Pizzarello ²⁵⁹ 2010
4	500	H ₂ O 5 mL HCOOH 5 mL HF/HCl 10 mL	60 60 80	2 2 6	Nucleic acids	Shimoyama ²⁶⁰ 1990
4	5000-18 350	Benzene 20 – 73 mL H ₂ O 20 – 73 mL HCOOH 40 – 146 mL	60	0.5	Pyrimidines & N-heterocyclic compounds	Stoks ^{261,262} 1979 & 1981
1	1000	HCOOH 8 mL	60	1	Nucleobases	Martins ²⁶³ 2008
1	1200	H ₂ O 3×300 mL	RT	46	Carboxamides	Cooper ¹⁴⁴ 1995
3	2000	HCl 10 mL (2 %)	RT	-	Sugars	Furukawa 2019
14	320-1611	Benzene/acetone 100 mL (8/2) H ₂ O / mL HCl (5 N) / mL	- Reflux Reflux	24	Amino acids & sugars	Kaplan ²⁶⁴ 1962

Because the targeted amino acids and sugars are water soluble, the use of such a mixture is not necessary, but could be justified if it could provide a protective effect during extraction, such as inhibition of degradation reactions. In addition, because ion exchange chromatography must be used after the extraction process, the use of a solvent other than water or a mixture of solvents raises questions about compatibility, purification performance, and fractionation, although isopropanol has the advantage of not dissolving salts and leading to cleaner samples²⁴⁹.

Another striking result is the efficiency of sonication on the extraction of all the compounds mentioned. Indeed, without sonication, the best recoveries were obtained after 140 h at 60 °C of conventional shaking²⁴⁸. At the same temperature and using sonication, similar or even slightly higher recoveries were reported (generally > 80%) with a duration of only 15 min for alanine, glycine, and glutamic acid. The recovery of serine could be increased from 20 to 80%. Compared to the often-applied extraction temperature of 100 °C, shown in **Table 12**, this lower extraction temperature should be preferred to preserve carbohydrates and amino acids. Thus, sonication appears to be an excellent compromise to ensure mild extraction conditions. Nevertheless, it should be mentioned that sonication is not without risk for the sample. These pulsed ultrasonic waves involve a cavitation phenomenon that creates tiny bubbles followed by their implosive collapse. Local temperatures and pressures can reach values as high as 5200 K and 500 atm²⁶⁵, and 1900 K at the bulk-cavitation bubble interface. It is also reported that these hot spots can dissociate water, creating hydroxyl radicals²⁶⁶ that can further oxidize organic compounds. As a result, compounds can be degraded by thermolysis in the center of the cavitation bubble or oxidized by sonolysis *via* hydroxyl radicals at the edge of the bubble and in the bulk as these radicals escape the interface²⁶⁷. Fortunately, the efficiency of this sonolysis process is low for hydrophilic compounds compared to hydrophobic compounds, making the extraction of amino acids and sugars suitable using sonication. Generation of hydroxyl radicals is also frequency dependent²⁶⁶, making low frequencies less likely to lead to degradation. Intensity is also an important parameter because the extraction of the analytes increases with the amplitude of vibration, until a maximum value is reached²⁶⁸. High values are not necessarily required because they could promote premature degradation of analytes.

In addition to the degradation pathways mentioned above, another extraction risk would be the polymerization of sugar molecules i.e., *caramelization*, which occurs at high temperature and involves complex sets of reactions such as dehydration and polymerization. This reaction can occur in solution or in the dry state and is dependent on pH and concentration. Ratsimba *et al.*²⁶⁹ studied the *caramelization* process of D-glucose, D-fructose, and sucrose by GC-MS and showed that for D-glucose, 1,6-anhydro- β -D-glucopyranose and 1,6-anhydro- β -D-glucofuranose as well as complex disaccharides were synthesized. Another striking finding was the presence of D-mannose and D-fructose, which could result in the Bruyn-Alberda van Ekenstein Lobry enolization process of D-glucose. It is essential to point out that the *caramelization* of D-glucose was performed under concentrated conditions (2.5 kg D-glucose in 250 ml water) at 170 °C for 2.8 h. Obviously, the amounts expected in extraterrestrial samples are much lower than the amounts used in this study. It does, however, testify that prolonged treatment at high temperature can induce structural changes and oligomerization of sugars. Apart from simple degradation,

isomerization is even more critical because it can lead to false detection of sugars not initially present in a sample.

2.4.2 Hydrolysis of meteoritic amino acids

In the case of amino acids, a hydrolysis step is required to cleave the oligomerized fraction and release the amino acids as monomers as mentioned in **Table 3**. This liquid hydrolysis is usually performed using concentrated 6 M HCl. Introduced by Tsugita *et al.*²⁷⁰, acid-vapor hydrolysis has notable features compared to traditional liquid hydrolysis of peptides. Contamination has been reported to be about 10-times lower, with a shorter hydrolysis time but using a higher temperature. Indeed, about 22.5 minutes at 158 °C showed better yields than traditional hydrolysis at 106 °C for 72 h. Because direct contact is made between the sample and the acid in traditional hydrolysis, washing steps are required to remove the acid, which is not the case with acid-vapor hydrolysis. Moreover, trifluoroacetic acid was used in conjunction with hydrochloric acid to better recover hydrophobic amino acids²⁷¹ such as isoleucine and valine that are known to be less sensitive to bond cleavage in dipeptides. At first glance, acid-vapor hydrolysis appears attractive but suffers from increased racemization²⁷². Racemization of amino acids under conventional hydrolysis conditions is known to occur and is dependent on pH and temperature²⁷³, but experiments with free amino acids and peptides have shown a more critical effect under acidic vapor conditions. Starting with the free L-enantiomer, the percentage of free D-alanine found in the acid-vapor analysis was $2.7 \pm 0.1\%$, whereas it was only $0.6 \pm 0.0\%$ in the liquid-phase hydrolysis. For aspartic acid, $8.5 \pm 0.3\%$ is reported versus $3.2 \pm 0.0\%$, respectively, and protein studies showed a similar trend.

In the end, water still appears to be the best extraction solvent for the simultaneous extraction of amino acids and sugars. It is also more appropriate to use it as a pure solvent to decrease the risk of contamination and potential disruption of ion exchange columns. Preserving the chemical structure and initial amount of analytes while optimizing their extraction is a major concern and leads to consider sonication to improve extraction under mild conditions ($T < 60^\circ\text{C}$ and $t < 1$ h). In the case of amino acids, a classical hydrolysis should be preferred to avoid increased racemization. If contamination occurs, it will be discussed and compared between proteinogenic and non-proteinogenic amino acids.

2.5 CONCLUSION

The investigation of chiral compounds in extraterrestrial samples can be conducted using a powerful tool like GC×GC. Improved separation and enantioseparation can be achieved through column coupling, and

improved detectability is achieved through the modulation process, making this technique particularly suitable for trace analysis. The first column used is chiral to allow enantioseparation of derivatives, and cyclodextrins occupy an important place in the separation of amino acids and sugars due to their separation mechanism, which forms diastereomeric complexes with chiral guests. The efficiency of separation and enantioseparation also depends on the derivatization procedure, which has a great impact on other parameters such as volatility, detectability, and stability. It is therefore carefully selected, especially in the case of sugars that can lead to many isomers by intramolecular cyclization. The objective of the next chapter is to focus on the development of an analytical procedure to study *ees* in extraterrestrial samples through amino acid and sugar derivatization studies, as well as extraction and purification steps.

CHAPTER III

Toward the development of a complete analytical procedure to investigate extraterrestrial and laboratory-produced extraterrestrial samples

3.1 GENERAL APPROACH

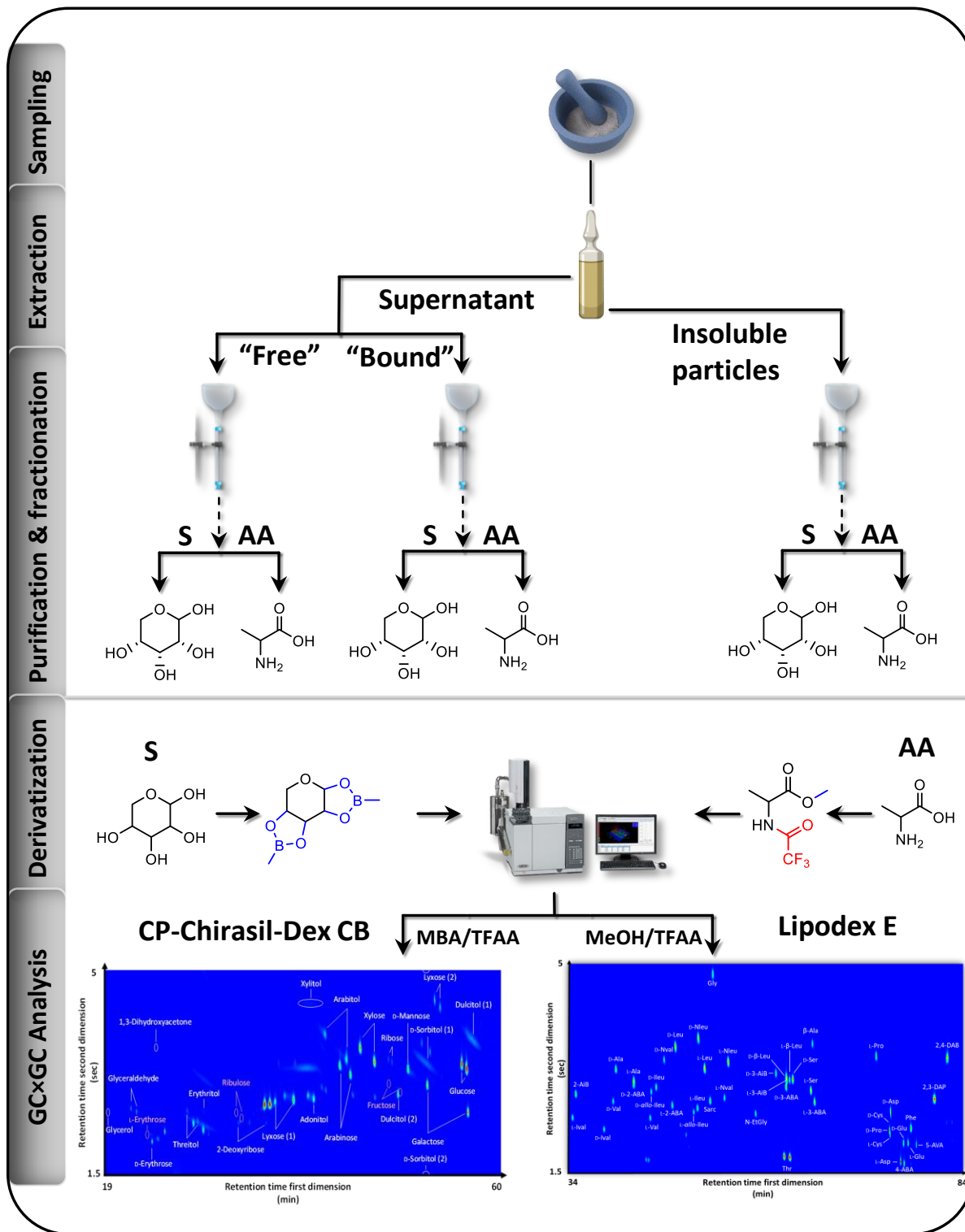


Figure 31. General scheme of sampling, extraction, fractionation and purification, derivatization and analysis of a meteorite sample. S – Sugars fraction, AA – Amino acids fraction.

The general procedure described in **Figure 31** was inspired by various previously published papers on the extraction, fractionation, purification, derivatization and analysis of meteorite samples and have been further optimized to meet our research goals. Each step is briefly presented below to provide an overview of the protocol. **Sampling** - Approximately 1 g of fragment (i.e., meteorite, serpentine procedural blank, etc.) is finely ground using a ceramic mortar and pestle to increase the contact area and facilitate the release of organic compounds. **Extraction** - The resulting powder (or interstellar ice analog) is hydrolyzed with water at 100 °C for 24 h (for amino acid target analysis) or room temperature for 24 h in a flame-sealed ampoule to recover the organic compounds. After cooling and centrifugation, the supernatant is separated from the insoluble solid material. It is then divided into two equal volumes to study free and oligomerized species such as amino acids and sugars separately. The *free* part does not undergo any additional step before fractionation while the *bound* part is hydrolyzed in 6 M HCl at 100 °C for 24 h to cleave any oligomeric bonds. Furthermore, the *insoluble* part is also hydrolyzed in HCl under the same conditions as mentioned above in order to better harvest the trapped organic compounds. **Purification & fractionation** - For each *free*, *bound* and *insoluble* part, sugars (S) and amino acids (AA) are separated by cation exchange chromatography *via* a sulfonated poly(styrene-co-divinylbenzene) resin. In its original H⁺ form, the resin readily binds positively charged molecules such as amino acids, metal cations and other salts allowing purification of these fractions. **Derivatization** - Sugars and amino acids are made volatile and suitable for GC analysis through two-step derivatizations. **GC×GC analysis** - AAs are derivatized with the MeOH/TFAA method and analyzed on a Lipodex E column while sugars are derivatized with the MBA/TFAA method and analyzed on a CP-Chirasil-Dex CB column. These methods and columns were selected for their selectivity, separation, enantioseparation and reliability.

3.2 DERIVATIZATION & GC×GC ANALYSIS

3.2.1 MeOH/TFAA derivatization of amino acids

3.2.1.1 *Materials and methods*

3.2.1.1.1 Reagents

Standards and reagents used in this study were purchased from Sigma-Aldrich, Fluka, or Acros Organics. The purity of DL and L amino acids was greater than 98% in all cases. Water used in all steps of the study – tool cleaning and sample processing – was obtained using a Milli-Q Direct 8 apparatus (18.2 MΩ.cm at 25 °C, < 5 ppb total organic carbon). All glassware was washed several times with ethanol and Milli-Q water, wrapped in aluminum foil, and then heated to 500 °C for at least 5 h to remove any organic

contaminants. PTFE-lined lids and caps were washed in the same manner. Pipette tips and inserts of GC×GC vials were used without further cleaning.

To prepare the amino acid stock solution, individual amino acids were weighed, mixed, dissolved in Milli-Q water, and then merged into a single solution. A different amino acid stock solution was also prepared for the *ee* experiments using only 10 amino acids for simplicity. The concentration of amino acids was corrected depending on the purity of the standard.

3.2.1.1.2 Derivatization

Diluted series of the stock solutions were transformed into *N*-trifluoroacetyl-*O*-methyl ester derivatives following the procedure reported by Fox *et al.*²²⁵ with some modifications. A volume of 50 µL of the aqueous amino acid solution was taken from a Reacti-vial® and dried under a gentle stream of nitrogen. Then, 200 µL of a MeOH/AcOCl solution (4:1, *v:v*) was added and the reaction mixture was stirred for 10 seconds and heated to 110 °C for 1 hour. The mixture was then cooled and dried under a stream of nitrogen. At this point, the sample was not completely dried, but about 1 – 2 µL remained to minimize the loss of the most volatile compounds after the first derivatization step. Next, 200 µL of a DCM/TFAA solution (4:1, *v:v*) was added, the reaction medium was stirred for 10 s, and then heated at 100 °C for 20 min. The solution was cooled again and then dried by a stream of nitrogen. Care must be taken to use a very gentle nitrogen stream to avoid over drying and losing important volatile compounds. Finally, the residue was dissolved in 50 µL of CHCl₃ containing 10⁻⁵ M methyl laurate as an internal standard and transferred to 1 mL GC vials equipped with 100 µL inserts for enantioselective GC×GC analyses.

3.2.1.1.3 GC×GC-TOFMS

Enantioselective analysis was performed using a GC×GC Pegasus IV D instrument coupled to a time-of-flight mass spectrometer (LECO, St Joseph, Michigan, USA). The MS system was operated at a storage rate of 150 Hz, with a mass range of 50-400 amu. The detector voltage was set at 1650 V, or 1800 V for the method detection limit (MDL), with a solvent delay of 15 minutes. The temperature of the ion source and injector was 230 °C. A Lipodex E column (25 m × 0.25 mm, 0.12 µm film thickness, Agilent-Varian, Santa Clara, California, USA) in the first dimension coupled with a DB Wax column (1.4 m × 0.1 mm, 0.1 µm film thickness) in the second dimension were used. Modulation between the columns was provided by a two-stage thermal jet modulator using liquid nitrogen. Helium was used as the carrier gas at a constant flow rate of 1 mL/min. Samples were injected in splitless mode, and the MS transfer line was maintained at 240 °C during analysis. A modulation period of 5 s was applied. The temperature of the primary column

was held at 40 °C for 1 min, then increased to 80 °C at a rate of 10 °C/min and held for 10 min, then heated to 125 °C at a rate of 1 °C/min, followed by a rate of 2 °C/min to 190 °C and held for 1 min. The secondary oven used a temperature offset of 30 °C. The modulator temperature was set 15 °C higher than the secondary oven. Depending on the purpose of the experiment, samples were injected multiple times to calculate peak areas with reliable statistical error bars. ChromaTOF™ software from LECO Corp. was used to quantify the analytes. The software integration was manually changed, when necessary, to correct the automatic data processing by the software.

3.2.1.2 Identification of amino acids

As derivatization has already been reported in the literature using the Lipodex E column, the elution orders allowed for the identification of several amino acids. However, identifying unreported peaks without access to their mass spectra is a more difficult task. In order to assign each peak to an amino acid, each amino acid was derivatized and injected independently to get access to its mass spectrum and retention time.

3.2.1.2.1 Mass spectrum & fragmentations

Unfortunately, mass spectral databases and articles were not very helpful in terms of availability of mass spectra to identify all of the investigated amino acids. After identifying each amino acid, a comprehensive list of their mass spectra was made and is available in **Table S 1** (p. 157). The interpretation of the mass fragmentations of the methyl ester of *N*-trifluoroacetyl amino acids has been little described, although some unusual fragmentation pathways with this derivatization have been reported²⁵⁸. **Figure 32** shows the mass spectrum and fragmentation of alanine. Since alanine is a well-studied amino acid, a detailed explanation of the fragmentation pattern is proposed.

Common fragmentation of derivatives involves $m/z = 69$ and $m/z = 59$, corresponding to the α -cleavage of the trifluoroacetyl carbonyl, in red, and the ester carbonyl, in blue, respectively. Primary amide functions are generally difficult to break in contrast to secondary amide functions in *N*-ethylglycine and proline, for example. The ester function is frequently lost because it can be stabilized as a $-C\equiv O^+$ ion or lead to a cyclic fragment due to the attack of the nitrogen on the carbonyl of the ester group. These 2 forms have an m/z difference of 1 because the hydrogen bound to the nitrogen is removed. This occurs notably for the amino acids 3-Aib, 4-Aba and 5-Ava. McLafferty rearrangement competes with α -cleavage of carbonyls when it can occur. Both carbonyls lead to McLafferty rearrangement, but McLafferty rearrangement of the ester carbonyl is more likely to be observed. Some amino acids show unusual peaks

such as $m/z = 78$ and $m/z = 106$. Both of these peaks result from the subsequent decomposition of the $m/z = 126$ fragment, as detailed by Manhas *et al.*²⁵⁸ and are shown below. The mass fragment $m/z = 106$ is obtained after the loss of HF from $m/z = 126$. The mass fragment $m/z = 78$ is obtained after the loss of CO from $m/z = 106$.

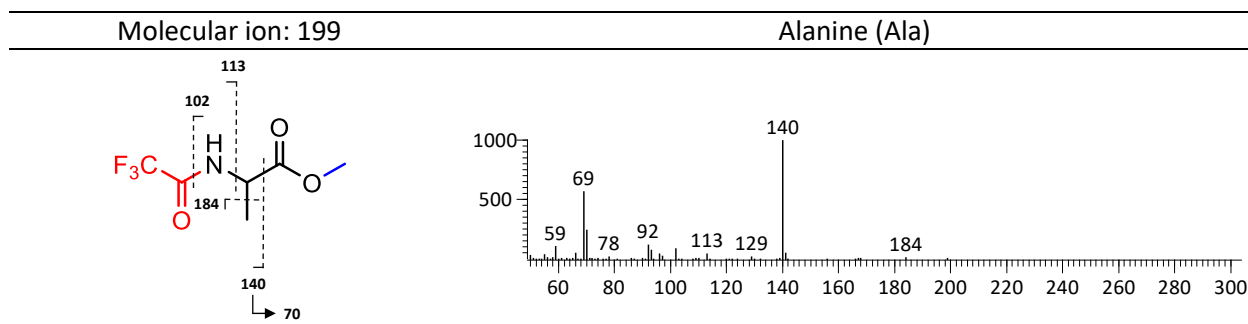
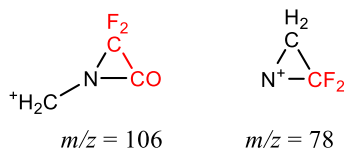


Figure 32. Mass spectrum & fragmentation of alanine as *N*-trifluoroacetyl methyl ester derivative.

$m/z = 199$ corresponds to the molecular ion.

$m/z = 140$ is obtained by α -cleavage of the ester (left side) and is the base peak. The positive charge is located on N.

$m/z = 59$ corresponds to $m/z = 140$ by-product. The positive charge is stabilized with the oxygen lone pair thus leading to an acylium ion.

$m/z = 168$ also corresponds to an alpha cleavage but occurs on the other side (right side) of the ester functional group and is also leading to an acylium ion.

$m/z = 167$ corresponds to the formation of a cycle initiated by the attack of nitrogen on the carbonyl with the removal of CH_3O^- .

$m/z = 70$ corresponds to further decomposition of $m/z = 140$.

$m/z = 184$ is obtained by σ -cleavage of the side-chain methyl group.

$m/z = 113$ is obtained by McLafferty rearrangement on the amide functional group.

$m/z = 55$ corresponds to $m/z = 113$ by-product's further decomposition into $\text{CH}_2=\text{CH}-\text{C}\equiv\text{O}^+$.

$m/z = 69$ is obtained by α -cleavage of the amide's carbonyl (left side) and corresponds to CF_3^+

$m/z = 102$ is obtained by α -cleavage of the amide's carbonyl (right side) and corresponds to $\text{F}_3\text{C}-\text{C}\equiv\text{O}^+$. Its by product corresponds to $m/z = 102$.

$m/z = 92$ fragmentation is unknown.

3.2.1.3 Overall resolution & enantioseparation

Figure 33 shows that enantioseparation is achieved for a large portion of the amino acids and that good overall resolution can be obtained using the chosen derivatization method in combination with enantio-GC×GC-TOFMS. Difficulties in resolving L-Ala from D-2-ABA as well as L-3-Aib/D-3-Aba/ β -Leu and β -Leu/D-Ser are unavoidable even after program optimization. Each amino acid was injected individually to allow identification. The order of elution of the enantiomers is based on the work of Fox *et al.*²²⁵ but was confirmed for Ala, Asp, Val, 2-Aba, Leu, Thr, Nva, Ile, Iva, and Pro using a solution with 5% *ee*. Most of the time, the D-enantiomer elutes before the L-enantiomer. The α -methylated amino acids tend to have a reversed order as pointed out by Fox *et al.*²²⁵ and verified for Iva. This reversed elution order was also observed for Pro – which is a secondary amine forming a pyrrolidine ring on the α -carbon. Coelutions of some analytes of interest can be avoided using a CP-Chirasil-Dex CB column, as shown in **Figure 34**. Using the same temperature program, the derivatives have a shorter elution time, about 15 minutes. Ala and 2-Aba are well resolved from each other and Phe is enantioseparated. The L-3-Aib/D-3-Aba/ β -Leu/D-Ser area is well spread using CP-Chirasil-Dex CB: 3-Aba, Ser, and 3-Aib are well resolved and enantioseparated whereas β -Leu is not enantioseparated. 2,4-Dab is still not enantioseparated. Moreover, 2-Aib and one Ala enantiomer are not observed in the chromatogram. Given the shorter retention times of all amino acids on the Chirasil-Dex compared with the Lipodex E column, it is most likely that they are hidden in the solvent delay. Overall, these 2 sets of columns appear to be complementary to achieve complete enantioseparation of the 30 amino acids investigated. A summary of *N*-trifluoroacetyl methyl ester amino acid derivatives in terms of characteristic fragment ions, retention time and method detection limit are reported **Table 13**. Asparagine turns into aspartic acid during the derivatization, as well as glutamine to glutamic acid.

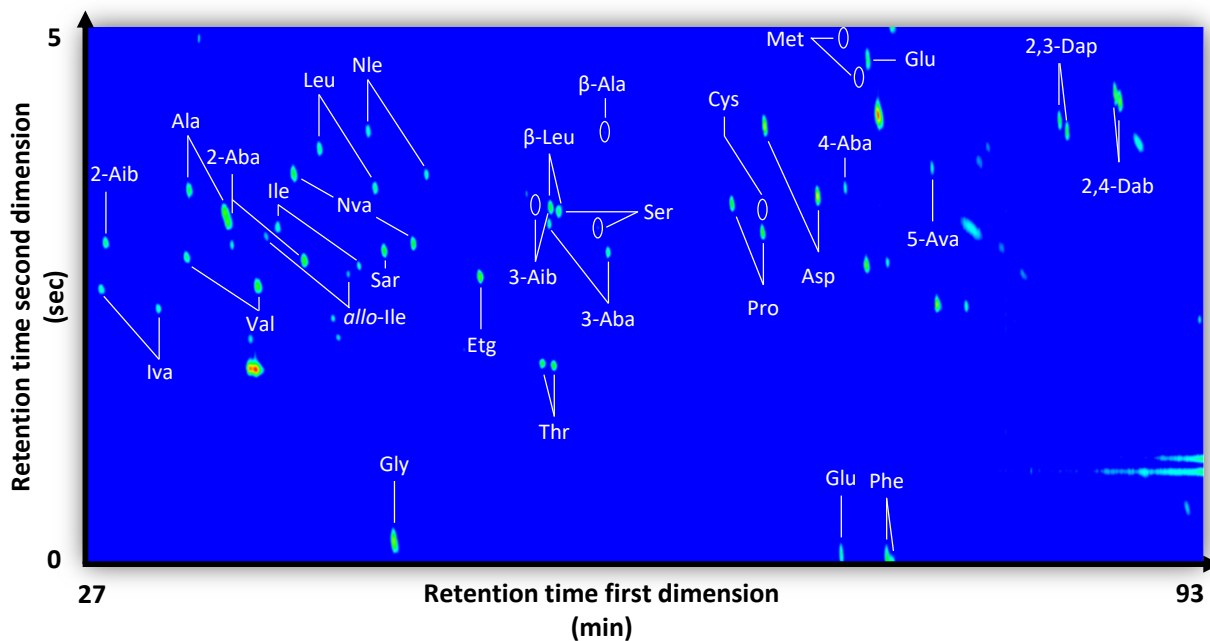


Figure 33. Two-dimensional chromatogram of MeOH/TFAA derivatized amino acids analyzed on a Lipodex E coupled to a DB-WAX column.

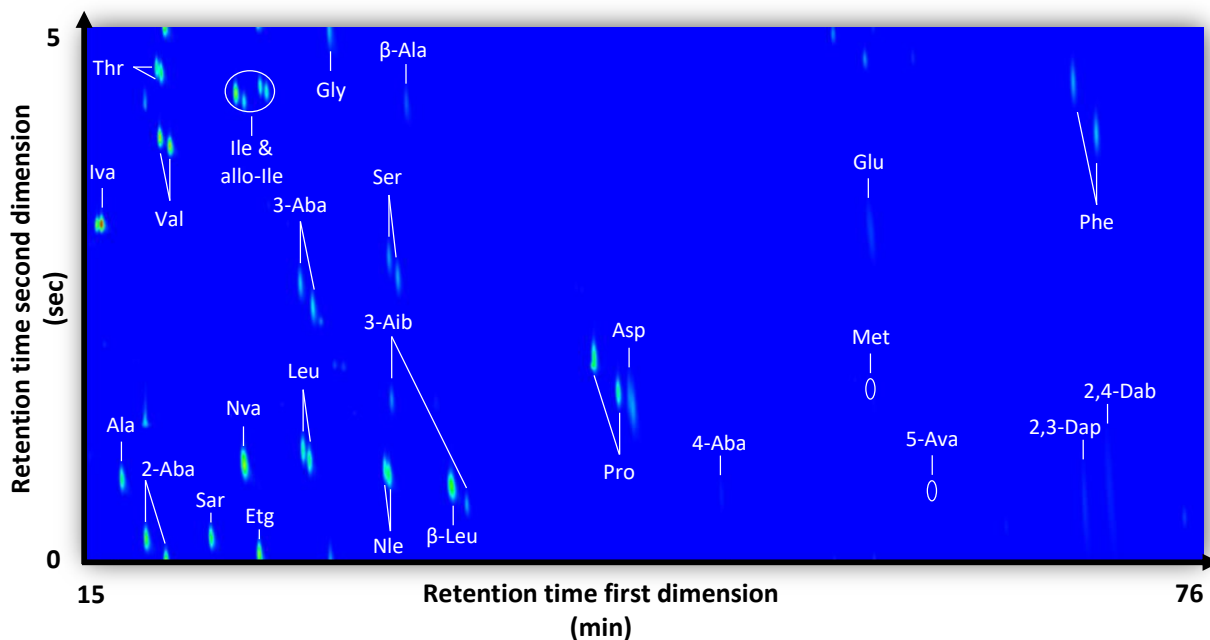


Figure 34. Two-dimensional chromatogram of MeOH/TFAA derivatized amino acids analyzed on a CP-Chirasil-Dex CB coupled to a DB-WAX column.

Table 13. Characterization of *N*-trifluoroacetyl methyl ester amino acid derivatives by mass spectra, retention time and method detection limit.

#	Compound	[M] ^{**}	Characteristic ions, <i>m/z</i>	<i>R</i> _{t1} ^a [min:sec]	<i>R</i> _{t2} ^b [sec]	<i>R</i> _s 1 st Dim. ^c	MDL (nM ; pg)
1	Glycine (Gly)	185	126, 69, 78, 56, 59, 88, 50, 106	45:20	0.27	-	43 ; 3.9
2	Sarcosine (Sar)	199	140, 69, 60, 78, 74, 90, 102, 199	44:45	2.91	-	33 ; 2.9
3	D-α-Alanine (D-Ala)	199	140, 69, 70, 92, 59, 102, 93, 66	33:10	3.46	2.8	27 ; 2.4
4	L-α-Alanine (L-Ala)	199	55, 69, 139, 70, 126, 167, 98, 59	35:15	3.27	-	32 ; 2.9
5	β-Alanine (β-Ala)	199	55, 69, 139, 70, 126, 167, 98, 59	57:50	3.99	-	21 ; 1.9
6	D-Serine (D-Ser)	311**	69, 138, 59, 110, 139, 153, 70, 96	55:20	3.32	4.2	28 ; 3.0
7	L-Serine (L-Ser)	311**	69, 138, 59, 110, 139, 153, 70, 96	57:25	3.12	-	22 ; 2.3
8	D-Cysteine ^d (D-Cys)	327**	69, 117, 59, 96, 61, 138, 129, 70	66:55	3.14	1	NF
9	L-Cysteine ^d (L-Cys)	327**	69, 117, 59, 96, 61, 138, 129, 70	67:15	3.08	-	NF
10	D-2,3-Diaminopropionic acid (D-2,3-Dap)	310**	69, 153, 185, 126, 78, 125, 96, 138	84:50	4.10	1.25	45 ; 4.7
11	L-2,3-Diaminopropionic acid (L-2,3-Dap)	310**	69, 153, 185, 126, 78, 125, 96, 138	85:15	4.01	-	44 ; 4.5
12	<i>N</i> -Ethylglycine (Etg)	213	126, 154, 69, 56, 140, 78, 74, 116	50:25	2.69	-	31 ; 3.2
13	2-Aminoisobutyric acid (2-Aib)	213*	154, 59, 69, 114, 84, 166, 138, 73	28:10	2.97	-	28 ; 2.9
14	D-2-Aminobutyric acid (D-2-Aba)	213*	154, 69, 126, 59, 56, 84, 96, 116	35:25	3.17	6.9	40 ; 4.1
15	L-2-Aminobutyric acid (L-2-Aba)	213*	154, 69, 126, 59, 56, 84, 96, 116	40:00	2.82	-	37 ; 3.8
16	D-3-Aminoisobutyric acid (D-3-Aib)	213	69, 88, 57, 153, 56, 126, 59, 84	53:10	3.44	3.4	23 ; 2.4
17	L-3-Aminoisobutyric acid (L-3-Aib)	213	69, 88, 57, 153, 56, 126, 59, 84	54:35	3.32	-	24 ; 2.5
18	D-3-Aminobutyric acid (D-3-Aba)	213	69, 140, 59, 70, 153, 74, 156, 102	54:30	3.16	7	45 ; 4.6 ^e
19	L-3-Aminobutyric acid (L-3-Aba)	213	69, 140, 59, 70, 153, 74, 156, 102	58:00	2.90	-	18 ; 1.8
20	4-Aminobutyric acid (4-Aba)	213	74, 69, 126, 59, 57, 182, 56, 78	72:05	3.49	-	13 ; 1.3
21	D-Aspartic acid (D-Asp)	257*	156, 59, 198, 69, 166, 85, 61, 71	67:20	4.04	6.3	41 ; 5.5
22	L-Aspartic acid (L-Asp)	257*	156, 59, 198, 69, 166, 85, 61, 71	70:30	3.40	-	41 ; 5.4
23	D-2,4-Diaminobutanoic acid (D-2,4-Dab)	324**	152, 69, 126, 153, 57, 56, 78, 185	88:10	4.33	NA	36 ; 4.2
24	L-2,4-Diaminobutanoic acid (L-2,4-Dab)	324**	152, 69, 126, 153, 57, 56, 78, 185	88:25	4.27	-	36 ; 4.2
25	D-Threonine (D-Thr)	325**	69, 152, 57, 153, 59, 185, 141, 96	54:05	1.88	1.3	28 ; 3.3
26	L-Threonine (L-Thr)	325**	69, 152, 57, 153, 59, 185, 141, 96	54:50	1.87	-	25 ; 3.0
27	D,L-Asparagine (D,L-Asn)	-	Aspartic Acid	-	-	-	-
28	D-Isovaline (D-Iva)	227*	55, 69, 168, 166, 114, 138, 59, 110	31:20	2.39	5.9	62 ; 7.2 ^e
29	L-Isovaline (L-Iva)	227*	55, 69, 168, 166, 114, 138, 59, 110	27:55	2.56	-	61 ; 7.1 ^e
30	D-Valine (D-Val)	227*	55, 153, 168, 69, 114, 125, 59, 56	33:00	2.85	7.3	29 ; 3.4
31	L-Valine (L-Val)	227*	55, 153, 168, 69, 114, 125, 59, 56	37:15	2.59	-	42 ; 4.9
32	D-Norvaline (D-Nva)	227*	55, 168, 126, 69, 114, 153, 59, 56	39:20	3.62	12.3	31 ; 3.6
33	L-Norvaline (L-Nva)	227*	55, 168, 126, 69, 114, 153, 59, 56	46:30	2.97	-	43 ; 5.1
34	D-Proline (D-Pro)	225	166, 69, 96, 71, 128, 68, 53, 167	67:10	3.09	3	24 ; 2.8
35	L-Proline (L-Pro)	225	166, 69, 96, 71, 128, 68, 53, 167	65:25	3.34	-	24 ; 2.8
36	5-Aminopentanoic acid (5-Ava)	227*	55, 126, 74, 69, 59, 139, 78, 82	77:15	3.68	-	NF
37	D-Glutamic acid (D-Glu)	271*	152, 69, 180, 212, 57, 59, 55, 82	71:50	0.16	3.2	29 ; 4.2
38	L-Glutamic acid (L-Glu)	271*	152, 69, 180, 212, 57, 59, 55, 82	73:25	4.66	-	28 ; 4.1
39	D-Methionine (D-Met)	259	61, 69, 153, 75, 185, 59, 152, 62	71:40	4.84	6.5	NF
40	L-Methionine (L-Met)	259	61, 69, 153, 75, 185, 59, 152, 62	72:45	4.53	-	NF
41	D-Isoleucine (D-Ile)	241*	69, 153, 185, 57, 182, 125, 126, 59	38:25	3.12	8.3	25 ; 3.3
42	L-Isoleucine (L-Ile)	241*	69, 153, 185, 57, 182, 125, 126, 59	43:15	2.78	-	32 ; 4.2
43	D- <i>allo</i> -Isoleucine (D- <i>allo</i> -Ile)	241*	69, 153, 185, 57, 182, 125, 126, 59	37:40	3.06	8.4	NA
44	L- <i>allo</i> -Isoleucine (L- <i>allo</i> -Ile)	241*	69, 153, 185, 57, 182, 125, 126, 59	42:35	2.70	-	28 ; 3.6
45	D-Leucine (D-Leu)	241*	69, 140, 182, 153, 70, 185, 55, 59	40:55	3.83	5.6	36 ; 4.8
46	L-Leucine (L-Leu)	241*	69, 140, 182, 153, 70, 185, 55, 59	44:10	3.48	-	25 ; 3.3
47	D-Norleucine (D-Nle)	241*	69, 182, 126, 153, 114, 70, 55, 59	43:45	4:00	7	28 ; 3.7
48	L-Norleucine (L-Nle)	241*	69, 182, 126, 153, 114, 70, 55, 59	47:15	3.61	-	30 ; 3.9
49	D-β-Leucine (D-β-Leu)	241*	156, 69, 198, 55, 59, 166, 139, 70	54:40	3.30	1	43 ; 5.6
50	L-β-Leucine (L-β-Leu)	241*	156, 69, 198, 55, 59, 166, 139, 70	55:05	3.27	-	22 ; 2.9
53	D-Phenylalanine (D-Phe)	275	91, 162, 69, 65, 131, 103, 77, 51	74:40	0.09	NA	23 ; 3.8
54	L-Phenylalanine (L-Phe)	275	91, 162, 69, 65, 131, 103, 77, 51	74:55	0.01	-	23 ; 3.8

*Molecular ion not detected. **Molecular ion detection is unknown. NA – Not applicable. NF – Not found. ^aRetention time first dimension. ^bRetention time second dimension. ^cValues found for 10⁻⁶ M. ^dValues obtained when injected alone at 10⁻⁴ M. ^eUnexpected coelution or peak absence on one sample over eight.

3.2.1.4 Repeatability

The repeatability of the derivatization was evaluated for nine replicate samples at 5×10^{-5} M injected once. The relative standard deviation (RSD) for each amino acid is shown in **Table 14**. For most amino acids the RSD was found to be between 3 and 7%, although high values, above 30%, were found for both enantiomers of 2,3-Dap, Thr and, in particular, for Met (118.54 & 114.07%). The average mean values (M_s) of Thr and Met are rather small with 0.05 and 0.22, respectively, explaining the relative increased RSD values, whereas the high RSDs observed for 2,3-Dap are more puzzling. Indeed, 5-Ava with a M_s value of 0.64 similar to the one of 2,3-Dap exhibits a relative standard deviation of only 8.93%. 2,4-Dab, which also contains 2 amine groups like 2,3-Dap has a standard deviation of only 4.11%. In addition, Cys is detected *randomly* and is therefore not investigated further. This implies that the MeOH/TFAA derivatization for amino acids containing sulfur, hydroxyl group or 2 amino groups is not robust, and therefore less suitable. Nevertheless, these results testify that for most amino acids, MeOH/TFAA derivatization seems reliable despite the risk of compound loss due to the high volatility of the synthesized derivatives. Indeed, Iva and 2-Aib are the first compounds to elute and show standard deviations of 3–4% and 8.68% respectively.

Table 14. Repeatability tests on 9 samples analyzed once for each amino acid at 5×10^{-5} M.

Compound	S ^a (%)	M _s ^b	Compound	S ^a (%)	M _s ^b	Compound	S ^a (%)	M _s ^b
Gly	4.28	8.64	D-Glu	6.75	1.96	D-3-Aba	5.86	2.42
Sar	4.95	8.33	L-Glu	4.43	2.06	L-3-Aba	4.9	2.46
D-α-Ala	5.08	10.68	D-Met	118.54	0.22	4-Aba	6.67	1.43
L-α-Ala	4.42	10.48	L-Met	114.07	0.22	D-Asp + Asn	3.95	2.81
β-Ala	5.13	3.49	D-Ile	4.45	2.34	L-Asp + Asn	3.69	2.83
D-Cys	ND	ND	L-Ile	4.34	2.32	DL-2,4-Dab	6.84	4.11
L-Cys	ND	ND	D- <i>allo</i> -Ile	4.83	1.54	D-Thr	34.85	0.05
D-2,3-Dap	38.14	0.80	L- <i>allo</i> -Ile	4.71	1.47	L-Thr	38.45	0.05
L-2,3-Dap	31.6	0.86	D-Leu	4.98	1.91	D-Iva	5.99	3.99
Etg	4.84	4.49	L-Leu	2.93	1.91	L-Iva	5.98	3.28
2-Aib	4.94	8.68	D-Nle	4.4	2.31	D-Val	4.51	3.70
D-2-Aba	4.17	6.66	L-Nle	5.16	2.33	L-Val	4.15	3.76
L-2-Aba	5.15	6.92	D-β-Leu	5.23	1.88	D-Nva	4.2	3.36
D-3-Aib	4.99	2.25	L-β-Leu	5.9	1.88	L-Nva	5.16	3.32
L-3-Aib	6.13	2.35	DL-Phe	5.25	5.22	D-Pro	5.91	4.87
5-Ava	8.93	0.64				L-Pro	4.99	4.95

ND – Not detected. ^aRelative standard deviation. ^b Ratio of amino acid over internal standard area. Temperature program slightly different than the one used in **Table 13**.

3.2.1.5 Linearity

The calibration curves for the amino acids show similar sensitivity given the slope values in **Table 15**. Indeed, for each enantiomer except phenylalanine, the same order of magnitude is reported. This means

Table 15. Regression data of the MeOH/TFAA calibration curve.

#	Compound	S^a	ΔS^b	I^c	ΔI^d	R^2
1	Glycine	7.79×10^4	210	3.80×10^{-2}	5.27×10^{-3}	0.9999
2	Sarcosine	7.76×10^4	187	-2.38×10^{-5}	4.70×10^{-3}	0.9999
3	D- α -Alanine	8.69×10^4	86.4	-4.49×10^{-3}	2.17×10^{-3}	0.9999
4	L- α -Alanine	8.74×10^4	102	-2.42×10^{-3}	2.56×10^{-3}	0.9999
5	β -Alanine	2.20×10^4	214	-6.42×10^{-3}	5.37×10^{-3}	0.9998
6	D-Serine	4.67×10^4	634	-1.98×10^{-2}	1.59×10^{-2}	0.9996
7	L-Serine	4.13×10^4	307	-7.22×10^{-3}	7.71×10^{-3}	0.9998
8	D-Cysteine ^e	NA	NA	NA	NA	NA
9	L-Cysteine ^e	NA	NA	NA	NA	NA
10	D-2,3-Diaminopropionic acid	5.70×10^4	308	-1.08×10^{-2}	7.75×10^{-3}	0.9999
11	L-2,3-Diaminopropionic acid					
12	N-Ethylglycine	4.69×10^4	122	-4.42×10^{-3}	3.06×10^{-3}	0.9999
13	2-Aminoisobutyric acid	6.80×10^4	60.7	-3.6×10^{-3}	1.53×10^{-3}	0.9999
14	D-2-Aminobutyric acid	5.80×10^4	152	-5.97×10^{-3}	3.81×10^{-3}	0.9999
15	L-2-Aminobutyric acid	6.28×10^4	436	8.23×10^{-3}	1.10×10^{-2}	0.9999
16	D-3-Aminoisobutyric acid	2.64×10^4	65.8	-2.4×10^{-3}	1.65×10^{-3}	0.9999
17	L-3-Aminoisobutyric acid	3.33×10^4	523	-1.46×10^{-2}	1.31×10^{-2}	0.9995
18	D-3-Aminobutyric acid	3.50×10^4	479	-1.31×10^{-2}	1.20×10^{-2}	0.9996
19	L-3-Aminobutyric acid	3.25×10^4	439	-1.22×10^{-2}	1.10×10^{-2}	0.9996
20	4-Aminobutyric acid	2.68×10^4	192	-5.69×10^{-3}	4.82×10^{-3}	0.9998
21	D-Aspartic acid + Asparagine	5.09×10^4	274	-9.3×10^{-3}	6.87×10^{-3}	0.9999
22	L-Aspartic acid + Asparagine	4.21×10^4	623	1.47×10^{-2}	1.56×10^{-2}	0.9995
23	D-2,4-Diaminobutanoic acid ^f	9.54×10^4	6540	-1.52×10^{-1}	1.64×10^{-1}	0.9906
24	L-2,4-Diaminobutanoic acid ^f					
25	D-Threonine	3.87×10^4	56.3	-2.67×10^{-3}	1.41×10^{-3}	0.9999
26	L-Threonine	4.58×10^4	402	-1.18×10^{-2}	1.01×10^{-2}	0.9998
27	DL-Asparagine					
28	D-Isovaline	2.57×10^4	110	1.11×10^{-3}	2.75×10^{-3}	0.9999
29	L-Isovaline	2.99×10^4	71.5	1.59×10^{-4}	1.80×10^{-3}	0.9999
30	D-Valine	3.30×10^4	24.7	-1.37×10^{-3}	6.21×10^{-4}	0.9999
31	L-Valine	3.26×10^4	180	3.73×10^{-3}	4.51×10^{-3}	0.9999
32	D-Norvaline	3.72×10^4	30.5	-1.18×10^{-3}	7.66×10^{-4}	0.9999
33	L-Norvaline	3.79×10^4	197	-6.25×10^{-3}	4.94×10^{-3}	0.9999
34	D-Proline	6.60×10^4	275	-9.34×10^{-3}	6.92×10^{-3}	0.9999
35	L-Proline	6.91×10^4	326	-1.05×10^{-2}	8.20×10^{-3}	0.9999
36	5-Aminopentanoic acid	1.71×10^4	177	-4.95×10^{-3}	4.44×10^{-3}	0.9997
37	D-Glutamic acid	5.78×10^4	982	-2.71×10^{-2}	2.47×10^{-2}	0.9994
38	L-Glutamic acid	5.03×10^4	526	-1.4×10^{-2}	1.32×10^{-2}	0.9997
39	D-Methionine ^g	-	-	-	-	-
40	L-Methionine ^g	-	-	-	-	-
41	D-Isoleucine	2.65×10^4	54.8	4.06×10^{-4}	1.38×10^{-3}	0.9999
42	L-Isoleucine	2.68×10^4	40.6	2.32×10^{-4}	1.02×10^{-3}	0.9999
43	D- <i>allo</i> -Isoleucine	1.82×10^4	105	-3.54×10^{-3}	2.64×10^{-3}	0.9999
44	L- <i>allo</i> -Isoleucine	1.61×10^4	52.8	6.35×10^{-4}	1.33×10^{-3}	0.9999
45	D-Leucine	2.41×10^4	93.1	-3.29×10^{-3}	2.34×10^{-3}	0.9999
46	L-Leucine	2.40×10^4	87.3	-3.15×10^{-3}	2.19×10^{-3}	0.9999
47	D-Norleucine	3.41×10^4	340	-1.03×10^{-2}	8.55×10^{-3}	0.9998
48	L-Norleucine	3.40×10^4	449	-1.26×10^{-2}	1.13×10^{-2}	0.9996
49	D- β -Leucine	3.43×10^4	501	-1.43×10^{-2}	1.26×10^{-2}	0.9995
50	L- β -Leucine	3.27×10^4	647	-1.82×10^{-2}	1.63×10^{-2}	0.9992
53	D-Phenylalanine					
54	L-Phenylalanine	2.11×10^5	393	-1.16×10^{-2}	9.86×10^{-3}	0.9999

^aSlope. ^bStandard error on S. ^cIntercept. ^dStandard error on I. ^eNot detected. ^fOne concentration missing. ^gOnly found at highest concentration. Data obtained using 4 concentrations: 5×10^{-5} M, 5×10^{-6} M, 5×10^{-7} M, and 5×10^{-8} M. For each concentration, 3 samples were prepared and analyzed.

that derivatization does not discriminate amino acid conversion, which is convenient especially for Iva and 2-Aib, which are priority targets in the analysis of extraterrestrial samples. In addition, the coefficient of determination R^2 is generally greater than 0.999 although three orders of magnitude of concentration are used. This suggests a wide range of applications of the method. The R^2 is used as an indicator of linearity with visual observation of the residual plot. For each amino acid, although the number of data points is small – four concentrations injected each 3 times – the residual plot appears to show uniformly scattered values around the x-axis and thus no bias in the method. The alanine residual plot is available in **Figure S 1** (p. 162).

3.2.1.6 Limit of detection

Despite its clear definition, the practical way to determine the *limit of detection* (LOD) is controversial and ambiguous because several methods and terms can be confused. The LOD is often estimated from a single sample measurement where the peak intensity is three times above the background noise. However, because the detector response to an analyte is Gaussian in shape, it is necessary to account for measurement fluctuations and confidence intervals. The method detection limit (MDL) is therefore more appropriate for determining the LOD, especially when very low concentrations of the analytes are of interest. This is because by using this method, fluctuations in the response of the instrument and the derivatization procedure are taken into account. The MDL should not be confused with the instrument detection limit (IDL) where multiple re-injections of a sample are performed (IDL) instead of a single injection of multiple samples (MDL). Here, splitless mode is used to provide the best injection for trace analysis, and the use of an internal standard to correct for injection fluctuations. Statistically, since only a set of samples from the population is taken – meaning that only a few measurements are made – the mean and standard deviation values are only estimates. In the case of the detection limit where the fluctuations are of interest – which means that the standard deviation is of interest – one way to establish a confidence interval of the standard deviation is to use the values of the one-sided students' t-distribution. The MDL is expressed as follows in **Equation 4**.

$$\mathbf{MDL = } t_{\alpha} S_s \text{ (in counts or area) leading to } \mathbf{MDL = } t_{\alpha} R_s Q_s 10^{-2} \text{ (in g or in M)} \quad \mathbf{Equation 4}$$

t_{α} is the $n-1$ one-sided Students' t-distribution value associated to the confidence interval α (no unit)

S_s is the standard deviation of the n analyzed samples (in counts or area)

R_s is the relative standard deviation of the n analyzed samples (in %)

Q_s is the theoretical analyzed quantity (in g) or concentration (in M)

Another method, using calibration curve data – based on the standard deviation extrapolated from the y-intercepts of the regression line – can provide an MDL value but also requires the preparation of several samples. Estimating a LOD using MDL is time consuming but more relevant for trace analysis. The concentration chosen to determine the MDL should be close to the MDL itself, with a peak intensity at least 10 times higher than the background. Since 30 amino acids are used in this study, the MDL of all these amino acids is chosen to be calculated without necessarily optimizing the intensity of each peak. It should be kept in mind that the MDLs displayed here may be overestimated or underestimated because it is not possible to optimize the concentration for all amino acids. The results of the MDLs are shown in **Table 13**. Reagent blanks were performed using TFAA ampoules before performing MDL injections. Only potential trace amounts of alanine were found when reagent blanks were analyzed at high detector voltage (1800 V), indicating that the TFAA ampoule is suitable for trace analysis.

A set of 8 separate experiments was performed to have a statistically relevant MDL. Thus, the t_{α} value for 7 degrees of freedom and 99% confidence was set to 2.998. The values of R_s are summarized in **Table 16**. Q_s is the quantity – near the MDL – used to determine the MDL. As an example, injecting 1 μL of a 5×10^{-8} M solution of D-alanine corresponds to $Q_s = 5.10^{-8} \times 10^{-6} \times 89.09 \text{ g/mol} = 4.5 \text{ pg}$. Then, the D-Ala LOD = $2.998 \times 18.2 \times 4.5 \times 10^{-12} \times 0.01 \approx 2.46 \text{ pg}$ corresponding to $2.73 \times 10^{-8} \text{ M}$.

Table 16. Relative standard deviation of 8 samples analyzed once using 5×10^{-8} M of each amino acid.

Compound	R_s^a (%)	Compound	R_s^a (%)	Compound	R_s^a (%)
Gly	29.0	L-3-Aib	16.3	L-3-Aba	11.8
Sar	22.0	D-Glu	19.2	4-Aba	8.4
D- α -Ala	18.2	L-Glu	18.4	D-Asp	27.5
L- α -Ala	21.4	D-Met ^b	-	L-Asp	27.3
β -Ala	13.9	L-Met ^b	-	DL-2,4-Dab	23.7
D-Ser	18.8	D-Ileu	16.9	D-Thr	18.4
L-Ser	14.8	L-Ileu	21.2	L-Thr	16.7
D-Cys	ND	L- <i>allo</i> -Ileu	18.4	D-Iva ^d	41.3
L-Cys	ND	D-Leu	24.2	L-Iva ^d	40.5
D-2,3-Dap	30.0	L-Leu	16.8	D-Val	19.2
L-2,3-Dap	29.1	D-Nle	18.6	L-Val	27.8
Etg	20.4	L-Nle	20.1	D-Nva	20.7
2-Aib	18.9	D- β -Leu	28.7	L-Nva	29.0
D-2-Aba	26.5	L- β -Leu	14.5	D-Pro	16.1
L-2-Aba	24.7	DL-Phe	15.4	L-Pro	16.2
D-3-Aib	15.4	D-3-Aba ^c	29.7	5-Ava	ND

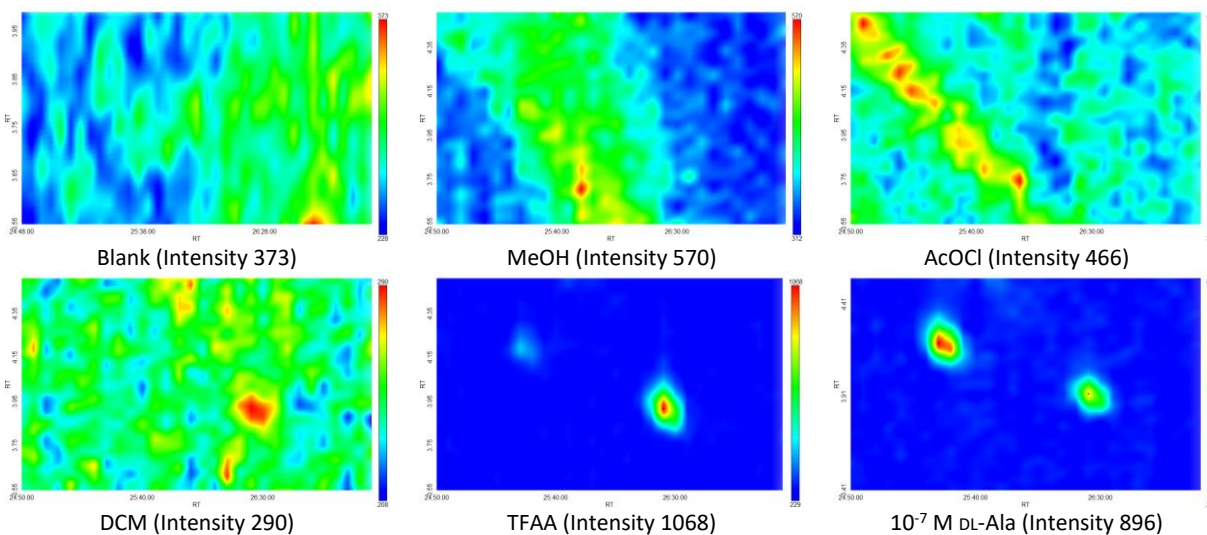
^aRelative standard deviation. ^bOnly detected in two samples. ^cUnexpected coelution with unknown compound on one sample.

^dPeak absence on one sample. ND – Not detected.

CONTAMINATION

In this study, experiments conducted to determine the detection limit of alanine showed that both the D and L forms of alanine were found, with a significant enantiomeric excess of the L enantiomer, as well as a very low detectability. This led to the consideration that contamination was likely. Free or polymerized alanine was investigated in methanol, acetyl chloride, dichloromethane and TFAA by derivatization of *N*(*O,S*)-ethoxy-carbonylheptafluorobutylester (ECHFBE). Since the detected alanine was fully derivatized, the first step reagents, methanol (MeOH) and acetyl chloride (AcOCl), were investigated for potential traces of free or polymerized alanine. 2 mL of each reagent were dried and derivatized to look for free alanine. Moreover, 2 mL of each reagent were dried and then hydrolyzed for 1 hour using a mixture of 200 μ L H₂O/AcOCl (4:1, v:v) at 110 °C to cleave potential traces of polyaniline followed by the ECHFBE derivatization. H₂O/AcOCl, like MeOH/AcOCl, forms hydrochloric acid (HCl) *in situ* which is required for the first esterification step of the MeOH/TFAA derivatization. The ECHFBE derivatization, which has been shown not to contain alanine (**Table 17**), was used. Indeed, the blank of the ECHFBE reagents showed no alanine presence, meaning that any alanine contamination from these reagents does not fall within the detection range of the instrument.

Table 17. Investigation of alanine contamination using 2 mL of dried reagent, hydrolyzed with H₂O/AcOCl and derivatized as ECHFBE derivatives. The ion *m/z* = 116, corresponding to the most intense alanine fragment, is displayed. A blank and a 10⁻⁷ M DL-alanine sample are also provided. The maximum intensity is also reported.



Surprisingly, neither MeOH nor AcOCl revealed free or polyaniline after derivatization (**Table 17**). The same search for free and polyaniline was performed on DCM and TFAA. The results showed that hydrolyzed TFAA contains a huge excess of L-alanine while unhydrolyzed TFAA shows no trace of alanine.

As expected, other proteinogenic amino acids such as phenylalanine, methionine or valine were found while *N*-ethylglycine – a non-proteinogenic amino acid – for example was not detected. It is interesting to note, that it is in the second step of the MeOH/TFAA derivatization – at 100 °C for 20 minutes – that alanine is released. For this to happen, an acidic medium is required. Since the reaction medium from the first step is very difficult to remove – it contains methanol, acetyl chloride, HCl, and methyl acetate – it is likely that HCl is still trapped in the remaining droplets and/or on the glass walls of the reaction vial and capable to hydrolyze alanine present in TFAA. Another explanation would be the presence of trifluoroacetic acid due to the reaction of TFAA and water in the atmosphere.

QUANTIFICATION OF ALANINE IN TFAA

Estimation of TFAA contamination was performed using an ECHFBE calibration of alanine, **Figure 35**. Five standards containing 10^{-5} , 5×10^{-6} , 10^{-6} , 5×10^{-7} and 2×10^{-7} M of each enantiomer of alanine were used. The calibration curve is shown below and includes hydrolyzed TFAA₁. Three different grades of TFAA were studied and analyzed at a high detector voltage of 1800 V. A few milliliters of each TFAA were dried, hydrolyzed as described above, and derivatized with ECHFBE. The important information is the order of magnitude of the contamination, which ranges from 10^{-8} to 10^{-10} M depending on the grade, **Table 18**. It is interesting to note, that the lowest contamination is obtained using TFAA in ampoules.

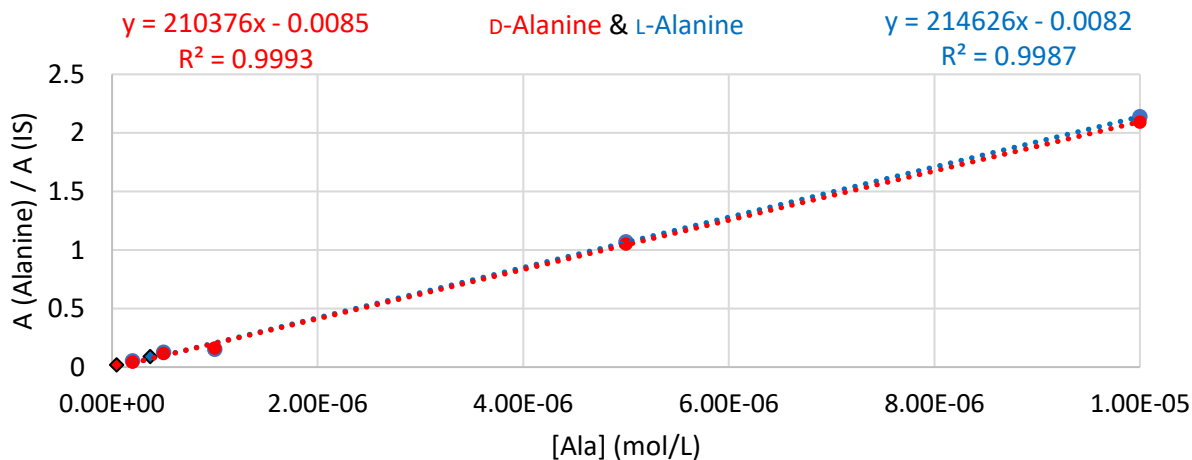


Figure 35. Calibration curve for *D*-Alanine and *L*-Alanine using ECHFBE derivatization. The small diamond on the calibration curve represents the concentration of alanine found in the TFAA₁ sample, 3.7×10^{-7} M.

Table 18. Alanine contamination in three different grades of TFAA.

	[D-Ala] (M)	[L-Ala] (M)	Sigma Reference
TFAA ₁	6.7×10 ⁻¹⁰	5.4 × 10 ⁻⁹	106232 - 25g
TFAA ₂	5.3×10 ⁻⁹	1.6 × 10 ⁻⁸	91719 - 10 × 1mL
TFAA ₃	NF	1.4 × 10 ⁻¹⁰	106232 - 10 × 1g

Since 4.7 mL were dried and analyzed in an approximately total volume of 69 μ L (50 μ L chloroform + 19 μ L 2,2,3,3,4,4,4-heptafluorobutanol), the actual concentration of L-alanine in TFAA₁ is calculated by **Equation 5**.

$$[\text{L-Ala}]_{\text{TFAA}_1} = \frac{[\text{L-Ala}]_{\text{TFAA}}^{\text{sample}} \times V_{\text{Analyzed}}}{V_{\text{TFAA}}} = \frac{3.7 \times 10^{-7} \times 0.069}{4.7} = 5.4 \times 10^{-9} \text{ M} \quad \text{Equation 5}$$

This contamination report is only an estimate of the actual alanine contamination because some of the concentrations were calculated by extrapolation to concentrations outside the linear range of the calibration curve.

OTHER PROTEINOGENIC AMINO ACID CONTAMINATION

Other amino acids were investigated, particularly in the most contaminated TFAA₂ where they are easier to detect. The presence of proteinogenic amino acids such as alanine, glycine, phenylalanine, glutamic acid, isoleucine, leucine, aspartic acid, proline was confirmed. We believe it is similar for the TFAA₃ (ampoule), because at least some of these amino acids including phenylalanine, alanine, glycine, and aspartic acid were found. Those amino acids are however not found when using the required 200 μ L of DCM/TFAA (4:1) (v:v).

3.2.1.7 Enantiomeric excess conservation

The enantiomeric excess (*ee*) is defined as the excess of one enantiomer over the other in a mixture of enantiomers. Thus, racemic mixtures have an *ee* equal to 0% while enantiopure compounds have an *ee* equal to 100%. In practice, when determining an *ee* using GC×GC, two limitations can be highlighted. The first concerns the purity of the standard used, which may be due either to the manufacturer's *ee* determination or to the evolution of the standard's *ee* over time. The second concerns artifacts and instrument limitations. Response variations between enantiomers, co-eluting impurities, lack of enantioresolution, or peak tailing can lead to an inaccurate determination of the absolute *ee* of the sample.

Thus, investigations of an apparent 5% ee_L using GC×GC was conducted by comparing the response of the racemic standard against a standard solution doped with 5% of the L-amino acid enantiomer. To determine the ees reliably and account for procedural and measurement fluctuations, 3 samples were derivatized and injected 3 times each.

Generally speaking, increasing the concentration leads to increased accuracy of the determined ee , as measurement fluctuations and integration errors are reduced. Thus, the S/N ratio is an important parameter that correlates with the determination of ee accuracy. **Figure 36**, reports the evolution of ee_L at four different concentrations and for 5 amino acids: 2,3-Dap, Ala, Glu, Iva and Pro. As expected, the standard deviation tends to be reduced at higher concentrations and ranges between $\pm 0.45\%$ and $\pm 1.07\%$ for the amino acids studied at 10^{-5} M. The accuracy of the ee at this concentration, on the other hand, is greater than 93.4% (Ala) for the amino acids studied except for Glu, with 82.8%. As calculated in **Table 3** (p. 24), the concentrations of amino acids in 1 g of the Murchison meteorite are between 10^{-5} and 10^{-4} M and are therefore sufficient for the accurate and precise determination of potential ees in 2,3-Dap, Ala, Iva and Pro. The most striking results are the huge standard deviations and lack of precision at 10^{-7} M, which is close to the detection limit of the method. Instead of obtaining ee_L of about 5%, negative values can be obtained for Ala and Glu, as well as standard deviations of up to $\pm 9.20\%$ for 2,3-Dap.

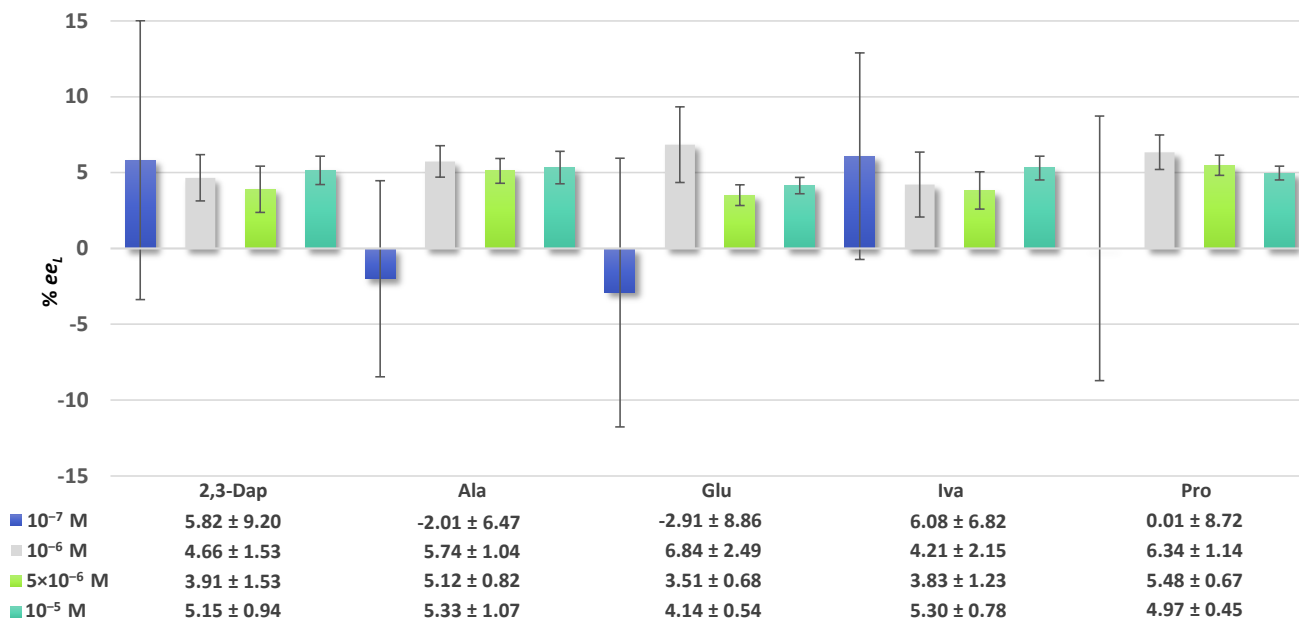


Figure 36. Evolution of ee over four concentrations of five 5% L-doped amino acids.

3.2.1.8 Stability

Stability regarding decomposition and/or evaporation of the derivatives was studied after 7 days. The derivatized sample was stored in a refrigerator at 4 °C. Three injections were performed before and after 7 days. Overall recoveries were generally between 80 and 100%, as shown in **Table 19**. The most volatile derivatives, i.e., the first third of the chromatogram, are closer to a recovery value of 80-90% than the other derivatives. The less volatile derivatives are closer to a recovery value of 90-100%. There are exceptions, however. Methionine has a recovery of only 50-55% despite its late elution time. This suggests, as mentioned in **3.2.1.4 Repeatability**, that the sulfur-containing derivatives, methionine, and cysteine, tend to decompose. Indeed, this may be particularly the case for cysteine because it is known that the *O*-trifluoroacetyl group is less stable than the *N*-trifluoroacetyl group towards hydrolysis²⁵⁹, meaning that the *S*-trifluoroacetyl group of cysteine is even more sensitive. Cysteine can form a dimer, cystine, through a disulfide bond that can prevent its detection as cysteine. However, tests on both cysteine and cystine standards did not show any dimerization of cysteine. Another example, serine, containing an *O*-trifluoroacetyl group, showed a good recovery of 100-110% but with a significant standard deviation of 20-25%.

Table 19. Recovery tests after 7 days using 5×10^{-5} M for each amino acid.

Compound	R ^a (%)	± (%) ^b	Compound	R ^a (%)	± (%) ^b	Compound	R ^a (%)	± (%) ^b
Gly	85.0	2.4	L-3-Aib	88.3	2.0	L-3-Aba	87.6	2.0
Sar	73.1	2.6	D-Glu	99.4	1.5	4-Aba	97.9	1.6
D-α-Ala	80.2	3.8	L-Glu	99.4	2.2	D-Asp	97.2	2.3
L-α-Ala	82.2	4.3	D-Met	52.4	3.2	L-Asp	97.4	1.8
β-Ala	97.8	2.3	L-Met	56.3	4.2	DL-2,4-Dab	103.8	7.3
D-Ser	99.8	19.6	D-Ileu	88.0	3.7	D-Thr	91.2	2.0
L-Ser	110.1	24.1	L-Ileu	93.7	3.7	L-Thr	80.3	4.6
D-Cys	ND	ND	L- <i>allo</i> -Ileu	82.2	2.7	D-Iva	79.8	5.1
L-Cys	ND	ND	D-Leu	86.5	3.7	L-Iva	86.6	5.1
D-2,3-Dap	104.1	6.7	L-Leu	79.1	2.5	D-Val	82.5	4.5
L-2,3-Dap	97.7	5.6	D-Nle	89.3	4.7	L-Val	86.4	4.4
Etg	86.5	3.1	L-Nle	88.1	3.5	D-Nva	86.7	3.0
2-Aib	77.6	4.5	DL-β-Leu	86.8	9.4	L-Nva	90.7	2.5
D-2-Aba	82.8	3.9	DL-Phe	100.5	2.7	D-Pro	89.6	2.9
L-2-Aba	82.7	4.1	D-3-Aba	80.1	5.9	L-Pro	98.9	2.8
D-3-Aib	93.1	3.3				5-Ava	80.1	5.9

^aRecoveries: ratio between samples at day 7 over day 0. ^bSamples analyzed three times at day 0, and three times at day 7. ND – Not detected.

3.2.1.9 Conclusion

MeOH/TFAA derivatization proves to be a convenient and powerful procedure to separate and enantioseparate most of the 30 amino acids used in this study when coupled to a GC×GC apparatus using a Lipodex E column in the 1st dimension. The utility of GC×GC is highlighted by the resolution of the 2nd column which avoids coelution of target analytes, outlying derivatization byproducts and lowers the detection limits of the method. For most amino acids, the following data are reported: method detection limit in the picogram range, relative standard deviation between 3-9%, standard deviation of enantiomeric excess in the 1% range at 10⁻⁵ M, and stability of derivatives after 7 days of 80-100%. Linearity is also evaluated over several orders of magnitude, from 5×10⁻⁸ M to 5×10⁻⁵ M. In addition, the first comprehensive listing of the mass spectrum of the *N*-trifluoroacetyl amino acid methyl ester allows for unambiguous identification of each amino acid. To compensate for the lack of resolution of a few targeted amino acids, a Chirasil-Dex column can be successfully used to complete the data set. As the derivatives have proven to be stable, it may be convenient and worthwhile to switch columns to obtain a thorough separation of targeted derivatives. This derivatization can find many applications in bioanalytical science but aims to be employed for extraterrestrial samples because of the previously mentioned advantages.

3.2.2 MBA/TFAA derivatization of sugars & sugar related compounds

3.2.2.1 Materials and methods

3.2.2.1.1 Reagents

Standards and reagents used in this study were purchased from Sigma-Aldrich, Fluka, or Acros Organics. The purity of DL and L sugars was greater than 98% in all cases. Water used for tool cleaning and sample processing was obtained using a Milli-Q Direct 8 apparatus (18.2 MΩ.cm at 25 °C, < 5 ppb total organic carbon). All glassware was washed several times with ethanol and Milli-Q water, wrapped in aluminum foil, and then heated to 500 °C for at least 5 h to remove any organic contaminants. PTFE-lined lids and caps were washed the same way. Biopur pipette tips and GC×GC vial inserts were used without further cleaning. To prepare the sugar stock solution, individual sugars were weighed, mixed, dissolved in Milli-Q water, and then merged into a single solution. The concentration of the sugars was corrected depending on the purity of the standard.

3.2.2.1.2 Derivatization

Diluted series of the sugar stock solutions were dried under a gentle flow of nitrogen until the water was completely removed. 50 μL of a 10 mg/mL methylboronic acid solution in pyridine was added, stirred for 10 seconds, and held at 60 $^{\circ}\text{C}$ for 30 minutes. The samples were then allowed to cool to room temperature for 2 minutes and carefully dried under nitrogen for approximately 40 to 50 minutes. 50 μL of a 1:1 (v:v) mixture of trifluoroacetic anhydride and ethyl acetate was added, stirred for 10 seconds and held at room temperature for 1 h. The samples were finally thoroughly dried under nitrogen and dissolved in 50 μL of ethyl acetate containing 10^{-6} M methyl myristate as an internal standard.

3.2.2.1.3 GC \times GC-TOFMS

Enantioselective analysis was performed using a GC \times GC Pegasus IV D instrument coupled to a time-of-flight mass spectrometer (LECO, St Joseph, Michigan, USA). The MS system was operated at a storage rate of 100 Hz, with a mass range of 25 to 400 amu. The detector voltage was set to 1650 V with a solvent delay of 12 minutes. The temperature of the ion source and injector was 230 $^{\circ}\text{C}$. A CP-Chirasil-Dex CB column (24.55 m \times 0.25 mm, film thickness 0.25 μm , Agilent-Varian, Santa Clara, California, USA) in the first dimension coupled with a DB Wax column (1.55 m \times 0.1 mm, film thickness 0.1 μm) in the second dimension were used. Modulation between the columns was provided by a two-stage thermal jet modulator using liquid nitrogen. Helium was used as the carrier gas at a constant flow rate of 1.2 mL/min. Samples were injected in splitless mode, and the MS transfer line was maintained at 240 $^{\circ}\text{C}$ during analyses. A modulation period of 5 s was applied. The temperature of the primary column was held at 55 $^{\circ}\text{C}$ for 1 min, then increased to 85 $^{\circ}\text{C}$ at a rate of 10 $^{\circ}\text{C}/\text{min}$ and held for 8 min. It was then increased to 125 $^{\circ}\text{C}$ at a rate of 2 $^{\circ}\text{C}/\text{min}$, then at a rate of 2 $^{\circ}\text{C}/\text{min}$ to 170 $^{\circ}\text{C}$. It finally reached 190 $^{\circ}\text{C}$ at a rate of 10 $^{\circ}\text{C}/\text{min}$ and was held at that temperature for 5 min. The secondary oven used a constant temperature offset of 25 $^{\circ}\text{C}$. The modulator temperature was set 15 $^{\circ}\text{C}$ higher than the secondary oven. Depending on the purpose of the experiment, samples were injected multiple times in order to calculate peak areas with reliable statistical error bars. ChromaTOFTM software from LECO Corp. was used to quantify the analytes. The integration range during quantification was manually changed, when necessary, to correct the automatic data processing by the software.

3.2.2.2 *Identification of sugars and sugar related compounds*

Previous experiments performed in the team allowed to easily identify most sugars as methylboronic ester derivatives thanks to their mass spectra and retention times such as glyceraldehyde, arabinose, xylose,

ribose and lyxose. However, several C₆ sugars such as glucose and galactose are not detected because of their free hydroxyl group. Interestingly, this is not necessarily the case for erythrose and 2-deoxyribose which also have a free hydroxyl group. Both, however, have lower detection limits, by about an order of magnitude. One solution to overcome this difficulty is to use acylation as a second derivatization step. This step significantly decreases the intensity of the derivatives using MBA only but could provide access to other classes of compounds such as sugar alcohols. However, this specific method has not been explored for this purpose, but it can be mentioned that S. Manhas *et al.*²⁶⁰ successfully used phenylboronic acid on glycerol, xylitol, ribitol, and L-arabitol to selectively protect diols for selective Fischer esterification. As pointed out by Van Dongen *et al.*²⁰⁴ using MBA/BSTFA for sugars, the difference in yield between monosaccharides could be due to the distance between the hydroxyl groups involved by the stereochemistry of the molecules²⁶¹. However, it seems that this stereochemistry leads to a unique sugar derivative because the authors report the appearance of several byproducts with prolonged reaction times with BSTFA. It then becomes clear that sugars and polyols with an even number of alcohols cannot necessarily be fully derivatized with MBA alone because the distance between the alcohols may be different depending on the alcohol conformer. They could be fully derivatized from MBA, fully derivatized from TFA, or lead to many MBA/TFA possibilities. This results in difficulties when trying to identify them using their mass spectra. Finally, sugar acids such as glyceric acid, threonic acid, erythronic acid, and gluconic acid were derivatized using MBA and MBA/TFAA but not detected. The mass spectra of the studied samples are available in **Table S 2** (p. 163), and data on the characteristics ions, and retention times are reported in **Table 20**.

3.2.2.2.1 Sugars

Glyceraldehyde, ribose, arabinose, xylose, and lyxose were previously identified as MBA derivatives, whereas galactose, glucose, and mannose were previously identified as MBA/TFA derivatives. Interestingly, lyxose showed two distinct peaks corresponding to either two MBA rings or an MBA ring with two TFA groups. A significant D-enantiomeric excess was used to confirm these two peaks. Van Dongen *et al.*²⁰⁴ reported only the latter while both coexist. It would seem natural for xylose to have the same two peaks, but only one form with two MBA rings was observed. This reinforces the scenario in which the conformation of the molecule plays a major role for the derivatives formed. Erythrose and 2-deoxyribose were identified as MBA derivatives, but the remaining alcohol would now be a TFA group thus changing the retention time and mass spectrum. Compared to the MBA derivative, 2-deoxyribose showed an intense $m/z = 69$ characteristic of TFA, but also two other ions, 140 and 224. The ion 85, on

Table 20. Characterization of MBA/TFAA sugar derivatives by mass spectra and retention time.

#	Compound	[M]**	Characteristic ions, <i>m/z</i>	<i>R</i> _{t1} ^a [min:sec]	<i>R</i> _{t2} ^b [sec]
1	Glycerol	380	69 (99.8) 153 (17.2) 43 (13.1) 97(12.1) 59 (11.7) 125 (6.7) 267 (1.0)	19:00	2.36
2	L-Glyceraldehyde	114	43 (99.8) 113 (95.7) 44 (70) 85 (53.5) 42 (50.7) 112 (45.3) 84 (37.6)	21:45	2.48
3	D-Glyceraldehyde	114	43 (99.8) 113 (95.7) 44 (70) 85 (53.5) 42 (50.7) 112 (45.3) 84 (37.6)	22:20	2.42
4	D-Erythrose	240	97 (99.9) 43 (72.9) 98 (48.9) 69 (39.8) 29 (23.6) 85 (23.1) 127 (22.5)	23:50	1.91
5	L-Erythrose*	240	97 (99.9) 43 (72.9) 98 (48.9) 69 (39.8) 29 (23.6) 85 (23.1) 127 (22.5)	23:05	2.14
6	1,3-Dihydroxyacetone	282	69 (99.8) 99 (30.3) 127 (27.4) 155 (12.9) 97 (99.8) 69 (83.2) 43 (31.3) 96 (25.5) 88 (20.5) 111 (10.7) 182 (2.3)	24:20	3.61
7	D-Threitol	338	97 (99.8) 69 (83.2) 43 (31.3) 96 (25.5) 88 (20.5) 111 (10.7) 182 (2.3)	27:20	2.44
8	L-Threitol	338	97 (99.8) 69 (83.2) 43 (31.3) 96 (25.5) 88 (20.5) 111 (10.7) 182 (2.3)	28:20	2.26
9	Erythritol	338	97 (99.8) 69 (94.5) 43 (34.4) 88 (26.8) 96 (24.6) 110 (13.3) 182 (2.4)	28:55	2.42
10	D-2-Deoxyribose	254	43 (99.9) 69 (85.2) 97 (32.2) 140 (22.0) 224 (4.2)	32:20	2.23
11	L-2-Deoxyribose	254	43 (99.9) 69 (85.2) 97 (32.2) 140 (22.0) 224 (4.2)	35:05	2.23
12	D-Lyxose (peak 1)	366	69 (99.8) 97 (57.0) 43 (42.8) 110 (37.5) 253 (5.0) 139 (4.7) 252 (4.1)	36:00	2.60
13	L-Lyxose (peak 1)	366	69 (99.8) 97 (57.0) 43 (42.8) 110 (37.5) 253 (5.0) 139 (4.7) 252 (4.1)	37:50	2.62
14	Xylitol	296	97 (99.8) 98 (87.5) 85 (85.2) 43 (56.5) 69 (50.7) 84 (32.1) 140 (5.5) 182 (2.1)	39:20	4.29
15	Adonitol	296	85 (99.9) 97 (86.3) 43 (73.5) 69 (55.3) 98 (43.6) 110 (23.1) 140 (9.3) 182 (4.9) 236 (1.3)	39:45	2.64
16	D-Arabitol	296	97 (99.8) 98 (85.0) 43 (68.8) 85 (67.8) 69 (50.0) 110 (17.0) 140 (8.6) 182 (3.6) 236 (1.0)	40:55	3.75
17	L-Arabitol	296	97 (99.8) 98 (85.0) 43 (68.8) 85 (67.8) 69 (50.0) 110 (17.0) 140 (8.6) 182 (3.6) 236 (1.0)	43:00	3.28
18	L-Arabinose	198	84 (99.8) 43 (34.4) 97 (26.7) 83 (26.2) 110 (20.8) 198 (0.5)	42:20	3.22
19	D-Arabinose	198	84 (99.8) 43 (34.4) 97 (26.7) 83 (26.2) 110 (20.8) 198 (0.5)	43:20	3.06
20	D-Xylose	198	97 (99.9) 84 (91.3) 43 (90.3) 110 (43.3) 85 (38.2) 139 (7.8) 126 (5.8) 168 (3.6)	44:20	3.52
21	L-Xylose	198	97 (99.9) 84 (91.3) 43 (90.3) 110 (43.3) 85 (38.2) 139 (7.8) 126 (5.8) 168 (3.6)	45:45	3.28
22	L-Ribose	198	84 (99.9) 97 (65.6) 43 (55.2) 110 (39.8) 139 (1.4) 152 (0.7)	47:05	3.33
23	D-Ribose	198	84 (99.9) 97 (65.6) 43 (55.2) 110 (39.8) 139 (1.4) 152 (0.7)	47:30	3.27
24	D-Mannose	324	85 (99.8) 84 (42.4) 97 (32.5) 43 (30.6) 69 (26.2) 127 (7.3) 210 (1.8) 182 (1.4)	49:05	3.16
25	D-Galactose	324	84 (99.8) 83 (24.2) 43 (20.8) 69 (15.1) 97 (13.3) 113 (4.7) 167 (0.9) 210 (0.7)	50:55	2.88
26	L-Galactose	324	84 (99.8) 83 (24.2) 43 (20.8) 69 (15.1) 97 (13.3) 113 (4.7) 167 (0.9) 210 (0.7)	54:55	2.42
27	L-Lyxose (peak 2)	198	97 (99.8) 43 (71.5) 84 (46.5) 110 (26.0) 139 (8.3) 126 (8.1) 168 (2.9)	51:40	4.34
28	D-Lyxose (peak 2)	198	97 (99.8) 43 (71.5) 84 (46.5) 110 (26.0) 139 (8.3) 126 (8.1) 168 (2.9)	52:10	4.22
29	L-Glucose	324	97 (99.8) 43 (75.4) 84 (55.5) 69 (48.7) 126 (41.6) 167 (7.7) 240 (6.5) 295 (1.3)	54:20	3.25
30	D-Glucose	324	97 (99.8) 43 (75.4) 84 (55.5) 69 (48.7) 126 (41.6) 167 (7.7) 240 (6.5) 295 (1.3)	54:50	3.16
31	Sorbitol (peak 1)	254	85 (99.9) 84 (35.1) 43 (20.7) 57 (14.8) 169 (4.2) 110 (4.1)	50:55	3.25
32	Sorbitol (peak 2)	254	85 (99.9) 97 (56.5) 84 (54.2) 43 (42.5) 57 (20.3) 69 (6.9) 110 (6.8) 169 (6.3)	50:50	0.01
33	Dulcitol (peak 1)	254	85 (99.9) 97 (58.6) 84 (49.3) 43 (45.0) 98 (22.0) 169 (6.7) 110 (5.9)	55:25	3.66
34	Dulcitol (peak 2)	422	97 (99.9) 69 (26.8) 96 (26.2) 43 (17.0) 98 (5.4) 211 (2.6) 295 (0.4)	48:05	2.72
35	L-Fructose*	324	97 (99.9) 69 (60.5) 43 (59.1) 110 (48.5) 84 (35.6) 197 (13.3) 155 (12.1) 127 (8.2)	46:50	2.96
36	D-Fructose*	324	97 (99.9) 69 (60.5) 43 (59.1) 110 (48.5) 84 (35.6) 197 (13.3) 155 (12.1) 127 (8.2)	48:10	2.79
37	L-Ribulose*	198	97 (99.8) 98 (55.7) 43 (54.6) 55 (19.8) 126 (10.2) 168 (5.7) 138 (3.8)	31:40	2.35
38	D-Ribulose*	198	97 (99.8) 98 (55.7) 43 (54.6) 55 (19.8) 126 (10.2) 168 (5.7) 138 (3.8)	32:45	2.29
39	Glycoaldehyde	198	43 (99.9) 113 (52.2) 112 (28.4) 85 (26.8) 84 (17.0) 69 (10.7)	< 12:00	-

*Retention times deducted from sample run as standards were not available during the experiment. Molecular ions were calculated assuming fully MBA and/or TFAA derivatized compounds.

the other hand, has faded. In the case of erythrose, the fragmentation pathways changed significantly with the addition of TFA. The only remaining common ion is $m/z = 85$ and it is now faint compared to $m/z = 43, 69$ and 97 .

3.2.2.2.2 Sugar alcohols

Glycerol, ethylene glycol, threitol, erythritol, arabitol, xylitol, adonitol, sorbitol, dulcitol, dihydroxyacetone, and glycolaldehyde dimer were studied. Ethylene glycol was not found but could elute very early, which explains its absence. Dihydroxyacetone and glycerol were only found as TFAA derivatives, which could be explained by the lack of conformational hindrance preventing MBA from derivatizing the two alcohol groups. Surprisingly, glycolaldehyde was found as a dimer and derivatized by MBA. As a dimer, its structure is very similar to that of glycerol, and one would expect similar reactivity. Its mass spectrum is close to glyceraldehyde with major fragment ions $43, 113$ and 85 , but their $m/z = 113$ fragmentation is different.

The structure of the following sugar alcohol derivatives is not fully elucidated but can be described in terms of MBA rings and TFA-derivatized hydroxyl numbers. Threitol and erythritol have identical mass spectra and correspond to a single MBA ring and TFA groups. It is likely that the MBA ring is located on centered hydroxyls because no $m/z = 85$ or 84 is observed. The major fragments are $m/z = 97, 69, 43$ and $m/z = 88, 110$ and 182 are characteristic of these C_4 sugar alcohols. Arabitol and xylitol have identical and similar mass spectra to adonitol. The mass spectra show the same major and characteristic ions as the C_4 sugar alcohols (the 88 ion is *replaced* by the 140 ion) but also show strong $m/z = 84, 85$, and 98 ions. Since the 85 and 97 ions are strongly represented in these C_5 sugar alcohols, it can be assumed that these compounds are derivatized as two 5-atom MBA rings and a TFA group. Interestingly, adonitol revealed the presence of 2 peaks with a similar mass spectrum reminiscent of a pair of enantiomers. Since it is a *meso* compound, the presence of MBA rings connecting the hydroxyls is likely to result in optical stereoisomers. The C_6 sugar alcohols, sorbitol and dulcitol, each show two peaks. The mass spectra of both sorbitol peaks are similar, while one of the dulcitol peaks resembles that of sorbitol and the other is faintly reminiscent of the C_4 sugar alcohols. The major fragments are $m/z = 85, 97$ and 43 and no $m/z = 69$ is observed. This suggests that all hydroxyls are derivatives of MBA. It is not clear whether the derivative consists of two 6-atom MBA rings and one 5-atom MBA ring or three 5-atom MBA rings. However, in the case of sorbitol, the first peak has stronger $m/z = 43$ and 97 and is therefore more likely to be representative of two 6-atom MBA rings and one 5-atom MBA ring, as fragmentation would more easily

lead to a charged 6-atom MBA ring with $m/z = 97$. In the case of dulcitol, these mass spectral characteristics are represented in the second peak. Concerning the first peak of dulcitol, no conclusion can be drawn on the structure of the derivative but the presence of at least 2 TFA groups given the intensity of $m/z = 69$ is suggested.

Interestingly, all sugar alcohols showed a significant tailing and peak width in the chromatogram, which increases with carbon number. At first glance, this should indicate the presence of underivatized hydroxyl(s) leading to undesired interactions with the capillary column. However, the relatively high intensities of $m/z = 69$ in some sugar alcohols (arabitol, erythritol, xylitol, adonitol) tend to consider the derivatives as TFA derivatives (apart from MBA) which is more consistent with the observed fragmentations. Then, the reasons why sugar alcohols tail remain unknown. Investigations to determine a more accurate structure could be performed at a lower ionization energy. Soft ionization could allow for better observation of higher m/z including the molecular ion.

3.2.2.3 Overall resolution and enantioseparation

Figure 37 shows that enantioseparation is achieved for all the compounds studied, and that a good overall separation can be obtained using the program provided. The only difficulty was found for the separation of fructose and dulcitol (peak 2), but this can be overcome by selecting an appropriate m/z for quantification. Regarding the order of elution, a certain trend can be noticed for erythrose, arabinose, ribose, and glucose, which share the same carbon configuration (except for the penultimate one) and whose L-enantiomer elutes before the D-enantiomer (**Figure 15**, p. 47). Similarly, xylose, lyxose (peak 1) and galactose have the D-enantiomer eluting before the L-enantiomer. In addition, the two ketoses, fructose and ribulose, show the same elution order (**Figure 16**, p. 47). Unfortunately, more data would be needed to confirm such a trend. As mentioned earlier, sugar alcohols are generally tailing, which can generate additional coelutions with non-target compounds. Moreover, the detectability and accuracy of the integrated area is reduced. Calibration curve data is available **Table S 3** (p. 167).

3.2.2.4 Conclusion

Although this method has not been studied as extensively as the MeOH/TFAA method described previously, several advantages can be highlighted. The separation and enantioseparation of sugars and sugar alcohols is efficient, except for fructose and dulcitol. The derivatization temperature is quite low with 60 °C and identical to the (S)-BuOH/TFAA method, which minimizes potential racemization and

degradation of sugars. Sugars, sugar alcohols, and deoxy sugars can be detected and quantified with this method, which is not the case for sugar acids. However, many sugar alcohols suffer from a significant tail in the first dimension that could prevent detection and/or quantification. This method was specifically designed for the study of sugars and sugar alcohols synthesized under hydrothermal conditions in a formose-type reaction (**4.2 Mineral-catalyzed formose reaction under hydrothermal conditions**). It can also be applied to extraterrestrial samples but suffers from higher limit of detections for C₃ to C₅ sugars compared to other sugar derivatization protocols.

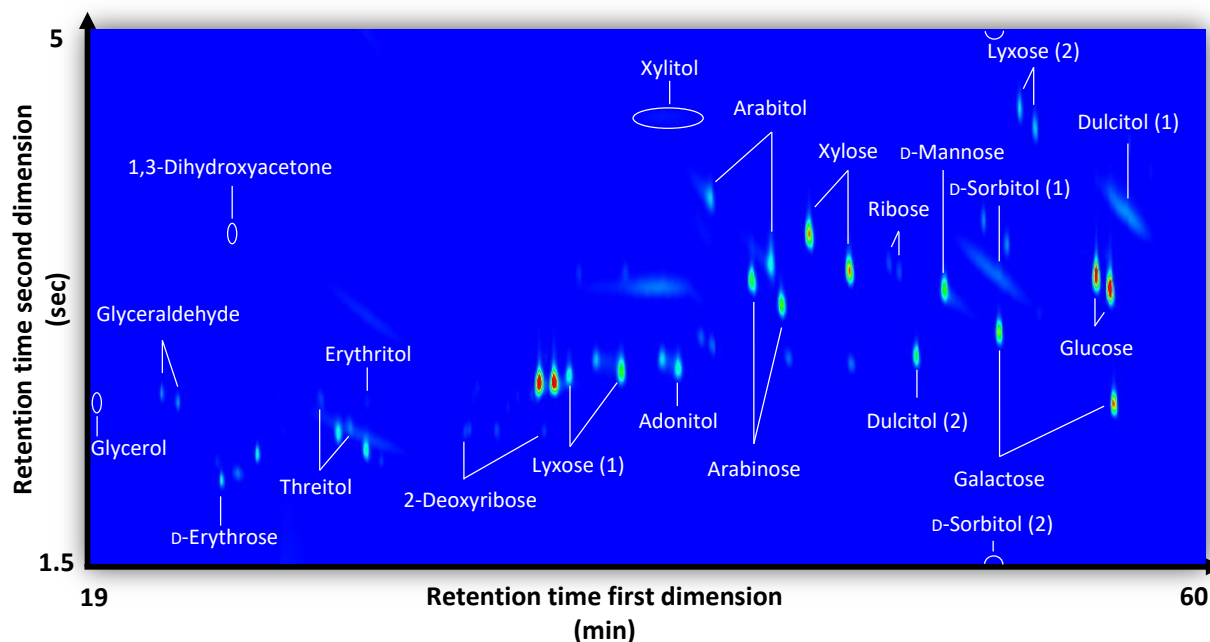


Figure 37. Two-dimensional chromatogram of MBA/TFAA derivatized sugars analyzed on a CP-Chirasil-Dex CB coupled to a DB-WAX column.

3.3 PURIFICATION & FRACTIONATION

3.3.1 Materials & methods

3.3.1.1 Materials & Reagents

The ion exchange chromatography (IEC) resin used was a BT AG® 50W-X8 biotech grade, 100-200 mesh in the H⁺ form from Bio-Rad. A Supelco Visiprep 12 DL vacuum manifold, and a KNF Laboport N 86 pump were used to elute the IEC solvents through disposable PTFE flow control valve packings from Supelco. Glass tubes (6 mL) and PTFE frits with 20 μm porosity from Supelco were used to retain the IEC resin. Duran 10 mL pear-shaped vials, a splash-proof adapter with return hole from Aldrich were used to recover

and concentrate the IEC eluates using a Büchi R-114 rotary evaporator and a B-480 water bath, as well as a Huber minichiller and a Vacuubrand PC 500 series pumping unit (and CVC 3000 vacuum regulator). Hydrochloric acid (ACS reagent $\geq 37\%$) from Sigma, ammonia (Ph. Eur. reagent 25% or 28 - 30%) from Supelco, and ethanol (Bioultra $\geq 99.8\%$) were used to condition the resin and/or elute the analytes.

Water used for tool cleaning and sample processing was obtained using a Milli-Q Direct 8 apparatus (18.2 M Ω .cm at 25 °C, < 5 ppb total organic carbon). All glassware was washed several times with ethanol and Milli-Q water, wrapped in aluminum foil, and then heated to 500 °C for at least 5 h to remove any organic contaminants. PTFE-lined lids and caps, plastic wire, and spatula were washed in the same manner. Pipette tips and GC \times GC vial inserts were used without further cleaning.

3.3.1.2 Column preparation & conditioning

About 1 g of resin was weighed into a clean beaker and poured with ethanol into a glass tube containing a teflon frit at the bottom. The beaker was rinsed several times with ethanol to recover as much of the resin particles as possible. The walls of the glass tube were cleaned, and excess ethanol was eluted under vacuum until the meniscus reached 0.5 cm above the resin bed. Approximately 10 ml of ethanol was used for the entire process. Bubbles in the resin were removed by stirring the resin/ethanol mixture for approximately 30 seconds with a spatula. The second Teflon frit was then added to the top of the resin to avoid disrupting the resin bed during further elution. Using a test tube, the top Teflon frit was lightly pressed toward the resin to remove bubbles.

The resin was then conditioned as follows: 4 bed volumes (BV) of 1 M HCl solution, 4 BV of Milli-Q water, 4 BV of 2 M NH₄OH, 4 BV of Milli-Q water, 4 BV of 1 M HCl, and 4 BV of Milli-Q. The pH was monitored to be neutral after the last Milli-Q washing step. During the first HCl rinse, the recovered solution had a brown tone. The prepared columns were used only once for each experiment.

REMARKS

- ◆ In theory, performing the first two conditioning steps (HCl followed by Milli-Q water) should be sufficient to clean, regenerate and equilibrate the column before introducing the sample. However, it would be preferable to simulate a complete elution in order to remove any trapped compounds that would only elute with NH₄OH.
- ◆ Ethanol is used instead of Milli-Q water to wet the Teflon frits and avoid additional bubbles, as Teflon is very hydrophobic. This also allows for additional washing with a less polar solvent.

- ◆ The bed volume is the volume of the cylinder containing the resin, calculated by the following equation: $BV = \pi \times r^2 \times h$ with r and h the radius and height of the cylinder, respectively. Note that the resin beads are swollen with solvent, so BV is defined as the volume occupied by the resin plus the solvent.
- ◆ 4 BV are used to avoid any loss of compound during the process. The cleaning and conditioning were therefore performed in the same way. As the elution is performed manually, the reproducibility can be affected by several parameters such as flow rate, flow variations and the presence of fine bubbles.
- ◆ As with all chromatographic techniques, injection plays an enormous role. A thin injection band is always sought after because it improves separation and detectability. Here, the additional aim was to avoid loss of analytes by dilution in the *solvent* fraction, **Figure 38**. Then, care must be taken to add the solvent dropwise during the elution process: the elution flow must be properly adjusted using the vacuum pump to allow dropwise addition without drying out the resin bed.
- ◆ Handmade columns were preferred over packaged columns because they are made of glass and can be washed and heated in a furnace to reduce any risk of contamination.
- ◆ A slight color change of the resin from dark brown to light brown is observed when the elution solvent is NH_4OH instead of water. It is likely that the counterion acts as an auxochrome and changes the chromophore properties of the resin.
- ◆ Originally, a longer column ($\approx 25 - 30$ cm) with an embedded glass frit (porosity 0: $160 - 250 \mu\text{m}$) was used, but the frit caused constantly column breakthroughs that could disrupt the subsequent derivatization. Moreover, this column size was not appropriate since only about 1 cm height was used for the resin. It is therefore less ergonomic and increases the risk of contamination. However, the use of smaller glass tubes usually requires a vacuum device to speed up the elution process.
- ◆ Calculations to compare the resin capacity and the content of the sample can be performed to ensure that the amino acids can be effectively filtered. Since the resin has a nominal capacity of 1.7 meq/mL^{186} , $1 \text{ eq} = 1 \text{ mole/valence}$, and *assuming* that amino acids have a valence equal to 1, 1 L of resin can hold up to 1.7 moles of amino acids, i.e., in our case, 1.25 mL (1 g resin with a nominal density of 0.8 g/mL) can hold up to about 2.13×10^{-3} mole. If we consider the worst case for the resin, i.e., all amino acids studied (≈ 30) have a content of 10^{-3} M (approximate concentration of glycine in 1 g Murchison) in $50 \mu\text{L}$, the total amount is about $10^{-3} \times 50 \times 10^{-6} \times 30 = 1.5 \times 10^{-6}$ M, which is about 3 orders of magnitude lower than the capacity of the resin. This is far from saturating the resin used, but it should be kept in mind that other positively charged compounds, such as ionic metals and nitrogen-bearing compounds from the extraterrestrial samples, will be retained and thus contribute to saturate the resin. Nevertheless,

calculations are made using the concentration of glycine, which is by far the most abundant of all the meteoritic amino acids. Saturation of the resin should therefore not occur.

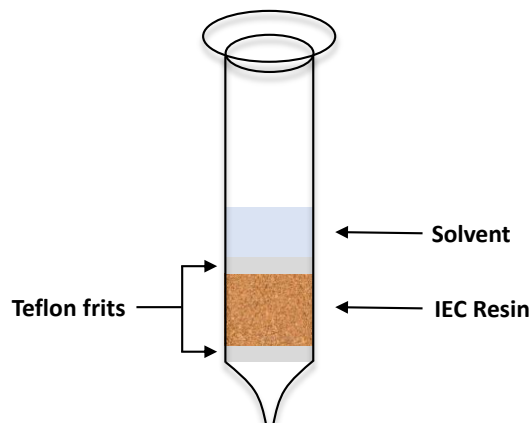


Figure 38. Schematic of glass tubes containing IEC resin and Teflon frits.

3.3.1.3 Sample purification and fractionation

After column conditioning, water was eluted until the meniscus was slightly above the level of the Teflon frit. A 10 mL pear-shaped flask was placed under the column to collect the upcoming sugar fraction. Then 50 μL of 5×10^{-6} M sugar standard mixture and 50 μL of 5×10^{-6} M amino acid standard mixture were gently added to the *solvent* section. Elution was performed using the vacuum pump, and the vacuum was manually controlled using a vent button. The elution rate was estimated to be between 10 and 20 cm/min, which is slightly faster than the 5 cm/min recommended in the column user manual¹⁸⁶. After the dropwise addition of 4 BV of water to recover the sugar fraction, elution was stopped, and a new flask was placed to recover the amino acid fraction. After the dropwise addition of 4 BV of 2 M NH_4OH , elution was stopped and both vials were stored and covered with aluminum foil after elution. As approximately 10 ml were recovered, a pre-concentration step of the fractions was performed using a rotary evaporator at 40 °C. Several vacuum steps were arranged at 500, 300, 100, 50, 25 and 10 mbar to avoid boiling (*bumping*) and thus loss of analyte. Although a clean splash adapter was used so that any solvent splash could be collected, this still presents a risk of analyte loss and should be avoided. The eluate was dried but not to complete dryness to minimize sample loss and polymerization reactions. The analytes in the pear-shape flask were recovered with 3×150 μL of water and transferred to a Reactival[®]. The water was then evaporated to complete dryness under a gentle flow of nitrogen. Derivatization of the amino acid fraction with MeOH/TFAA was performed after these steps.

3.3.2 Amino acid recoveries

The recovery values shown in **Figure 39** are the result of 3 IEC experiments versus 3 reference comparisons at the same 5×10^{-6} M concentration. Most recoveries are between 70 and 100%, which is an acceptable loss for this necessary purification and fractionation step. Methionine values are not reported because it was only detected in one sample. Amino acids such as Gly, β -Ala, L-Ala, D-2-Aba, 4-Aba and DL-2,4-Dab show recoveries above 100%. Particularly, β -alanine shows a recovery of 821.3%, which is consistent with an observed important contamination likely coming from the ammonia elution solvent (28 – 30%) rather than the resin itself. Follow-up studies using a different grade of ammonia (Ph. Eur. 25% reagent) gave more satisfactory results in terms of contamination. The highest contamination observed was for glycine, in the order of 10^{-6} M, while that for proline, phenylalanine, glutamic acid, serine, and threonine was less than 10^{-7} M. The 25% grade ammonia is therefore considered to be appropriate for future analysis.

Leu, Ile, *allo*-Ile, beta-Leu and Nle, like Iva, tend to have lower recoveries than the other amino acids. Those have the particularity of having a branched carbon side-chain (except Nle). Whether this influences the interaction with the resin and led to decreased recoveries is unsure given the relatively high errors bars in this experiment. Even if the addition of NH_4OH releases the amine group from its ionic bond with the sulfonate group, these interactions with the resin could slow down and prevent their elution. Another striking result is the poor recovery of Phe and 2,3-Dap. In the case of Phe, this could be due to a matrix interaction as the aromatic backbone of Phe may involve π -stacking with the divinylbenzene polystyrene sulfonate resin. For 2,3-Dap, its recovery differs notably from that of the homologous diamino acid 2,4-Dab. 2,3-Dap low recovery should be due to the poor repeatability of the derivatization (**Table 14**, relative standard deviation of 38%) but interestingly shows a low standard deviation of 3.1% here. On the other hand, the standard deviation of 2,4-Dab is relatively high (31.7%) compared to the other amino acids (even in the references) and cannot be explained because the repeatability tests (**Table 14**) showed a standard deviation of 6.8%, in the same range as the other amino acids.

A majority of amino acids tend to have an L-excess, which generally indicates contamination. However, Pro, and Ile, two proteinogenic amino acids tend to have an excess of D which challenges the contamination hypothesis. In addition, the large standard deviations make these assumptions difficult. Further experiments would then be required to ensure that the ion exchange resin does not bias the *ees*.

Table 21 is intended to give an overview of the *ee* bias that can be observed employing IEC, using Ala and Iva. Ala appears to be unaffected by the extraction and purification process, while Iva has a significant *ee*

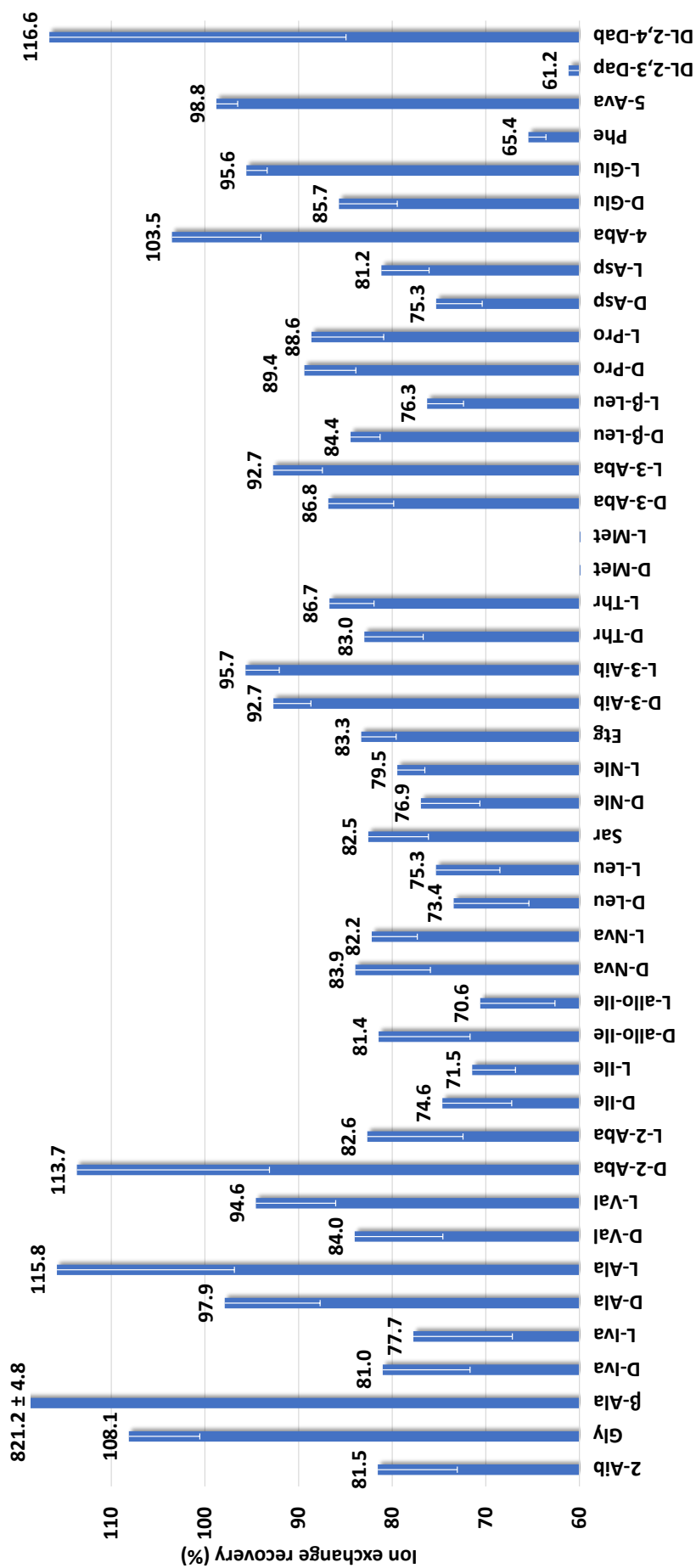


Figure 39. Recoveries of amino acids after ion exchange chromatography and MeOH/TFAA derivatized.

bias. Indeed, an ee_L of -7.19% corresponding to a $\Delta ee_L = 13.97\%$ between the reference and IEC is observed for Iva, while the standard deviations are equal to 0.54% (reference) and 1.32% (IEC). This result is particularly important because isovaline is a priority target in meteorite analysis. In addition, large excesses of L-Iva have sometimes been reported by Murchison meteorite analysis^{138,262}. A detailed investigation of the GCxGC chromatogram (**Figure 40**), however, revealed an abundant background noise from the derivatization reagents coeluting with the D-enantiomer of isovaline and thus induced this artificial bias. Sugars, on the other hand, were not studied here but were used in the first experiment (**Figure 39**). The estimation of the impact of sugars on amino acid recoveries is unfortunately difficult to assess in view of the data obtained. Indeed, using only amino acids, the recoveries of Ala (D: $97.9 \pm 10.2\%$, L: $115.8 \pm 19.0\%$) and Iva (D: $81.0 \pm 9.3\%$, L: $77.7 \pm 10.6\%$) are somewhat different from those obtained using both 5% ee_L amino acids and sugars. In the latter case, recoveries of Ala (D: $93.2 \pm 12.1\%$, L: $93.2 \pm 11.4\%$) and Iva (D: $119.1 \pm 10.6\%$, L: $89.3 \pm 13.0\%$) are slightly lower for Ala and significantly higher for Iva. However, as the recovery of Iva is greater than 100%, any conclusion is difficult to assess despite the reported standard deviations and background noise. Finally, sugars were not studied as thoroughly as amino acids with respect to IEC recoveries and ee bias. However, the following section provides preliminary results on the potential recoveries of sugars.

Table 21. Comparison of 5% ee_L doped amino acids at 10^{-5} M with and without ion exchange chromatography.

		Reference	IEC 1	IEC 2	IEC 3	IEC 4
Alanine	ee_L (%)	4.87	4.54	5.40	4.76	4.81
	σee_L (%)	0.21	0.11	0.07	0.13	0.10
Isovaline	ee_L (%)	6.78	-6.28	-9.04	-7.79	-5.65
	σee_L (%)	0.54	0.17	0.51	0.61	0.88

σee_L – Standard deviation of ee_L . In blue are highlighted the averages obtained for the reference and ion exchange chromatography experiments. In green are highlighted the standard deviations.

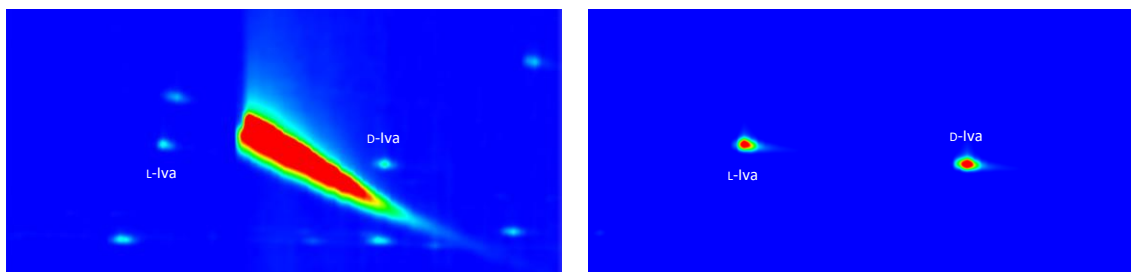


Figure 40. Two-dimensional chromatograms of Iva retention time area highlighting derivatization reagents background noise induced by IEC. On the left, the total-ion current is displayed. On the right, the $m/z = 168$ characteristic ion of Iva is displayed.

3.3.3 Early developments

The following section corresponds to previous research work in which alternative derivatization methods for amino acids and sugars were considered. For sugars, (S)-BuOH-TFAA derivatization was considered while for amino acids, ECHFBE was considered. Nevertheless, we assume that the results obtained can be transposed to other derivatizations, as long as this does not change the effect studied itself. The GC-FID was used with the *old/larger* IEC column configuration.

3.3.3.1 Recoveries of alanine and ribose

The required ammonia concentration and bed volumes were investigated to achieve high recoveries of alanine and ribose. As shown in **Table 22**, ribose recovery appeared to be slightly higher using 4 BV than 3 BV, although its value exceeded 100%. On the other hand, alanine was not detected using 3 BV, and only about 1.5% is reported using 4 BV. Thus, 4 BV will be retained, and the NH₄OH concentration will need to be increased to elute alanine that is still bound to the resin after 4 BV. To confirm that the resin does indeed bind alanine, an amino acid derivatization was performed on a sugar fraction and revealed no presence or breakthrough of alanine.

Table 22. Recovery of DL-alanine and DL-ribose by ion exchange chromatography for 3 and 4 bed volumes and with 1 M NH₄OH.

		Alanine (ECHFBE)	Ribose ((S)-BuOH/TFAA)
3 BV	D Recovery (%)	0	98.52 ± 4.48
	L Recovery (%)	0	98.46 ± 4.84
4 BV	D Recovery (%)	1.56 ± 6.63	109.14 ± 4.48
	L Recovery (%)	1.75 ± 6.44	105.77 ± 4.84

Standard deviations correspond to the 3 references, recoveries are based on only one sample.
GC-FID, *old* IEC setup, 10⁻³ M.

To ensure that the amino acids can be recovered, an experiment using 14.8 M NH₄OH was conducted and revealed high recoveries of about 99.5%. Further experiments led to the final selection of 2 M N₄OH as the optimal concentration (usually also used in the literature) and showed, using 4 BV (**Table 23**), for both compounds and both enantiomers, recoveries of around 95%. 3 references for alanine and 3 references for ribose were made to compare the results with 4 ion exchange chromatography experiments. However, the standard deviations (SD) are around 5% for alanine and 10% for ribose. The high SD for ribose is mainly due to the high SD of IEC, which is not the case for alanine. At this point, it is unclear whether this is from the derivatization itself or from the IEC treatment. Nevertheless, these results tend to be very satisfactory given the use of the IEC resin, rotary evaporator, and manual recovery in the pear-shaped flask. Furthermore, the change in *ees* (Δee_0 , the difference in *ee*₀ between IEC and reference) induced by the

resin for the racemic mixture was investigated but showed no significant difference as this difference is within the standard deviation range. Indeed, a -0.104 ± 0.152 is reported for alanine while 1.00 ± 1.21 is reported for ribose. However, this is not sufficient to conclude that there is no effect on *ee*. Studies using 5% *ee* on sugars should be performed to evaluate this effect on samples with effective *ee*. Interestingly, even though this column configuration led to resin breakthrough, it *seems* to have no impact on both derivatizations applied, but no general conclusions can be drawn as it could affect other compounds.

Table 23. Recoveries of DL-alanine and DL-ribose using ion exchange chromatography for 4 BV and using 2 M NH_4OH .

	Alanine (ECHFBE)	Ribose ((S)-BuOH/TFAA)
D Recovery (%)	96.69 ± 5.11	96.75 ± 10.31
L Recovery (%)	96.88 ± 5.26	94.71 ± 9.24
Δee_D (%)	-0.104 ± 0.152	1.00 ± 1.21

In parentheses, the derivatization used is detailed.

GC-FID, old IEC setup, 10^{-3} M.

3.3.3.2 Drying impact

The potential loss of sugars due to the drying step before derivatization was investigated. Each result shown in **Table 24**, corresponds to the relative recovery of a dried 50 μL standard (10^{-3} M) of two samples with different drying times derivatized using (S)-BuOH/TFAA. The dried sample corresponds to a 50 μL standard plus 450 μL water, evaporated to complete dryness under a gentle nitrogen stream. The overdried sample corresponds to a dried sample plus a 30 minutes overdrying. Two conclusions can be drawn from these data: the drying step has no impact in terms of ribose degradation, and overdrying does not induce analyte loss due to its volatility.

Table 24. Ribose recovery depending on the drying procedure before derivatization.

	Dried sample	Overdried sample
Relative recovery (%)	102.6 ± 3.3	102.2 ± 3.9

GC-FID, (S)-BuOH/TFAA, 10^{-3} M.

In addition, experiments of potential ribose loss using the rotary evaporator to concentrate the IEC eluate were performed but did not yield conclusive results and are therefore not reported here. However, the recovery results in **Table 23** consider the entire IEC process and discards major degradation or loss of analytes.

3.3.4 Conclusion

Ion exchange chromatography, used to purify samples from salts, is also useful for separating a sample into two distinct fractions of amino acids and sugars. This reduces the risk of disruption of subsequent derivatization. Initial experiments have shown, after optimization of ammonia concentration and bed volumes, that recoveries of alanine and ribose, used as model compounds, are above $95 \pm 10\%$. Nevertheless, comprehensive studies on 30 amino acids have shown that the recovery values can be significantly modified depending on the amino acid, as is the case for Phe or 2,3-Dap with recoveries of about 60%. Recoveries for other amino acids are generally between 70 and 100%. On the other hand, enantiomeric conservation tests using 5% doped L-amino acids showed no variation for Ala, but a serious reversal for Iva as a Δe_e of 13.97% is observed due to an abundant background noise from the derivatization reagents. Thus, further method and temperature program optimization are required to avoid such coelution as Iva is a notable amino acid in meteorites and that IEC is used as a pretreatment step. Finally, comprehensive investigations on the recovery of sugars should be carried out with particular emphasis on the preservation of such 5% excess.

3.4 SAMPLING & EXTRACTION

3.4.1 Materials & methods

Serpentine was used as a meteorite analog to simulate liquid-solid interactions and adsorption. It is typically used to perform procedural blanks when analyzing extraterrestrial samples. A porcelain mortar and pestle were used to grind the serpentine into fine grains. Pre-scored 5 mL Duran ampoules were used to perform the samples' water extraction in the presence of serpentine, and flame-sealed. A Sigma centrifuge was used to recover the supernatant from the serpentine grains and operated at 6000 rpm.

Water used for tool cleaning and sample processing was obtained using a Milli-Q Direct 8 apparatus (18.2 M Ω .cm at 25 °C, < 5 ppb total organic carbon). All glassware was washed several times with ethanol and Milli-Q water, wrapped in aluminum foil, and then heated to 500 °C for at least 5 h to remove any organic contaminants. The serpentine was heated to 500 °C for at least 5 h to degrade and remove any contaminants before being crushed.

3.4.2 Degradation of amino acids during hydrolysis

3.4.2.1 Procedure

The degradation of amino acids during water hydrolysis (24 h at 100 °C or room temperature) with and without serpentine was studied. When used, approximately 500 mg of serpentine was crushed to a fine powder and placed in a pre-scored ampoule using a spatula. The powder was then doped with 50 µL of a 5×10^{-5} M amino acid standard and allowed to dry for 2 h. For the remaining samples, 50 µL of this solution was placed to the bottom of the ampoule. Then, 3.5 mL of Milli-Q water to mimic the extraction of the powder from the mortar into the ampoule were added before flame-sealing and the hydrolysis. After the samples were cooled down, a centrifuge was used for 10 min, and the supernatant was recovered using a clean Pasteur pipette. 2 (or 3) additional 1 mL washes using water, vortex stirring, centrifugation and recovery of the supernatant were performed. The recovered extracts were purified on IEC detailed in **3.3.1.3 Sample purification and fractionation** (p. 97) and derivatized MeOH/TFAA, detailed in **3.2.1.1.2 Derivatization** (p. 73).

3.4.2.2 Results & discussion

As can be seen in **Table 25**, rinsing the powder 2 or 3 times with 1 mL after hydrolysis increases the recovery by 2% to no more than 4%, and should be used for meteorite analyses. In the presence of serpentine, amino acid recoveries after hydrolysis at 100 °C tend to be 5 – 10% lower, which could be consistent with mineral-catalyzed degradation/secondary products.

Table 25. Amino acids recoveries after water extraction.

	1	2	3	4
	Serpentine 100 °C, 24 h	Serpentine 100 °C, 24 h	- 100 °C, 24 h	- RT, 24 h
	Recovery 2×1 mL	Recovery 3×1 mL	Recovery 2×1 mL	Recovery 2×1 mL
D-Nva	115.7 ± 13.3	120.7 ± 13.4	92.7 ± 14.8	100.9 ± 13.6
L-Nva	96.0 ± 9.8	98.5 ± 9.8	80.5 ± 11.6	87.6 ± 10.0
D-Ala	93.1 ± 12.5	93.6 ± 12.6	97.0 ± 14.3	93.1 ± 12.8
L-Ala	94.4 ± 12.0	98.8 ± 12.1	93.8 ± 14.2	99.7 ± 12.3
D-Pro	83.2 ± 9.4	85.5 ± 9.4	92.5 ± 10.0	98.4 ± 9.5
L-Pro	82.9 ± 9.0	84.4 ± 9.1	94.6 ± 10.1	102.2 ± 9.1
D-Asp A	61.7 ± 11.5	64.0 ± 11.3	91.8 ± 11.4	77.8 ± 11.6
L-Asp A	70.9 ± 14.7	63.2 ± 11.0	94.2 ± 10.8	80.8 ± 10.7

New column, GC×GC-TOFMS, MeOH/TFAA, 5×10^{-5} M.

Curiously, D-Nva recoveries are significantly higher than L-Nva in all samples and should, at first glance, be consistent with contamination. Nevertheless, L-Nva is low in sample 4, which is also the case for Asp. In addition, high standard deviations greater than 10% are reported. Thus, questions about handling errors

can be raised, but also about the repeatability of the derivatization, discussed in the next section. The main conclusion here, despite the variability of the results obtained, is that at least 60% of the amino acids can be recovered by the process of water hydrolysis followed by IEC fractionation.

3.4.3 Degradation of amino acids in the presence of sugars

3.4.3.1 Procedure

To obtain an estimate of the recovery of the whole process and to evaluate the potential reactions occurring at elevated temperatures between amino acids and sugars, a mixture of both compound classes was used. Approximately 500 mg of serpentine was crushed with a mortar and pestle and then doped, in the mortar, with 50 μL of a 5×10^{-5} M sugar mixture and 50 μL of a 50×10^{-5} M amino acid mixture. The sample was then allowed to dry for 2 h, allowing adsorption of the compounds onto the serpentine. The mineral powder was crushed again and recovered using $6 \times 333 \mu\text{L} + 1 \text{ mL}$ water, until the mortar appeared clean, and placed in an ampoule. The top of the ampoule was washed with 500 μL to recover any remaining powder. Flame sealing, water hydrolysis, IEC, and derivatization were performed as previously described.

Table 26. Recoveries of Ala and Iva after mortar-doped serpentine, water hydrolysis and IEC.

	Recovery (%)
D-Ala	49.92 \pm 30.45
L-Ala	50.54 \pm 28.21
D-Iva	41.51 \pm 48.28
L-Iva	32.69 \pm 37.31

New column, GC \times GC-TOFMS, MeOH/TFAA, 5×10^{-5} M.

As can be seen in **Table 26**, lower recoveries are obtained than using only amino acids during hydrolysis. The recoveries of Ala decreased from more than 90% to about 50%. However, the experimental conditions are not exactly the same. Here, the amino acids and sugars were deposited on the mineral, but in the mortar and significant loss could occur even with careful washing of the mortar. The material is different and could adsorb these compounds better. So far, on other experiments, standard deviations were in the range of 5 – 15%, which gives a relatively high but acceptable uncertainty on the result obtained considering the number of measurements and steps performed. Here, standard deviations greater than 30% could, at first glance, correspond to poor repeatability of the mineral doping in the mortar. However, the reference standard deviations for Ala and Iva are in the range of 17 – 25%, suggesting a problem with the repeatability of the derivatization. For this reason, this derivatization method was studied in detail in **3.2.1 MeOH/TFAA derivatization of amino acids**. Therefore, it cannot be concluded that there is any

impact of sugars. Unfortunately, no further experiments were performed using the full procedure because derivatization and IEC recoveries were studied preferentially.

3.4.4 Conclusion

Further analyses must be performed to study the behavior of amino acids and sugars throughout the procedure. The water hydrolysis in the presence of sugars and amino acids will be of great importance as both can react and decrease the recovered quantities. However, this should be studied using sonication to avoid their degradation and reaction. The presence of serpentine could also have an impact on their recoveries. HCl hydrolysis of recovered amino acids is also of great interest for these recoveries. Racemization and *ees* should be studied in both cases as they will be investigated on a real sample.

3.5 CONCLUSION

Sampling, extraction, purification, fractionation, derivatization, and GC×GC analysis constitute numerous steps to be investigated, methods to be developed, and experience to be gained. Although, unfortunately, the development of a complete procedure to study *ees* in extraterrestrial samples has not yet been achieved, considerable progress has been made. A ready-to-use amino acid derivatization for trace analysis and *ees* studies of 30 amino acids is now available for extraterrestrial and simulated samples. A derivatization of sugars, based on the previous team's laboratory experiments, has been extended to sugar alcohols and the sugar data set has been enriched and can be further studied for application to extraterrestrial and simulated samples. Expertise in purification and fractionation steps using handmade IEC columns and glass reaction tubes was developed and showed recoveries of 70 – 100% for amino acids. Sugars, on the other hand, were only studied through ribose in early developments but showed recoveries greater than 95%. As with amino acids, further studies are needed on recoveries and *ees*. The sources of contamination highlighted for amino acids are a major problem, but reagents and materials are now identified for further experiments. Sampling and extraction remain the least studied steps. Extraction will, in the future, be performed using sonication. The water extraction shown here, however, testifies that no major degradation occurred during this step and implies that water extraction by sonication should lead to better recoveries. In addition, the use of sonication could reduce the risk of mineral-catalyzed degradation/byproducts, compared to the conventional water extraction at 100 °C for 24 h.

CHAPTER IV

Applications of the optimized method to complex samples

4.1 AMINO ACID SYNTHESIS STARTING FROM HEXAMETHYLENETETRAMINE

This study is a follow-up to previously published work by V. Vinogradoff *et al.*¹⁵⁹ on the formation of amino acids from hexamethylenetetramine (HMT) under hydrothermal conditions, at pH 10 and 150 °C for 2, 7 or 31 days. Multiple parameters can have an impact on the synthesis of amino acids in parent bodies: composition of organic and mineral phases, pH, concentrations, temperature, oxidation state, relative water content and degree of aqueous alteration. The influence of the presence of phyllosilicates (Al-rich smectite or Fe-rich smectite) or carboxylic acids was studied and showed significant differences in the abundance for glycine, alanine and 4-aminobutyric acid compared to HMT alone. The highest abundance of amino acids reported was for the use of phyllosilicates, but the results for carboxylic acids led to consider the formose reaction with ammonia and Maillard-type reactions as possible synthetic routes. Indeed, the decomposition of HMT leads to the initial reactants of these reactions such as formaldehyde and amines.

Here, only the sample containing HMT has been studied and two main objectives are highlighted. The first is to compare the results obtained – using ion exchange chromatography purification and MeOH/TFAA derivatization – with those reported by the authors. The second objective is to search for other amino acids not previously detected due to higher detection limits.

4.1.1 Materials and methods

The samples received from the *Physique des Interactions Ioniques et Moléculaires* (PIIM) laboratory at Aix-Marseille Université consisted of a liquid and a solid part of about 5-7 μL in total. The initial concentration of HMT was 2 M compared to 0.2 M in the previous work¹⁵⁹. The degradation time of HMT was set to 31 days for both sample sets.

Each sample (2 μL for liquid 1 and liquid 2 samples, and the remaining solid portion) was subjected to 24 h of water hydrolysis at 100 °C in a flame-sealed glass ampoule. Each sample was then divided into 2 equal parts, the first untreated, and the second hydrolyzed with 6 M HCl for 24 h at 100 °C in a flame-sealed ampoule. Each part was then purified and fractionated using ion exchange chromatography, **Figure 41**, detailed in **3.3.1.3 Sample purification and fractionation** (p. 97). The amino acid fractions were derivatized with the MeOH/TFAA procedure and analyzed by GC \times GC-TOFMS, the conditions of which are detailed **3.2.1.1.2 Derivatization** (p. 73) and **3.2.1.1.3 GC \times GC-TOFMS** (p. 73). Each sample was injected twice. Concentrations were corrected using ion exchange chromatography recoveries of amino acids.

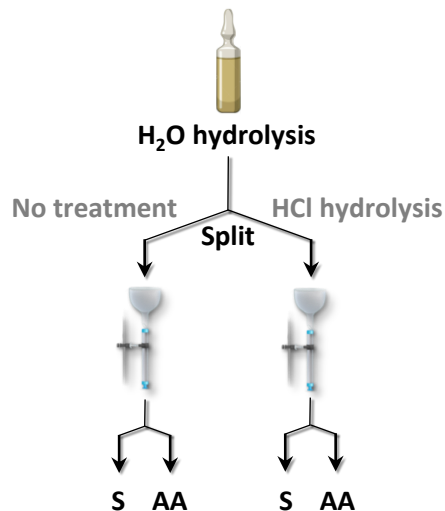


Figure 41. Schematic of the HMT sample processing. *S* represents the sugar fraction and *AA* the amino acid fraction.

4.1.2 Amino acids content

To compare the reported and obtained values, the amounts obtained here were divided by 10 to match the original 0.2 M experiment, **Table 27**. It is interesting to note, for the solid and both liquid 1 and liquid 2 samples, the difference between the free and hydrolyzed content obtained. Since each sample was equally fractionated into a *free* and *HCl-hydrolyzed* fraction, the difference between the two values corresponds either to variations in the cleavage of the oligomerized amino acids or to their degradation under the chosen hydrolysis conditions. It is also possible that the use of 6 M HCl, even after drying, may have an impact on MeOH/TFAA derivatization, even though the first derivatization step requires an acidic medium. However, no real trend can be established between the two liquid fractions and on the solid fraction. Therefore, it is difficult to know whether insufficient bond cleavage or degradation have occurred. Glycine, for example, appears to have an increased content between the free and hydrolyzed portion for the solid samples (690 μM to 831 μM) and the first liquid (584 μM to 711 μM). However, the second liquid sample only increased from 487 μM to 493 μM , which is not significant. In addition, glycine is known to be a contaminant present in ammonia that is required for IEC elution. Another hypothesis would be the lack of homogeneity of the sample, as the solid part is more like a gel and the second liquid sample was more difficult to sample as only liquid sample without any solid/gel fraction.

Table 27. Comparison of the amino acid content reported in the original study¹⁵⁹ and in the present work.

Amino acids	#C	Reported 0.2 M (μ M)	Obtained 0.2 M** (μ M)	Obtained 2 M* (μ M)	Solid		Liquid 1		Liquid 2	
					Free	HCl hydrolysis	Free	HCl hydrolysis	Free	HCl hydrolysis
Gly	2	573.44 \pm 15.15	379.69	3796.90	689.81	830.71	584.24	711.47	487.21	493.45
β -Ala	3	15.35 \pm 0.38	33.02	330.24	65.47	63.74	54.82	51.92	46.90	47.40
D- α -Ala	3	30.31 \pm 2.11	128.92	1289.18	158.05	135.84	92.02	115.88	113.23	73.32
L- α -Ala	3		141.21	126.94	77.75	96.44	89.59	68.91		
Sarc	3	-	159.94	1599.37	314.12	385.82	122.87	318.77	223.68	234.12
D-3-Aib	4	2.39 \pm 0.77	10.17	101.73	10.56	11.24	9.84	8.91	7.98	8.37
L-3-Aib	4		8.40	8.98	7.57	7.11	6.13	6.65		
D-3-Aba	4	1.22 \pm 1.05	3.79	37.87	3.52	3.70	3.11	2.62	2.59	2.80
L-3-Aba	4		4.02	3.81	3.33	2.72	2.83	2.82		
D-2-Aba	4	1.22 \pm 0.27	1.71	17.15	-	2.48	-	1.42	-	1.53
L-2-Aba	4				2.44	2.61	1.64	1.53	1.75	1.76
4-Aba	4	11.01 \pm 2.88	1.05	10.53	1.84	2.23	1.45	1.62	1.47	1.93
DL-2,4-Dab	4	-	0.57	5.73	1.25	0.98	1.05	0.73	0.91	0.81
D-Glu	5	< 0.1	1.26	12.60	0.04	0.12	0.03	0.08	0.02	0.11
L-Glu	5				1.28	2.08	3.01	1.47	1.36	3.00
D-Pro	5	< 0.1	0.58	5.83	0.35	0.38	0.35	0.27	0.27	0.30
L-Pro	5				0.58	0.81	0.85	0.51	0.48	0.67
2-Aib	4	-	0.26	2.57	-	0.83	0.65	0.55	-	0.54
D-Val	5	< 0.1	0.36	3.64	0.29	0.30	0.22	0.19	0.16	0.18
L-Val	5				0.35	0.61	0.36	0.29	0.29	0.40
D-Asp	4	< 0.1	0.36	3.62	-	0.30	0.18	0.09	0.02	0.27
L-Asp	4				0.20	0.80	0.76	0.41	0.27	0.32
Etg	4		0.27	2.74	0.52	0.60	0.44	0.37	0.38	0.43
DL-2,3-Dap	3		0.16	1.56	-	0.75	0.00	0.24	-	0.56
D-Thr	4	< 0.1	0.09	0.92	-	-	-	-	-	-
L-Thr	4				0.06	0.31	0.17	0.10	0.09	0.18
DL-Phe	9	-	0.16	1.55	0.23	0.18	0.49	0.23	0.26	0.17
5-Ava	5	-	0.03	0.33	0.06	0.06	0.18	0.04	-	-
D-Leu	6		0.11	1.06	0.00	0.00	0.00	0.00	0.00	0.00
L-Leu	6				0.10	0.25	0.25	0.15	0.13	0.18

*Total amino acid content obtained through the sum of the solid and liquid values. **This content was divided by 10 to obtain an equivalent of 0.2 M HMT for comparison with data reported in the original study.

As can be seen in **Table 28**, the trend in amino acid content previously reported¹⁵⁹ and obtained here is similar. The most abundant amino acids are C₃ (Gly, Sar, α -Ala, β -Ala) compared to C₄ (β -Aib, β -Aba, α -Aba, γ -Aba). However, differences in abundances can be noted. We found that Gly is about 1.5 times and γ -Aba 10 times less abundant in our experiments, while α -Ala is 4 times and, β -Ala 2 times more abundant

compared to the previous experiments. These differences could originate from the difference in HMT concentration, which was 0.2 M for the reported study, and 2 M for the present work. As a general trend, α - (except glycine) and β -amino acids tend to be found in higher amounts using a more concentrated HMT. Conversely, the content of 4-Aba, a γ -amino acid, is much lower than reported in the original study.

Table 28. Comparison of the amino acids content between the work of V. Vinogradoff *et al.*¹⁵⁹ and the presented study.

		Amino acids content													
Reported	Gly	>>	α -Ala	>	β -Ala	>	γ -Aba	>	β -Aib	>	α -Aba	=	β -Aba		
Here	Gly	>	Sar	>	α -Ala	>	β -Ala	>>	β -Aib	>	β -Aba	>	α -Aba	>	γ -Aba

As considered by V. Vinogradoff *et al.*¹⁵⁹, these amino acids could be formed by a formose-type reaction in parallel with Maillard-type reactions, **Figure 42**. Under this assumption and using highly concentrated HMT, it is likely that the kinetics of the formose and Maillard-type reactions would be altered and lead to a higher abundance of low molecular weight amino acids. Because glycolaldehyde and glyceraldehyde would be more rapidly converted to amino acids (while assuming that tetrose formation is relatively slow), the equilibrium would have shifted to the production of glycolaldehyde and glyceraldehyde (Le Châtelier's principle), and thus of α - and β -amino acids rather than γ -amino acids. Thus, it would be interesting to study the sugar content of the 0.2 M and 2 M HMT samples to examine the relative proportions of tetroses and glyceraldehyde. Since IEC was employed, the sugar fractions were studied simultaneously using MBA derivatization. Surprisingly, no sugars were detected except for arabinose and xylose, which were also found in the procedural blank. From this perspective, one might assume that no formose-type reaction occurred. However, as we will point out in the next section, the lifetime of the sugars synthesized by the formose reaction is generally on the order of days. Indeed, after 45 days, no sugar content was found while the present experiment used 31 days of reaction time. Unfortunately, derivatization with MBA (used for the lower limit of detection) did not detect sugar alcohols, unlike the MBA/TFAA used in the next section. At the time these experiments were performed, the presence of these sugar alcohols and in particular glycerol at long reaction times was unknown. Thus, investigations of sugars in HMT samples should be performed using shorter reaction times or MBA/TFAA to identify sugar alcohols.

4.1.3 Other detected amino acids

Compared with previous work, several additional amino acids were successfully detected including Sar, DL-2,4-Dab, DL-Glu, DL-Pro, 2-Aib, DL-Val, DL-Asp, Etg, DL-2,3-Dap, DL-Thr, DL-Phe, 5-Ava, and DL-Leu. Eight of these were not investigated in the previous study and thus show that either a higher HMT concentration

led to amino acid formation above instrumental detection limit or that our analytical device allowed for improved identification. The detection of the other five amino acids targeted but not detected in the previous work, Glu, Pro, Val, Asp and Thr, can mainly be explained by the lack of amino acid content in the original study, due to the use of 0.2 M HMT, which did not allow such detection. Nevertheless, the reported detection limits for the AccQ:Tag (6-aminoquinolyl-*N*-hydroxysuccinimidyl carbamate) derivatization used in the original study are in the 10^{-7} M range using the UHPL-UV instrument²⁷⁴, whereas they are in the 10^{-8} M range using MeOH/TFAA followed by GC×GC-TOFMS.

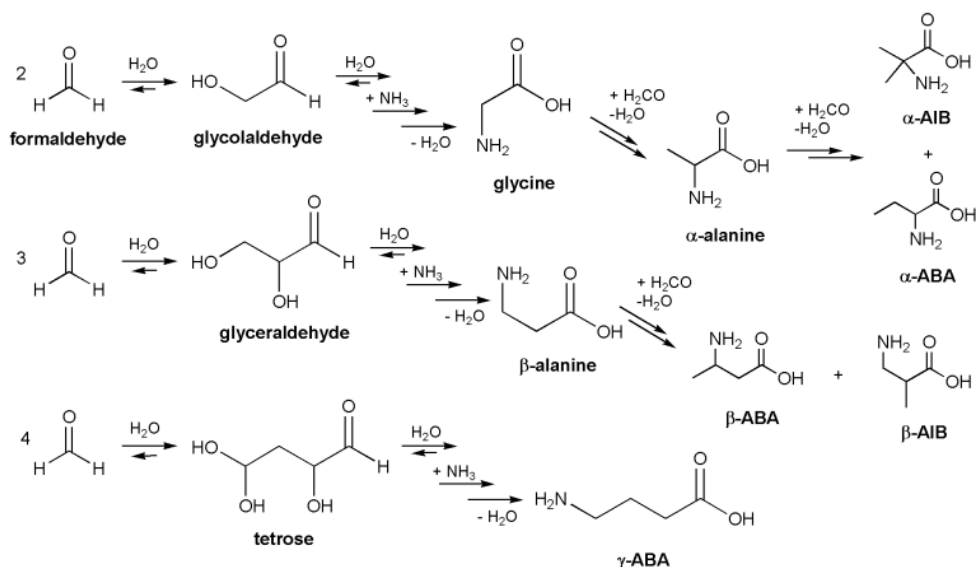


Figure 42. Proposed pathway for the formation of amino acids from the decomposition of HMT followed by the formose reaction in the presence of ammonia. From V. Vinogradoff et al.¹⁵⁹

4.1.4 Conclusion

The analysis of the HMT samples indicates that ion exchange chromatography coupled with MeOH/TFAA derivatization is suitable for the analysis of complex samples. This notably allowed the identification of 13 additional amino acids not detected in the original study. The comparison with the original study is limited because the samples used different concentrations, were not derivatized with the same procedure nor on the same apparatus. Nevertheless, the same trend in amino acid abundance was measured. This first analysis of a complex sample serves mainly to justify the applicability of the developed protocol to other extraterrestrial-like samples. Future applications of this procedure would be the analysis of interstellar ice analogs that allows the simultaneous investigation of amino acid and sugar fractions.

4.2 MINERAL-CATALYZED FORMOSE REACTION UNDER HYDROTHERMAL CONDITIONS

In this study, several main objectives can be highlighted. The first is to investigate whether olivine is capable of initiating a formose-type reaction under hydrothermal conditions. The second is to compare the mineral-catalyzed synthesis of sugars with the classical calcium hydroxide catalyst in terms of sugar diversity and kinetics. Finally, the potential induction of *e*es into the sugars formed under hydrothermal conditions and the presence of the olivine mineral are investigated. This study focuses on longer reaction times, between 2 and 45 days, whereas classical experiments on the formose reaction are generally performed within minutes up to hours.

4.2.1 Materials and methods

The samples received (about 200 μ L each) from the *Physique des Interactions Ioniques et Moléculaires* (PIIM) laboratory, Aix-Marseille Université were used without any treatment before the drying step and subsequent derivatization. 20 μ L of the supernatant of each sample was placed in a Reactival® and dried under a gentle stream of nitrogen. MBA/TFAA derivatization and GC \times GC-TOFMS conditions were as detailed in **3.2.2.1.2 Derivatization** (p. 89) and **3.2.2.1.3 GC \times GC-TOFMS** (p. 89). Quantification of sugars and sugar alcohols is based on the calibration curves provided in this same section. Due to GC \times GC maintenance between the analyses of samples from day 7 and day 45 that altered the sensitivity of the instrument, another calibration curve dedicated to day 45 was performed to reliably quantify the sugars in these samples. The calibration curve data is available in **Table S 4** (p. 168).

For the samples received, formose reaction experiments were performed in aqueous systems and under anoxic atmosphere at 80 °C. The mineral olivine was chosen as a model silicate given its abundance in the solar system, and as a catalyst for the formose reaction. As shown in **Table 29**, various experimental conditions and combinations of formaldehyde (F), glycolaldehyde (G), calcium hydroxide (Ca(OH)₂ denoted by α), and olivine (O) were tested. Formaldehyde was introduced as paraformaldehyde (PFA, which is a polyoxymethylene with a low degree of polymerization, typically between 8 and 100 units) that was depolymerized during the experiments by heat treatment under acidic conditions. The weight ratios used in these experiments were set to 10:1 for F/(G or α) and 10:1 for O/F. The prepared mixtures were then loaded into closed cells in an argon glovebox and then heated to 80 °C. Once the experiments were started, three durations (day 2, day 7, and day 45) were studied for their sugar content.

Table 29. Overview of samples studied in this work.

<i>Composition</i>	<i>Day 2</i>	<i>Day 7</i>	<i>Day 45</i>
Formaldehyde + Glycolaldehyde	FG2 (pH = 4 – 5)	FG7 (pH = 3 – 4)	FG45 (pH = 4)
Formaldehyde + Olivine	FO2 (pH = 6 – 7)	FO7 (pH = 6 – 7)	FO45 (pH = 6)
Formaldehyde + Olivine + Glycolaldehyde	FGO2 (pH = 7)	FGO7 (pH = 6 – 7)	FGO45 (pH = 7)
Olivine	O2*	O7*	-
Formaldehyde	F2*	-	F45*
Formaldehyde + Calcium hydroxide	F2 α (pH = 5 – 6)	F7 α (pH = 5)	-
Formaldehyde + Glycolaldehyde + Calcium hydroxide	FG2 α (pH = 6 – 7)	FG7 α (pH = 5)	-

*Samples derivatized once and analyzed once, - Samples not supplied. Other samples were derivatized twice and analyzed twice.

4.2.2 Derivatization approach

At first glance, (S)-BuOH/TFAA derivatization would be an excellent option, as sugars, sugar alcohols and sugar acids could be derivatized and analyzed. However, it should be kept in mind that a formose reaction leads to a wide variety of sugars, sugar alcohols, sugar acids, and substituted sugars, and could potentially involve many co-elutions, even with a powerful separation technique such as GC \times GC. Since this derivatization leads to many forms for each sugar, an alternative derivatization such as an MBA-based derivatization would offer more selectivity. MBA/TFAA seems to be a better choice than MBA because of the detection of sugar alcohols at the expense of sugar intensity. Nevertheless, the amount of sugars expected in this formose reaction are high (preliminary results from *PIIM* analyses) and may justify the use of MBA/TFAA derivatization. In addition, the TFA-derivatized compounds show an intense $m/z = 69$ peak, while the other peaks tend to be much smaller. Unfortunately, the $m/z = 69$ ion is associated with high noise and often an inability to integrate properly in case of coelution because it is a common mass for derivatives. Thus, alternative m/z ratios have to be used to reliably quantify the targeted molecules. MBA/TFAA then appears to be a more appropriate choice as some MBA/TFAA derivatized sugars would only be MBA derivatives. Another consideration is the impact of the matrix on derivatization. Because the first (S)-BuOH/TFAA step is performed in an acidic medium (using acetyl chloride to form HCl *in situ*), this derivatization is less likely to be affected by the pH of the samples, which is between 3 and 7. On the other hand, the first step of MBA/TFAA derivatization is rather performed in basic medium (in pyridine) and could have an impact on the reactivity of MBA. A first test on FGO2 was performed and led to consider MBA/TFAA as a better choice. Indeed, as shown in **Figure 43**, MBA/TFAA shows a better distribution of compounds using $m/z = 43$ (characteristic of MBA ring fragmentation) than (S)-BuOH/TFAA using $m/z = 57$ (characteristic of (S)-BuOH fragmentation), **Figure 44**, with optimized temperature programs. The

intensities of the highest peaks, in red, are of the same order of magnitude (more intense for (S)-BuOH/TFAA by a factor of 2.5). Therefore, MBA/TFAA could reduce the risk of coelution when integrating sugar peaks. In addition, glyceraldehyde is not detected with (S)-BuOH/TFAA and is of great interest because it is the simplest sugar and one of the first aldol reaction products from glycolaldehyde. Finally, *ee* will be studied and better results in terms of accuracy were found for the MBA (not MBA/TFAA) derivatization than for the (S)-BuOH/TFAA derivatization. This again led to the final decision to select MBA/TFAA as a better compromise for the overall analysis.

Since the MBA/TFAA derivatization was chosen to quantify sugars and study potential enantiomeric excesses, the BSTFA derivatization was used to complete the dataset of synthesized sugar acids, branched sugars, and other characteristic formose reaction products that could not be studied with MBA/TFAA.

Qualitative examination of the sugar acids and other relevant formose reaction products presented in **Table 30** tends to confirm a formose reaction under the experimental conditions. In the case of FGO2, most of the listed compounds and especially 2-hydroxymethylglycerol (HMG) and 2-hydroxymethyltetritol (HMT*) were detected while this was not the case for FG2 α . As discussed in **4.2.3 Evolution of sugars content**, this could be due to kinetic differences as olivine and calcium hydroxide seem to catalyze the reaction at different rates. On the other hand, the presence of sugar acids is a good indicator of the formose reaction in terms of the diversity of products synthesized. This diversity is highlighted through **Figure 45** showing chromatograms of FGO2, FG2 α , FGO7 and FG7 α . Ion 43, characteristic of polyols, is displayed. Trimethylsilyl derivatives were identified and searched according to the work of C. Meinert *et al.*⁹⁵, providing exhaustive information on characteristic ions and retention times.

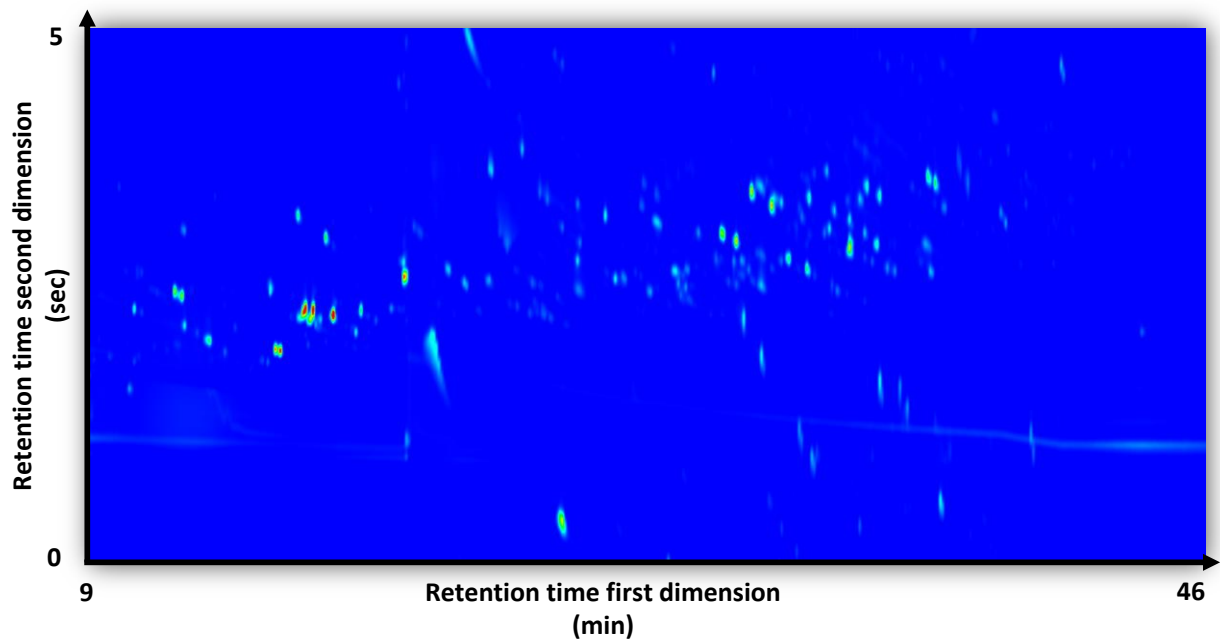


Figure 43. Two-dimensional chromatogram of MBA/TFAA derivatized FGO2 sample analyzed on CP-Chirasil-Dex CB coupled to DB-WAX columns. Ion 43, characteristic of MBA fragmentation, is displayed.

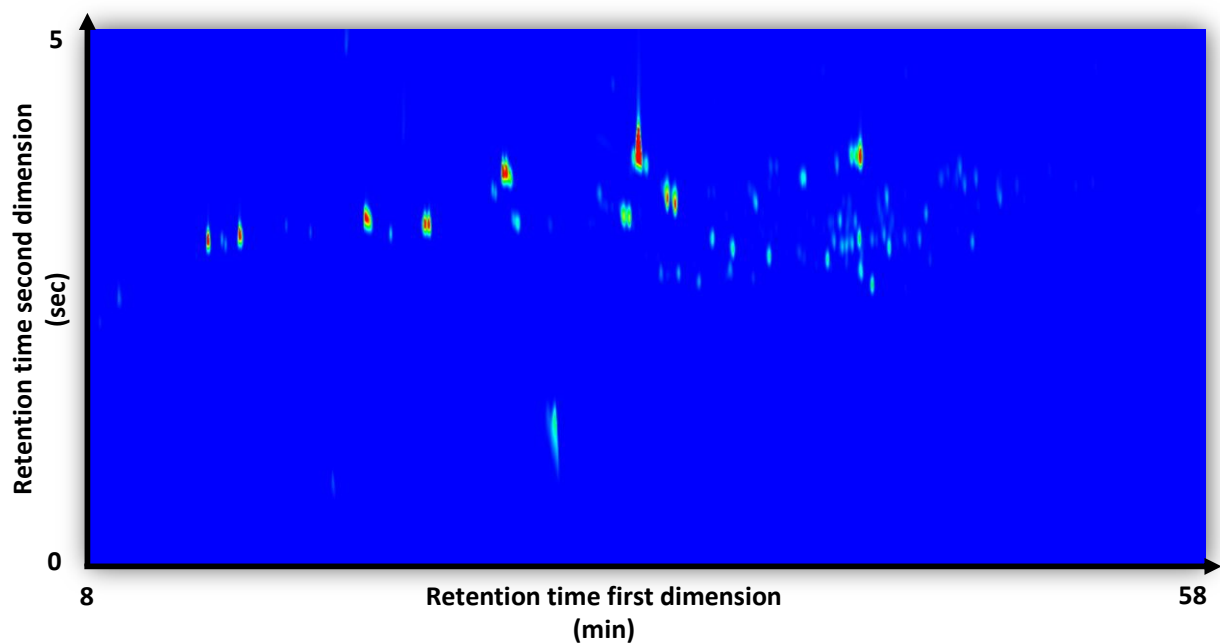


Figure 44. Two-dimensional chromatogram of (S)-BuOH/TFAA derivatized FGO2 sample analyzed on CP-Chirasil-Dex CB coupled to DB-WAX columns. Ion 57, characteristic of (S)-BuOH fragmentation, is displayed.

Table 30. Qualitative analysis of some relevant formose reaction products using BSTFA derivatization.

	Compounds	FG2 α	FGO2
Branched compounds	2-Methylglyceric acid	✓	×
	2-Methylglycerol	ND	✓
	2-Hydroxymethylglycerol	ND	✓
	2-Hydroxymethyltetritol	ND	✓
Sugar acids	Glyceric acid*	✓	✓
	Erythronic acid*	ND	✓
	Threonic acid*	ND	✓
	Ribonic acid**	✓	✓
	Arabinoic acid**	✓	✓
	Xylonic acid**	✓	✓
Hydroxycarboxylic acids	Lyxonic acid**	✓	✓
	Glycolic acid	ND	✓
	Lactic acid	✓	✓
	3-Hydroxypropanoic acid	×	✓
	2-Hydroxybutyric acid (R & S)	ND	✓
	3-Hydroxyisobutyric acid	×	✓
	3-Hydroxybutyric acid (R & S)	×	×

✓ Detected, × Not detected, ND - Not determined due to noise & weak signal, *Verified with sugar acid standards, **Assumed to be these acids as retention times and mass spectrum are similar but shifted.

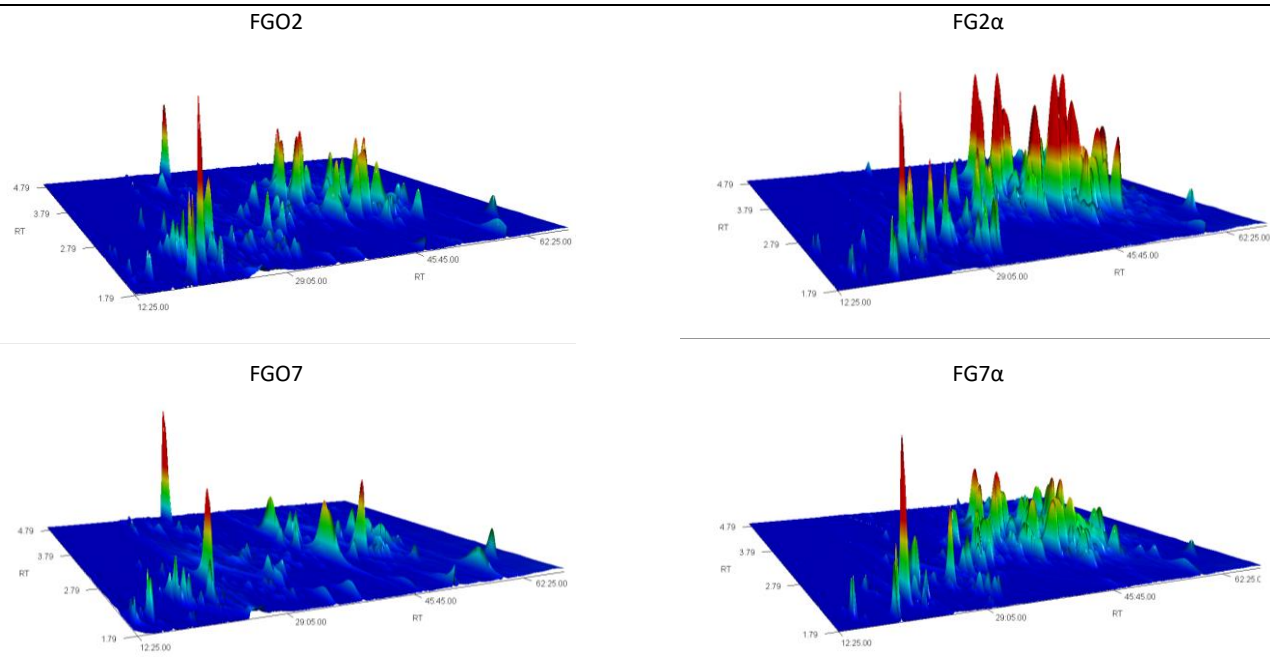


Figure 45. Two-dimensional chromatograms of FGO2, FG2 α , FGO7 and FG7 α . Ion 43, characteristic of polyols is displayed and shows the diversity of synthesized compounds and relative differences between calcium hydroxide and olivine.

4.2.3 Evolution of sugars content

As can be seen, from **Figure 46**, the highest sugar abundancies are obtained for FG2 α using the traditional calcium hydroxide catalyst of the formose reaction. Concentrations up to 1.16×10^{-3} M were found for DL-xylose. Using olivine, the highest concentration found was also for xylose with 3.90×10^{-4} M in FGO2. Unsurprisingly, the presence of glycolaldehyde in addition to formaldehyde leads to higher sugar content: 6.65×10^{-4} M and 9.83×10^{-4} M are reported for F7 α and FG7 α , respectively, whereas 2.97×10^{-4} M and 3.90×10^{-4} M are reported for FO2 and FGO2, respectively. Similarly, using Ca(OH)₂, the presence of glycolaldehyde greatly impacts the kinetics of C₅ and C₆ sugar formation. Indeed, almost no sugar content was reported for F2 α and 6.65×10^{-4} M for F7 α , whereas the highest reported values 1.16×10^{-3} M and 9.83×10^{-4} M are for FG2 α and FG7 α . Furthermore, comparing F2 α (almost zero sugar content) and FO2 (2.97×10^{-4} M for lyxose), it appears that olivine is a better catalyst than Ca(OH)₂ when using only formaldehyde.

Both catalysts lead to a wide variety of compounds, as can be seen in **Figure 45**, including sugars and sugar-related compounds. Indeed, although we have focused here on quantifying 10 sugars and 6 sugar alcohols (and their enantiomers, when possible), many other chromatographic peaks could correspond to sugars formed in those samples. Using aldonitrile acetate (ANA) derivatization, the *PIIM* team estimated that about 35 peaks could be associated with oses or polyols in the highly concentrated samples (FO2, FO7, FGO2, FG2 α , and FG7 α) by comparing their mass spectra and the NIST database. As a reminder, the major drawback of ANA derivatization is the lack of enantioseparation of C₄, C₅, and C₆ sugars.

Furthermore, the abundance of sugars formed is also an interesting result of this study. C₅ sugars are found in highest amount in all samples compared to C₄ or C₆ sugars. It is interesting to note that between days 2 and 7, a decrease in C₅ sugars is expected and obtained, while an increase in C₆ sugars is expected but not obtained. It is therefore possible that aldopentoses (ribose, arabinose, lyxose, xylose) are more likely to isomerize into ketopentoses (e.g., ribulose) than to produce aldohexoses by aldol reaction (**Figure 8**, p. 30). Surprisingly, the ribulose content is barely detectable, which undermines this hypothesis. Similarly, fructose should increase since aldohexoses (e.g., glucose and galactose) can isomerize to ketohexoses (e.g., fructose) but follows the same trend as glucose and galactose with a very high content compared to ribulose. In the end, it is likely that all the sugars studied here remain in equilibrium with each other and decrease overall with time, probably leading to branched sugars and secondary products before being degraded. It should be noted that fructose and ribulose were not directly quantified because

no calibration curve was available for these compounds. Their concentration was approximated using the calibration curve of xylose but with a correction factor because they were injected at a single concentration. Therefore, the concentration values obtained must be considered as rough estimates, but the trend between samples should be accurate.

Another important result is the presence of 2-deoxyribose in several samples. Although this compound has been previously detected with other deoxysugars²⁷⁵ under hydrothermal conditions, its presence indicates that formation of this compound could have been occurred during parent body processing of meteorites in the presence of phyllosilicates such as olivine. The synthesis of deoxy sugars would not be due to the formose reaction but could be the result of the combination of acetaldehyde and formaldehyde in the presence of a divalent metal oxide, or the combination of glyceraldehyde and acetaldehyde²⁷⁶. Here, this study reveals that a similar range of 2-deoxyribose concentration is achieved using calcium hydroxide (2.82×10^{-6} M for FG2 α and 1.09×10^{-5} M for F7 α) and olivine (2.73×10^{-6} M for FGO2 and 1.01×10^{-5} M for FGO7) catalysts.

The general trend is that C₅ sugars are most abundant on days 2 and 7. This would, however, need to be correlated with the total amount of C₆ sugars, as only glucose and galactose were quantified. Unfortunately, mannose could not be identified because the chromatogram is too crowded in its retention area. An intermediate time between day 7 and day 45 would have been interesting to study to follow the decrease in sugar content and to confirm if C₅ and C₆ sugars decrease in the same manner as previously reported. Among C₅ sugars, xylose and lyxose are more abundant than ribose and arabinose in FG2 α . On the other hand, xylose and arabinose are more abundant in F7 α , FG7 α , FO2, FO7, FGO2, and FGO7. This finding is very interesting because one would expect the same sugar content for each C₅ sugar in all samples, or the same imbalance pattern between FG2 α , F7 α , and FO2 for example. Thus, it appears that the presence of glycolaldehyde in Ca(OH)₂-containing samples promotes the synthesis of xylose and lyxose (FG2 α) and subsequently improves the degradation and/or conversion kinetics of lyxose. Concerning the olivine-containing samples, the trend with and without glycolaldehyde remains the same but the relative intensities can be discussed, especially for FO2 where ribose is close to arabinose in terms of content. It would have been interesting to have data on threose to look for variations between threose and erythrose contents. Unfortunately, threose was not found in any samples, assuming that threose and erythrose share the same mass spectrum. The most plausible explanation would be that threose has a different MBA

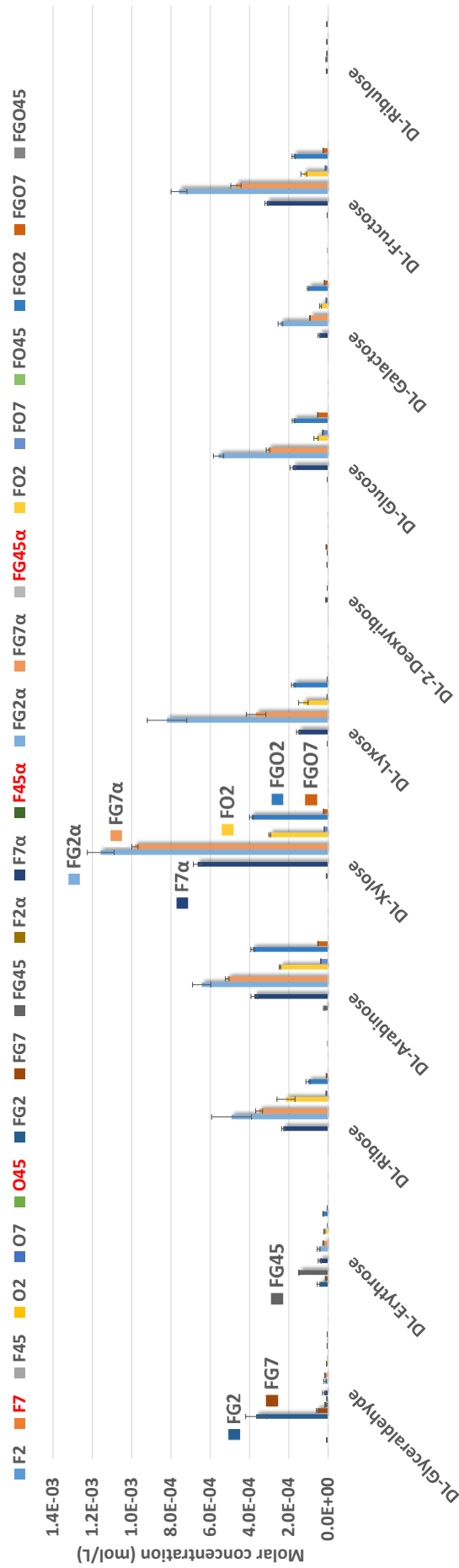


Figure 46. Evolution of sugar content using calcium hydroxide and olivine as catalysts for the formose reaction on days 2, 7 and 45. In red are highlighted samples not received.

ring location, resulting in different fragmentation patterns. Unfortunately, no threose standard was available to test this hypothesis.

The lifetime of sugars under hydrothermal conditions is very limited as none were found in samples FGO45 or FO45. Unfortunately, data from F45 α and FG45 α are missing but should show the same result because the Ca(OH)₂-catalyzed formose reaction is known to rapidly degrade sugars²⁷⁷. However, this shows that olivine does not provide better preservation of the synthesized sugars under these conditions.

Even in the absence of catalysts, the reaction occurs slowly, as the glyceraldehyde content is high in FG2, about 3.67×10^{-4} M, and decreases to 5.53×10^{-5} M in FG7 and 1.57×10^{-5} M in FG45. At the same time, for these samples, the concentration of erythrose is relatively high compared to the other samples, and highest for FG45 at 1.48×10^{-4} M. Higher carbon-containing sugars are only detected in samples FG45 and F45 samples with very low concentrations in the range of 10^{-6} – 10^{-5} M.

4.2.4 Evolution of sugar alcohols content

As can be seen in **Figure 47**, the evolution of the sugar alcohol content is less obvious than in the case of sugars. However, the most important information is the considerable increase in glycerol concentration after 45 days under hydrothermal conditions. Concentrations ranging from 6.24×10^{-3} M and 1.04×10^{-2} M were found for F45, FG45, FO45, and FGO45 while the day 2 and 7 samples were, at best, in the 10^{-5} M range. Glycerol can be obtained by the well-known Cannizzaro reaction of glyceraldehyde and formaldehyde¹⁵⁴, reduction of glyceraldehyde and even dihydroxyacetone. Given the low concentrations of glyceraldehyde and dihydroxyacetone on days 2 and 7, it is likely that the oligomerized sugars were reduced and/or cleaved because they were not detected after 45 days. Indeed, if it formed from glyceraldehyde, its synthesis from formaldehyde would have resulted in the detection of another low molecular weight sugar such as erythrose. The higher content of C₄ erythritol in FO45 and FGO45 tends to confirm this trend where sugars are degraded to lower molecular weight sugar alcohols. Interestingly, no such high values are reported for F45 and FG45 relative to glycerol. Thus, olivine could have an increased impact on the reduction and cleavage of sugars since the glycerol content is also higher at day 45 for samples containing olivine. A difference in pH can be noted between the day 45 samples, where the olivine-containing samples FO45 and FGO45 are less acidic (pH_{FO45} = 6, pH_{FGO45} = 7) than FG45 (pH_{FG45} = 4). The role of olivine as a pH buffer may therefore alter the mechanism by which sugars are degraded and reduced along with different kinetics. Unfortunately, no data are available for F45 α and FG45 α to support

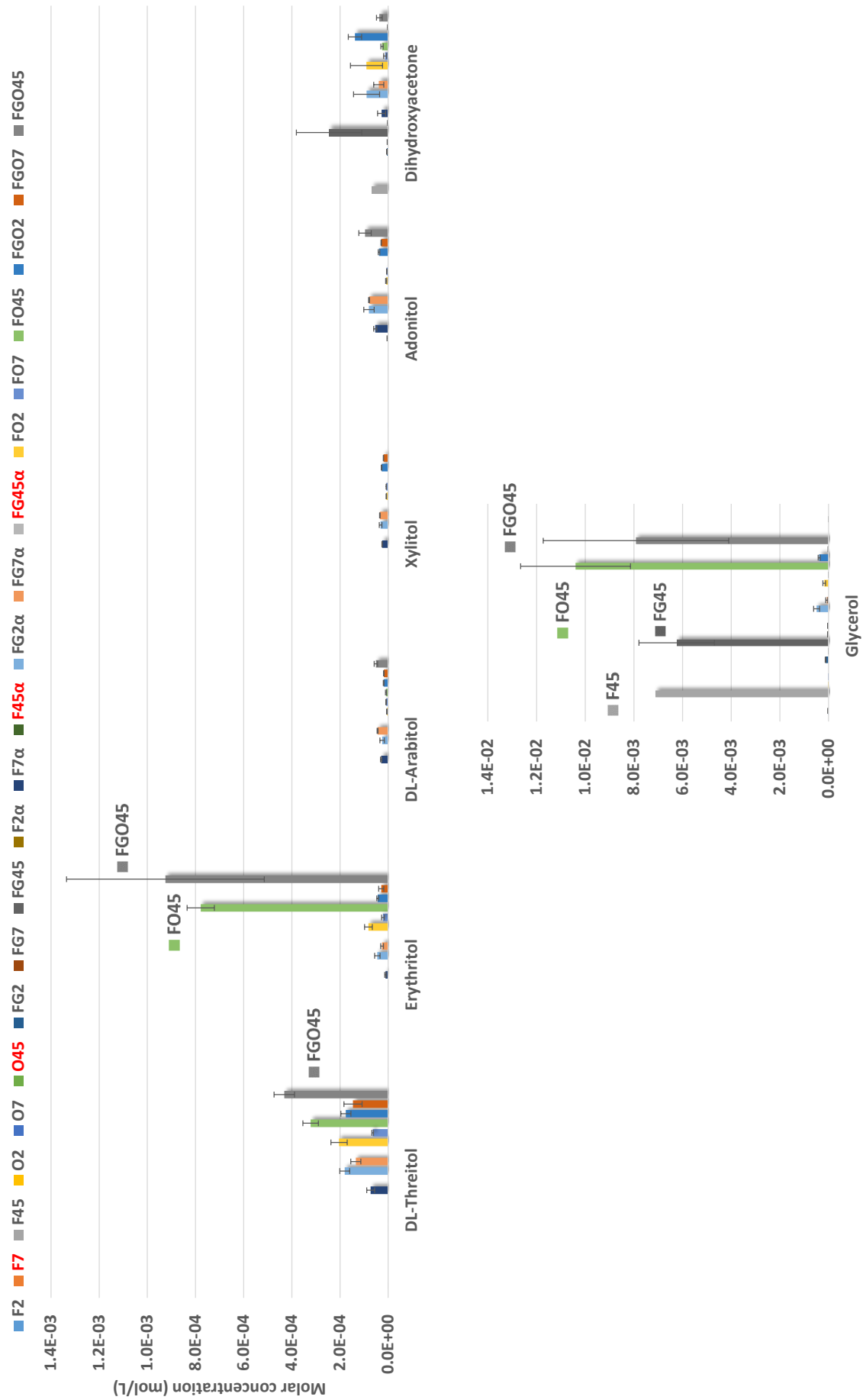


Figure 47. Evolution of sugar alcohols and dihydroxyacetone content using calcium hydroxide and olivine as catalysts for the formose reaction on days 2, 7, and 45. In red are highlighted samples not received.

these conclusions. The drop in pH of the formose reaction is an indicator of the Cannizzaro reaction which leads to alcohols and carboxylic acids²⁷⁸. The formation of various carboxylic acids in large quantities could be responsible of this drop as *e.g.*, glyceraldehyde can lead to glyceric acid and glycerol, glycolaldehyde to glycolic acid and ethylene glycol, and formaldehyde to formic acid and methanol¹⁵⁴. The detection of glycolic acid and especially glyceric acid, linked to glycerol formation, thus tend to support a Cannizzaro reaction. However, no standards were run at this point to investigate formic acid.

4.2.5 Enantiomeric excesses investigation

One of the objectives of the study was to search for potential *ees* in sugars formed under mineral-catalyzed hydrothermal conditions. However, in most cases, coelutions of the enantiomers were observed, even after selecting the most appropriate *m/z* for integration and quantification. In addition, sugars and sugar alcohols were sometimes quantified close to the limit of quantification, resulting in high *ee* errors. Thus, the *ee* obtained cannot be considered reliable. As an example, 2-deoxyribose, **Figure 48**, shows a *D-ee* of -21% with a relatively low standard deviation of 3.5%. However, the detected signal is very low in abundance, noisy, and it is difficult to assess whether coelution is occurring. Therefore, this value cannot be considered for any interpretation. On the other hand, lyxose and glucose are opposite examples, *i.e.*, they show high intensities (*S/N* is in the order of magnitude of 3000) and no visible significant coelution. The maximum *ee* values for lyxose and glucose are -4.48 ± 0.77 and 1.84 ± 0.29 , respectively. The other reported *ees* for these compounds are in the same range and have the same sign. Two conclusions can be drawn: (*i*) the number of analyses (4) to study these *ees* is small compared to the discussion in **3.2.1.7 Enantiomeric excess conservation** (p. 85) and (*ii*) a reproducible bias may be included in the results as many peak slices are integrated (due to GC×GC and peak tailing). Ultimately, a more comprehensive study of the derivatization in terms of *ee* should be performed before evaluating any significant *ee*. Thus, since no major enantiomeric imbalances were found, this led to the consideration that the compounds were synthesized in racemic proportions because olivine is not a chiral mineral and Ca(OH)_2 should not trigger *ees*.

4.2.6 Conclusion

Even with careful selection of the MBA/TFAA derivatization procedure, the use of a powerful resolution tool such as GC×GC, and selection of appropriate ions for quantification, coelutions of nontargeted compounds with the targeted enantiomers occurred and prevented accurate *ee* determination. The formose reaction was confirmed using well-known formose products with BSTFA derivatization, but it

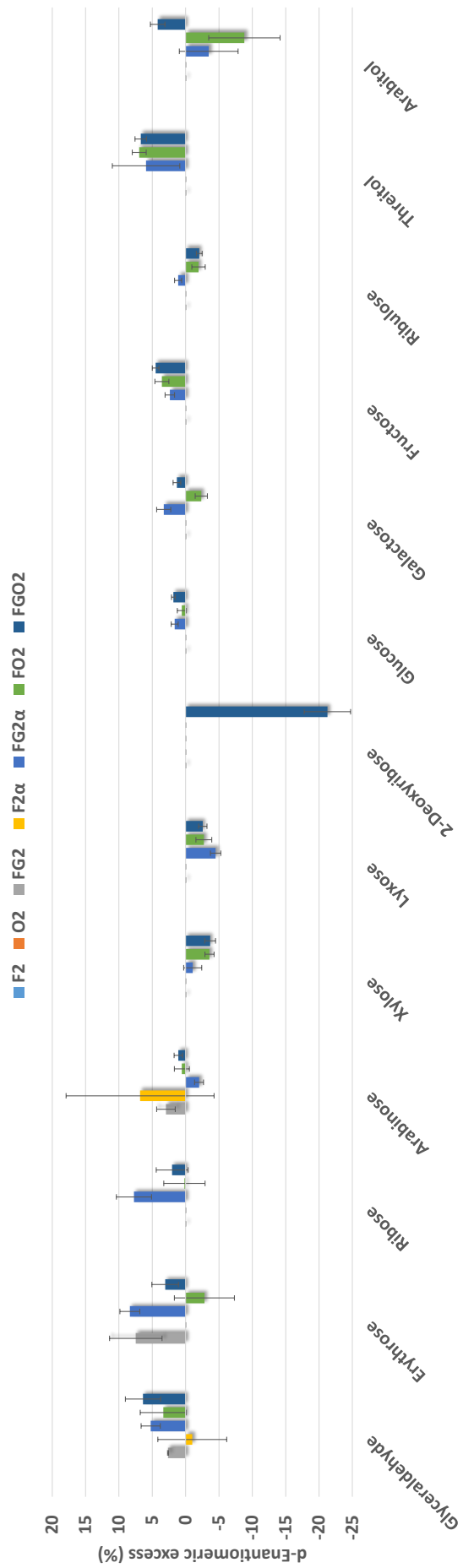


Figure 48. D-Enantiomeric excess in calcium hydroxide and olivine catalyzed formose reaction on day 2.

remains a complex sample that is difficult to analyze but may correspond in diversity to a true extraterrestrial sample. Nevertheless, the quantification of both sugar enantiomers and sugar alcohols led to interesting results concerning their evolution over a long period of time, up to 45 days, whereas studies on the formose reaction generally focus on shorter time scales. On the one hand, the sugars are rapidly synthesized over a period of at least 2 days and 7 days and are then probably transformed into branched or reduced sugars and degraded into lower molecular weight sugar alcohols as observed at day 45. In addition, olivine appears to be a better catalyst than $\text{Ca}(\text{OH})_2$ using formaldehyde only, despite lower molar concentrations of sugars have been reported. The detection of 2-deoxyribose is consistent with other studies conducted but is unlikely to be due to the formose reaction itself. It is nevertheless evidence that this life-required compound can be obtained under hydrothermal conditions in small quantities and gives clues to its plausible presence in extraterrestrial samples. Investigations on other timescales, i.e., first reaction hours, day 1 and between days 7 and 45 would be interesting to better understand the differences between calcium hydroxide and olivine catalysis. Besides, F45 α and FG45 α sample analyses would have provided valuable information on the stability of sugar alcohols using calcium hydroxide. Unfortunately, these samples were not available, and no comparison can be made with olivine. Finally, significant standard deviations are reported for sugars and especially sugar alcohols. These errors may be due to extrapolation out of the linear range that was evaluated for the $5 \times 10^{-6} \text{ M} - 10^{-4} \text{ M}$ range. Values as high as $1.2 \times 10^{-3} \text{ M}$ are however reported for sugars, and up to 10^{-2} M for sugar alcohols. In addition, the presence of contaminants such as metals and other species could interfere with the derivatization, as no ion exchange chromatography purification was employed.

CONCLUSION & PERSPECTIVES

Where and how life emerged are still ongoing questions. All living organisms use proteins consisting of L-amino acids and DNA/RNA consisting of D-2-deoxyribose/D-ribose. Finding clues to the origin of this biological homochirality would help to understand how life evolved. Despite numerous theories about the emergence of enantiomeric excesses *via* a symmetry breaking event followed by amplification mechanisms, no conclusion can be drawn about which is responsible for life's enantiomeric selection. Thus, it is still unclear whether this selection occurred *via* a deterministic or random mechanism.

However, since meteorite analyses have shown the presence of amino acids and sugar derivatives, whose *ees* follows the same trend as life's homochirality, as well as of circularly polarized light, capable of inducing *ees*, in the interstellar medium, a plausible scenario would be that these biosignatures form on dust grains and that an enantiomer is selected by enantioselective synthesis or photolysis. It is therefore of interest to develop analytical procedures to investigate the organic content of meteorites and samples returned from asteroids or other astrophysical objects in our solar system to study the abiotic synthesis of chiral biosignatures. This manuscript has attempted to investigate this challenge.

Since amino acids and sugars are priority targets in this analysis, a suitable derivatization method must be employed. The methanol/trifluoroacetic anhydride derivatization for amino acids, which has been used especially for isovaline, showed suitable overall resolution and enantioseparation of about 30 amino acids by GC×GC-TOFMS. The lack of absolute resolution can be overcome by using a CP-Chirasil-Dex CB instead of a Lipodex E stationary phase as primary column. Repeatability, linearity, stability, mass fragmentation, and conservation of enantiomeric excess have been studied, and this method is now ready to be used for extraterrestrial samples. Sugars, on the other hand, are much more challenging, as 5 different stereoisomers of a single enantiomer can be found in equilibrium due to intramolecular cyclization, which leads to 5- and 6-carbon rings. Many derivatization procedures have been developed in the literature, but none of them is a remarkable compromise. It must be adapted to the purpose of the analysis. Thus, methylboronic acid/trifluoroacetic anhydride has been proposed as an alternative allowing the separation and enantioseparation of about 15 sugars and sugar alcohols. The main known drawbacks of this method are the non-detection of sugar acids as well as the tailing of high molecular weight sugar alcohols during GC×GC analysis. In addition, the use of trifluoroacetic anhydride is a compromise as the detection limits of C₂ to C₅ sugars are lowered using this second derivatization step but allows the detection of *conformer compatible* sugars, sugar alcohols and deoxy sugars.

Prior to derivatization of extraterrestrial or extraterrestrial-like samples, a purification and desalting step is usually performed to avoid subsequent derivatization disruption and allows for the selection of compounds by cationic filtering. Using such a configuration, and MeOH/TFAA derivatization, amino acid recoveries were studied and showed values between 61.2% and 115.8%. However, contamination was reported but was mainly due to the quality of the ammonia used as elution solvent in the fractionation step, which was particularly the case for β -alanine with recoveries above 800%. The know-how of handmade columns was developed, and early developments of ion exchange chromatography showed recoveries of alanine around $95 \pm 5\%$ as well as recoveries of ribose around $96 \pm 10\%$ which is promising for sugar recoveries.

Sampling and extraction were the last to be studied in the entire procedure, but the first tests on amino acids using water hydrolysis showed overall recoveries in the range of 61.7% to 120.7%. Unfortunately, no data are available for sugars and further experiments should be conducted on sugars with an amino acid/sugar mixture to discard or not degradation by the Maillard reaction. On the other hand, sonication is considered to be an efficient method to safely extract sugars and amino acids and will be used for further testing. Based on the derivatization methods studied or developed and using ion exchange chromatography, two types of simulated samples were analyzed.

The first, the formose reaction, is known to lead to a wide variety of sugars, sugar alcohols, and sugar acids, and has been shown to be mineral-catalyzed in the presence of olivine, a very abundant mineral in the solar system. Many minerals, including olivine, exhibit this property and this work shows that olivine can act as a formose reaction catalyst starting from formaldehyde under hydrothermal conditions. However, the data obtained do not allow us to conclude whether olivine produces more, or more diverse sugars compared to the traditional calcium hydroxide catalyst during the whole process, although the highest values reported are for calcium hydroxide. Although the abundances of sugars are known to decrease rapidly, another interesting result is the impressive lifetime of sugar alcohols that are still present after 45 days of hydrothermal alteration while sugars have not been detected. Furthermore, given the surprisingly high glycerol content after 45 days and the low content of potential precursors such as glyceraldehyde and dihydroxyacetone throughout days 2 and 7, it is likely that sugars at some point stop gaining in complexity and are instead degraded and reduced to smaller sugar alcohols and sugar acids *via* the Cannizzaro reaction. In some ways, this corroborates the results of meteorite analysis where high molecular weight sugars and sugar derivatives are not detected. The detection of 2-deoxyribose is

consistent with other work, which gives clues to the possible presence of this life-required compound in extraterrestrial matter. The evolution of sugars from C₅ to C₆, however, did not show the expected trend. Indeed, the C₅ and C₆ aldoses and ketoses decrease in abundance in a similar way while an increase in C₆ should theoretically be obtained.

The availability of interstellar formaldehyde for such a reaction to occur is often discussed. Hexamethylenetetramine (HMT), which was recently analyzed directly in an extraterrestrial sample, could be a feedstock for both formaldehyde and ammonia, and is the second application of this manuscript. Interestingly, HMT is also known to potentially lead to amino acids during parent body alteration processes. The present work, using methanol/trifluoroacetic anhydride derivatization and ion exchange chromatography, detected 13 additional amino acids compared to previous works. Because a higher concentration of HMT led to a higher abundance of low-molecular-weight amino acids, it is likely that the formose reaction in the presence of ammonia (sugar model) favored the synthesis of α - and β -amino acids rather than γ -amino acids. However, this result should be correlated with the analysis of sugars to examine their relative proportions. Indeed, even if the analyzed sugar fractions did not show the presence of any sugars, they still could have been formed and be degraded as 31 days of hydrothermal treatment was used. Unfortunately, MBA/TFAA derivatization, which was not used, would have been a better alternative to detect sugar alcohols and discuss whether sugars and sugar derivatives were formed. Nevertheless, the HMT analysis represents our first analysis of a complex sample using the entire procedure (except for the sample extraction part) that proved to be effective.

The objectives defined at the beginning of this manuscript were to develop a procedure to extract, purify, fractionate, derivatize, and analyze extraterrestrial samples. Derivatization and GC \times GC analysis of amino acids and sugars have been studied and are suitable for this purpose, but the MBA/TFAA derivatization for sugars would require more exhaustive experiments. Purification and fractionation by ion exchange chromatography showed good recoveries for amino acids and ribose. The main advantages are the simultaneous study of amino acids and sugars on a single sample and desalting. Further research is needed to estimate the recovery of other sugars. Sampling and extraction require extensive investigations, especially since sonication will be used for future sample processing, which has not been studied here. Nevertheless, hydrolysis with water did not show any degradation of the amino acids. Future applications of this procedure concern the analysis of interstellar ice analogs irradiated by circularly polarized light, the analysis of hydrothermal-altered samples and the analysis of meteorites.

REFERENCES

- (1) Tetz, V. V.; Tetz, G. V. A New Biological Definition of Life. *Biomol. Concepts* **2020**, *11* (1), 1–6. <https://doi.org/10.1515/bmc-2020-0001>.
- (2) Avalos, M.; Babiano, R.; Cintas, P.; Jiménez, J. L.; Palacios, J. C. From Parity to Chirality: Chemical Implications Revisited. *Tetrahedron Asymmetry* **2000**, *11* (14), 2845–2874. [https://doi.org/10.1016/S0957-4166\(00\)00265-2](https://doi.org/10.1016/S0957-4166(00)00265-2).
- (3) Aliashkevich, A.; Alvarez, L.; Cava, F. New Insights Into the Mechanisms and Biological Roles of D-Amino Acids in Complex Eco-Systems. *Front. Microbiol.* **2018**, *9*, 683. <https://doi.org/10.3389/fmicb.2018.00683>.
- (4) Pikuta, E. V.; Hoover, R. B.; Klyce, B.; Davies, P. C. W.; Davies, P. Bacterial Utilization of L -Sugars and D -Amino Acids; Hoover, R. B., Levin, G. V., Rozanov, A. Y., Eds.; San Diego, California, USA, 2006; p 63090A. <https://doi.org/10.1117/12.690434>.
- (5) Fujii, N. [No Title Found]. *Orig. Life Evol. Biosph.* **2002**, *32* (2), 103–127. <https://doi.org/10.1023/A:1016031014871>.
- (6) Sandars, P. G. H. A Toy Model for the Generation of Homochirality during Polymerization. *Orig. Life Evol. Biosph.* **2003**, *33* (6), 575–587. <https://doi.org/10.1023/A:1025705401769>.
- (7) Herbst, E.; van Dishoeck, E. F. Complex Organic Interstellar Molecules. *Annu. Rev. Astron. Astrophys.* **2009**, *47* (1), 427–480. <https://doi.org/10.1146/annurev-astro-082708-101654>.
- (8) Irvine, W. M. The Molecular Composition of Dense Interstellar Clouds. In *Chemistry in Space*; Greenberg, J. M., Pirronello, V., Eds.; Springer Netherlands: Dordrecht, 1991; pp 89–121. https://doi.org/10.1007/978-94-009-0695-2_4.
- (9) Bonner, W. A. Origins of Chiral Homogeneity in Nature. In *Topics in Stereochemistry*; Eliel, E. L., Wilen, S. H., Eds.; John Wiley & Sons, Inc.: Hoboken, NJ, USA, 2007; pp 1–96. <https://doi.org/10.1002/9780470147276.ch1>.
- (10) MacDermott, A. J. 8.2 Perspective and Concepts: Biomolecular Significance of Homochirality: The Origin of the Homochiral Signature of Life. In *Comprehensive Chirality*; Elsevier, 2012; pp 11–38. <https://doi.org/10.1016/B978-0-08-095167-6.00804-1>.
- (11) Barron, L. D. *Molecular Light Scattering and Optical Activity*, 2nd ed.; Cambridge University Press, 2004. <https://doi.org/10.1017/CBO9780511535468>.
- (12) Rikken, G. L. J. A.; Raupach, E. Enantioselective Magnetochiral Photochemistry. *Nature* **2000**, *405* (6789), 932–935. <https://doi.org/10.1038/35016043>.
- (13) Wu, C. S.; Ambler, E.; Hayward, R. W.; Hoppes, D. D.; Hudson, R. P. Experimental Test of Parity Conservation in Beta Decay. *Phys. Rev.* **1957**, *105* (4), 1413–1415. <https://doi.org/10.1103/PhysRev.105.1413>.
- (14) Hegstrom, R. A. Parity Violation and Chiral Symmetry Breaking of a Racemic Mixture. *Biosystems* **1987**, *20* (1), 49–56. [https://doi.org/10.1016/0303-2647\(87\)90019-0](https://doi.org/10.1016/0303-2647(87)90019-0).
- (15) Reiner, C.; Nicholson, G. J.; Nagel, U.; Schurig, V. Evaluation of Enantioselective Gas Chromatography for the Determination of Minute Deviations from Racemic Composition of α -Amino Acids with Emphasis on Tyrosine: Accuracy and Precision of the Method. *Chirality* **2007**, *19* (5), 401–414. <https://doi.org/10.1002/chir.20390>.
- (16) Tranter, G. E. The Parity Violating Energy Differences between the Enantiomers of α -Amino Acids. *Mol. Phys.* **1985**, *56* (4), 825–838. <https://doi.org/10.1080/00268978500102741>.

-
- (17) Wolfram Hans-Peter Thiemann. A Short History of the Investigation of the Origin of the Terrestrial Biosphere's Homochirality (Some Personal Remarks, Recalling Historical Milestones). *Journal of Interdisciplinary Methodologies and Issues in Science* **2018**. <https://doi.org/hal-01819743>.
- (18) Hawbaker, N. A.; Blackmond, D. G. Energy Threshold for Chiral Symmetry Breaking in Molecular Self-Replication. *Nat. Chem.* **2019**, *11* (10), 957–962. <https://doi.org/10.1038/s41557-019-0321-Y>.
- (19) Hegstrom, R. A. Weak Neutral Current and β Radiolysis Effects on the Origin of Biomolecular Chirality. *Nature* **1985**, *315* (6022), 749–750. <https://doi.org/10.1038/315749a0>.
- (20) Inoue, Y.; Ramamurthy, V. *Chiral Photochemistry*; Marcel Dekker: New York, 2004.
- (21) Cocke, W. J.; Muncaster, G. W.; Gehrels, T. Upper Limit to Circular Polarization of Optical Pulsar NP 0532. *Astrophys. J.* **1971**, *169*, L119. <https://doi.org/10.1086/180825>.
- (22) Bailey, J.; Chrysostomou, A.; Hough, J. H.; Gledhill, T. M.; McCall, A.; Clark, S.; Ménard, F.; Tamura, M. Circular Polarization in Star- Formation Regions: Implications for Biomolecular Homochirality. *Science* **1998**, *281* (5377), 672–674. <https://doi.org/10.1126/science.281.5377.672>.
- (23) Fukue, T.; Tamura, M.; Kandori, R.; Kusakabe, N.; Hough, J. H.; Bailey, J.; Whittet, D. C. B.; Lucas, P. W.; Nakajima, Y.; Hashimoto, J. Extended High Circular Polarization in the Orion Massive Star Forming Region: Implications for the Origin of Homochirality in the Solar System. *Orig. Life Evol. Biospheres* **2010**, *40* (3), 335–346. <https://doi.org/10.1007/s11084-010-9206-1>.
- (24) Kwon, J.; Tamura, M.; Lucas, P. W.; Hashimoto, J.; Kusakabe, N.; Kandori, R.; Nakajima, Y.; Nagayama, T.; Nagata, T.; Hough, J. H. NEAR-INFRARED CIRCULAR POLARIZATION IMAGES OF NGC 6334-V. *Astrophys. J.* **2013**, *765* (1), L6. <https://doi.org/10.1088/2041-8205/765/1/L6>.
- (25) Lucas, P. W.; Hough, J. H.; Bailey, J.; Chrysostomou, A.; Gledhill, T. M.; McCall, A. UV Circular Polarisation in Star Formation Regions: The Origin of Homochirality? *Orig. Life Evol. Biospheres* **2005**, *35* (1), 29–60. <https://doi.org/10.1007/s11084-005-7770-6>.
- (26) Yoo, S.; Park, Q.-H. Enhancement of Chiroptical Signals by Circular Differential Mie Scattering of Nanoparticles. *Sci. Rep.* **2015**, *5* (1), 14463. <https://doi.org/10.1038/srep14463>.
- (27) Bailey, J. Astronomical Sources of Circularly Polarized Light and the Origin of Homochirality. *Orig. Life Evol. Biosph.* **2001**, *31* (1/2), 167–183. <https://doi.org/10.1023/A:1006751425919>.
- (28) Meinert, C.; de Marcellus, P.; Le Sergeant d'Hendecourt, L.; Nahon, L.; Jones, N. C.; Hoffmann, S. V.; Bredehöft, J. H.; Meierhenrich, U. J. Photochirogenesis: Photochemical Models on the Absolute Asymmetric Formation of Amino Acids in Interstellar Space. *Phys. Life Rev.* **2011**, *8* (3), 307–330. <https://doi.org/10.1016/j.pprev.2011.08.005>.
- (29) Meinert, C.; Bredehöft, J. H.; Filippi, J.-J.; Baraud, Y.; Nahon, L.; Wien, F.; Jones, N. C.; Hoffmann, S. V.; Meierhenrich, U. J. Anisotropy Spectra of Amino Acids. *Angew. Chem. Int. Ed.* **2012**, *51* (18), 4484–4487. <https://doi.org/10.1002/anie.201108997>.
- (30) Balavoine, G.; Moradpour, A.; Kagan, H. B. Preparation of Chiral Compounds with High Optical Purity by Irradiation with Circularly Polarized Light, a Model Reaction for the Prebiotic Generation of Optical Activity. *J. Am. Chem. Soc.* **1974**, *96* (16), 5152–5158. <https://doi.org/10.1021/ja00823a023>.
- (31) Kuhn, W.; Braun, E. Photochemische Erzeugung optisch aktiver Stoffe. *Naturwissenschaften* **1929**, *17* (14), 227–228. <https://doi.org/10.1007/BF01506782>.

- (32) Flores, J. J.; Bonner, W. A.; Massey, G. A. Asymmetric Photolysis of (RS)-Leucine with Circularly Polarized Ultraviolet Light. *J. Am. Chem. Soc.* **1977**, *99* (11), 3622–3625. <https://doi.org/10.1021/ja00453a018>.
- (33) Kagan, H.; Moradpour, A.; Nicoud, J. F.; Balavoine, G.; Martin, R. H.; Cosyn, J. P. Photochemistry with Circularly Polarised Light. II) Asymmetric Synthesis of Octa and Nonahelicene. *Tetrahedron Lett.* **1971**, *12* (27), 2479–2482. [https://doi.org/10.1016/S0040-4039\(01\)96896-0](https://doi.org/10.1016/S0040-4039(01)96896-0).
- (34) Myrgorodska, I.; Meinert, C.; Hoffmann, S. V.; Jones, N. C.; Nahon, L.; Meierhenrich, U. J. Light on Chirality: Absolute Asymmetric Formation of Chiral Molecules Relevant in Prebiotic Evolution. *ChemPlusChem* **2017**, *82* (1), 74–87. <https://doi.org/10.1002/cplu.201600214>.
- (35) Snyder, P. A.; Vipond, P. M.; Johnson, W. C. Circular Dichroism of the Alkyl Amino Acids in the Vacuum Ultraviolet. *Biopolymers* **1973**, *12* (5), 975–992. <https://doi.org/10.1002/bip.1973.360120504>.
- (36) Matsuo, K.; Gekko, K. Vacuum-Ultraviolet Circular Dichroism Study of Saccharides by Synchrotron Radiation Spectrophotometry. *Carbohydr. Res.* **2004**, *339* (3), 591–597. <https://doi.org/10.1016/j.carres.2003.11.019>.
- (37) Nielsen, S. B.; Chakraborty, T.; Hoffmann, S. V. Synchrotron Radiation Circular Dichroism Spectroscopy of Ribose and Deoxyribose Sugars, Adenosine, AMP and DAMP Nucleotides. *ChemPhysChem* **2005**, *6* (12), 2619–2624. <https://doi.org/10.1002/cphc.200500236>.
- (38) Meierhenrich, U. J.; Nahon, L.; Alcaraz, C.; Bredehöft, J. H.; Hoffmann, S. V.; Barbier, B.; Brack, A. Asymmetric Vacuum UV Photolysis of the Amino Acid Leucine in the Solid State. *Angew. Chem. Int. Ed.* **2005**, *44* (35), 5630–5634. <https://doi.org/10.1002/anie.200501311>.
- (39) Meinert, C.; Hoffmann, S. V.; Cassam-Chenaï, P.; Evans, A. C.; Giri, C.; Nahon, L.; Meierhenrich, U. J. Photonenergy-Controlled Symmetry Breaking with Circularly Polarized Light. *Angew. Chem. Int. Ed.* **2014**, *53* (1), 210–214. <https://doi.org/10.1002/anie.201307855>.
- (40) Tia, M.; Cunha de Miranda, B.; Daly, S.; Gaie-Levrel, F.; Garcia, G. A.; Nahon, L.; Powis, I. VUV Photodynamics and Chiral Asymmetry in the Photoionization of Gas Phase Alanine Enantiomers. *J. Phys. Chem. A* **2014**, *118* (15), 2765–2779. <https://doi.org/10.1021/jp5016142>.
- (41) Meinert, C.; Garcia, A. D.; Topin, J.; Jones, N. C.; Diekmann, M.; Berger, R.; Nahon, L.; Hoffmann, S. V.; Meierhenrich, U. J. Amino Acid Gas Phase Circular Dichroism and Implications for the Origin of Biomolecular Asymmetry. *Nat. Commun.* **2022**, *13* (1), 502. <https://doi.org/10.1038/s41467-022-28184-0>.
- (42) Tia, M.; Cunha de Miranda, B.; Daly, S.; Gaie-Levrel, F.; Garcia, G. A.; Nahon, L.; Powis, I. VUV Photodynamics and Chiral Asymmetry in the Photoionization of Gas Phase Alanine Enantiomers. *J. Phys. Chem. A* **2014**, *118* (15), 2765–2779. <https://doi.org/10.1021/jp5016142>.
- (43) Glavin, D. P.; Burton, A. S.; Elsilá, J. E.; Aponte, J. C.; Dworkin, J. P. The Search for Chiral Asymmetry as a Potential Biosignature in Our Solar System. *Chem. Rev.* **2020**, *120* (11), 4660–4689. <https://doi.org/10.1021/acs.chemrev.9b00474>.
- (44) Blackmond, D. G. The Origin of Biological Homochirality. *Cold Spring Harb. Perspect. Biol.* **2019**, *11* (3), a032540. <https://doi.org/10.1101/cshperspect.a032540>.
- (45) Jacques, J.; Collet, A.; Wilen, S. H. *Enantiomers, Racemates, and Resolutions*; Wiley, 1981.

- (46) Viedma, C.; Ortiz, J. E.; Torres, T. de; Izumi, T.; Blackmond, D. G. Evolution of Solid Phase Homochirality for a Proteinogenic Amino Acid. *J. Am. Chem. Soc.* **2008**, *130* (46), 15274–15275. <https://doi.org/10.1021/ja8074506>.
- (47) Viedma, C. Chiral Symmetry Breaking During Crystallization: Complete Chiral Purity Induced by Nonlinear Autocatalysis and Recycling. *Phys. Rev. Lett.* **2005**, *94* (6), 065504. <https://doi.org/10.1103/PhysRevLett.94.065504>.
- (48) Ostwald, W. Studien Über Die Bildung Und Umwandlung Fester Körper: 1. Abhandlung: Übersättigung Und Überkaltung. *Z. Für Phys. Chem.* **1897**, *22U* (1), 289–330. <https://doi.org/doi:10.1515/zpch-1897-2233>.
- (49) Noorduyn, W. L.; Izumi, T.; Millemaggi, A.; Leeman, M.; Meekes, H.; Van Enkevort, W. J. P.; Kellogg, R. M.; Kaptein, B.; Vlieg, E.; Blackmond, D. G. Emergence of a Single Solid Chiral State from a Nearly Racemic Amino Acid Derivative. *J. Am. Chem. Soc.* **2008**, *130* (4), 1158–1159. <https://doi.org/10.1021/ja7106349>.
- (50) Frank, F. C. On Spontaneous Asymmetric Synthesis. *Biochim. Biophys. Acta* **1953**, *11*, 459–463. [https://doi.org/10.1016/0006-3002\(53\)90082-1](https://doi.org/10.1016/0006-3002(53)90082-1).
- (51) Bryliakov, K. P. Chemical Mechanisms of Prebiotic Chirality Amplification. *Research* **2020**, *2020*, 1–8. <https://doi.org/10.34133/2020/5689246>.
- (52) Soai, K.; Shibata, T.; Morioka, H.; Choji, K. Asymmetric Autocatalysis and Amplification of Enantiomeric Excess of a Chiral Molecule. *Nature* **1995**, *378* (6559), 767–768. <https://doi.org/10.1038/378767a0>.
- (53) Soai, K.; Niwa, S.; Hori, H. Asymmetric Self-Catalytic Reaction. Self-Production of Chiral 1-(3-Pyridyl)Alkanols as Chiral Self-Catalysts in the Enantioselective Addition of Dialkylzinc Reagents to Pyridine-3-Carbaldehyde. *J. Chem. Soc. Chem. Commun.* **1990**, No. 14, 982. <https://doi.org/10.1039/c39900000982>.
- (54) Talsi, E. P.; Samsonenko, D. G.; Bryliakov, K. P. Asymmetric Autoamplification in the Oxidative Kinetic Resolution of Secondary Benzylic Alcohols Catalyzed by Manganese Complexes. *ChemCatChem* **2017**, *9* (13), 2599–2607. <https://doi.org/10.1002/cctc.201700438>.
- (55) Talsi, E. P.; Bryliakov, K. P. Autoamplification-Enhanced Oxidative Kinetic Resolution of *Sec*-Alcohols and Alkyl Mandelates, and Its Kinetic Model. *ChemCatChem* **2018**, *10* (12), 2693–2699. <https://doi.org/10.1002/cctc.201800180>.
- (56) Geiger, Y.; Achard, T.; Maise-François, A.; Bellemin-Lapponnaz, S. Hyperpositive Nonlinear Effects in Asymmetric Catalysis. *Nat. Catal.* **2020**, *3* (5), 422–426. <https://doi.org/10.1038/s41929-020-0441-1>.
- (57) Steendam, R. R. E.; Verkade, J. M. M.; van Benthem, T. J. B.; Meekes, H.; van Enkevort, W. J. P.; Raap, J.; Rutjes, F. P. J. T.; Vlieg, E. Emergence of Single-Molecular Chirality from Achiral Reactants. *Nat. Commun.* **2014**, *5* (1), 5543. <https://doi.org/10.1038/ncomms6543>.
- (58) Miyagawa, S.; Aiba, S.; Kawamoto, H.; Tokunaga, Y.; Kawasaki, T. Absolute Asymmetric Strecker Synthesis in a Mixed Aqueous Medium: Reliable Access to Enantioenriched α -Aminonitrile. *Org. Biomol. Chem.* **2019**, *17* (5), 1238–1244. <https://doi.org/10.1039/C8OB03092H>.
- (59) Breslow, R.; Cheng, Z.-L. L-Amino Acids Catalyze the Formation of an Excess of D-Glyceraldehyde, and Thus of Other D Sugars, under Credible Prebiotic Conditions. *Proc. Natl. Acad. Sci.* **2010**, *107* (13), 5723–5725. <https://doi.org/10.1073/pnas.1001639107>.

- (60) Powner, M. W.; Gerland, B.; Sutherland, J. D. Synthesis of Activated Pyrimidine Ribonucleotides in Prebiotically Plausible Conditions. *Nature* **2009**, *459* (7244), 239–242. <https://doi.org/10.1038/nature08013>.
- (61) Hein, J. E.; Tse, E.; Blackmond, D. G. A Route to Enantiopure RNA Precursors from Nearly Racemic Starting Materials. *Nat. Chem.* **2011**, *3* (9), 704–706. <https://doi.org/10.1038/nchem.1108>.
- (62) Morowitz, H. J. A Mechanism for the Amplification of Fluctuations in Racemic Mixtures. *J. Theor. Biol.* **1969**, *25* (3), 491–494. [https://doi.org/10.1016/S0022-5193\(69\)80035-4](https://doi.org/10.1016/S0022-5193(69)80035-4).
- (63) Klussmann, M.; Iwamura, H.; Mathew, S. P.; Wells, D. H.; Pandya, U.; Armstrong, A.; Blackmond, D. G. Thermodynamic Control of Asymmetric Amplification in Amino Acid Catalysis. *Nature* **2006**, *441* (7093), 621–623. <https://doi.org/10.1038/nature04780>.
- (64) Klussmann, M.; White, A. J. P.; Armstrong, A.; Blackmond, D. G. Rationalization and Prediction of Solution Enantiomeric Excess in Ternary Phase Systems. *Angew. Chem. Int. Ed.* **2006**, *45* (47), 7985–7989. <https://doi.org/10.1002/anie.200602520>.
- (65) Klussmann, M.; Izumi, T.; White, A. J. P.; Armstrong, A.; Blackmond, D. G. Emergence of Solution-Phase Homochirality via Crystal Engineering of Amino Acids. *J. Am. Chem. Soc.* **2007**, *129* (24), 7657–7660. <https://doi.org/10.1021/ja0708870>.
- (66) Kondepudi, D. K.; Kaufman, R. J.; Singh, N. Chiral Symmetry Breaking in Sodium Chlorate Crystallization. *Science* **1990**, *250* (4983), 975–976. <https://doi.org/10.1126/science.250.4983.975>.
- (67) Langenbeck, W.; Triem, G. Zur Theorie Der Erhaltung Und Entstehung Optischer Aktivität in Der Natur. *Z. Für Phys. Chem.* **1936**, *177A* (1), 401–408. <https://doi.org/10.1515/zpch-1936-17737>.
- (68) Blair, N. E.; Bonner, W. A. Experiments of the Amplification of Optical Activity. *Orig. Life* **1980**, *10* (3), 255–263. <https://doi.org/10.1007/BF00928403>.
- (69) Wolfire, M. G.; McKee, C. F.; Hollenbach, D.; Tielens, A. Neutral Atomic Phases of the Interstellar Medium in the Galaxy. *Astrophys. J.* **2003**, *587* (1), 278.
- (70) Ehrenfreund, P.; Cami, J. Cosmic Carbon Chemistry: From the Interstellar Medium to the Early Earth. *Cold Spring Harb. Perspect. Biol.* **2010**, *2* (12), a002097–a002097. <https://doi.org/10.1101/cshperspect.a002097>.
- (71) Wooden, D. H.; Charnley, S. B.; Ehrenfreund, P. *Composition and Evolution of Interstellar Clouds: Comets II*; University of Arizona Press, Tucson, 2005.
- (72) Burke, D. J.; Brown, W. A. Ice in Space: Surface Science Investigations of the Thermal Desorption of Model Interstellar Ices on Dust Grain Analogue Surfaces. *Phys. Chem. Chem. Phys.* **2010**, *12* (23), 5947. <https://doi.org/10.1039/b917005g>.
- (73) D’Hendecourt, L. B.; Allamandola, L. J.; Greenberg, J. M. Time Dependent Chemistry in Dense Molecular Clouds. I. Grain Surface Reactions, Gas/Grain Interactions and Infrared Spectroscopy. *âp* **1985**, *152*, 130–150.
- (74) Chiar, J. E. The Nature and Evolution of Interstellar Ices. *Orig. Life Evol. Biosph.* **1997**, *27* (1/3), 79–100. <https://doi.org/10.1023/A:1006518029497>.
- (75) Garrod, R. T.; Weaver, S. L. W.; Herbst, E. Complex Chemistry in Star-Forming Regions: An Expanded Gas-Grain Warm-up Chemical Model. *Astrophys. J.* **2008**, *682* (1), 283–302. <https://doi.org/10.1086/588035>.

-
- (76) Moore, M. H.; Donn, B.; Khanna, R.; A'Hearn, M. F. Studies of Proton-Irradiated Cometary-Type Ice Mixtures. *Icarus* **1983**, *54* (3), 388–405. [https://doi.org/10.1016/0019-1035\(83\)90236-1](https://doi.org/10.1016/0019-1035(83)90236-1).
- (77) Millar, T. J. Molecules in High-Mass Star-Forming Regions - Theory and Observation. In *Science with the Atacama Large Millimeter Array (ALMA)*; 1999; p 38.
- (78) Dartois, E. The Ice Survey Opportunity of ISO. *Space Sci. Rev.* **2005**, *119* (1–4), 293–310. <https://doi.org/10.1007/s11214-005-8059-9>.
- (79) Ehrenfreund, P.; Kerkhof, O.; Schutte, W.; Boogert, A.; Gerakines, P.; Dartois, E.; D'Hendecourt, L.; Tielens, A.; Dishoeck, V.; Whittet, D. Laboratory Studies of Thermally Processed H₂O-CH₃OH-CO₂ Ice Mixtures and Their Astrophysical Implications. *Astron. Astrophys.* **1999**, *350*, 240–253.
- (80) D'Hendecourt, L. B.; Allamandola, L. J.; Greenberg, J. M. Time Dependent Chemistry in Dense Molecular Clouds. I. Grain Surface Reactions, Gas/Grain Interactions and Infrared Spectroscopy. *\aap* **1985**, *152*, 130–150.
- (81) Tielens, A. G. G. M.; Hagen, W. Model Calculations of the Molecular Composition of Interstellar Grain Mantles. *\aap* **1982**, *114* (2), 245–260.
- (82) Ehrenfreund, P.; Boogert, A. C. A.; Gerakines, P. A.; Tielens, A. G. G. M.; van Dishoeck, E. F. Infrared Spectroscopy of Interstellar Apolar Ice Analogs. *\aap* **1997**, *328*, 649–669.
- (83) Smoluchowski, R. Solar System Ice: Amorphous or Crystalline? *Science* **1983**, *222* (4620), 161–163. <https://doi.org/10.1126/science.222.4620.161>.
- (84) Bernstein, M. P.; Dworkin, J. P.; Sandford, S. A.; Cooper, G. W.; Allamandola, L. J. Racemic Amino Acids from the Ultraviolet Photolysis of Interstellar Ice Analogues. *Nature* **2002**, *416* (6879), 401–403. <https://doi.org/10.1038/416401a>.
- (85) Muñoz Caro, G. M.; Meierhenrich, U. J.; Schutte, W. A.; Barbier, B.; Arcones Segovia, A.; Rosenbauer, H.; Thiemann, W. H.-P.; Brack, A.; Greenberg, J. M. Amino Acids from Ultraviolet Irradiation of Interstellar Ice Analogues. *Nature* **2002**, *416* (6879), 403–406. <https://doi.org/10.1038/416403a>.
- (86) de Marcellus, P.; Meinert, C.; Nuevo, M.; Filippi, J.-J.; Danger, G.; Deboffle, D.; Nahon, L.; Le Sergeant d'Hendecourt, L.; Meierhenrich, U. J. NON-RACEMIC AMINO ACID PRODUCTION BY ULTRAVIOLET IRRADIATION OF ACHIRAL INTERSTELLAR ICE ANALOGS WITH CIRCULARLY POLARIZED LIGHT. *Astrophys. J.* **2011**, *727* (2), L27. <https://doi.org/10.1088/2041-8205/727/2/L27>.
- (87) Cronin, J. R.; Pizzarello, S. Amino Acid Enantiomer Excesses in Meteorites: Origin and Significance. *Adv. Space Res.* **1999**, *23* (2), 293–299. [https://doi.org/10.1016/S0273-1177\(99\)00050-2](https://doi.org/10.1016/S0273-1177(99)00050-2).
- (88) Pizzarello, S.; Zolensky, M.; Turk, K. A. Nonracemic Isovaline in the Murchison Meteorite: Chiral Distribution and Mineral Association. *Geochim. Cosmochim. Acta* **2003**, *67* (8), 1589–1595. [https://doi.org/10.1016/S0016-7037\(02\)01283-8](https://doi.org/10.1016/S0016-7037(02)01283-8).
- (89) Glavin, D. P.; Dworkin, J. P. Enrichment of the Amino Acid L-Isovaline by Aqueous Alteration on CI and CM Meteorite Parent Bodies. *Proc. Natl. Acad. Sci.* **2009**, *106* (14), 5487–5492. <https://doi.org/10.1073/pnas.0811618106>.
- (90) Agúndez, M.; Cernicharo, J.; Decin, L.; Encrenaz, P.; Teyssier, D. CONFIRMATION OF CIRCUMSTELLAR PHOSPHINE. *Astrophys. J.* **2014**, *790* (2), L27. <https://doi.org/10.1088/2041-8205/790/2/L27>.

- (91) Turner, A. M.; Bergantini, A.; Abplanalp, M. J.; Zhu, C.; Góbi, S.; Sun, B.-J.; Chao, K.-H.; Chang, A. H. H.; Meinert, C.; Kaiser, R. I. An Interstellar Synthesis of Phosphorus Oxoacids. *Nat. Commun.* **2018**, *9* (1), 3851. <https://doi.org/10.1038/s41467-018-06415-7>.
- (92) Nam, I.; Lee, J. K.; Nam, H. G.; Zare, R. N. Abiotic Production of Sugar Phosphates and Uridine Ribonucleoside in Aqueous Microdroplets. *Proc. Natl. Acad. Sci.* **2017**, *114* (47), 12396–12400. <https://doi.org/10.1073/pnas.1714896114>.
- (93) Turner, A. M.; Abplanalp, M. J.; Bergantini, A.; Frigge, R.; Zhu, C.; Sun, B.-J.; Hsiao, C.-T.; Chang, A. H. H.; Meinert, C.; Kaiser, R. I. Origin of Alkylphosphonic Acids in the Interstellar Medium. *Sci. Adv.* **2019**, *5* (8), eaaw4307. <https://doi.org/10.1126/sciadv.aaw4307>.
- (94) Cooper, G. W.; Onwo, W. M.; Cronin, J. R. Alkyl Phosphonic Acids and Sulfonic Acids in the Murchison Meteorite. *Geochim. Cosmochim. Acta* **1992**, *56* (11), 4109–4115. [https://doi.org/10.1016/0016-7037\(92\)90023-C](https://doi.org/10.1016/0016-7037(92)90023-C).
- (95) Meinert, C.; Myrgorodska, I.; de Marcellus, P.; Buhse, T.; Nahon, L.; Hoffmann, S. V.; d’Hendecourt, L. L. S.; Meierhenrich, U. J. Ribose and Related Sugars from Ultraviolet Irradiation of Interstellar Ice Analogs. *Science* **2016**, *352* (6282), 208–212. <https://doi.org/10.1126/science.aad8137>.
- (96) Furukawa, Y.; Chikaraishi, Y.; Ohkouchi, N.; Ogawa, N. O.; Glavin, D. P.; Dworkin, J. P.; Abe, C.; Nakamura, T. Extraterrestrial Ribose and Other Sugars in Primitive Meteorites. *Proc. Natl. Acad. Sci.* **2019**, *116* (49), 24440–24445. <https://doi.org/10.1073/pnas.1907169116>.
- (97) Breslow, R. On the Mechanism of the Formose Reaction. *Tetrahedron Lett.* **1959**, *1* (21), 22–26. [https://doi.org/10.1016/S0040-4039\(01\)99487-0](https://doi.org/10.1016/S0040-4039(01)99487-0).
- (98) Oba, Y.; Takano, Y.; Naraoka, H.; Watanabe, N.; Kouchi, A. Nucleobase Synthesis in Interstellar Ices. *Nat. Commun.* **2019**, *10* (1), 4413. <https://doi.org/10.1038/s41467-019-12404-1>.
- (99) Saladino, R.; Carota, E.; Botta, G.; Kapralov, M.; Timoshenko, G. N.; Rozanov, A. Y.; Krasavin, E.; Di Mauro, E. Meteorite-Catalyzed Syntheses of Nucleosides and of Other Prebiotic Compounds from Formamide under Proton Irradiation. *Proc. Natl. Acad. Sci.* **2015**, *112* (21), E2746–E2755. <https://doi.org/10.1073/pnas.1422225112>.
- (100) Menor-Salván, C.; Ruiz-Bermejo, Dra. M.; Guzmán, M. I.; Osuna-Esteban, S.; Veintemillas-Verdaguer, S. Synthesis of Pyrimidines and Triazines in Ice: Implications for the Prebiotic Chemistry of Nucleobases. *Chem. - Eur. J.* **2009**, *15* (17), 4411–4418. <https://doi.org/10.1002/chem.200802656>.
- (101) Weisberg, M. K.; McCoy, T. J.; Krot, A. N. Systematics and Evaluation of Meteorite Classification. In *Meteorites and the Early Solar System II*; Lauretta, D. S., McSween, H. Y., Eds.; 2006; p 19.
- (102) Gilmour, I. Structural and Isotopic Analysis of Organic Matter in Carbonaceous Chondrites. In *Treatise on Geochemistry*; Elsevier, 2003; pp 269–290. <https://doi.org/10.1016/B0-08-043751-6/01146-4>.
- (103) Monica M. Grady. *Catalogue of Meteorites*; 5th Edition; Cambridge University Press, 2000.
- (104) Bischoff, A.; Geiger, T. Meteorites from the Sahara: Find Locations, Shock Classification, Degree of Weathering and Pairing. *Meteoritics* **1995**, *30* (1), 113–122. <https://doi.org/10.1111/j.1945-5100.1995.tb01219.x>.

-
- (105) Garcia, A.; Meinert, C.; Sugahara, H.; Jones, N.; Hoffmann, S.; Meierhenrich, U. The Astrophysical Formation of Asymmetric Molecules and the Emergence of a Chiral Bias. *Life* **2019**, *9* (1), 29. <https://doi.org/10.3390/life9010029>.
- (106) Cooper, G.; Kimmich, N.; Belisle, W.; Sarinana, J.; Brabham, K.; Garrel, L. Carbonaceous Meteorites as a Source of Sugar-Related Organic Compounds for the Early Earth. *Nature* **2001**, *414* (6866), 879–883. <https://doi.org/10.1038/414879a>.
- (107) Cronin, J. R.; Chang, S. Organic Matter in Meteorites: Molecular and Isotopic Analyses of the Murchison Meteorite. In *The Chemistry of Life's Origins*; Greenberg, J. M., Mendoza-Gómez, C. X., Pirronello, V., Eds.; NATO Advanced Study Institute (ASI) Series C; 1993; Vol. 416, pp 209–258.
- (108) Fox, S.; Gspandl, A.; Weng, F. M. Acceleration of Amino Acid Racemization by Isovaline: Possible Implications for Homochirality and Biosignature Search. *Int. J. Astrobiol.* **2020**, *19* (3), 276–282. <https://doi.org/10.1017/S1473550420000014>.
- (109) Furukawa, Y.; Chikaraishi, Y.; Ohkouchi, N.; Ogawa, N. O.; Glavin, D. P.; Dworkin, J. P.; Abe, C.; Nakamura, T. Extraterrestrial Ribose and Other Sugars in Primitive Meteorites. *Proc. Natl. Acad. Sci.* **2019**, *116* (49), 24440–24445. <https://doi.org/10.1073/pnas.1907169116>.
- (110) Koga, T.; Naraoka, H. A New Family of Extraterrestrial Amino Acids in the Murchison Meteorite. *Sci. Rep.* **2017**, *7* (1), 636. <https://doi.org/10.1038/s41598-017-00693-9>.
- (111) Cooper, G.; Kimmich, N.; Belisle, W.; Sarinana, J.; Brabham, K.; Garrel, L. Carbonaceous Meteorites as a Source of Sugar-Related Organic Compounds for the Early Earth. *Nature* **2001**, *414* (6866), 879–883. <https://doi.org/10.1038/414879a>.
- (112) Furukawa, Y.; Chikaraishi, Y.; Ohkouchi, N.; Ogawa, N. O.; Glavin, D. P.; Dworkin, J. P.; Abe, C.; Nakamura, T. Extraterrestrial Ribose and Other Sugars in Primitive Meteorites. *Proc. Natl. Acad. Sci.* **2019**, *116* (49), 24440–24445. <https://doi.org/10.1073/pnas.1907169116>.
- (113) Cooper, G.; Rios, A. C. Enantiomer Excesses of Rare and Common Sugar Derivatives in Carbonaceous Meteorites. *Proc. Natl. Acad. Sci.* **2016**, *113* (24), E3322–E3331. <https://doi.org/10.1073/pnas.1603030113>.
- (114) Whipple, F. L. A Comet Model. I. The Acceleration of Comet Encke. *Astrophys. J.* **1950**, *111*, 375. <https://doi.org/10.1086/145272>.
- (115) Cochran, A. L.; Levasseur-Regourd, A.-C.; Cordiner, M.; Hadamcik, E.; Lasue, J.; Gicquel, A.; Schleicher, D. G.; Charnley, S. B.; Mumma, M. J.; Paganini, L.; Bockelée-Morvan, D.; Biver, N.; Kuan, Y.-J. The Composition of Comets. *Space Sci. Rev.* **2015**, *197* (1–4), 9–46. <https://doi.org/10.1007/s11214-015-0183-6>.
- (116) Greenberg, J. M. Making a Comet Nucleus. *Ap* **1998**, *330*, 375–380.
- (117) Combi, M. R.; Harris, W. M.; Smyth, W. H. Gas Dynamics and Kinetics in the Cometary Coma: Theory and Observations. In *Comets II*; Festou, M. C., Keller, H. U., Weaver, H. A., Eds.; 2004; p 523.
- (118) Hsieh, H. H. Asteroid–Comet Continuum Objects in the Solar System. *Philos. Trans. R. Soc. Math. Phys. Eng. Sci.* **2017**, *375* (2097), 20160259. <https://doi.org/10.1098/rsta.2016.0259>.
- (119) Ulamec, S.; Fantinati, C.; Maibaum, M.; Geurts, K.; Biele, J.; Jansen, S.; Küchemann, O.; Cozzoni, B.; Finke, F.; Lommatsch, V.; Moussi-Soffys, A.; Delmas, C.; O'Rourke, L. Rosetta Lander – Landing and Operations on Comet 67P/Churyumov–Gerasimenko. *Acta Astronaut.* **2016**, *125*, 80–91. <https://doi.org/10.1016/j.actaastro.2015.11.029>.

- (120) Goesmann, F.; Rosenbauer, H.; Bredehöft, J. H.; Cabane, M.; Ehrenfreund, P.; Gautier, T.; Giri, C.; Krüger, H.; Le Roy, L.; MacDermott, A. J.; McKenna-Lawlor, S.; Meierhenrich, U. J.; Caro, G. M. M.; Raulin, F.; Roll, R.; Steele, A.; Steininger, H.; Sternberg, R.; Szopa, C.; Thiemann, W.; Ulamec, S. Organic Compounds on Comet 67P/Churyumov-Gerasimenko Revealed by COSAC Mass Spectrometry. *Science* **2015**, *349* (6247), aab0689. <https://doi.org/10.1126/science.aab0689>.
- (121) Altwegg, K.; Balsiger, H.; Bar-Nun, A.; Berthelier, J.-J.; Bieler, A.; Bochslers, P.; Briois, C.; Calmonte, U.; Combi, M. R.; Cottin, H.; De Keyser, J.; Dhooghe, F.; Fiethe, B.; Fuselier, S. A.; Gasc, S.; Gombosi, T. I.; Hansen, K. C.; Haessig, M.; Jäckel, A.; Kopp, E.; Korth, A.; Le Roy, L.; Mall, U.; Marty, B.; Mousis, O.; Owen, T.; Rème, H.; Rubin, M.; Sémon, T.; Tzou, C.-Y.; Hunter Waite, J.; Wurz, P. Prebiotic Chemicals—Amino Acid and Phosphorus—in the Coma of Comet 67P/Churyumov-Gerasimenko. *Sci. Adv.* **2016**, *2* (5), e1600285. <https://doi.org/10.1126/sciadv.1600285>.
- (122) Gross, D.; Grodsky, G. On the Sublimation of Amino Acids and Peptides. *J. Am. Chem. Soc.* **1955**, *77* (6), 1678–1680. <https://doi.org/10.1021/ja01611a085>.
- (123) Tenenbaum, E. D.; Woolf, N. J.; Ziurys, L. M. Identification of Phosphorus Monoxide ($X^2\Pi_r$) in VY Canis Majoris: Detection of the First P–O Bond in Space. *Astrophys. J.* **2007**, *666* (1), L29–L32. <https://doi.org/10.1086/521361>.
- (124) Ziurys, L. M. Detection of Interstellar PN - The First Phosphorus-Bearing Species Observed in Molecular Clouds. *Astrophys. J.* **1987**, *321*, L81. <https://doi.org/10.1086/185010>.
- (125) Guélin, M.; Cernicharo, J.; Paubert, G.; Turner, B. E. Free Cp in Irc+ 10216. *Astron. Astrophys.* **1990**, *230*, L9–L11.
- (126) Agúndez, M.; Cernicharo, J.; Guélin, M. Discovery of Phosphaethyne (HCP) in Space: Phosphorus Chemistry in Circumstellar Envelopes. *Astrophys. J.* **2007**, *662* (2), L91–L94. <https://doi.org/10.1086/519561>.
- (127) Maciá, E. The Role of Phosphorus in Chemical Evolution. *Chem. Soc. Rev.* **2005**, *34* (8), 691. <https://doi.org/10.1039/b416855k>.
- (128) Cruikshank, D. P.; Kerridge, J. F. Organic Material: Asteroids, Meteorites, and Planetary Satellites. *Exobiol. Sol. Syst. Explor.* **1992**.
- (129) Martins, Z.; Chan, Q. H. S.; Bonal, L.; King, A.; Yabuta, H. Organic Matter in the Solar System—Implications for Future on-Site and Sample Return Missions. *Space Sci. Rev.* **2020**, *216* (4), 54. <https://doi.org/10.1007/s11214-020-00679-6>.
- (130) Cruikshank, D. P.; Brown, R. H. Organic Matter on Asteroid 130 Elektra. *Science* **1987**, *238* (4824), 183–184.
- (131) Campins, H.; Hargrove, K.; Pinilla-Alonso, N.; Howell, E. S.; Kelley, M. S.; Licandro, J.; Mothé-Diniz, T.; Fernández, Y.; Ziffer, J. Water Ice and Organics on the Surface of the Asteroid 24 Themis. *Nature* **2010**, *464* (7293), 1320–1321.
- (132) Rivkin, A. S.; Emery, J. P. Detection of Ice and Organics on an Asteroidal Surface. *Nature* **2010**, *464* (7293), 1322–1323.
- (133) De Sanctis, M. C.; Ammannito, E.; McSween, H. Y.; Raponi, A.; Marchi, S.; Capaccioni, F.; Capria, M. T.; Carrozzo, F. G.; Ciarniello, M.; Fonte, S. Localized Aliphatic Organic Material on the Surface of Ceres. *Science* **2017**, *355* (6326), 719–722.

- (134) Pieters, C. M.; Nathues, A.; Thangjam, G.; Hoffmann, M.; Platz, T.; De Sanctis, M. C.; Ammannito, E.; Tosi, F.; Zambon, F.; Pasckert, J. H. Geologic Constraints on the Origin of Red Organic-rich Material on Ceres. *Meteorit. Planet. Sci.* **2018**, *53* (9), 1983–1998.
- (135) Naraoka, H.; Mita, H.; Hamase, K.; Mita, M.; Yabuta, H.; Saito, K.; Fukushima, K.; Kitajima, F.; Sandford, S. A.; Nakamura, T.; Noguchi, T.; Okazaki, R.; Nagao, K.; Ebihara, M.; Yurimoto, H.; Tsuchiyama, A.; Abe, M.; Shirai, K.; Ueno, M.; Yada, T.; Ishibashi, Y.; Okada, T.; Fujimura, A.; Mukai, T.; Yoshikawa, M.; Kawaguchi, J. Preliminary Organic Compound Analysis of Microparticles Returned from Asteroid 25143 Itokawa by the Hayabusa Mission. *Geochem. J.* **2012**, *46* (1), 61–72. <https://doi.org/10.2343/geochemj.1.0134>.
- (136) Yada, T.; Abe, M.; Okada, T.; Nakato, A.; Yogata, K.; Miyazaki, A.; Hatakeda, K.; Kumagai, K.; Nishimura, M.; Hitomi, Y.; Soejima, H.; Yoshitake, M.; Iwamae, A.; Furuya, S.; Uesugi, M.; Karouji, Y.; Usui, T.; Hayashi, T.; Yamamoto, D.; Fukai, R.; Sugita, S.; Cho, Y.; Yumoto, K.; Yabe, Y.; Bibring, J.-P.; Pilorget, C.; Hamm, V.; Brunetto, R.; Riu, L.; Lourit, L.; Loizeau, D.; Lequertier, G.; Moussi-Soffys, A.; Tachibana, S.; Sawada, H.; Okazaki, R.; Takano, Y.; Sakamoto, K.; Miura, Y. N.; Yano, H.; Ireland, T. R.; Yamada, T.; Fujimoto, M.; Kitazato, K.; Namiki, N.; Arakawa, M.; Hirata, N.; Yurimoto, H.; Nakamura, T.; Noguchi, T.; Yabuta, H.; Naraoka, H.; Ito, M.; Nakamura, E.; Uesugi, K.; Kobayashi, K.; Michikami, T.; Kikuchi, H.; Hirata, N.; Ishihara, Y.; Matsumoto, K.; Noda, H.; Noguchi, R.; Shimaki, Y.; Shirai, K.; Ogawa, K.; Wada, K.; Senshu, H.; Yamamoto, Y.; Morota, T.; Honda, R.; Honda, C.; Yokota, Y.; Matsuoka, M.; Sakatani, N.; Tatsumi, E.; Miura, A.; Yamada, M.; Fujii, A.; Hirose, C.; Hosoda, S.; Ikeda, H.; Iwata, T.; Kikuchi, S.; Mimasu, Y.; Mori, O.; Ogawa, N.; Ono, G.; Shimada, T.; Soldini, S.; Takahashi, T.; Takei, Y.; Takeuchi, H.; Tsukizaki, R.; Yoshikawa, K.; Terui, F.; Nakazawa, S.; Tanaka, S.; Saiki, T.; Yoshikawa, M.; Watanabe, S.; Tsuda, Y. Preliminary Analysis of the Hayabusa2 Samples Returned from C-Type Asteroid Ryugu. *Nat. Astron.* **2022**, *6* (2), 214–220. <https://doi.org/10.1038/s41550-021-01550-6>.
- (137) Parker, E. T.; Chan, Q. H. S.; Glavin, D. P.; Dworkin, J. P. Non-protein Amino Acids Identified in Carbon-rich Hayabusa Particles. *Meteorit. Planet. Sci.* **2022**, maps.13794. <https://doi.org/10.1111/maps.13794>.
- (138) Cronin, J. R.; Pizzarello, S.; Epstein, S.; Krishnamurthy, R. V. Molecular and Isotopic Analyses of the Hydroxy Acids, Dicarboxylic Acids, and Hydroxydicarboxylic Acids of the Murchison Meteorite. *Geochim. Cosmochim. Acta* **1993**, *57* (19), 4745–4752. [https://doi.org/10.1016/0016-7037\(93\)90197-5](https://doi.org/10.1016/0016-7037(93)90197-5).
- (139) Pizzarello, S.; Cooper, G. W.; Flynn, G. J. The Nature and Distribution of the Organic Material in Carbonaceous Chondrites and Interplanetary Dust Particles. In *Meteorites and the Early Solar System II*; Lauretta, D. S., McSween, H. Y., Eds.; 2006; p 625.
- (140) Hudson, R.; Lewis, A.; Moore, M.; Dworkin, J.; Martin, M. Enigmatic Isovaline: Investigating the Stability, Racemization, and Formation of a Non-Biological Meteoritic Amino Acid. *Bioastronomy 2007 Mol. Microbes Extraterr. Life* **2009**, *420*.
- (141) Hayatsu, R.; Studier, M. H.; Anders, E. Origin of Organic Matter in Early Solar System—IV. Amino Acids: Confirmation of Catalytic Synthesis by Mass Spectrometry. *Geochim. Cosmochim. Acta* **1971**, *35* (9), 939–951. [https://doi.org/10.1016/0016-7037\(71\)90007-X](https://doi.org/10.1016/0016-7037(71)90007-X).
- (142) Buc, S. R.; Ford, J. H.; Wise, E. C. An Improved Synthesis of β -Alanine. *J. Am. Chem. Soc.* **1945**, *67* (1), 92–94. <https://doi.org/10.1021/ja01217a033>.

- (143) Burton, A. S.; Stern, J. C.; Elsila, J. E.; Glavin, D. P.; Dworkin, J. P. Understanding Prebiotic Chemistry through the Analysis of Extraterrestrial Amino Acids and Nucleobases in Meteorites. *Chem. Soc. Rev.* **2012**, *41* (16), 5459. <https://doi.org/10.1039/c2cs35109a>.
- (144) Cooper, G. W.; Cronin, J. R. Linear and Cyclic Aliphatic Carboxamides of the Murchison Meteorite: Hydrolyzable Derivatives of Amino Acids and Other Carboxylic Acids. *Geochim. Cosmochim. Acta* **1995**, *59* (5), 1003–1015. [https://doi.org/10.1016/0016-7037\(95\)00018-6](https://doi.org/10.1016/0016-7037(95)00018-6).
- (145) Matthews, C.; Nelson, J.; Varma, P.; Minard, R. Deuterolysis of Amino Acid Precursors: Evidence for Hydrogen Cyanide Polymers as Protein Ancestors. *Science* **1977**, *198* (4317), 622–625.
- (146) Blagojevic, V.; Petrie, S.; Bohme, D. K. Gas-Phase Syntheses for Interstellar Carboxylic and Amino Acids. *Mon. Not. R. Astron. Soc.* **2003**, *339* (1), L7–L11. <https://doi.org/10.1046/j.1365-8711.2003.06351.x>.
- (147) Strecker, A. Ueber die künstliche Bildung der Milchsäure und einen neuen, dem Glycocoll homologen Körper; *Ann. Chem. Pharm.* **1850**, *75* (1), 27–45. <https://doi.org/10.1002/jlac.18500750103>.
- (148) Butlerov, A. M. Einiges Über Die Chemische Structur Der Körper. *Z. Für Chem.* **1861**, *4*, 549–560.
- (149) Appayee, C.; Breslow, R. Deuterium Studies Reveal a New Mechanism for the Formose Reaction Involving Hydride Shifts. *J. Am. Chem. Soc.* **2014**, *136* (10), 3720–3723. <https://doi.org/10.1021/ja410886c>.
- (150) Cairns-Smith, A. G.; Ingram, P.; Walker, G. L. Formose Production by Minerals: Possible Relevance to the Origin of Life. *J. Theor. Biol.* **1972**, *35* (3), 601–604. [https://doi.org/10.1016/0022-5193\(72\)90153-1](https://doi.org/10.1016/0022-5193(72)90153-1).
- (151) Omran, A. Plausibility of the Formose Reaction in Alkaline Hydrothermal/Vent Environments. *Orig. Life Evol. Biospheres* **2020**. <https://doi.org/10.1007/s11084-020-09599-5>.
- (152) Eckhardt, A. K.; Linden, M. M.; Wende, R. C.; Bernhardt, B.; Schreiner, P. R. Gas-Phase Sugar Formation Using Hydroxymethylene as the Reactive Formaldehyde Isomer. *Nat. Chem.* **2018**, *10* (11), 1141–1147. <https://doi.org/10.1038/s41557-018-0128-2>.
- (153) Larralde, R.; Robertson, M. P.; Miller, S. L. Rates of Decomposition of Ribose and Other Sugars: Implications for Chemical Evolution. *Proc. Natl. Acad. Sci.* **1995**, *92* (18), 8158–8160. <https://doi.org/10.1073/pnas.92.18.8158>.
- (154) Haas, M.; Lamour, S.; Christ, S. B.; Trapp, O. Mineral-Mediated Carbohydrate Synthesis by Mechanical Forces in a Primordial Geochemical Setting. *Commun. Chem.* **2020**, *3* (1), 140. <https://doi.org/10.1038/s42004-020-00387-w>.
- (155) Fox, S. W.; Windsor, C. R. Synthesis of Amino Acids by the Heating of Formaldehyde and Ammonia. *Science* **1970**, *170* (3961), 984–986. <https://doi.org/10.1126/science.170.3961.984>.
- (156) Oba, Y.; Takano, Y.; Naraoka, H.; Kouchi, A.; Watanabe, N. Deuterium Fractionation upon the Formation of Hexamethylenetetramines through Photochemical Reactions of Interstellar Ice Analogs Containing Deuterated Methanol Isotopologues. *Astrophys. J.* **2017**, *849* (2), 122. <https://doi.org/10.3847/1538-4357/aa8ea5>.
- (157) Ehrenfreund, P.; Charnley, S. B. Organic Molecules in the Interstellar Medium, Comets, and Meteorites: A Voyage from Dark Clouds to the Early Earth. *Annu. Rev. Astron. Astrophys.* **2000**, *38* (1), 427–483. <https://doi.org/10.1146/annurev.astro.38.1.427>.

- (158) Oba, Y.; Takano, Y.; Naraoka, H.; Furukawa, Y.; Glavin, D. P.; Dworkin, J. P.; Tachibana, S. Extraterrestrial Hexamethylenetetramine in Meteorites—a Precursor of Prebiotic Chemistry in the Inner Solar System. *Nat. Commun.* **2020**, *11* (1), 6243. <https://doi.org/10.1038/s41467-020-20038-x>.
- (159) Vinogradoff, V.; Remusat, L.; McLain, H. L.; Aponte, J. C.; Bernard, S.; Danger, G.; Dworkin, J. P.; Elsila, J. E.; Jaber, M. Impact of Phyllosilicates on Amino Acid Formation under Asteroidal Conditions. *ACS Earth Space Chem.* **2020**, *4* (8), 1398–1407. <https://doi.org/10.1021/acsearthspacechem.0c00137>.
- (160) Vinogradoff, V.; Bernard, S.; Le Guillou, C.; Remusat, L. Evolution of Interstellar Organic Compounds under Asteroidal Hydrothermal Conditions. *Icarus* **2018**, *305*, 358–370. <https://doi.org/10.1016/j.icarus.2017.12.019>.
- (161) Muñoz Caro, G. M.; Schutte, W. A. UV-Photoprocessing of Interstellar Ice Analogs: New Infrared Spectroscopic Results. *Astron. Astrophys.* **2003**, *412* (1), 121–132. <https://doi.org/10.1051/0004-6361:20031408>.
- (162) Bernstein, M. P.; Sandford, S. A.; Allamandola, L. J.; Chang, S.; Scharberg, M. A. Organic Compounds Produced by Photolysis of Realistic Interstellar and Cometary Ice Analogs Containing Methanol. *Astrophys. J.* **1995**, *454*, 327. <https://doi.org/10.1086/176485>.
- (163) Fernandez, X.; Filippi, J.-J.; Jeanville, M. Chromatographie en phase gazeuse à deux dimensions : GC-GC et GCxGC. *Tech. Anal.* **2011**. <https://doi.org/10.51257/a-v1-p1489>.
- (164) Gordon, B. M.; Uhrig, M. S.; Borgerding, M. F.; Chung, H. L.; Coleman, W. M.; Elder, J. F.; Giles, J. A.; Moore, D. S.; Rix, C. E.; White, E. L. Analysis of Flue-Cured Tobacco Essential Oil by Hyphenated Analytical Techniques. *J. Chromatogr. Sci.* **1988**, *26* (4), 174–180. <https://doi.org/10.1093/chromsci/26.4.174>.
- (165) Liu, Z.; Phillips, J. B. Comprehensive Two-Dimensional Gas Chromatography Using an On-Column Thermal Modulator Interface. *J. Chromatogr. Sci.* **1991**, *29* (6), 227–231. <https://doi.org/10.1093/chromsci/29.6.227>.
- (166) Lee, A. L.; Bartle, K. D.; Lewis, A. C. A Model of Peak Amplitude Enhancement in Orthogonal Two-Dimensional Gas Chromatography. *Anal. Chem.* **2001**, *73* (6), 1330–1335. <https://doi.org/10.1021/ac001120s>.
- (167) Matisová, E.; Dömötöröová, M. Fast Gas Chromatography and Its Use in Trace Analysis. *J. Chromatogr. A* **2003**, *1000* (1–2), 199–221. [https://doi.org/10.1016/S0021-9673\(03\)00310-8](https://doi.org/10.1016/S0021-9673(03)00310-8).
- (168) Giddings, J. C. Two-Dimensional Separations: Concept and Promise. *Anal. Chem.* **1984**, *56* (12), 1258A–1270A. <https://doi.org/10.1021/ac00276a003>.
- (169) Bahaghighat, H. D.; Freye, C. E.; Synovec, R. E. Recent Advances in Modulator Technology for Comprehensive Two Dimensional Gas Chromatography. *TrAC Trends Anal. Chem.* **2019**, *113*, 379–391. <https://doi.org/10.1016/j.trac.2018.04.016>.
- (170) Bruckner, C. A.; Prazen, B. J.; Synovec, R. E. Comprehensive Two-Dimensional High-Speed Gas Chromatography with Chemometric Analysis. *Anal. Chem.* **1998**, *70* (14), 2796–2804. <https://doi.org/10.1021/ac980164m>.
- (171) Muscalu, A. M.; Edwards, M.; Górecki, T.; Reiner, E. J. Evaluation of a Single-Stage Consumable-Free Modulator for Comprehensive Two-Dimensional Gas Chromatography: Analysis of

- Polychlorinated Biphenyls, Organochlorine Pesticides and Chlorobenzenes. *J. Chromatogr. A* **2015**, *1391*, 93–101. <https://doi.org/10.1016/j.chroma.2015.02.074>.
- (172) Wohlfahrt, S.; Fischer, M.; Varga, J.; Saraji-Bozorgzad, M.-R.; Matuschek, G.; Denner, T.; Zimmermann, R. Dual-Stage Consumable-Free Thermal Modulator for the Hyphenation of Thermal Analysis, Gas Chromatography, and Mass Spectrometry. *Anal. Chem.* **2016**, *88* (1), 640–644. <https://doi.org/10.1021/acs.analchem.5b04183>.
- (173) Freye, C. E.; Mu, L.; Synovec, R. E. High Temperature Diaphragm Valve-Based Comprehensive Two-Dimensional Gas Chromatography. *J. Chromatogr. A* **2015**, *1424*, 127–133. <https://doi.org/10.1016/j.chroma.2015.10.098>.
- (174) Tranchida, P. Q.; Franchina, F. A.; Dugo, P.; Mondello, L. Use of Greatly-Reduced Gas Flows in Flow-Modulated Comprehensive Two-Dimensional Gas Chromatography-Mass Spectrometry. *J. Chromatogr. A* **2014**, *1359*, 271–276. <https://doi.org/10.1016/j.chroma.2014.07.054>.
- (175) Phillips, J. B.; Ledford, E. B. Thermal Modulation: A Chemical Instrumentation Component of Potential Value in Improving Portability. 7.
- (176) Phillips, J. B.; Gaines, R. B.; Blomberg, J. A Robust Thermal Modulator for Comprehensive Two-Dimensional Gas Chromatography. 8.
- (177) Marriott, P. J.; Kinghorn, R. M. Longitudinally Modulated Cryogenic System. A Generally Applicable Approach to Solute Trapping and Mobilization in Gas Chromatography. *Anal. Chem.* **1997**, *69* (13), 2582–2588. <https://doi.org/10.1021/ac961310w>.
- (178) Harynuk, J.; Górecki, T. New Liquid Nitrogen Cryogenic Modulator for Comprehensive Two-Dimensional Gas Chromatography. *J. Chromatogr. A* **2003**, *1019* (1–2), 53–63. <https://doi.org/10.1016/j.chroma.2003.08.097>.
- (179) Seeley, J. V.; Kramp, F.; Hicks, C. J. Comprehensive Two-Dimensional Gas Chromatography via Differential Flow Modulation. *Anal. Chem.* **2000**, *72* (18), 4346–4352. <https://doi.org/10.1021/ac000249z>.
- (180) Wang, F. C.-Y. New Valve Switching Modulator for Comprehensive Two-Dimensional Gas Chromatography. *J. Chromatogr. A* **2008**, *1188* (2), 274–280. <https://doi.org/10.1016/j.chroma.2008.02.104>.
- (181) Vendevre, C.; Ruiz-Guerrero, R.; Bertoncini, F.; Duval, L.; Thiébaud, D. Comprehensive Two-Dimensional Gas Chromatography for Detailed Characterisation of Petroleum Products. *Oil Gas Sci. Technol. - Rev. IFP* **2007**, *62* (1), 43–55. <https://doi.org/10.2516/ogst:2007004>.
- (182) Bertoncini, F.; Vendevre, C.; Thiébaud, D. Interest and Applications of Multidimensional Gas Chromatography for Trace Analysis in the Petroleum Industry. *Oil Gas Sci. Technol.* **2005**, *60* (6), 937–950. <https://doi.org/10.2516/ogst:2005066>.
- (183) Blase, R. C.; Llera, K.; Luspay-Kuti, A.; Libarondi, M. The Importance of Detector Acquisition Rate in Comprehensive Two-Dimensional Gas Chromatography (GC×GC). *Sep. Sci. Technol.* **2014**, *49* (6), 847–853. <https://doi.org/10.1080/01496395.2013.866961>.
- (184) Libarondi, M.; Binkley, J. Comparing the Capabilities of Time-of-Flight and Quadrupole Mass Spectrometers. *LCGC Suppl.* **2010**, *8* (3), 28–33.
- (185) Bramer, S. E. V. *An Introduction to Mass Spectrometry*; 1998.

- (186) Mamyrin, B. A.; Karataev, V. I.; Shmikk, D. V.; Zagulin, V. A. The Mass-Reflectron, a New Nonmagnetic Time-of-Flight Mass Spectrometer with High Resolution. *Sov. J. Exp. Theor. Phys.* **1973**, *37*, 45.
- (187) Li, S.; Purdy, W. C. Cyclodextrins and Their Applications in Analytical Chemistry. *Chem. Rev.* **1992**, *92* (6), 1457–1470. <https://doi.org/10.1021/cr00014a009>.
- (188) Bender, H. (1→4)- α -D-Glucopyranosyltransfer-produkte aus cyclohexaamylose. *Carbohydr. Res.* **1978**, *65* (1), 85–97. [https://doi.org/10.1016/S0008-6215\(00\)84215-9](https://doi.org/10.1016/S0008-6215(00)84215-9).
- (189) *Cyclodextrins and Their Complexes: Chemistry, Analytical Methods, Applications*, 1st ed.; Dodziuk, H., Ed.; Wiley, 2006. <https://doi.org/10.1002/3527608982>.
- (190) Upadhyay, S. K.; Kumar, G. NMR and Molecular Modelling Studies on the Interaction of Fluconazole with β -Cyclodextrin. *Chem. Cent. J.* **2009**, *3* (1), 9. <https://doi.org/10.1186/1752-153X-3-9>.
- (191) Dai, Y.; Hai, J.; Tang, W.; Ng, S.-C. Cyclodextrin-Based Chiral Stationary Phases for Gas Chromatography. In *Modified Cyclodextrins for Chiral Separation*; Tang, W., Ng, S.-C., Sun, D., Eds.; Springer Berlin Heidelberg: Berlin, Heidelberg, 2013; pp 27–66. https://doi.org/10.1007/978-3-642-37648-1_2.
- (192) Davis, M. E.; Brewster, M. E. Cyclodextrin-Based Pharmaceuticals: Past, Present and Future. *Nat. Rev. Drug Discov.* **2004**, *3* (12), 1023–1035. <https://doi.org/10.1038/nrd1576>.
- (193) Melton, L. D.; Slessor, K. N. Synthesis of Monosubstituted Cyclohexaamyloses. *Carbohydr. Res.* **1971**, *18* (1), 29–37. [https://doi.org/10.1016/S0008-6215\(00\)80256-6](https://doi.org/10.1016/S0008-6215(00)80256-6).
- (194) Tabushi, I.; Shimokawa, K.; Fujita, K. Specific Bifunctionalization on Cyclodextrin. *Tetrahedron Lett.* **1977**, *18* (18), 1527–1530. [https://doi.org/10.1016/S0040-4039\(01\)93093-X](https://doi.org/10.1016/S0040-4039(01)93093-X).
- (195) Ciucanu, I.; Kerek, F. A Simple and Rapid Method for the Permethylolation of Carbohydrates. *Carbohydr. Res.* **1984**, *131* (2), 209–217. [https://doi.org/10.1016/0008-6215\(84\)85242-8](https://doi.org/10.1016/0008-6215(84)85242-8).
- (196) König, W. A.; Krebber, R.; Mischnick, P. Cyclodextrins as Chiral Stationary Phases in Capillary Gas Chromatography. Part V: Octakis(3-O-Butyryl-2,6-Di-O-Pentyl)- γ -Cyclodextrin. *J. High Resolut. Chromatogr.* **1989**, *12* (11), 732–738. <https://doi.org/10.1002/jhrc.1240121108>.
- (197) Freissinet, C.; Buch, A.; Szopa, C.; Sternberg, R. Enantiomeric Separation of Volatile Organics by Gas Chromatography for the in Situ Analysis of Extraterrestrial Materials: Kinetics and Thermodynamics Investigation of Various Chiral Stationary Phases. *J. Chromatogr. A* **2013**, *1306*, 59–71. <https://doi.org/10.1016/j.chroma.2013.07.058>.
- (198) Aponte, J. C.; Elsila, J. E.; Hein, J. E.; Dworkin, J. P.; Glavin, D. P.; McLain, H. L.; Parker, E. T.; Cao, T.; Berger, E. L.; Burton, A. S. Analysis of Amino Acids, Hydroxy Acids, and Amines in CR Chondrites. *Meteorit. Planet. Sci.* **2020**, *55* (11), 2422–2439. <https://doi.org/10.1111/maps.13586>.
- (199) Talebi, M.; Patil, R. A.; Armstrong, D. W. Gas Chromatography Columns Using Ionic Liquids as Stationary Phase. In *Commercial Applications of Ionic Liquids*; Shiflett, M. B., Ed.; Green Chemistry and Sustainable Technology; Springer International Publishing: Cham, 2020; pp 131–165. https://doi.org/10.1007/978-3-030-35245-5_6.
- (200) Lambertus, G. R.; Crank, J. A.; McGuigan, M. E.; Kendler, S.; Armstrong, D. W.; Sacks, R. D. Rapid Determination of Complex Mixtures by Dual-Column Gas Chromatography with a Novel Stationary Phase Combination and Spectrometric Detection. *J. Chromatogr. A* **2006**, *1135* (2), 230–240. <https://doi.org/10.1016/j.chroma.2006.09.086>.

- (201) Nan, H.; Anderson, J. L. Ionic Liquid Stationary Phases for Multidimensional Gas Chromatography. *TrAC Trends Anal. Chem.* **2018**, *105*, 367–379. <https://doi.org/10.1016/j.trac.2018.03.020>.
- (202) Siegler, W. C.; Crank, J. A.; Armstrong, D. W.; Synovec, R. E. Increasing Selectivity in Comprehensive Three-Dimensional Gas Chromatography via an Ionic Liquid Stationary Phase Column in One Dimension. *J. Chromatogr. A* **2010**, *1217* (18), 3144–3149. <https://doi.org/10.1016/j.chroma.2010.02.082>.
- (203) Cardinael, P.; Casabianca, H.; Peulon-Agasse, V.; Berthod, A. Sample Derivatization in Separation Science. In *Analytical Separation Science*; Pino, V., Anderson, J. L., Berthod, A., Stalcup, A. M., Eds.; Wiley-VCH Verlag GmbH & Co. KGaA: Weinheim, Germany, 2015; pp 063–063. <https://doi.org/10.1002/9783527678129.assep063>.
- (204) Meinert, C.; Meierhenrich, U. J. Derivatization and Multidimensional Gas-Chromatographic Resolution of α -Alkyl and α -Dialkyl Amino Acid Enantiomers. *ChemPlusChem* **2014**, *79* (6), 781–785. <https://doi.org/10.1002/cplu.201300328>.
- (205) Reiner, C.; Nicholson, G. J.; Nagel, U.; Schurig, V. Evaluation of Enantioselective Gas Chromatography for the Determination of Minute Deviations from Racemic Composition of α -Amino Acids with Emphasis on Tyrosine: Accuracy and Precision of the Method. *Chirality* **2007**, *19* (5), 401–414. <https://doi.org/10.1002/chir.20390>.
- (206) Bio-rad. AG[®] 50W and AG MP-50 Cation Exchange Resins - Instruction Manual.
- (207) Huck, C. W.; Huber, C. G.; Bonn, G. K. Chapter 5 HPLC of Carbohydrates with Cation- and Anion-Exchange Silica and Resin-Based Stationary Phases. In *Journal of Chromatography Library*; Elsevier, 2002; Vol. 66, pp 165–205. [https://doi.org/10.1016/S0301-4770\(02\)80030-6](https://doi.org/10.1016/S0301-4770(02)80030-6).
- (208) Huber, C. G.; Bonn, G. K. Chapter 4 HPLC of Carbohydrates with Cation- and Anion-Exchange Silica and Resin-Based Stationary Phases. In *Journal of Chromatography Library*; Elsevier, 1995; Vol. 58, pp 147–180. [https://doi.org/10.1016/S0301-4770\(08\)60509-6](https://doi.org/10.1016/S0301-4770(08)60509-6).
- (209) Qin, L.; Dauphas, N.; Janney, P. E.; Wadhwa, M. Analytical Developments for High-Precision Measurements of W Isotopes in Iron Meteorites. *Anal. Chem.* **2007**, *79* (8), 3148–3154. <https://doi.org/10.1021/ac062040c>.
- (210) Hogenboom, J. A.; D’Incecco, P.; Fuselli, F.; Pellegrino, L. Ion-Exchange Chromatographic Method for the Determination of the Free Amino Acid Composition of Cheese and Other Dairy Products: An Inter-Laboratory Validation Study. *Food Anal. Methods* **2017**, *10* (9), 3137–3148. <https://doi.org/10.1007/s12161-017-0876-4>.
- (211) Wu, A. C.; Witt, T.; Gilbert, R. G. Characterization Methods for Starch-Based Materials: State of the Art and Perspectives. *Aust. J. Chem.* **2013**, *66* (12), 1550. <https://doi.org/10.1071/CH13397>.
- (212) Erik, K.; Knudsen, B.; Laerke, H. N.; Jørgensen, H. Carbohydrates and Carbohydrate Utilization in Swine. In *Sustainable Swine Nutrition*; Chiba, L. I., Ed.; Blackwell Publishing Ltd.: Oxford, UK, 2012; pp 109–137. <https://doi.org/10.1002/9781118491454.ch5>.
- (213) Navarro, D. M. D. L.; Abelilla, J. J.; Stein, H. H. Structures and Characteristics of Carbohydrates in Diets Fed to Pigs: A Review. *J. Anim. Sci. Biotechnol.* **2019**, *10* (1), 39. <https://doi.org/10.1186/s40104-019-0345-6>.
- (214) Franks, F.; Lillford, P. J.; Robinson, G. Isomeric Equilibria of Monosaccharides in Solution. Influence of Solvent and Temperature. *J. Chem. Soc. Faraday Trans. 1 Phys. Chem. Condens. Phases* **1989**, *85* (8), 2417. <https://doi.org/10.1039/f19898502417>.

- (215) Kamerling, J. P. Basics Concepts and Nomenclature Recommendations in Carbohydrate Chemistry. In *Comprehensive Glycoscience*; Elsevier, 2007; pp 1–38. <https://doi.org/10.1016/B978-044451967-2/00001-5>.
- (216) Blakeney, A. B.; Harris, P. J.; Henry, R. J.; Stone, B. A. A Simple and Rapid Preparation of Alditol Acetates for Monosaccharide Analysis. *Carbohydr. Res.* **1983**, *113* (2), 291–299. [https://doi.org/10.1016/0008-6215\(83\)88244-5](https://doi.org/10.1016/0008-6215(83)88244-5).
- (217) Cooper, G.; Yim, S.; Lanoiselée, J.; Sorden, S.; Ramirez, F. G. The Baseline Resolution of Aldo-Monosaccharide Enantiomers: Simplified GC–MS Analyses Using Acetal-Trifluoroacetyl Derivatives for Complex Samples. *J. Chromatogr. B* **2019**, *1126–1127*, 121761. <https://doi.org/10.1016/j.jchromb.2019.121761>.
- (218) Li, B. W.; Schuhmann, P. J. Gas Chromatographic Analysis of Sugars in Granola Cereals. *J. Food Sci.* **1981**, *46* (2), 425–427. <https://doi.org/10.1111/j.1365-2621.1981.tb04876.x>.
- (219) Churms, S. C. Recent Developments in the Chromatographic Analysis of Carbohydrates. *J. Chromatogr. A* **1990**, *500*, 555–583. [https://doi.org/10.1016/S0021-9673\(00\)96092-8](https://doi.org/10.1016/S0021-9673(00)96092-8).
- (220) Willis, D. E. GC Analysis of C2-C7 Carbohydrates as the Trimethylsilyl-Oxime Derivatives on Packed and Capillary Columns. *J. Chromatogr. Sci.* **1983**, *21* (3), 132–138. <https://doi.org/10.1093/chromsci/21.3.132>.
- (221) Guerrant, G. O.; Moss, C. Wayne. Determination of Monosaccharides as Aldononitrile, O-Methyloxime, Alditol, and Cyclitol Acetate Derivatives by Gas Chromatography. *Anal. Chem.* **1984**, *56* (4), 633–638. <https://doi.org/10.1021/ac00268a010>.
- (222) Wohl, A. Abbau Des Traubenzuckers. *Berichte Dtsch. Chem. Ges.* **1893**, *26* (1), 730–744. <https://doi.org/10.1002/cber.189302601150>.
- (223) Garcia, A. The Origins of Homochirality : Study by Two-Dimensional Gas Chromatography. phdthesis, Université Côte d’Azur, 2021.
- (224) Schummer, C.; Delhomme, O.; Appenzeller, B.; Wennig, R.; Millet, M. Comparison of MTBSTFA and BSTFA in Derivatization Reactions of Polar Compounds Prior to GC/MS Analysis. *Talanta* **2009**, *77* (4), 1473–1482. <https://doi.org/10.1016/j.talanta.2008.09.043>.
- (225) van Dongen, B. E.; Schouten, S.; Damsté, J. S. S. Gas Chromatography/Combustion/Isotope-Ratio-Monitoring Mass Spectrometric Analysis of Methylboronic Derivatives of Monosaccharides: A New Method for Determining Natural ¹³ C Abundances of Carbohydrates: ¹³ C Analysis of Monosaccharides. *Rapid Commun. Mass Spectrom.* **2001**, *15* (7), 496–500. <https://doi.org/10.1002/rcm.259>.
- (226) Faraco, M.; Fico, D.; Pennetta, A.; De Benedetto, G. E. New Evidences on Efficacy of Boronic Acid-Based Derivatization Method to Identify Sugars in Plant Material by Gas Chromatography–Mass Spectrometry. *Talanta* **2016**, *159*, 40–46. <https://doi.org/10.1016/j.talanta.2016.06.004>.
- (227) Lu, Y.; Freeland, S. On the Evolution of the Standard Amino-Acid Alphabet. *Genome Biol.* **2006**, *7* (1), 102. <https://doi.org/10.1186/gb-2006-7-1-102>.
- (228) Zhang, Y.; Baranov, P. V.; Atkins, J. F.; Gladyshev, V. N. Pyrrolysine and Selenocysteine Use Dissimilar Decoding Strategies. *J. Biol. Chem.* **2005**, *280* (21), 20740–20751. <https://doi.org/10.1074/jbc.M501458200>.

- (229) Simkus, D. N.; Aponte, J. C.; Elsila, J. E.; Parker, E. T.; Glavin, D. P.; Dworkin, J. P. Methodologies for Analyzing Soluble Organic Compounds in Extraterrestrial Samples: Amino Acids, Amines, Monocarboxylic Acids, Aldehydes, and Ketones. **2019**, 30.
- (230) Freissinet, C.; Buch, A.; Sternberg, R.; Szopa, C.; Geffroy-Rodier, C.; Jelinek, C.; Stambouli, M. Search for Evidence of Life in Space: Analysis of Enantiomeric Organic Molecules by N,N-Dimethylformamide Dimethylacetal Derivative Dependant Gas Chromatography–Mass Spectrometry. *J. Chromatogr. A* **2010**, 1217 (5), 731–740. <https://doi.org/10.1016/j.chroma.2009.11.009>.
- (231) Rodier, C.; Sternberg, R.; Raulin, F.; Vidal-Madjar, C. Chemical Derivatization of Amino Acids for in Situ Analysis of Martian Samples by Gas Chromatography. *J. Chromatogr. A* **2001**, 915 (1–2), 199–207. [https://doi.org/10.1016/S0021-9673\(01\)00625-2](https://doi.org/10.1016/S0021-9673(01)00625-2).
- (232) Nuevo, M.; Bredehöft, J. H.; Meierhenrich, U. J.; d’Hendecourt, L.; Thiemann, W. H.-P. Urea, Glycolic Acid, and Glycerol in an Organic Residue Produced by Ultraviolet Irradiation of Interstellar/Pre-Cometary Ice Analogs. *Astrobiology* **2010**, 10 (2), 245–256. <https://doi.org/10.1089/ast.2009.0358>.
- (233) Myrgorodska, I.; Meinert, C.; Martins, Z.; le Sergeant d’Hendecourt, L.; Meierhenrich, U. J. Quantitative Enantioseparation of Amino Acids by Comprehensive Two-Dimensional Gas Chromatography Applied to Non-Terrestrial Samples. *J. Chromatogr. A* **2016**, 1433, 131–136. <https://doi.org/10.1016/j.chroma.2016.01.014>.
- (234) Weygand, F.; Röpsch, A. N-Trifluoroacetyl-aminosäuren, XIV.N-Trifluoroacetylierungen von Aminosäuren und Peptiden mit Trifluoressigsäure-phenylester. *Chem. Ber.* **1959**, 92 (9), 2095–2099. <https://doi.org/10.1002/cber.19590920921>.
- (235) Chan, H.-S.; Martins, Z.; Sephton, M. A. Amino Acid Analyses of Type 3 Chondrites Colony, Ornans, Chainpur, and Bishunpur: Amino Acid Analysis of Type 3 Chondrites. *Meteorit. Planet. Sci.* **2012**, 47 (9), 1502–1516. <https://doi.org/10.1111/j.1945-5100.2012.01413.x>.
- (236) Martins, Z.; Price, M. C.; Goldman, N.; Sephton, M. A.; Burchell, M. J. Shock Synthesis of Amino Acids from Impacting Cometary and Icy Planet Surface Analogues. *Nat. Geosci.* **2013**, 6 (12), 1045–1049. <https://doi.org/10.1038/ngeo1930>.
- (237) Cliffe, A. J. Determination of Some Amino Acids by Gas Chromatography of Derivatives. 9.
- (238) Roach, D.; W. Gehrke, C. Direct Esterification of the Protein Amino Acids. *J. Chromatogr. A* **1969**, 44, 269–278. [https://doi.org/10.1016/S0021-9673\(01\)92537-3](https://doi.org/10.1016/S0021-9673(01)92537-3).
- (239) Lamkin, W. M.; Gehrke, C. W. Quantitative Gas Chromatography of Amino Acids. Preparation of n-Butyl N-Trifluoroacetyl Esters. 7.
- (240) Chimiak, L.; Elsila, J. E.; Dallas, B.; Dworkin, J. P.; Aponte, J. C.; Sessions, A. L.; Eiler, J. M. Carbon Isotope Evidence for the Substrates and Mechanisms of Prebiotic Synthesis in the Early Solar System. *Geochim. Cosmochim. Acta* **2021**, 292, 188–202. <https://doi.org/10.1016/j.gca.2020.09.026>.
- (241) Frank, H.; Bimboes, D.; Nicholson, G. J. A Modified Procedure for Acid-Catalyzed Esterification with Isopropanol. *Chromatographia* **1979**, 12 (3), 168–170. <https://doi.org/10.1007/BF02314873>.
- (242) Fox, S.; Strasdeit, H.; Haasmann, S.; Brückner, H. Gas Chromatographic Separation of Stereoisomers of Non-Protein Amino Acids on Modified γ -Cyclodextrin Stationary Phase. *J. Chromatogr. A* **2015**, 1411, 101–109. <https://doi.org/10.1016/j.chroma.2015.07.082>.

- (243) Cruickshank, P. A.; Sheehan, J. C. Gas Chromatographic Analysis of Amino Acids as *N*-Trifluoroacetylmino Acid Methyl Esters. *Anal. Chem.* **1964**, *36* (7), 1191–1197. <https://doi.org/10.1021/ac60213a009>.
- (244) Corr, L. T.; Berstan, R.; Evershed, R. P. Development of *N*-Acetyl Methyl Ester Derivatives for the Determination of $\delta^{13}\text{C}$ Values of Amino Acids Using Gas Chromatography-Combustion- Isotope Ratio Mass Spectrometry. *Anal. Chem.* **2007**, *79* (23), 9082–9090. <https://doi.org/10.1021/ac071223b>.
- (245) Saroff, H. A.; Karmen, A. Gas Chromatography of the *N*-Trifluoroacetylmethyl Esters of the Amino Acids. *Anal. Biochem.* **1960**, *1* (4–5), 344–350. [https://doi.org/10.1016/0003-2697\(60\)90032-4](https://doi.org/10.1016/0003-2697(60)90032-4).
- (246) Rodier, C.; Sternberg, R.; Szopa, C.; Buch, A.; Cabane, M.; Raulin, F. Search for Organics in Extraterrestrial Environments by in Situ Gas Chromatography Analysis. *Adv. Space Res.* **2005**, *36* (2), 195–200. <https://doi.org/10.1016/j.asr.2004.12.072>.
- (247) Hemmler, D.; Roullier-Gall, C.; Marshall, J. W.; Rychlik, M.; Taylor, A. J.; Schmitt-Kopplin, P. Evolution of Complex Maillard Chemical Reactions, Resolved in Time. *Sci. Rep.* **2017**, *7* (1), 3227. <https://doi.org/10.1038/s41598-017-03691-z>.
- (248) Buch, A.; Sternberg, R.; Meunier, D.; Rodier, C.; Laurent, C.; Raulin, F.; Vidal-Madjar, C. Solvent Extraction of Organic Molecules of Exobiological Interest for in Situ Analysis of the Martian Soil. *J. Chromatogr. A* **2003**, *999* (1–2), 165–174. [https://doi.org/10.1016/S0021-9673\(03\)00494-1](https://doi.org/10.1016/S0021-9673(03)00494-1).
- (249) Buch, A.; Glavin, D. P.; Sternberg, R.; Szopa, C.; Rodier, C.; Navarro-González, R.; Raulin, F.; Cabane, M.; Mahaffy, P. R. A New Extraction Technique for in Situ Analyses of Amino and Carboxylic Acids on Mars by Gas Chromatography Mass Spectrometry. *Planet. Space Sci.* **2006**, *54* (15), 1592–1599. <https://doi.org/10.1016/j.pss.2006.05.041>.
- (250) Aponte, J. C.; Whitaker, D.; Powner, M. W.; Elsila, J. E.; Dworkin, J. P. Analyses of Aliphatic Aldehydes and Ketones in Carbonaceous Chondrites. *ACS Earth Space Chem.* **2019**, *3* (3), 463–472. <https://doi.org/10.1021/acsearthspacechem.9b00006>.
- (251) Aponte, J. C.; Woodward, H. K.; Abreu, N. M.; Elsila, J. E.; Dworkin, J. P. Molecular Distribution, ^{13}C -isotope, and Enantiomeric Compositions of Carbonaceous Chondrite Monocarboxylic Acids. *Meteorit. Planet. Sci.* **2019**, *54* (2), 415–430. <https://doi.org/10.1111/maps.13216>.
- (252) Pizzarello, S.; Yarnes, C. T. The Soluble Organic Compounds of the Mukundpura Meteorite: A New CM Chondrite Fall. *Planet. Space Sci.* **2018**, *164*, 127–131. <https://doi.org/10.1016/j.pss.2018.07.002>.
- (253) Aponte, J. C.; McLain, H. L.; Dworkin, J. P.; Elsila, J. E. Aliphatic Amines in Antarctic CR2, CM2, and CM1/2 Carbonaceous Chondrites. *Geochim. Cosmochim. Acta* **2016**, *189*, 296–311. <https://doi.org/10.1016/j.gca.2016.06.018>.
- (254) Aponte, J. C.; Dworkin, J. P.; Elsila, J. E. Assessing the Origins of Aliphatic Amines in the Murchison Meteorite from Their Compound-Specific Carbon Isotopic Ratios and Enantiomeric Composition. *Geochim. Cosmochim. Acta* **2014**, *141*, 331–345. <https://doi.org/10.1016/j.gca.2014.06.035>.
- (255) Aponte, J. C.; Tarozo, R.; Alexandre, M. R.; Alexander, C. M. O.; Charnley, S. B.; Hallmann, C.; Summons, R. E.; Huang, Y. Chirality of Meteoritic Free and IOM-Derived Monocarboxylic Acids and Implications for Prebiotic Organic Synthesis. *Geochim. Cosmochim. Acta* **2014**, *131*, 1–12. <https://doi.org/10.1016/j.gca.2014.01.035>.

- (256) Pizzarello, S.; Davidowski, S. K.; Holland, G. P.; Williams, L. B. Processing of Meteoritic Organic Materials as a Possible Analog of Early Molecular Evolution in Planetary Environments. *Proc. Natl. Acad. Sci.* **2013**, *110* (39), 15614–15619. <https://doi.org/10.1073/pnas.1309113110>.
- (257) Pizzarello, S.; Schrader, D. L.; Monroe, A. A.; Lauretta, D. S. Large Enantiomeric Excesses in Primitive Meteorites and the Diverse Effects of Water in Cosmochemical Evolution. *Proc. Natl. Acad. Sci.* **2012**, *109* (30), 11949–11954. <https://doi.org/10.1073/pnas.1204865109>.
- (258) Pizzarello, S.; Williams, L. B.; Lehman, J.; Holland, G. P.; Yarger, J. L. Abundant Ammonia in Primitive Asteroids and the Case for a Possible Exobiology. *Proc. Natl. Acad. Sci.* **2011**, *108* (11), 4303–4306. <https://doi.org/10.1073/pnas.1014961108>.
- (259) Pizzarello, S.; Wang, Y.; Chaban, G. M. A Comparative Study of the Hydroxy Acids from the Murchison, GRA 95229 and LAP 02342 Meteorites. *Geochim. Cosmochim. Acta* **2010**, *74* (21), 6206–6217. <https://doi.org/10.1016/j.gca.2010.08.013>.
- (260) Shimoyama, A.; Hagishita, S.; Harada, K. Search for Nucleic Acid Bases in Carbonaceous Chondrites from Antarctica. *Geochem. J.* **1990**, *24* (5), 343–348. <https://doi.org/10.2343/geochemj.24.343>.
- (261) Stoks, P. G.; Schwartz, A. W. Uracil in Carbonaceous Meteorites. *Nature* **1979**, *282* (5740), 709–710. <https://doi.org/10.1038/282709a0>.
- (262) Stoks, P. G.; Schwartz, A. W. Nitrogen-Heterocyclic Compounds in Meteorites: Significance and Mechanisms of Formation. *Geochim. Cosmochim. Acta* **1981**, *45* (4), 563–569. [https://doi.org/10.1016/0016-7037\(81\)90189-7](https://doi.org/10.1016/0016-7037(81)90189-7).
- (263) Martins, Z.; Botta, O.; Fogel, M. L.; Sephton, M. A.; Glavin, D. P.; Watson, J. S.; Dworkin, J. P.; Schwartz, A. W.; Ehrenfreund, P. Extraterrestrial Nucleobases in the Murchison Meteorite. *Earth Planet. Sci. Lett.* **2008**, *270* (1–2), 130–136. <https://doi.org/10.1016/j.epsl.2008.03.026>.
- (264) Kaplan, I. R.; Degens, E. T.; Reuter, J. H. Organic Compounds in Stony Meteorites. *Geochim. Cosmochim. Acta* **1963**, *27* (7), 805–834. [https://doi.org/10.1016/0016-7037\(63\)90045-0](https://doi.org/10.1016/0016-7037(63)90045-0).
- (265) Yentür, G.; Dükkancı, M. Synergistic Effect of Sonication on Photocatalytic Oxidation of Pharmaceutical Drug Carbamazepine. *Ultrason. Sonochem.* **2021**, *78*, 105749. <https://doi.org/10.1016/j.ultsonch.2021.105749>.
- (266) Ali, F.; Reinert, L.; Levêque, J.-M.; Duclaux, L.; Muller, F.; Saeed, S.; Shah, S. S. Effect of Sonication Conditions: Solvent, Time, Temperature and Reactor Type on the Preparation of Micron Sized Vermiculite Particles. *Ultrason. Sonochem.* **2014**, *21* (3), 1002–1009. <https://doi.org/10.1016/j.ultsonch.2013.10.010>.
- (267) Xiao, R.; Diaz-Rivera, D.; Weavers, L. K. Factors Influencing Pharmaceutical and Personal Care Product Degradation in Aqueous Solution Using Pulsed Wave Ultrasound. *Ind. Eng. Chem. Res.* **2013**, *52* (8), 2824–2831. <https://doi.org/10.1021/ie303052a>.
- (268) Santos, H. M.; Lodeiro, C.; Capelo-Martnez, J.-L. The Power of Ultrasound. In *Ultrasound in Chemistry*; Capelo-Martnez, J.-L., Ed.; Wiley-VCH Verlag GmbH & Co. KGaA: Weinheim, Germany, 2008; pp 1–16. <https://doi.org/10.1002/9783527623501.ch1>.
- (269) Ratsimba, V.; Fernández, J. M. G.; Defaye, J.; Nigay, H.; Voilley, A. Qualitative and Quantitative Evaluation of Mono- and Disaccharides in d-Fructose, d-Glucose and Sucrose Caramels by Gas–Liquid Chromatography–Mass Spectrometry. *J. Chromatogr. A* **1999**, *844* (1–2), 283–293. [https://doi.org/10.1016/S0021-9673\(99\)00322-2](https://doi.org/10.1016/S0021-9673(99)00322-2).

-
- (270) Tsugita, A.; Uchida, T.; Mewes, H. W.; Ataka, T. A Rapid Vapor-Phase Acid (Hydrochloric Acid and Trifluoroacetic Acid) Hydrolysis of Peptide and Protein. *J. Biochem. (Tokyo)* **1987**, *102* (6), 1593–1597. <https://doi.org/10.1093/oxfordjournals.jbchem.a122209>.
- (271) Palecz, B. Enthalpic Homogeneous Pair Interaction Coefficients of L- α -Amino Acids as a Hydrophobicity Parameter of Amino Acid Side Chains. *J. Am. Chem. Soc.* **2002**, *124* (21), 6003–6008. <https://doi.org/10.1021/ja011937i>.
- (272) Kaiser, K.; Benner, R. Hydrolysis-Induced Racemization of Amino Acids: Hydrolysis-Induced Amino Acid Racemization. *Limnol. Oceanogr. Methods* **2005**, *3* (8), 318–325. <https://doi.org/10.4319/lom.2005.3.318>.
- (273) Bada, J. L. Kinetics of Racemization of Amino Acids as a Function of PH. *J. Am. Chem. Soc.* **1972**, *94* (4), 1371–1373. <https://doi.org/10.1021/ja00759a064>.
- (274) Guba, A.; Bába, O.; Tózsér, J.; Csósz, É.; Kalló, G. Fast and Sensitive Quantification of AccQ-Tag Derivatized Amino Acids and Biogenic Amines by UHPLC-UV Analysis from Complex Biological Samples. *Metabolites* **2022**, *12* (3), 272. <https://doi.org/10.3390/metabo12030272>.
- (275) Kopetzki, D.; Antonietti, M. Hydrothermal Formose Reaction. *New J. Chem.* **2011**, *35* (9), 1787. <https://doi.org/10.1039/c1nj20191c>.
- (276) Oró, J.; Cox, A. Non-Enzymic Synthesis of 2-Deoxyribose; FEDERATION AMER SOC EXP BIOL 9650 ROCKVILLE PIKE, BETHESDA, MD 20814-3998, 1962; Vol. 21, p 80.
- (277) de Bruijn, J. M.; Kieboom, A. P. G.; van Bekkum, H. Alkaline Degradation of Monosaccharides V: Kinetics of the Alkaline Isomerization and Degradation of Monosaccharides. *Recl. Trav. Chim. Pays-Bas* **2010**, *106* (2), 35–43. <https://doi.org/10.1002/recl.19871060201>.
- (278) Omran, A.; Menor-Salvan, C.; Springsteen, G.; Pasek, M. The Messy Alkaline Formose Reaction and Its Link to Metabolism. *Life* **2020**, *10* (8), 125. <https://doi.org/10.3390/life10080125>.

SUPPLEMENTARY MATERIALS

Table S 1. Mass spectrum & fragmentation patterns of *N*-trifluoroacetyl amino acid methyl ester derivatives.

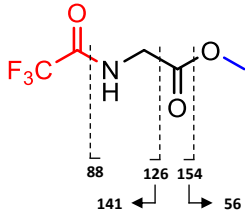
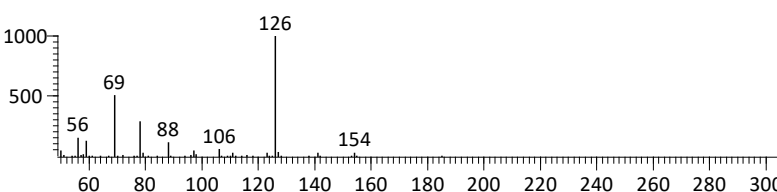
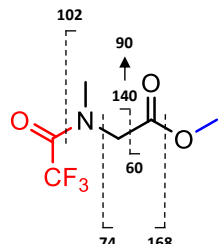
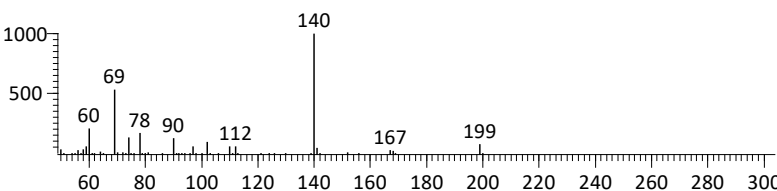
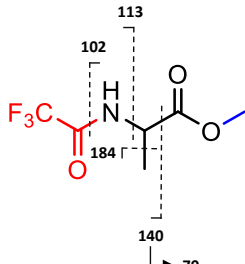
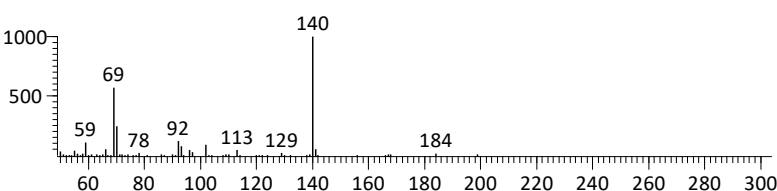
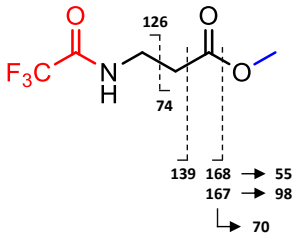
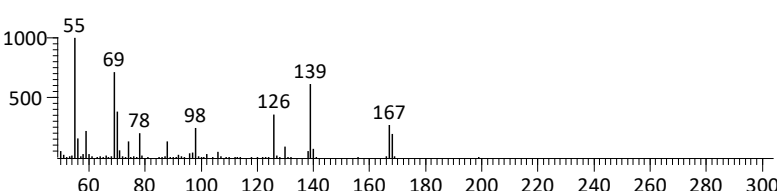
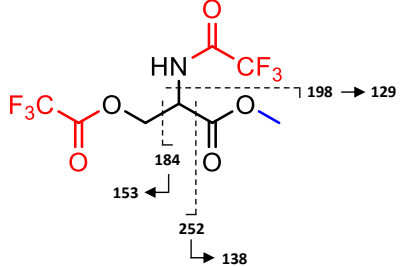
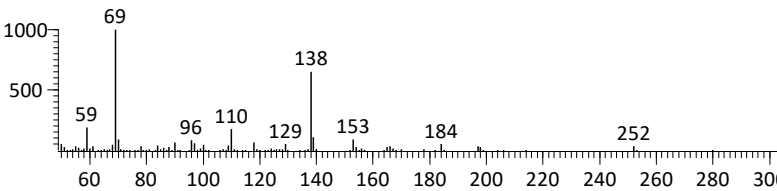
<p>Molecular ion: 185</p> 	<p>Glycine (Gly)</p> 
<p>Molecular ion: 199</p> 	<p>Sarcosine (Sar)</p> 
<p>Molecular ion: 199</p> 	<p>Alanine (Ala)</p> 
<p>Molecular ion: 199</p> 	<p>β-Alanine (β-Ala)</p> 
<p>Molecular ion: 311</p> 	<p>Serine (Ser)</p> 

Table S 1. Continued.

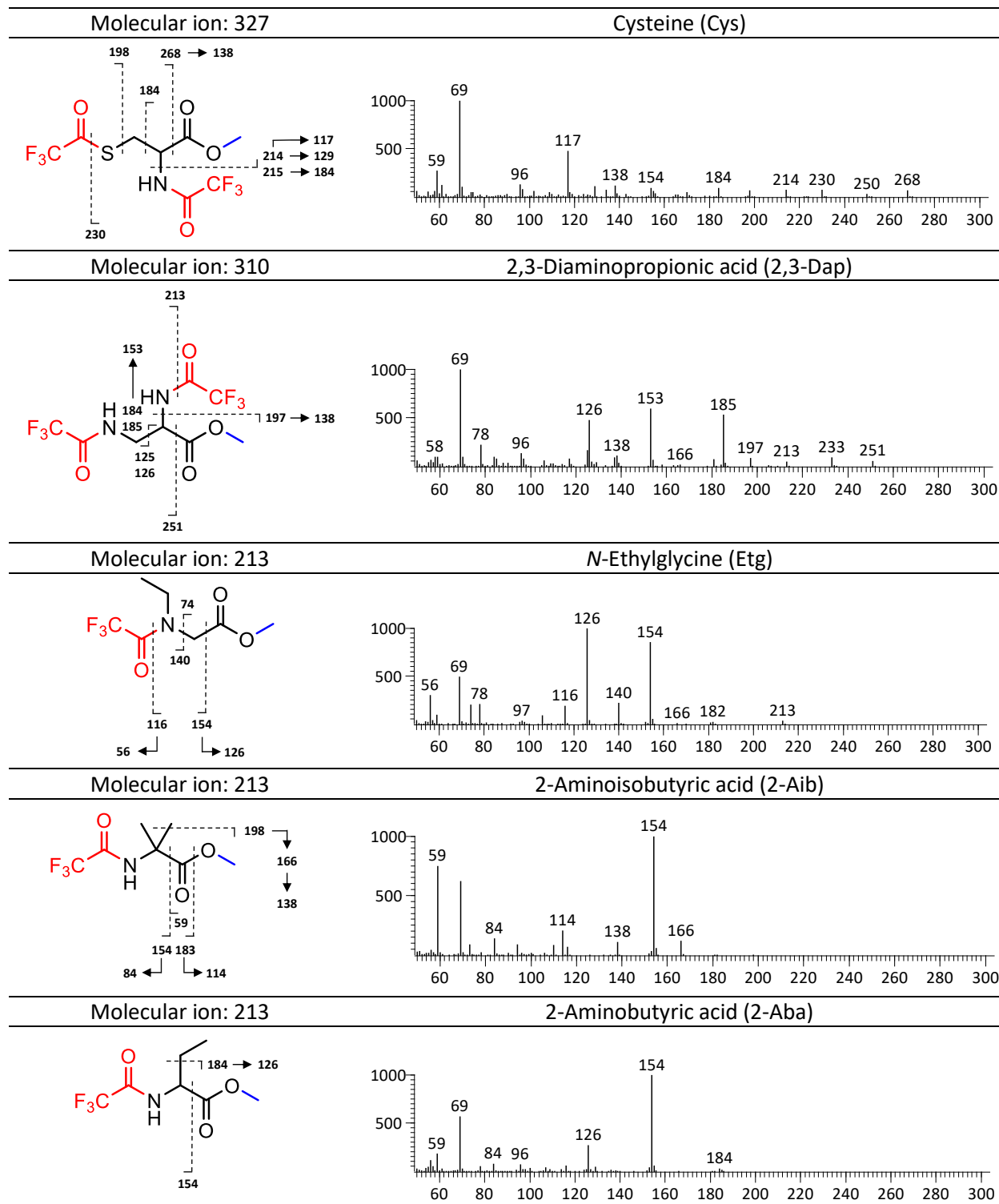


Table S 1. Continued.

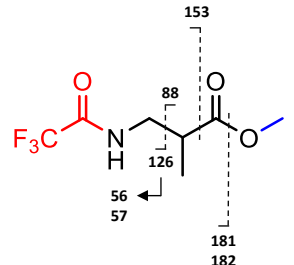
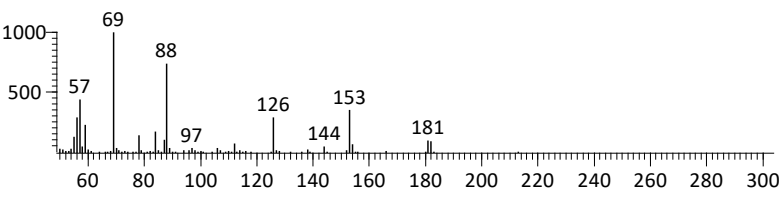
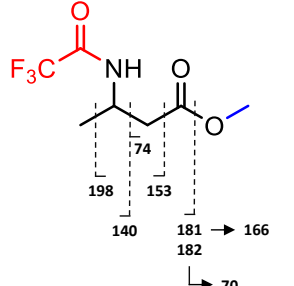
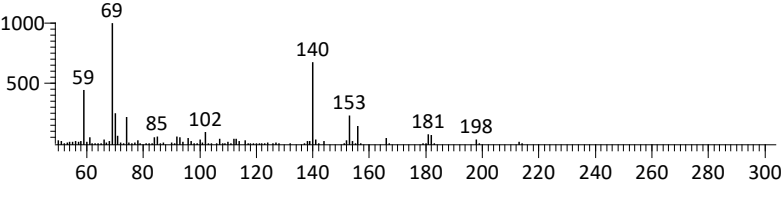
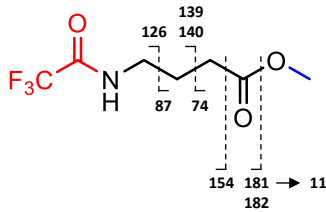
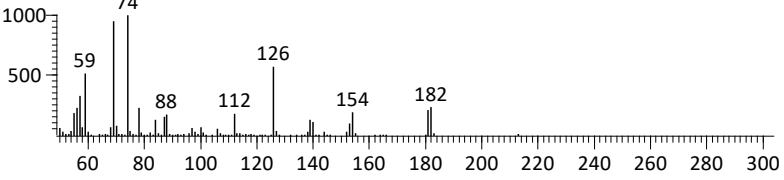
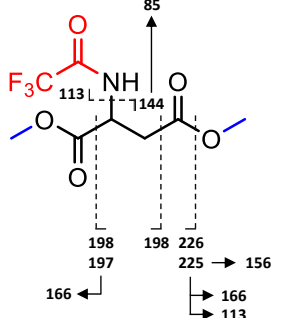
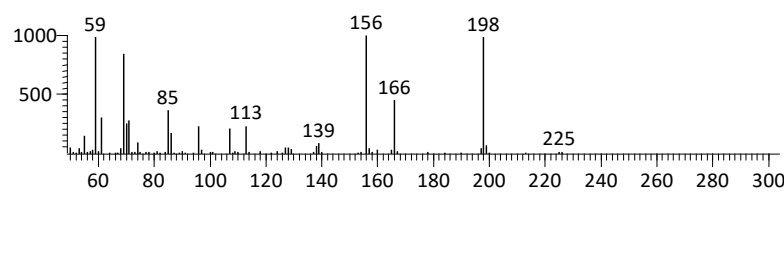
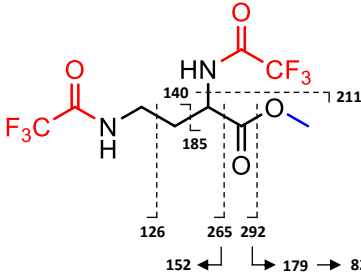
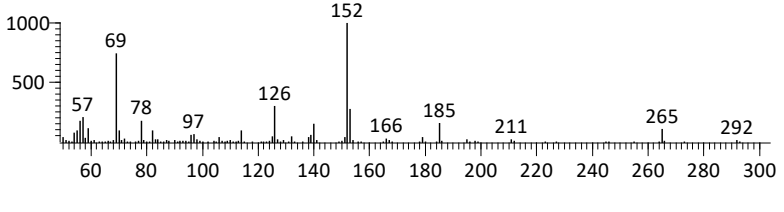
<p>Molecular ion: 213</p> 	<p>3-Aminoisobutyric acid (3-Aib)</p> 
<p>Molecular ion: 213</p> 	<p>3-Aminobutyric acid (3-Aba)</p> 
<p>Molecular ion: 213</p> 	<p>4-Aminobutyric acid (4-Aba)</p> 
<p>Molecular ion: 257</p> 	<p>Aspartic acid (Asp)</p> 
<p>Molecular ion: 324</p> 	<p>2,4-Diaminobutanoic acid (2,4-Dab)</p> 

Table S 1. Continued.

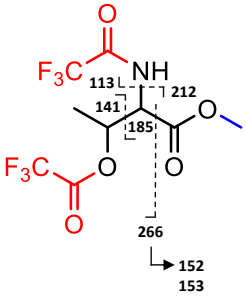
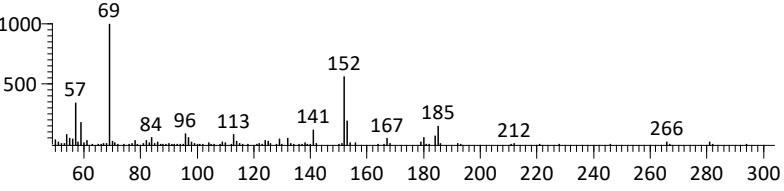
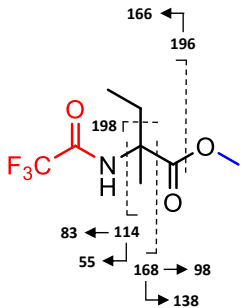
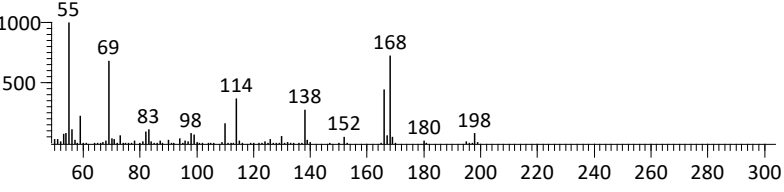
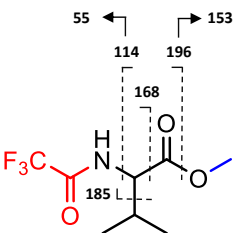
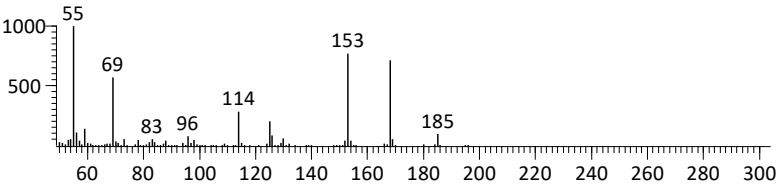
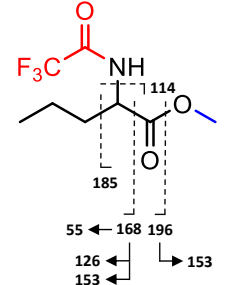
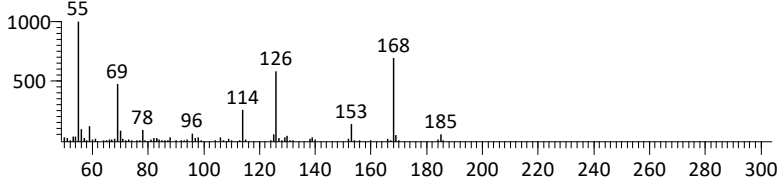
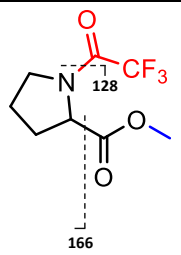
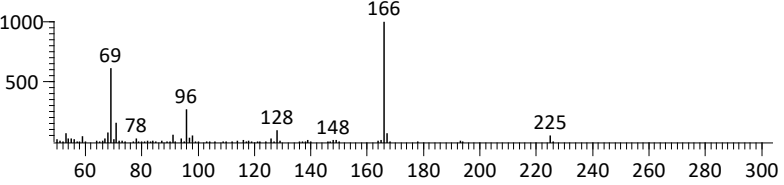
<p>Molecular ion: 325</p> 	<p>Threonine (Thr)</p> 
<p>Molecular ion: 227</p> 	<p>Isovaline (Iva)</p> 
<p>Molecular ion: 227</p> 	<p>Valine (Val)</p> 
<p>Molecular ion: 227</p> 	<p>Norvaline (Nva)</p> 
<p>Molecular ion: 225</p> 	<p>Proline (Pro)</p> 

Table S 1. Continued.

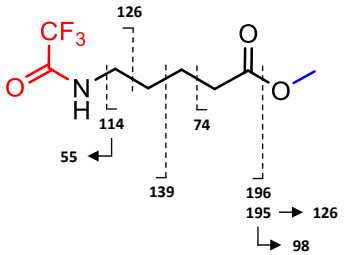
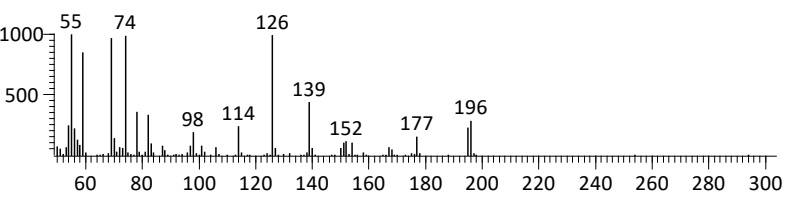
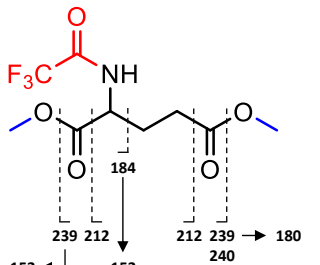
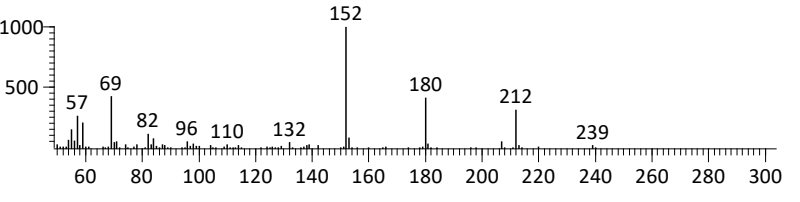
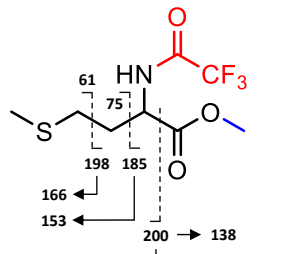
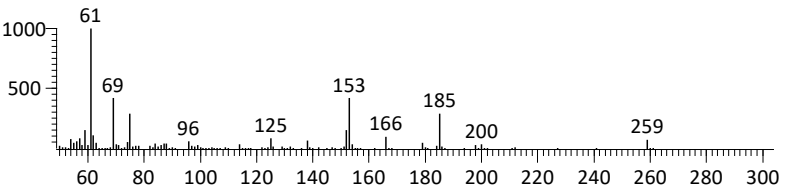
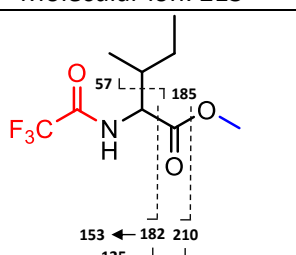
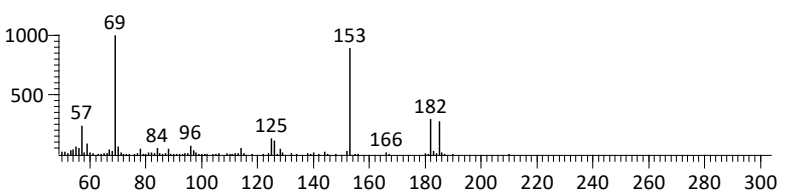
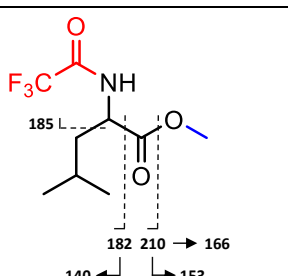
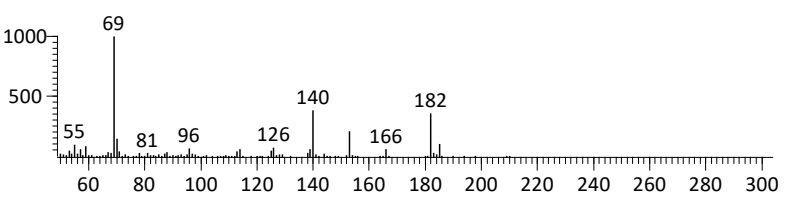
<p>Molecular ion: 227</p> 	<p>5-Aminopentanoic acid (5-Ava)</p> 
<p>Molecular ion: 271</p> 	<p>Glutamic acid (Glu)</p> 
<p>Molecular ion: 259</p> 	<p>Methionine (Met)</p> 
<p>Molecular ion: 213</p> 	<p>Isoleucine (Ile) & <i>allo</i>-Isoleucine (<i>allo</i>-Ile)</p> 
<p>Molecular ion: 241</p> 	<p>Leucine (Leu)</p> 

Table S 1. Continued.

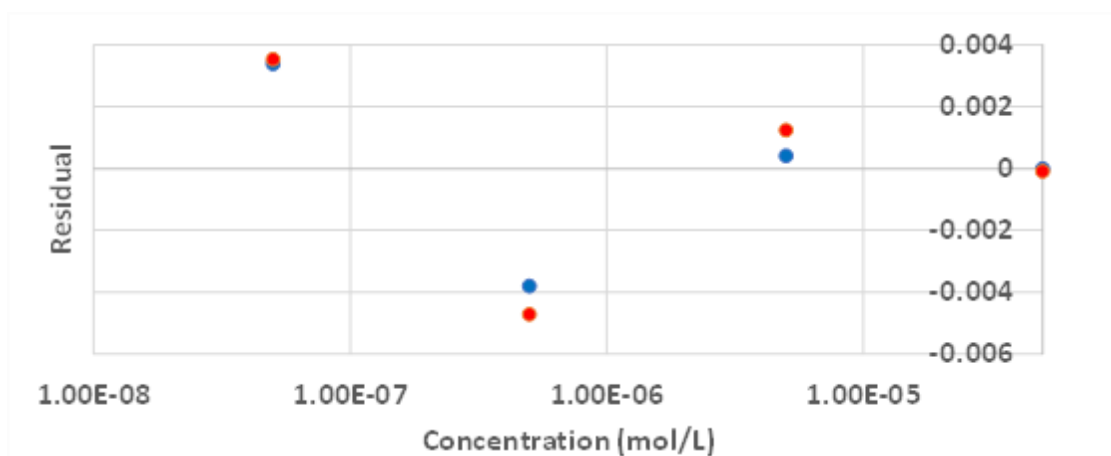
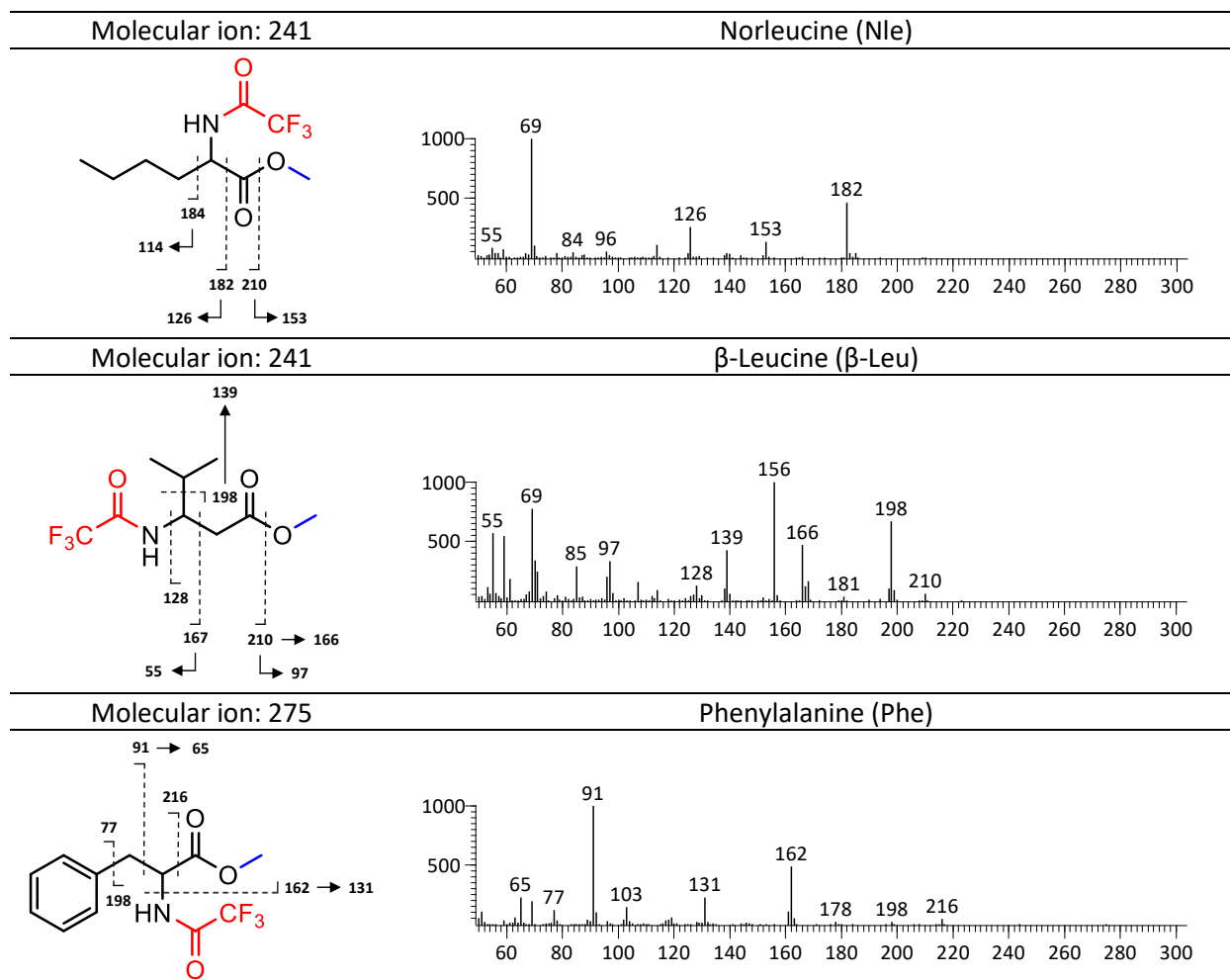


Figure S 1. Alanine residual plot calculated from the calibration curve. Residual values displayed are the difference between the predicted value from the calibration curve, and the obtained value, for each concentration.

Table S 2. Mass spectrum of MBA/TFAA derivatized sugars and sugar related compounds.

Molecular ion: 198	Glycolaldehyde (dimer)
TFAA group(s): 1 MBA ring(s): 1	
Molecular ion: 380	Glycerol
TFAA group(s): 3 MBA ring(s): 0	
Molecular ion: 114	Glyceraldehyde
TFAA group(s): 0 MBA ring(s): 1	
Molecular ion: 240	Erythrose
TFAA group(s): 1 MBA ring(s): 1	
Molecular ion: 282	1,3-Dihydroxyacetone
TFAA group(s): 2 MBA ring(s): 0	
Molecular ion: 338	Threitol
TFAA group(s): 2 MBA ring(s): 1	

Table S 2. Continued.

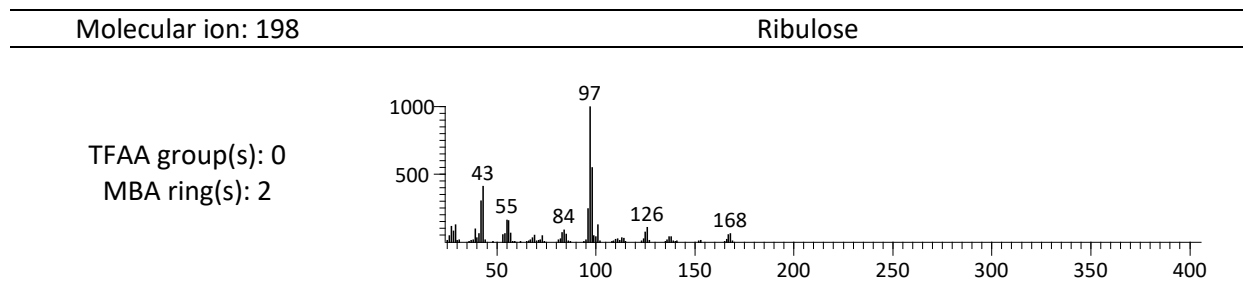
Molecular ion: 338	Erythritol
TFAA group(s): 2 MBA ring(s): 1	<p>Mass spectrum of Erythritol showing relative intensity (0 to 1000) versus m/z (0 to 400). The base peak is at m/z 97. Other significant peaks are labeled at m/z 43, 55, 69, 88, 110, and 182.</p>
Molecular ion: 254	2-Deoxyribose
TFAA group(s): 1 MBA ring(s): 1	<p>Mass spectrum of 2-Deoxyribose showing relative intensity (0 to 1000) versus m/z (0 to 400). The base peak is at m/z 43. Other significant peaks are labeled at m/z 57, 69, 84, 97, 140, 166, 195, and 224.</p>
Molecular ion: 366	Lyxose (peak 1)
TFAA group(s): 2 MBA ring(s): 1	<p>Mass spectrum of Lyxose (peak 1) showing relative intensity (0 to 1000) versus m/z (0 to 400). The base peak is at m/z 69. Other significant peaks are labeled at m/z 43, 55, 85, 97, 139, 182, 223, and 253.</p>
Molecular ion: 198	Lyxose (peak 2)
TFAA group(s): 0 MBA ring(s): 2	<p>Mass spectrum of Lyxose (peak 2) showing relative intensity (0 to 1000) versus m/z (0 to 400). The base peak is at m/z 97. Other significant peaks are labeled at m/z 43, 57, 84, 110, 139, and 168.</p>
Molecular ion: 296	Xylitol
TFAA group(s): 1 MBA ring(s): 2	<p>Mass spectrum of Xylitol showing relative intensity (0 to 1000) versus m/z (0 to 400). The base peak is at m/z 97. Other significant peaks are labeled at m/z 43, 57, 69, 140, and 182.</p>
Molecular ion: 296	Adonitol
TFAA group(s): 1 MBA ring(s): 2	<p>Mass spectrum of Adonitol showing relative intensity (0 to 1000) versus m/z (0 to 400). The base peak is at m/z 85. Other significant peaks are labeled at m/z 43, 57, 69, 110, 140, 182, and 236.</p>

Table S 2. Continued.

Molecular ion: 296	Arabitol
TFAA group(s): 1 MBA ring(s): 2	
Molecular ion: 198	Arabinose
TFAA group(s): 0 MBA ring(s): 2	
Molecular ion: 198	Xylose
TFAA group(s): 0 MBA ring(s): 2	
Molecular ion: 198	Ribose
TFAA group(s): 0 MBA ring(s): 2	
Molecular ion: 324	Mannose
TFAA group(s): 1 MBA ring(s): 2	
Molecular ion: 324	Galactose
TFAA group(s): 1 MBA ring(s): 2	

Table S 2. Continued.

Molecular ion: 324	Glucose
TFAA group(s): 1 MBA ring(s): 2	<p>Mass spectrum for Glucose. The x-axis represents m/z from 0 to 400, and the y-axis represents relative intensity from 0 to 1000. The base peak is at m/z 97. Other significant peaks are labeled at m/z 43, 57, 84, 113, 126, 139, 167, 240, and 295.</p>
Molecular ion: 254	Sorbitol (peak 1)
TFAA group(s): 0 MBA ring(s): 3	<p>Mass spectrum for Sorbitol (peak 1). The x-axis represents m/z from 0 to 400, and the y-axis represents relative intensity from 0 to 1000. The base peak is at m/z 85. Other significant peaks are labeled at m/z 43, 69, 97, and 169.</p>
Molecular ion: 254	Sorbitol (peak 2)
TFAA group(s): 0 MBA ring(s): 3	<p>Mass spectrum for Sorbitol (peak 2). The x-axis represents m/z from 0 to 400, and the y-axis represents relative intensity from 0 to 1000. The base peak is at m/z 85. Other significant peaks are labeled at m/z 43, 57, 97, 110, 169, and 194.</p>
Molecular ion: 254	Dulcitol (peak 1)
TFAA group(s): 0 MBA ring(s): 3	<p>Mass spectrum for Dulcitol (peak 1). The x-axis represents m/z from 0 to 400, and the y-axis represents relative intensity from 0 to 1000. The base peak is at m/z 85. Other significant peaks are labeled at m/z 43, 57, 97, 110, 139, and 169.</p>
Molecular ion: 422	Dulcitol (peak 2)
TFAA group(s): 2 MBA ring(s): 2	<p>Mass spectrum for Dulcitol (peak 2). The x-axis represents m/z from 0 to 400, and the y-axis represents relative intensity from 0 to 1000. The base peak is at m/z 97. Other significant peaks are labeled at m/z 43, 69, 84, 111, and 211.</p>
Molecular ion: 324	Fructose
TFAA group(s): 1 MBA ring(s): 2	<p>Mass spectrum for Fructose. The x-axis represents m/z from 0 to 400, and the y-axis represents relative intensity from 0 to 1000. The base peak is at m/z 97. Other significant peaks are labeled at m/z 43, 55, 69, 84, 110, 127, 155, and 197.</p>

Table S 2. Continued.

Table S 3. Regression data of the MBA/TFAA calibration curve, used for days 2 and 7.

#	Compound	S^a (M^{-1})	ΔS^b (M^{-1})	R^2
1	D-Glyceraldehyde	6.51×10^3	231	0.99748
2	L-Glyceraldehyde	6.09×10^3	211	0.99756
3	D-Erythrose	2.33×10^3	78.2	0.99774
4	D-Ribose	1.02×10^4	272	0.99858
5	L-Ribose	1.03×10^4	271	0.99863
6	D-Arabinose	1.31×10^5	3327	0.99871
7	L-Arabinose	1.29×10^5	2963	0.99895
8	D-Xylose	5.34×10^4	1301	0.99881
9	L-Xylose	5.00×10^4	1121	0.99900
10	D-Lyxose	1.36×10^3	15	0.99976
11	L-Lyxose	1.42×10^3	17	0.99972
12	D-2-Deoxyribose	1.86×10^3	20	0.99976
13	L-2-Deoxyribose	2.14×10^3	35	0.99947
14	D-Glucose	3.74×10^4	830	0.99901
15	L-Glucose	3.26×10^4	480	0.99956
16	D-Galactose	1.88×10^5	3199	0.99942
17	L-Galactose	2.25×10^5	4961	0.99902
18	Glycerol	1.01×10^4	534	0.99441
19	D-Threitol	1.14×10^3	50	0.99623
20	L-Threitol	1.04×10^3	42	0.99677
21	Erythritol	8.10×10^2	13	0.99952
22	D-Arabitol	2.01×10^3	64	0.99797
23	L-Arabitol	1.84×10^3	62	0.99774
24	Xylitol	1.64×10^4	417	0.99871
25	Adonitol	1.76×10^3	53	0.99821
26	Dihydroxyacetone	8.67×10^2	18	0.99914

^aSlope. ^bStandard error on S . Intercept was set to 0. Data obtained using 3 concentrations: 10^{-4} M, 10^{-5} M and 5×10^{-6} M. For each concentration, 2 samples were prepared and analyzed 3 times.

Table S 4. Regression data of the MBA/TFAA calibration curve, used for day 45.

#	Compound	S^a (M ⁻¹)	ΔS^b (M ⁻¹)	R^2
1	D-Glyceraldehyde	1.63×10^3	49	0.99732
2	L-Glyceraldehyde	1.58×10^3	50	0.99698
3	D-Erythrose	2.59×10^2	46	0.94090
4	D-Ribose	4.96×10^3	145	0.99743
5	L-Ribose	4.80×10^3	121	0.99810
6	D-Arabinose	2.79×10^4	1606	0.99012
7	L-Arabinose	2.90×10^4	1369	0.99334
8	D-Xylose	1.82×10^4	272	0.99933
9	L-Xylose	1.78×10^4	273	0.99929
10	D-Lyxose	8.68×10^2	13	0.99933
11	L-Lyxose	8.75×10^2	12	0.99941
12	D-Glucose	2.79×10^4	936	0.99662
13	L-Glucose	2.59×10^4	668	0.99801
14	D-Galactose	1.52×10^5	4822	0.99699
15	L-Galactose	1.70×10^5	4571	0.99783
16	Glycerol	2.95×10^3	605	0.88776
17	D-Threitol	1.09×10^3	29	0.99861
18	L-Threitol	9.66×10^2	24	0.99872
19	Erythritol	2.02×10^2	8	0.99720
20	D-Arabitol	1.34×10^3	49	0.99737
21	L-Arabitol	1.28×10^3	58	0.99591
22	Adonitol	8.69×10^2	15	0.99941
23	Dihydroxyacetone	8.93×10^1	21	0.86171

^aSlope. ^bStandard error on S. Intercept was set to 0. Data obtained using 4 concentrations: 5×10^{-5} M, 10^{-5} M, 5×10^{-6} M and 10^{-6} M. For each concentration, 1 sample was prepared and analyzed 2 times.

